DEPARTMENT OF CIVIL ENGINEERING

Powder packing optimisation for clinker reduction in concrete

19 February 2018

Prepared by: Matthew Holmes

Supervisor: Emeritus Prof Mark Alexander

Submitted in partial fulfilment of a Master of Science degree in Civil Engineering in Civil Infrastructure Management and Maintenance

Plagiarism Declaration

- I know the meaning of plagiarism and declare that all the work in the document, save for that which is properly acknowledged using the UCT Harvard Convention for citation and referencing, is my own.
- This dissertation has been submitted to the Turnitin module and I confirm that my supervisor has seen my report and any concerns revealed by such have been resolved with my supervisor.

Matthew Stuart Holmes Signed by candidate

Acknowledgements

I would like to express my sincere gratitude towards my supervisor Emeritus Prof. Mark Alexander for his continuous support and guidance throughout this research project. This research would not have been possible without the committed assistance of Nooredien Hassen, Tahir Mukaddam and the University of Cape Town (UCT) concrete laboratory staff. The invaluable assistance of the UCT Chemical Engineering Department is also acknowledged along with the assistance of the Electron Microscope Unit at UCT.

I would also like to thank the '6th floor squad' for always lending a helping hand when needed and for many eventful lunch-times. Lastly, but far from least, I would like to thank Bryony Clark for her perseverance in editing this document and my family and fiancé for their unrelenting support. Your work behind the scenes has not gone unnoticed.

Summary

Globally, concrete is the most used construction material. Its embodied energy is relatively low, yet due to the vast quantities that are produced annually, it has substantial greenhouse gas (GHG) emissions associated with it. Of the concrete constituents, the manufacture of clinker - the basis of all conventional cements - contributes the most significant emissions. Therefore, to reduce the emissions associated with concrete manufacture, there has been extensive research into how clinker content can be reduced without compromising desired concrete properties. Existing methods for clinker reduction have, however, only allowed clinker replacement to a limited extent.

This research investigated the more efficient use of clinker to minimise clinker content required to achieve desired mechanical and durability properties of concrete. The optimisation of powder (materials < 125 μm) packing, using filler materials with varying fineness, was identified to potentially increase clinker efficiency. The optimisation undertaken was the maximisation of powder packing density but without adversely affecting workability. The investigation entailed the application of analytical particle packing density models as well as experimental investigation. Two particle packing models, the Compaction Interaction Packing Model (CIPM) and the Modified Andreasen and Andersen Curve (MAAC) were applied.

Various methods for determining the packing density of powder combinations were investigated which informed the use of the mixing energy test to provide experimental packing density data for the modelling procedures. The CIPM was used to optimise the powder phases of concrete as it incorporated the effect of surface forces on powder packing and the MAAC was used to complete the optimisation of fine and coarse aggregate materials. It was necessary to calibrate the CIPM through the selection of various model constants, based on the minimisation of the average error associated with predicted packing density.

Despite the incorporation of surface force effects, the CIPM did not predict the trend in packing density observed for various experimental powder combinations with consistent accuracy. Combinations of cement with limestone of high and low fineness (relative to cement) were most accurately predicted but combinations with limestones of similar fineness to cement were less accurate. It was therefore apparent that the model inadequately accounted for the effects of varying particle size and the corresponding influence of surface forces on these particles. However, for practicality, model constants which minimised overall error were used to determine powder combinations enabling maximum packing density for use in optimised concrete mix design.

Concrete mixes were designed in 2 phases. Initially water content was fixed, and limestone content was successively increased to 40 vol. % (Phase 1). Despite the formation of mixtures according to maximum packing density, the results showed that optimisation of packing density with a fixed water content was insufficient to reduce clinker content without adversely affecting compressive strength. However, workability was maintained without excessive superplasticiser (SP) dosage and oxygen permeability, water sorptivity and accelerated drying shrinkage were either improved or not adversely affected. This was attributed to the ability of fine fillers to prevent interconnectivity of the pore structure and the decreased volume of gel hydration products leading to reduced drying shrinkage.

Compressive strength was tested for a binary (cement/limestone) and ternary (cement /limestone/fly ash (FA)) binder blend for Phase 2 in conjunction with a substantially reduced water content. Workability was adversely affected and both mixes required high SP doses, however, the FA blend required a relatively lower dose. Compressive strength was again decreased relative to the reference mix but when comparing Phase 1 and 2 mixes with predicted strength for equivalent w/c ratios, compressive strength was relatively unchanged, inferring little benefit of packing optimisation.

However, binder efficiency indices ('bi') (between 5.3 and 6.9 $kg/m^3/MPa$) were reduced relative to data from previous investigations with similar strength class (between 10 to 20 $kg/m^3/MPa$), inferring increased binder performance. Powder packing optimisation thereby has the potential to enable clinker reduction, particularly for lower strength grade concrete, without adversely affecting compressive strength. Furthermore, the relatively unaffected durability indicators portray the beneficial effects of powder packing optimisation on increasing the impenetrability of concrete microstructure and its potential use in applications where durability is of importance. These findings may also point to further possible reductions in the binder efficiency index below 5 $kg/m^3/MPa$ if water content is further reduced (to maintain low water: cement ratio) and reactive SCMs are incorporated. However, further investigation and understanding of the fundamentals of powder packing is necessary to achieve a fully predictive process of low-clinker concrete mix design that can be universally applicable.

Table of Contents

List of Figures

List of Tables

Abbreviations

ACI	:	American concrete institute
C&CI	:	Cement and Concrete Institute
CH	:	Calcium hydroxide
CIPM	:	Compaction Interaction Packing Model
CO_2e	:	Carbon dioxide equivalent (w.r.t. GHG emissions)
CPM	:	Compressible Packing Model
CSI	:	Cement sustainability initiative
CSF	:	Condensed Silica Fume
C-S-H	:	Calcium Silicate Hydrate
FA	:	Fly Ash
GGBS	:	Ground Granulated Blast Furnace Slag
GGCS	:	Ground Granulated Corex Slag
GHG	:	Greenhouse Gas
GNR	:	Getting the numbers right project (WBCSD)
GWP	:	Global warming potential
HPC	:	High performance concrete
IPS	:	Interparticle Separation Distance (viscosity prediction model)
LPDM	:	Linear Packing Density Model
MAAC	:	Modified Andreasen and Andersen Curve
PC	:	Portland Cement
PCE	:	Poly-carboxylate ether
PSD	:	Particle size distribution
SCM	:	Supplementary cementitious material
SEM	:	Scan Electron Microscopy
SP	:	Superplasticiser
WBCSD	:	World business council for sustainable development
w/b	:	Water: binder ratio (only reactive binder)
w/p	:	Water: powder ratio
w/c	:	Water: cement ratio
w/cm	:	Water: cementitious material ratio (Wet packing test)
INT'_{ni}	:	Natural interference (viscosity prediction model)
XRD	:	X-ray diffraction

Notation and symbols

Greek

α : Packing density of a mixture

α_{exp} : Experimentally determined packing density of a mixture [-]

α_i : Packing density of dominant size class *i* [-]

α_j : Packing density of size class *j* [-]

α_t : Calculated packing density of a mixture (CIPM)

β : Virtual packing density of a particle mixture (CIPM)

β_i : Virtual packing density of size class *i* [-]

β_j : Virtual packing density of size class *j* [-]

β_t : Calculated virtual packing density of a mixture [-]

β_{ti} : Calculated virtual packing density of a mixture when size class *i* is dominant [-]

φ_i : Partial volume: the volume occupied by size class *i* in a unit volume [-]

φ_i^* : Maximum partial volume that size class *i* may occupy given the presence of other particles [-]

φ_j : Partial volume: the volume occupied by size class *j* in a unit volume [-]

Latin

a_{ij} : Factor which describes the loosening effect caused by the particles in size class *j* on the packing density of the particles in size class *i* [-]

$a_{ij,c}$: Factor which describes the loosening effect caused by the particles in class j on the packing of the particles in class i for the determination of φi^* [-]

b_{ij} : Factor which describes the wall effect caused by the particles in class j on the packing of the particles in class i [-]

$b_{ij,c}$: Factor which describes the wall effect caused by the particles in class *j* on the packing of the particles in class *i* to determine φ_i^* [-]

C_a : Compaction-interaction constant within the loosening effect $a_{ij,c}$ [-]

C_b : Compaction-interaction constant within the wall effect $b_{ij,c}$ [-]

d : Particle diameter (µm) (CIPM)

D : Particle diameter (µm) (MAAC)

d_c : Cut-off diameter in the CIPM below which compaction-interaction is taken into account [µm]

d_i : Diameter of dominant size class *i* [µm]

d_j : Diameter of size class *j* [µm]

d_{small} : Diameter of size class consisting of small particles [µm]

d_{large} : Diameter of size class consisting of large particles [µm]

D_L : Diameter of maximum particle size in a mixture [µm]

D_s : Diameter of minimum particle size in a mixture [µm]

H : Experimental dissipative parameter (viscosity prediction model)

i : Nomenclature for the dominant size class in a mixture

j : Nomenclature for a size class in a mixture

K : Compaction index [-]

K_{exp}: Experimental compaction index associated with the experimental measurement of packing density

K_i: Partial compaction index of size class *i* within the CIPM [-]. The summation of K_i across all size classes in a mixture equates to the compaction index (K_t)

K_t : Compaction index associated with a mixture in the CIPM [-]

L_a : Compaction-interaction constant within the loosening effect a_{ij} [-]

L_b : Compaction-interaction constant within the wall effect b_{ij} [-]

q : Distribution modulus (exponent in MAAC equation) [-]

r_i : Volume fraction of size class *i* [-]

r_j : Volume fraction of size class *j* [-]

1 Introduction

1.1 Background

The construction industry is a primary stakeholder in the development of a country, which is of utmost importance for a developing country such as South Africa. However, this industry also contributes substantial Greenhouse gas (GHG) emissions at an unsustainable rate (U.S. Geological Survey, 2016; Witi & Stevens, 2014). It is therefore important to integrate sustainable processes into all aspects of this industry to ensure sustainable development for time to come.

To compare the impact of different GHGs, the term 'Global Warming Potential' (GWP) was developed as a measure of the energy absorbed by 1 tonne of gas over a given period of time, relative to the energy absorbed by 1 tonne of carbon dioxide (CO_2) (which is taken to be 1). Therefore, to indicate the impact of a particular GHG, it is common convention to quote the CO_2 equivalent emissions (CO_2e emissions) associated with a GHG.

Vast CO_2e emissions are associated with construction materials due to fossil-fuelled, energy intensive processes required for the conversion of raw materials to high quality construction materials. Furthermore, by-products of these processes include CO_2e emissions and therefore the careful selection of appropriate construction materials is becoming increasingly important to achieve an environmentally sustainable construction industry.

Relative to other common construction materials, concrete does not have substantial associated CO_2e emissions. A report compiled for the Cement and Concrete Institute of Southern Africa (InEnergy, 2010) showed concrete to have between 195 and 483 kg CO_2/t associated with it, depending on various material constituents, whereas steel reinforcing, for example, had associated with it 2735 kg/CO_2/t. However, it is the most widely used construction material (Van Den Heede & De Belie, 2012) with approximately 1 tonne being produced annually for every living human being (Flower & Sanjayan, 2007), causing its cumulative associated CO_2e emissions to be of concern when attempting to achieve environmental sustainability. (InEnergy, 2010)

When considering the individual materials that make up concrete, cement represents the primary contributor of GHGs, contributing between 5 and 7 % of global anthropogenic CO_2e emissions (Van Den Heede & De Belie, 2012). This is largely due to the production of clinker, a major constituent of Portland cement. Its production is extremely energy intensive and entails the burning of fossil fuels, liberating GHGs, as does the calcination process (required to convert $CaCO_3$ to CaO) which alone accounts for 0.52 tonnes CO_2e emissions per tonne clinker produced (Witi & Stevens, 2014). Additionally, emissions associated with mining, crushing, milling and transportation of raw and processed materials cannot be overlooked when considering the total CO_2e emissions associated with clinker.

The reduction in clinker content of concrete is therefore recognised as having the potential to enable a significant reduction in emissions associated with concrete manufacture. However, this material is also responsible for providing the binding capacity within a concrete mix when it hydrates in the presence of water. Therefore, along with the potential reduction in emissions with a decrease in clinker content, it is as important to consider the binding capacity (which ultimately enables the robust engineering properties of concrete) and how these can still be achieved with a decreased clinker content.

The realisation for the increased sustainability of concrete with a reduction of clinker content is not a recent development and has received research interest for some time (Lothenbach *et al.*, 2011; Imbabi *et al.*, 2012; Proske *et al.*, 2014; Scrivener *et al.*, 2016). Studies have included the investigation of materials to replace clinker which offer varying degrees of cementing capacity as a result of various chemical reactions. These range from those which undergo latent hydraulic reactions or pozzolanic reactions which both form hydration products similar to the hydration of clinker to 'alternate' binders, the reactions of which produce hydration products completely different to the hydration of clinker (Grieve, 2009).

Furthermore, recent investigations continue to use clinker but optimise the packing of concrete materials to reduce the required clinker content (Fennis, 2011; Knop *et al.*, 2014; Proske *et al.*, 2014; Yu *et al.*, 2015). It has been observed that with an increased packing density of constituent materials, concrete properties benefit from a denser microstructure and a stiffer, less permeable material is attained. Decreased void space also demands less water and can potentially allow decreased water content while maintaining workability. Should the optimisation of the packing of concrete materials enhance concrete properties, it is likely that the clinker content may be reduced to an extent without diminishing the required engineering properties.

Methods to increase and optimise the packing density of coarse aggregate particles are well documented. Packing models have been developed which can reasonably accurately predict the packing density of a given particle size distribution (PSD) of coarse aggregate particles(Jones *et al.*, 2002; Alexander & Mindess, 2005; Loseby, 2014). However, the extent to which the optimisation of coarse aggregate packing influences the eventual concrete properties is not as great as the extent to which powder material (<125 μm) packing influences eventual concrete properties.

Although the packing of the entire range of materials is important, the optimisation of powder packing appears to provide the greatest potential for clinker reduction. However, there is no consensus on the best technique to optimise packing. Several optimisation attempts have been in the form of applying coarse aggregate packing models to powder packing (Jones *et al.*, 2002; Knop & Peled, 2016). This has often led to inaccurate prediction of powder packing density due to the different influences on these materials when compared with coarse aggregate particles.

Influences specific to powder packing have more recently been acknowledged in packing models. Fennis (2011) incorporated an increased effect of surface forces with a decrease in particle size. Furthermore, there has been suggestion that maximising packing density (the objective of most particle packing models) to ultimately enable clinker reduction should rather be reconsidered as being an implication of optimising paste rheology and, instead, not the sole objective of the optimisation process (John *et al.*, 2017).

However, the consensus is that with a better consideration of the influences specific to powder packing (primarily, the effect of surface forces but also aspects such as particle shape and surface morphology) the accuracy with which powder packing can be modelled will be increased. Subsequently, this should enable the optimisation of this phase, be it through increasing packing density or achieving this indirectly through optimising rheology properties.

Investigations into these principles have enabled better particle packing, and reported concrete properties were either enhanced or not adversely affected, realising the potential for a reduction in clinker content. Yet, concrete mix design in South Africa currently only indirectly

considers the packing of constituent materials and does so largely for coarse and fine aggregate materials. Therefore, application of powder packing optimisation techniques to reduce clinker in this context needs to be quantified. The accuracy of newly developed packing models and their applicability to the concrete materials commonly used in the Western Cape needs to be tested. With the quantification of the potential for clinker reduction by powder packing optimisation using modelling techniques, a powerful tool for use in concrete mix design could be achieved. Such a tool could aid the development of low-clinker concretes and reduce GHGs associated with concrete manufacture in the Western Cape.

1.2 Problem Statement

Powder packing optimisation has been identified to potentially enable the reduction of clinker content of concrete and therefore associated GHGs. Particle packing models of varying theory, complexity and practicality have been developed to optimise particle packing density but the most appropriate methods to enable the reduction of clinker are still unclear. The ability of existing models to account for influences specific to powder packing needs to be investigated, and conclusions drawn with respect to the suitability of packing models for use in reducing the clinker content of concrete.

1.3 Research objectives

The overarching objective for this research is to reduce the clinker content of concrete without adversely affecting desired concrete properties. To achieve this general objective, the following subsidiary objectives are defined:

- To determine which particle packing model/s is/are best suited for the prediction of the packing density of powder materials (<125 μm)
- To investigate experimental methods for the assessment of powder packing density
- To determine the accuracy with which particle packing models can predict the packing density of powders
- To apply particle packing modelling to optimise concrete mix design by maximising powder packing density without adversely affecting workability
- To determine the extent that fine fillers can aid powder packing optimisation
- To determine the extent that powder packing optimisation can reduce the clinker content of concrete according to the binder efficiency index (bi)*

*Amount of reactive binder (kg) per cubic meter of concrete required to achieve 1 MPa of compressive strength at 28 days (Damineli *et al.*, 2010).

1.4 Scope and limitations

The scope for this research is represented in Figure 1-1 and includes the following limitations:

- Consideration was given to the packing of the entire spectrum of concrete constituents, but focus was given to the packing of powder materials
- The application of particle packing modelling techniques required various assumptions, which are described in the relevant sections concerning their implementation

- Refinement of the mix design process with the incorporation of modelling outputs was not possible due to imposed time constraints. Therefore, only a limited range of concrete mix designs and concrete properties were tested.
- Materials used in the experimental program were limited to those supplied and used locally in the Western Cape

1.5 Plan of development

This dissertation is divided into 7 chapters as follows:

Chapter 1: Introduction - A general overview of the research topic is provided. Background information is given to support the relevance of the research along with the problem statement, objectives, scope and limitations.

Chapter 2: Review of literature - An in-depth analysis of literature pertaining to the need for clinker reduction, existing strategies therefore and potential new strategies are reviewed with a focus given to particle packing modelling.

Chapter 3: Preliminary experimental investigation - Methodology for preliminary experimental investigations is given. This chapter entails the analysis of constituent material properties and the evaluation of various experimental techniques for the determination of packing density.

Chapter 4: Particle packing modelling - Particle packing modelling methodology is described, covering the integration of the Compaction Interaction Packing Model (CIPM) with the Modified Andreasen and Andersen Curve (MAAC) and their implementation in Microsoft Excel.

Chapter 5: Implementation of modelling outputs - Methodology regarding the use of modelling outputs in two phases of concrete mix design is discussed along with the methods used to test the fresh and hardened concrete properties of interest.

Chapter 6: Results and discussions - A detailed discussion of findings from modelling and experimental work is presented. Findings concerning constituent material properties are discussed along with the selection of the most appropriate method for measuring powder packing density, the calibration and use of the combined particle packing models, resulting concrete mix designs, fresh and hardened concrete properties and the ability of powder packing optimisation to allow for clinker reduction in concrete.

Chapter 7: Conclusions and recommendations – Conclusions based on the findings presented in the previous chapters are provided and recommendations for future research and application of low-clinker concrete are proposed.

Appendices: - Provision of additional information.

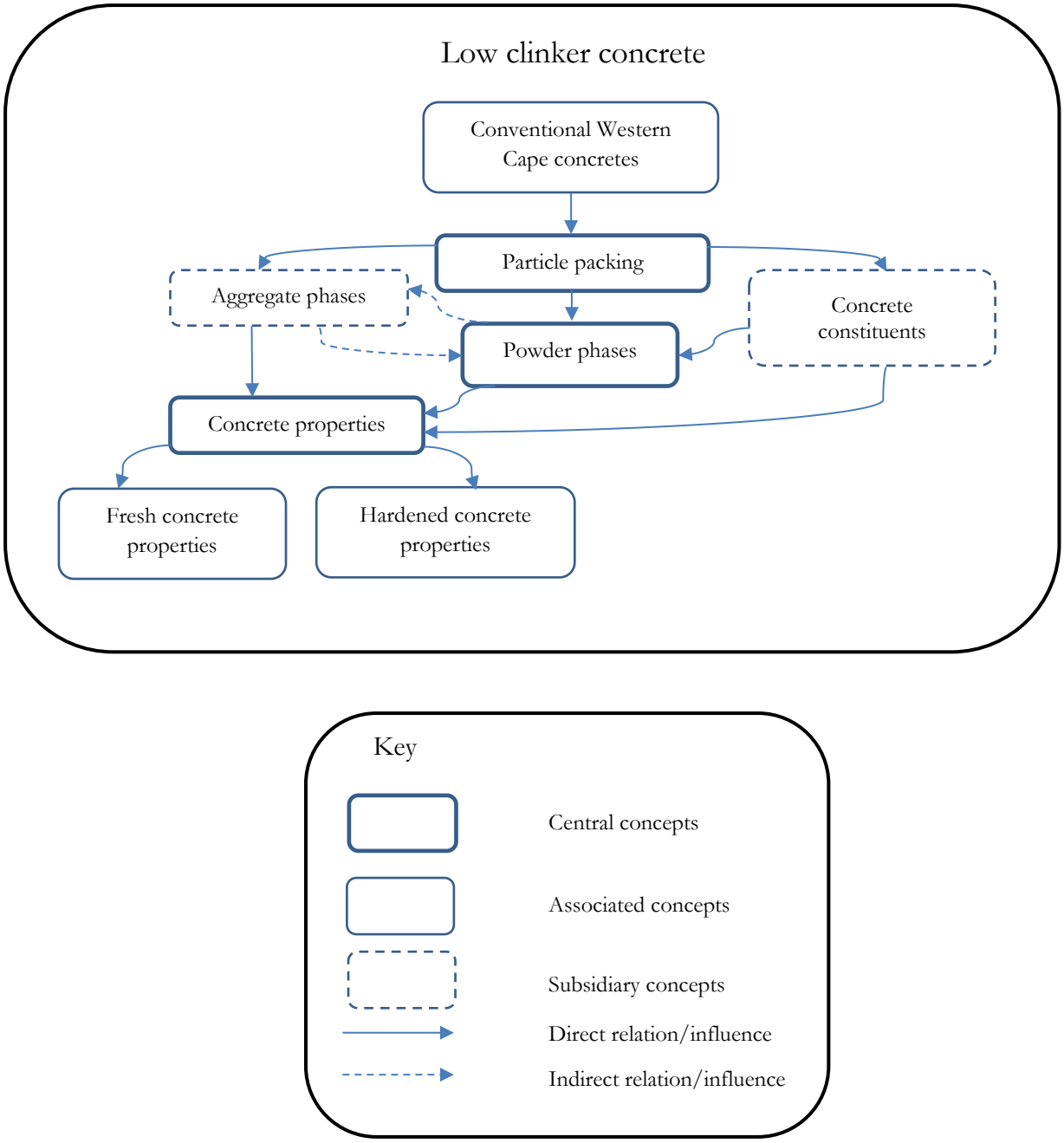

Figure 1-1: Research scope and conceptual framework

2 Review of Literature

This review addresses literature concerning the need for a reduction in the emissions associated with concrete manufacture and discusses existing strategies to achieve this. Commentary is given concerning the extent to which emissions have been reduced with existing strategies and recent advancements in this field involving the optimisation of the powder phases of concrete are introduced. Focus is given to the packing of concrete materials, the modelling thereof and why this field is of interest for the reduction of the clinker content.

2.1 Low clinker concrete

2.1.1 A need for clinker reduction in concrete

Concrete is well recognised for its competent engineering properties, robust nature and ability to be used under almost any circumstance and therefore has been, and will continue to be, used extensively worldwide for time to come. Carbon dioxide equivalent (CO_2e) emissions for 30 MPa concrete comprising commonly used South African concrete materials show that emissions are highly dependent on the concrete mix design considered, ranging between 195 and 483 kg CO_2e /m^3 concrete (InEnergy, 2010). In comparison to another widely used construction material, such as reinforcing steel that has been reported to have CO_2e emissions of 2735 kg CO_2e /t (InEnergy, 2010), concrete has substantially lower associated emissions. However, despite these findings, the global mass production of concrete, approximately 1 tonne/capita (Flower & Sanjayan, 2007) and, more broadly, the production of all cement based materials, within the range of 4.8 to 5.5 t/capita (Scrivener *et al.*, 2016), results in significant Greenhouse Gases (GHGs) being associated with its manufacture.

With the realisation of the need for sustainable construction methods and materials, the reduction of GHGs associated with concrete manufacture has attracted substantial research. Various methodologies have been proposed to reduce emissions, yet there is an underlying finding that remains unchanged: there is no probable replacement for concrete as a construction material in its entirety. Instead, the most reasonable, economically viable solution that has presented itself is the optimisation of the use of concrete constituents and in that way, reducing the emissions associated with its manufacture and the impact that it has on the environment (Scrivener *et al.*, 2016).

The demand for concrete is continuously increasing in developing countries, such as South Africa, and the supply and manufacture of its constituents will need to meet this demand. Associated emissions range from those which come from the extraction of raw material resources to processing and manufacture and the energy required to do so, as well as the emissions from chemical reactions required to produce its constituents. Furthermore, there are other indirect emissions due to transportation from an initial processing plant to a final processing plant or destination, which have significant contributions to the overall CO_2e emissions associated with the end-product (InEnergy, 2010).

To adequately consider all emissions associated with concrete, due consideration would have to be given to the entire lifecycle of concrete, such as research by Muigai (2014). However, considering the individual materials that make up common structural concrete, there is

overwhelming evidence for Portland cement (PC) being the primary contributor to CO_2 emissions associated with concrete, contributing between 5 and 7 % of global anthropogenic CO_2 emissions.(Van Den Heede & De Belie, 2012; Proske *et al.*, 2014; Damineli *et al.*, 2016; Scrivener *et al.*, 2016; John *et al.*, 2017).

To substantiate this point, the World Business Council for Sustainable Development Cement Sustainability Initiative (WBCSD- CSI) have compiled a database comprising CO_2 and energy statistics associated with the global cement industry, reporting the global total cement production for the year 2014 as approximately 4.2 billion tons (WBCSD-CSI, 2016). The 'Getting the Numbers Right' (GNR) project, led by the WBCSD, forms the basis of this database and represents 21 % of global cement production. Cumulatively, 934 global cement manufacturing facilities took part in the project and produced more than 877 million tons of cement in 2014, equating to an excess of 563 million tons of CO_2 emissions (excluding CO_2 from on-site power generation) (see Figure 2-1).

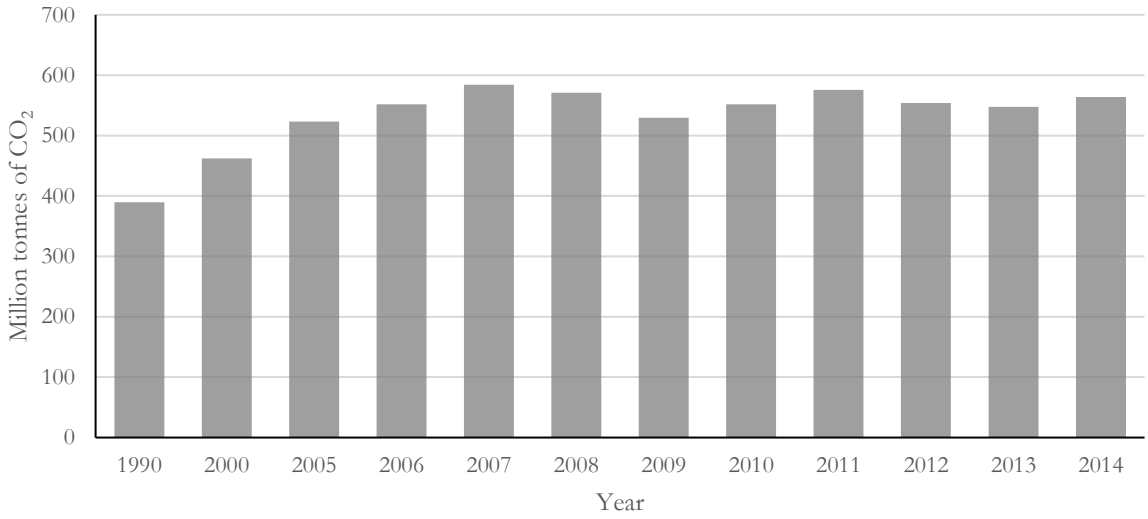

Figure 2-1: Total gross CO_2 emissions from cement production for all GNR participants (WBCSD-CSI, 2016).

Due to PC having a substantially larger emission factor (approximately 1 t CO_2e/t clinker) relative to concrete as a whole, even small reductions in the volume of clinker included in concrete will contribute to reducing CO_2e emissions (InEnergy, 2010). Furthermore, reduced clinker content would not only reduce GHG emissions directly but have a ripple effect in reducing those associated indirectly with clinker manufacture (e.g. transportation, fuels for heating and coal-burning power generation).

2.1.2 Current strategies for clinker substitution

Clinker content reduction has been the interest of global research for some time (Lothenbach *et al.*, 2011; Imbabi *et al.*, 2012; Proske *et al.*, 2014). The focus has primarily been on the partial replacement of clinker with inert (or relatively inert) filler materials and the use of supplementary cementitious materials (SCMs) that enable the formation of cementing compounds similar to clinker hydration products (calcium silicate hydrates (C-S-H)).

Despite some of the earliest use of fillers being reported in the USA in 1912 (due to economic constraints), their use in concrete was only standardised in the 1980s (John *et al.*, 2017). Subsequently, several national standards include the use of fillers and the South African national standard for cements, SANS 50197-1 (2013), which follows the European national standard, EN197-1 (2011), allows up to 35 % of limestone filler substitution. While this has the potential to allow large clinker replacement, filler contents in the range of 35 % are rarely reported and are usually substantially less (see § 2.1.3).

Pozzolanic and latent hydraulic SCMs are also commonly used as partial replacement materials in South Africa. Fly ash (FA), a by-product of coal-burning power generation, is the most commonly used pozzolanic SCM. Pozzolanic binders do not react with water but instead, after the hydration of clinker has progressed sufficiently, pozzolanic binders react with calcium hydroxide solution within concrete pores. The reaction products comprise calcium silicate and calcium aluminate compounds, similar to hydrated PC (Hewlett, 2004).

Common latent hydraulic SCMs are ground granulated blastfurnace and corex slag (GGBS and GGCS respectively), the latter more specific to the Western Cape. Latent hydraulic binders only react with water to form cementing compounds once they have been alkali activated (Hewlett, 2004). When used in a blend with PC, the hydration of clinker liberates calcium hydroxide which provides the necessary alkali activation of the latent hydraulic binder. Reactions following the alkali activation enable the formation of hydration products that are very similar to those of clinker, except for there being no liberation of calcium hydroxide (Grieve, 2009).

The replacement of clinker with SCMs have the potential to reduce CO_2e emissions associated with concrete while providing a use for by-products that would otherwise need to be disposed of. Furthermore, they have other associated benefits such as the refinement of concrete microstructure and potential ability to bind and prevent the ingress of deleterious ions.

SCMs are combined with PC either by inter-grinding during the cement manufacturing process or by blending the SCM with clinker after the grinding process, either by the cement manufacturer or by the user when making a concrete mix. The formation of blended cement by inter-grinding relatively soft SCMs with clinker has been found to result in the preferential grinding of the softer SCM relative to the harder clinker and increases the fineness of the eventual Portland-composite cement (Voglis *et al.*, 2005). However, this depends on the characteristics of the SCM being used. Alternatively, the separate milling of clinker and the SCM followed by blending ensure that the fineness of each material can be controlled as the fineness of each component material is independent of another.

Despite the standardisation of SCMs and relatively large allowable replacement of clinker in South African standards, on average, cement comprises only 20 % SCM and/or filler material and PC makes up the remaining component (Scrivener *et al.*, 2016). Concerning the future use of commonly-used clinker substitutes, limestone is the most abundant whereas suitable sources of GGBS and FA are less so and likely to be limited to only 15 -25 % of global cement consumption. In addition to these materials, more recent studies consider the combined use of calcined clays and fine limestone to achieve a relatively inexpensive, low CO_2 system (Juenger *et al.*, 2011). Such methodology makes use of widely available raw materials and has potential to replace up to 50 % of clinker while enabling equivalent performance to existing cements (Scrivener *et al.*, 2016).

The UNEP report on eco-efficient cements (Scrivener *et al.*, 2016) established two primary areas that have potential to enable significant reductions in GHGs associated with cement and concrete materials that do not require costly investment. These are the increased use of SCMs that have low associated GHGs as partial replacement for PC, and the more efficient use of PC. The first requires sustainable exploitation of existing SCMs and increasing use of and research into newly identified SCMs such as calcined clays and agricultural ashes. Proske *et al.* (2013) also reported that the largest reduction in GHGs could be achieved with the combined use of limestone and reactive SCMs. Specifically, they reported a reduction of 60 % of GWP with the use of GGBS and limestone relative to conventional concrete.

The second area identified requires the use of highly reactive cements (usually finer ground), particle packing optimisation and increased filler contents with the use of effective dispersants to increase PC efficiency (Scrivener *et al.*, 2016). This is largely due to an increase in the packing density (see § 2.3.1) of the particulate mixture and less water being required to fill interstitial space enabling the reduction of the water: cement ratio and less cement being required to achieve a desired strength. Figure 2-2 represents the case of PC particles (grey) dispersed in water in the presence of a larger (brown) particle. Surface forces govern PC packing density and cause smaller PC particles to adhere to the surface of larger particles as well as the formation of PC agglomerates. These phenomena cause the overall packing density to be low. Figure 2-3 represents the same scenario with the addition of an effective dispersant. Surface forces are temporarily nullified, breaking agglomerates and allowing particles to act as single entities, leading to a localised increase in the packing density. Figure 2-4 portrays the addition of a filler material to the scenario described in Figure 2-3. The filler material, with a wider particle size range than PC, fills interstitial space and further increases packing density. Scrivener *et al.* (2016) mentioned that the combination of these techniques with substantial water content reduction was expected to enable the current average limestone content of 7 % to be increased to 50 %, while still enabling adequate performance.

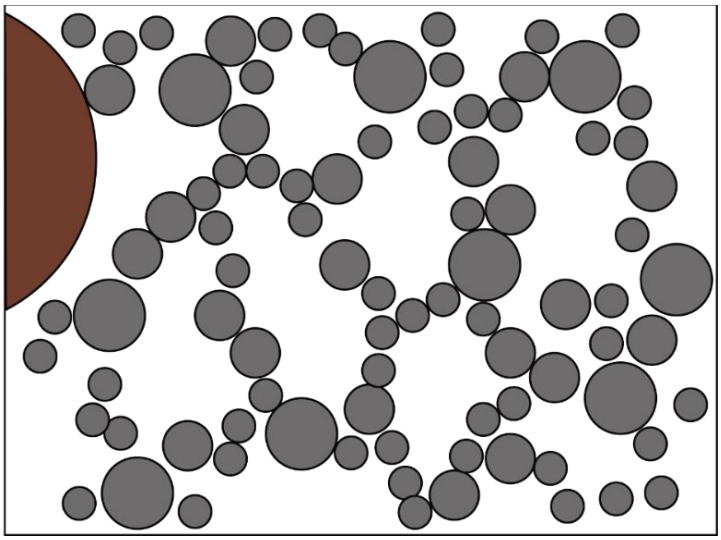

Figure 2-2: Surface forces govern PC packing in water. (PC particles – grey, larger aggregate particle – brown). Adapted from Proske *et al.* (2013).

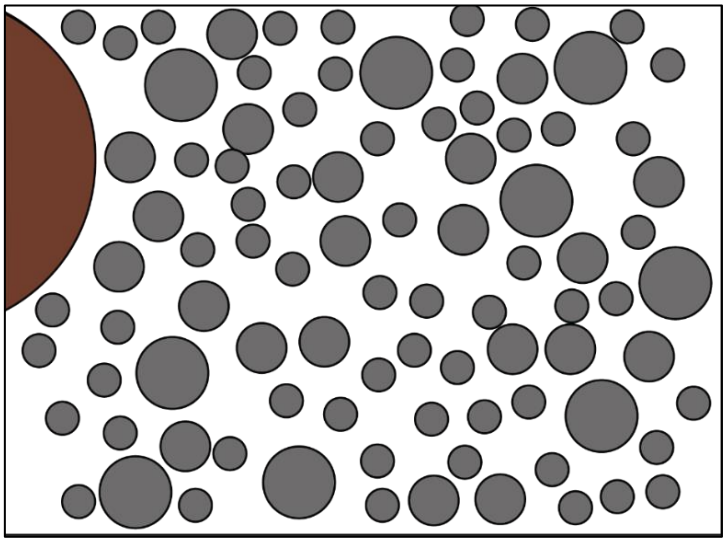

Figure 2-3: Surface forces nullified using a dispersant. Agglomerates are broken. Adapted from Proske *et al.* (2013).

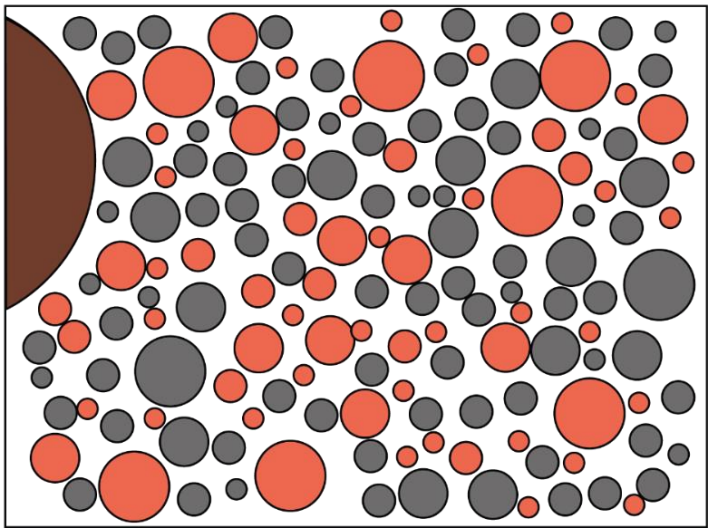

Figure 2-4: A filler material (orange) is added to the system in Figure 2-3. Packing density is increased. Adapted from Proske *et al.* (2013).

In addition to these strategies, other approaches of non-Portland cement clinkers have been proposed as alternative, longer-term solutions such as belite-ye'elimite-ferrite (BYF) clinkers, alkali activated binder technologies, concrete products produced by carbonation as opposed to hydration and the exploitation of abundant ultramafic rocks as an alternative raw material to limestone (Scrivener *et al.*, 2016). However, these latter strategies are not likely to offer effective alternatives to PC in the near future due to necessary further research and development, manufacturing processes being energy and/or capital intensive, or their application being limited to a niche markets and therefore not likely to have a significant impact on the global CO_2 footprint associated with PC (Scrivener *et al.*, 2016).

2.1.3 The extent to which SCMs have enabled clinker reduction

Although SCMs can replace a portion of clinker without detrimentally affecting concrete properties, often actually leading to an enhancement of the concrete microstructure (Juenger & Siddique, 2015), this method alone appears to be limited, considering the current average percentage replacement of clinker with these materials.

Despite some countries allowing relatively large filler and SCM contents, (see some of the maximum allowable replacement levels in Table 2-1 according to SANS 50197-1 (2013) and a global perspective of allowable limestone content according to various national standards in Figure 2-5) the GNR project (WBCSD-CSI, 2016) showed that, as a percentage of the total volume of cement produced, limestone filler accounted for 7 %, followed by GGBS at 5 %, FA at 3 %, pozzolana at 3 % and other materials 1 %.

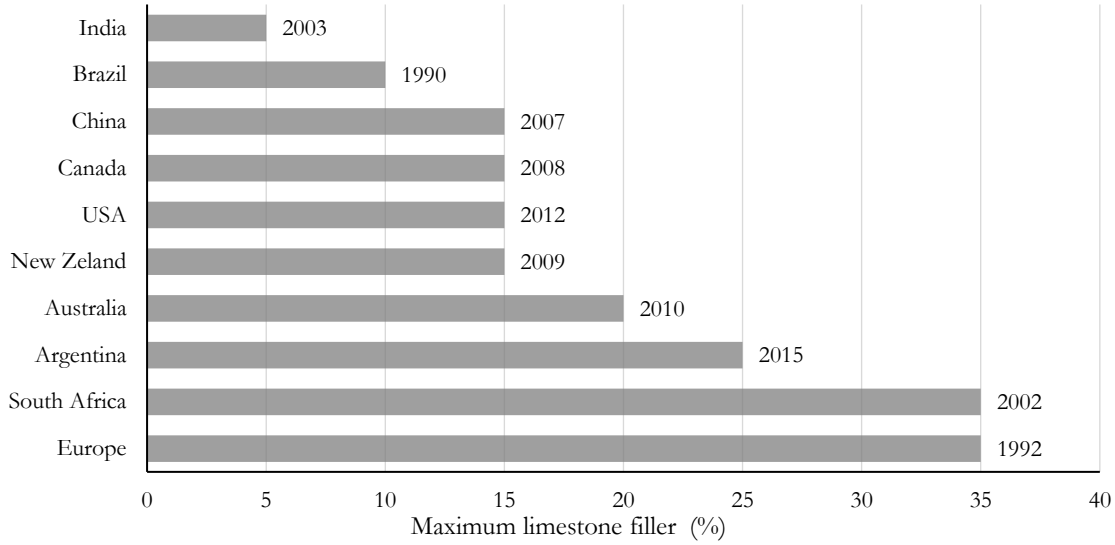

Figure 2-5: Maximum limestone filler (mass %) in standardised cements. The year of the first publication of the standard is shown alongside the data (John *et al.*, 2017)

The relatively low application of these large, allowable replacements (especially seen in the South African National Standard) is likely due to the dilution of clinker with increasing SCM replacement or relatively inert filler material. A lower concentration of clinker or reactive SCM, causes a lower rate (as well as absolute) increase in the solid volume of hydration products (John *et al.*, 2017). This in-turn leads to increased capillary porosity, decreasing strength and affecting durability properties adversely. This dilution effect can be partially compensated by using more reactive, high-fineness cements as well as fillers that are substantially finer than clinker. However, there exists a limit beyond which further dilution of clinker results, instead, in an increase in the environmental impact of the blended cement.

To assess the efficiency of the replacement of clinker with various SCMs, Damineli *et al.* (2010) developed the binder intensity index (bi) as a measure of the amount of reactive binder per cubic metre of concrete (kg/m^3) necessary to achieve 1 MPa of compressive strength. Damineli *et al.* (2010) showed that a binder intensity of approximately 5 kg/m^3 MPa^{-1} was feasible and has

been achieved for many concretes with compressive strength > 50 MPa. However, for concretes with lower strength grades, substantially higher binder intensity indexes were reported, in the range of 10 to 20 kg/m^3 MPa^{-1} (Figure 2-6). This was attributed to the specification of minimum cement content in national standards and shows that performance gains are possible (Damineli *et al.*, 2010)

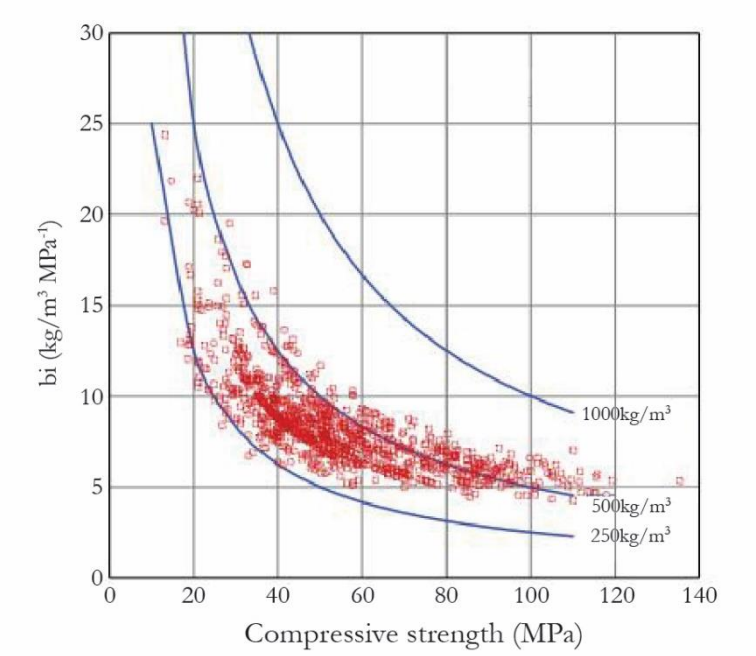

Figure 2-6: Data collected by Damineli *et al.* (2010) showing binder intensity index versus 28 day strength. Equipotential lines represent concretes with equivalent total binder quantities.

Considering the environmental impact at the exit gate of the cement manufacturer, dilution of clinker could be regarded as having reduced CO_2 and energy usage however this does not accurately represent the implications of using a cement with highly diluted clinker content. For example, when making concrete with the goal of obtaining a specified strength class using a low strength grade cement (e.g. 32.5 N containing high limestone content), a substantially higher cement content would be required to reach the specified strength relative to the use of a high strength grade cement (e.g. 52.5 N). Thereby, there would be an overall increase in the environmental impact of the concrete made using the cement containing high limestone content (John *et al.*, 2017).

Therefore, solely increasing SCM/filler content in cements cannot realistically reduce the environmental impact of concrete due to an increasing dilution effect with an increase in SCM/filler content. For increased clinker replacement, the dilution effect needs to be compensated and a possible solution is the reduction of water content in concrete (Fennis, 2011; Li & Kwan, 2013; Proske *et al.*, 2013; John *et al.*, 2017). Fundamentally, this requires an increase in the packing density of constituent materials to minimise interparticle void space needing to be filled with water. Increasing packing density is not a new development but has been of research interest for some time, one of the earliest recorded cases being that by Fuller and Thompson (1907). However, with increased packing density of constituent materials, greater internal friction is introduced into the system, creating potential problems for ensuring workable concrete.

Table 2-1: Composition of standardised blended cements after SANS 50197-1 (2013)

Cement Type	Notation of product		Composition by percentage mass								
						Pozzolana		Fly ash			
			Clinker	Blastfurnace slag	Silica fume	Natural	Natural Calcined	Siliceous	Calcareous	Limestone	Minor additional constituents
CEM II	Portland-Limestone cement	CEM II A – L	80 – 94	-	-	-	-	-	-	6 – 20	0 – 5
		CEM II B - L	65 – 79	-	-	-	-	-	-	21 – 35	0 – 5
CEM III	Blastfurnace cement	CEM II A	35 – 64	36 – 65	-	-	-	-	-	-	0 – 5
		CEM III B	20 – 34	66 – 80	-	-	-	-	-	-	0 – 5
		CEM III C	5 – 19	81 – 95	-	-	-	-	-	-	0 – 5
CEM IV	Pozzolanic cement	CEM IV A	65 – 89	-	<---------- 11 – 35 ---------->					-	0 – 5
		CEM IV B	45 – 64	-	<---------- 36 – 55 ---------->					-	0 – 5
CEM V	Composite cement	CEM V A	40 – 64	18 – 30	-	<----------18 – 30 ---------->			-	-	0 – 5
		CEM V B	20 - 39	31 – 50	-	<----------31 – 50 ---------->			-	-	0 – 5

This calls for careful optimisation of the particle structure to achieve a balance between increased packing density and necessary workability. Consideration must be given to individual constituent material properties as well as how all material constituents interact/perform together. This should involve investigation into the water demand of constituent materials, the factors affecting this such as exposed surface area, particle shape and surface morphology as well as the mechanisms influencing the packing of particles similar to those influencing water demand. Furthermore, absolute particle size and particle size distribution, surface force effects and the influence of applied compaction energy must be considered.

2.1.4 Low-clinker concrete properties

SCMs and fillers have not always been used with the primary intention of decreasing GHGs associated with concrete manufacture. These materials are also used to achieve the particular concrete properties that they enable when blended with PC. When sufficient portions of clinker and SCM/filler are combined, the resulting synergistic behaviour is usually one which benefits concrete properties relative to using pure PC (Thomas, 2007).

The following section discusses concrete properties resulting from the partial replacement of PC with SCMs. Brief consideration is given to SCMs commonly used in the Western Cape and focus is given to the use of limestone filler and its synergistic use with common reactive SCMs as its abundance has been acknowledged (Scrivener *et al.*, 2016). The use of limestone filler is of particular interest for this research to assess its ability to increase powder phase packing density. Detailed reviews of concrete properties resulting from the replacement of clinker with common, as well as less common, SCMs have been given by Siddique & Khan (2011), Ramezanianpour (2014) and Juenger *et al.* (2011).

Aside from the inherent properties associated with the composition of various SCMs and fillers, it is important to consider the varying manufacturing processes, purity of the material as well as whether the material was inter-ground, blended or added when mixing concrete constituents to be able to fully assess the way in which the SCM/filler affects concrete properties (Lollini *et al.*, 2014; Ramezanianpour, 2014).

2.1.4.1 Fresh concrete properties

Common SCMs tend to be of similar or higher fineness than plain PC and for the case of inter-ground limestone, the softer limestone is usually preferentially ground over clinker, giving it a higher fineness. With a decrease in particle size there is an increase in wettable surface area and the potential to increase the water demand of a mixture as well as cause the formation of agglomerates. Agglomerates cause local high porosity, trapping excess water and negatively impact workability (Juenger & Siddique, 2015).

Of the common reactive SCMs, the inclusion of GGCS has in instances been found to improve workability to a small degree, however improved workability due to the inclusion of FA is significantly more pronounced (Grieve, 2009). The spherical particle shape of FA creates a ball bearing effect, allowing material particles to pass one another with less friction.

To counteract increasing water demand, water-reducing admixtures are applied so as not to affect water: cement ratios (w/c). However, increasing replacement ratios demand lower w/c ratios and lower water contents to maintain hardened concrete properties. Therefore, larger quantities

of superplasticiser (SP) are required. It is important to ensure the compatibility of admixtures with SCMs due to reports of diminishing effectiveness, particularly with the use of natural pozzolana (Juenger & Siddique, 2015).

Concerning the use of limestone as a replacement material, Ramezanianpour (2014) reported existing literature to present contradictory findings concerning the effects on fresh concrete properties. Some reported increased workability yet others reported this to be dependent on the fineness and replacement level of limestone while others noted no significant effects for limestone replacements up to 12 % (Mohammadi & South, 2016). Explanations offered concerned the range of the particle size distribution of limestone. High water demands were expected for narrowly distributed materials whereas wider distributions were thought to have lower water demands. Furthermore, the influence of limestone on water demand was also inferred to depend on the size distribution of PC to which the limestone was added.

Proske *et al.* (2014) made concrete with high-volume limestone replacements (up 65 % mass of powders) and were able to maintain workability similar to reference 40 MPa mixes with PC content as low as 150 kg/m^3 and water content in the range of 145 l/m^3. On reducing the cement content, they maintained a set powder content (material sub 125 μm) of 440 kg/m^3 to ensure fluidity of the mix and incorporated FA as a reactive SCM (likely to have benefited workability due to its spherical shape). SP dosage also had to be increased to a maximum dosage of 6.9 kg/m^3 versus a maximum dosage of 3 kg/m^3 for the reference mixes.

Proske *et al.* (2014) mention that a sharp decrease in water content required careful optimisation of the particle size distribution and packing of particles less than 125 μm. A portion of two 'ordinary' fineness limestones used (Blaine values of 5000 cm^2/g and 3100 cm^2/g) was replaced by a finer limestone (Blaine value of 16000 cm^2/g) resulting in a significant decrease in the viscosity of the mix. The effects on the viscosity by the substitution of ordinary fineness limestone with the finer limestone could be related to the expulsion of excess water from interstitial space, allowing excess water to be used for lubrication of particle movement.

2.1.4.2 Early age concrete properties

Besides the varying reactivity of SCMs having the potential to produce cementing products given the correct chemical composition and environment, they have long been known to influence the hydration of clinker, and therefore fresh and hardened concrete properties, by their physical presence, which has been termed the 'filler' effect. Principal factors controlling the filler effect are the replacement level and fineness of the SCM. Berodier & Scrivener (2014) address two mechanisms describing the effect. The first entails the dilution of cement particles by SCM and results in more space being available for the formation of clinker hydration products. The second is the nucleation of C-S-H on the filler surface, causing an increased hydration rate. Both are acknowledged by several other authors (Voglis *et al.*, 2005; De Weerdt *et al.*, 2011; Kumar *et al.*, 2013; Juenger & Siddique, 2015; Moon *et al.*, 2017).

Monitoring hydration heat using isothermal calorimetry, Berodier & Scrivener (2014) analysed the filler effect of four different materials, namely, quartz, slag, fly ash and limestone. They found that, there exists a direct link between the acceleration slope leading up to the peak of the heat of hydration and density of C-S-H nucleation and that there is little or no effect on the growth rate of C-S-H. Limestone had the greatest density of C-S-H nuclei on its surfaces and

therefore a larger accelerating effect on hydration. The authors attributed this to the partial dissolution of calcium carbonate or the provision of a favourable surface structure providing a template for C-S-H precipitation (Berodier & Scrivener, 2014). Juenger & Siddique (2015) report work by Antoni *et al.* who observed an increased presence of portlandite ($Ca(OH)_2$) in cement pastes using quartz as an inert filler. This implied an increase in the degree of the hydration of PC and represented the filler effect.

Although limestone filler was originally thought to be an inert filler material which only enhanced the hydration of clinker, calcium carbonate is now known to react in the presence of available aluminates (De Weerdt *et al.*, 2011; Juenger & Siddique, 2015). Its reaction results in the creation of further hydration products and therefore limestone substitution of up to 10 % has been reported to not detrimentally affect concrete strength, and lower replacements of approximately 5 % have been reported to enhance properties relative to pure PC mixtures (Scrivener *et al.*, 2016). Larger replacements, in the range of 15 to 25 %, are reportedly possible without detrimentally affecting concrete strength if clinker reactivity is increased by grinding it to a higher fineness (Ramezanianpour, 2014). Contrarily, the use of pozzolanic SCMs generally decrease early age strength due to the dilution of PC and the delayed onset of their reaction. This has been compensated for by including small limestone replacements to enhance hydration at an early age, such as 5 % limestone with 10 % metakaolin (Juenger & Siddique, 2015) where compressive strength was higher than a reference mixture at both early and later ages.

GGBS, despite being a reactive SCM, may retard setting, the extent being dependent on the % PC replacement. However, comparatively, GGCS was found to have higher CaO, Al_2O_3 and MgO concentrations, indicating that it should have higher hydraulic activity than GGBS that is of equivalent fineness. This should lead to a more rapid reaction than the conventional GGBS, reducing the extent of retardation (Alexander *et al.*, 2003). The reaction of FA relies on the presence of PC hydration products ($Ca(OH)_2$) and therefore, it too increases setting time with increasing PC replacement. As a result, both SCMs can lower the heat of hydration which is beneficial for certain applications (Grieve, 2009).

De Weerdt *et al.* (2011) qualitatively assessed hydration products using X-ray diffraction (XRD) and, after 1 day, found similar hydration products in all mortar mixes under consideration (plain PC, PC and FA, PC and Limestone, and ternary blends of PC, FA and Limestone). At later ages, 28 days onwards, they found ettringite, calcium monocarboaluminate and calcium hemicarbonate hydrate in mixtures containing limestone. In the absence of limestone, however, only calcium monosulphate hydrate and ettringite were observed.

De Weerdt *et al.* (2011) attributed the consumption of calcium hydroxide (CH) associated with the minor replacement of PC with limestone (5 %) to the formation of hemicarbonate where PC supplied the calcium required for the reaction. However, the effect of a minor addition of limestone was more pronounced for their ternary mixtures containing PC, FA and limestone. Aluminates are liberated during the dissolution of FA and cause the sulphate/aluminate ratio to be decreased. Sulphate depletion causes more ettringite to decompose and react with additional aluminates to form calcium monosulphoaluminate hydrate. The presence of limestone in this environment has a stabilising effect as it reacts with the additional aluminates provided by FA, forming calcium monocarboaluminate hydrates. The combination of these reactions results in increased ettringite, more chemically bound water and a larger volume of hydrates, causing

decreased porosity and therefore increased strength (De Weerdt *et al.*, 2011). Similarly, Bentz *et al.* (2012) reported synergistic behaviour due to the filler effect with the inclusion of limestone in high volume FA cements to counter delayed setting time and low early age mechanical properties. Subsequently, ternary blends comprising GGBS, limestone and PC resulted in the production of hemicarboaluminate and the use of metakaolin in place of GGBS in the same ternary blend led to the formation of hemicarboaluminate and mono carboaluminate (Juenger & Siddique, 2015).

2.1.4.3 Later age concrete properties

Compressive strength

Increasing the replacement of PC with materials offering little or no cementing capacity, keeping all other parameters the same, results in detrimental effects to compressive strength due to increased dilution of the clinker and increased spanning distance of C-S-H. Considering total binder content to include limestone and PC, with increasing limestone replacement and maintenance of a water: binder ratio (w/b) at 0.5, De Weerdt *et al.* (2011) reported a decrease in compressive strength at all ages. Their investigation did not explicitly involve powder material optimisation although they offered reasoning for the selection of the fineness of FA and limestone filler based on previous investigations into effective particle size distributions (De Weerdt *et al.*, 2011). However, they did mention that limestone replacements may have had a more beneficial effect at lower w/b ratios. Although the inclusion of FA and GGCS also tend to cause low early age strengths, their slower strength development causes the formation of a refined concrete microstructure and therefore tend to enable increased later age compressive strength relative to conventional concretes (Grieve, 2009).

De Weerdt *et al.* (2011) also analysed mixtures with FA as a replacement and later, ternary blends with FA and limestone, and found FA-only replacements up to 15 % still obtained similar compressive strength to 100 % PC mixtures at an early age (1 day). Higher replacement led to decreased early age strength but, by 90 and 140 days, strengths were equivalent to the reference mixture.

Proske *et al.* (2014) achieved similar compressive strength to 40 MPa reference concrete (with PC content between 240 and 270 kg/m^3) using high limestone replacement as well as ternary blends of limestone and FA, such that PC content was reduced to 150 kg/m^3. This was primarily enabled by a substantial decrease in the water content but required further modifications so not to affect fresh concrete properties (§ 2.1.4.1). Proske *et al.* (2014) also found the replacement of a portion of the two ordinary fineness limestones with a finer limestone increased compressive strength relative to the reference mixture and attributed this to increased homogeneity of the microstructure and improved interfacial transition zones. Moon *et al.* (2017) reported similar findings regarding the effects of limestone fineness but also found compressive strength to be more sensitive to clinker fineness than that of limestone.

Müller *et al.* (2014) blended quartz powder of varying fineness with CEM I, using the combined input from the Compaction Interaction Packing Model (CIPM) and the Modified Andreasen and Andersen Curve (MAAC) (discussed further in § 2.4.1 and 2.4.2 respectively). For PC contents of 113 and 109 kg/m^3 28 day compressive strength was 41 and 20 MPa respectively (the former having a water: cement ratio of 0.691 and the latter, 1.049). Binder intensity indices (see § 2.1.3) for these mixes were 2.75 and 5.45 kg /m^3 MPa^{-1} respectively, showing the possibility

for increased binder efficiency when effectively proportioned materials are used in conjunction with reduced water content.

Transport properties

The increased fineness of SCMs and their consumption of $Ca(OH)_2$ to produce dense C-S-H has resulted in improved pore structure, reducing permeability and sorptivity. Slowed strength development with the use of GGCS aids in the refinement of concrete pore structure, reducing permeability. Furthermore, its chemical composition enables the binding of chlorides, increasing resistance against chloride ingress. The use of FA also leads to reduced concrete permeability as well as offers protection against alkali silica reaction and improved sulphate resistance (Grieve, 2009). Regarding newer SCMs, Juenger & Siddique, (2015) found that the replacement of up to 10 % of PC with metakaolin could reduce concrete porosity but replacement in excess thereof resulted in increased porosity.

Lollini *et al.* (2014) quote previous findings regarding the carbonation resistance of Portland-limestone concretes where it was found that carbonation rates increased relative to PC concretes at the same water binder ratio but that carbonation resistance of concretes of equivalent strength was similar. However, Tsivilis *et al.* (2002) made limestone replacements up to 35 % that were inter-ground with clinker and achieved equivalent carbonation resistance.

There have been reports of increased and decreased resistance to chloride ingress in concretes containing limestone replacements. Increased resistance was attributed to the filler effect whereas decreased resistance was thought to be due to the reaction of limestone and aluminates forming compounds which have lower chloride binding capacity than aluminates in PC. Negligible differences in the resistance to chloride ingress were reported for replacements of up to 15 % by other authors (Lollini *et al.*, 2014).

Ramezanianpour (2014) reported general findings for Portland-limestone cements whereby the nucleation effect of fine limestone refined the concrete pore structure, reducing inter-connectivity of pores, resulting in reduced permeability. However, cases of increased gas permeability despite decreased sorptivity were also reported. This was attributed to changes in the total volume and distribution of pores due to the filler and dilution effects characteristic of limestone cements. Lollini *et al.* (2014) acknowledged that results concerning the effects of limestone replacement on gas, water and oxygen permeability from various studies are controversial and appear to lack any kind of trend. Lollini *et al.* (2014) constructed mixtures with 15 and 30 % limestone replacement, using PC and limestone (of similar median particle size (7,5 μm) to PC but with coarser maximum particle size) and, for the 15 % replacements, reported reduced compressive strength and resistance to chloride ingress but inconclusive results regarding resistance to carbonation. For 30 % replacement, they reported a worsening of all the above-mentioned properties.

Drying shrinkage

Dhir *et al.* (2007) reported reductions in shrinkage as limestone replacement increased up to 45 %. Mohammadi & South (2016) makes reference to other investigations confirming similar findings as does Bentz *et al.* (2009) for the replacement of limestone up to 10 %. Reasoning offered was that increased dilution of clinker by limestone resulted in decreased C-S-H gel and overall decreased volume of water contained within gel pores. Therefore, as the removal of this water

accounts for substantial drying shrinkage strains (Alexander & Beushausen, 2009), a decrease in its volume results in decreased drying shrinkage.

Mohammadi & South (2016) noted minor increases (3.6 %) in the drying shrinkage of their 12 % limestone mixtures relative to control mixtures containing 5 % limestone. As the absolute drying shrinkage was significantly below Australian allowable limits, they concluded that the increase was negligible. Palm *et al.* (2016) found shrinkage of 50 % limestone replacement mixtures to be highly dependent on the quality of limestone used. Shrinkage strains at 112 days for a mixture using 98 % $CaCO_3$ limestone had comparable shrinkage to a reference mixture containing no limestone. However, mixtures using another limestone (74 % $CaCO_3$) gave shrinkage strains that were 40 and 65 % greater than reference mixtures using CEM II A-LL with w/c = 0.50 and 0.60 respectively. The lower purity limestone had a presence of clay minerals, likely responsible for increased drying shrinkage (Palm *et al.*, 2016). The authors described the potential mechanism causing increased shrinkage to comprise of the initial swelling of the clay in the presence of water, followed by the drying of the microstructure where the clay particles have the tendency to attract each other and lead to increased shrinkage.

2.2 Existing concrete mix design methodologies

Globally, mix design processes vary and can be attributed to variations in locally available materials (Alexander & Mindess, 2005). The South African approach, namely the 'C&CI Method of Mix Design' (Addis and Goodman, 2009) is based on ACI 211.1-91(2002) but has been adapted for local application. Concerning the selection of aggregate quantities, the method broadly makes two assumptions:

- The water requirement for a given combination of materials and consistence (slump) is relatively constant regardless of the cement content
- For a given mixture of materials, there exists an optimum stone content which is dependent on size, shape and compacted bulk density of the stone, fineness modulus of the sand and the required consistence of the concrete

Water requirement and optimum stone content are therefore functions of the aggregate properties, maximum stone size and consistence (Alexander & Mindess, 2005). The method allows the use of various binder materials but only covers conventional concretes (as opposed to making consideration for the design of high performance concretes (HPC)). Constituent quantities are calculated on a mass basis with the requirement that the sum of the absolute volume of constituents equates to the total volume of concrete.

The C&CI method has been specifically formulated to suit common South African practise, which usually involves the use of crushed aggregates and gap-graded mixtures (Alexander & Mindess, 2005). Particle shapes resulting from crushing are often angular and potentially flaky, depending on the crushing processes and nature of the parent rock. The implementation of gap-graded mixtures thereby aims to reduce internal friction due to aggregate interlock by angular particles and enable sufficiently workable mixtures.

This method differs from other methods such as those used in the United Kingdom (UK) and North America (ACI) where common practise has been the use of natural aggregates in continuously-graded mixtures (although both standards do account for the potential use of

crushed aggregates). Natural aggregates tend to be smoother and have better, rounded particle shapes from attrition. Thereby, this allows them to be used in continuously graded mixtures without detrimentally affecting workability.

All methods account for the fineness of fine aggregate, either by the fineness modulus (C&CI and ACI) or by the proportion of material finer than 600 μm (UK), as well as the maximum size of the coarse aggregate. Only the C&CI method qualitatively considers characteristics of the fine aggregate separately from the stone, allowing an increase/decrease of water content based on the subjective assessment of fine aggregate quality. ACI acknowledges the effect of fine aggregate properties on workability but does not account for this explicitly (Alexander & Mindess, 2005).

The ACI method considers coarse aggregate properties indirectly by measuring the dry-rodded bulk density and the C&CI method does so by measuring the compacted bulk density of the stone. However, the UK method only indirectly accounts for the shape of the coarse aggregate by adjustments to the water content based on whether the aggregate is crushed or uncrushed. Despite some differences, Alexander & Mindess (2005) showed that these three mix designs methods tend to approximately the same outcome and concluded that, "no one method is 'better' than another, but may be more suitable with certain types of materials." (Alexander & Mindess, 2005: 219)

Therefore, when it comes to optimising concrete powder phases, existing methodologies for conventional concretes fail to explicitly account for the characteristics of these materials and how they interact and pack together. The design process is usually one which seeks to achieve the overall economy of a mix. Furthermore, important properties influencing aggregate packing in a concrete mix such as particle shape, texture and grading are only implicitly considered in existing methods by ensuring that materials fall within certain permissible limits, such as those specified in SANS 1083 (2006). If the powder phases of concrete are to be optimised, more specific consideration needs to be given to the factors influencing their interactions and ability to pack together.

2.3 Particle packing optimisation

Particle packing optimisation in the past has focused on enhancing the economy of concrete or achieving high density and strength, and it is now of interest to reduce concrete's environmental impact. However, in each of these cases, the term 'optimisation' would have had different implications. It is therefore important to define the inferences of the term 'optimisation' in the context of this research. It is impossible to optimise all concrete properties simultaneously as it is almost always the case that the optimisation of one property leads to the detriment of another.

Optimising the packing of particulate materials usually refers to the maximisation of packing density (portrayed in *Eqn. 2-1* with V_p and V_b representing the solid volume and bulk volume of the particles respectively). However, this invariably results in a particle mixture having decreased mobility due to increased internal friction, and in the case of concrete, cause workability to be detrimentally affected.

$$\alpha = \frac{V_p}{V_b} \qquad \textit{Eqn. 2-1}$$

It is important not to neglect the effect of the optimisation of a single property on the remaining concrete properties due to the implication that an entire range of concrete properties need to meet minimum specification to ensure the practicality of the material (e.g. efficient mixing, placing, compaction and finishing). Therefore, optimisation of the packing of particulate materials within the context of this research implies the maximisation of packing density to an extent that fresh concrete properties are not adversely affected.

2.3.1 Packing density

The packing density of a particulate mixture is defined as the solid volume of particulate material in a unit total volume (de Larrard, 1999). Packing density is of concern for composite materials, like concrete, where the aim is to combine granular materials in such a way that porosity (void space) can be minimised to benefit mechanical properties and improve impenetrability.

The packing density of a material is not an intrinsic property of the material but, is reliant on several influencing factors. De Larrard (1999) defines three main factors influencing packing density of a poly-disperse granular mixture:

- The size of the particulate material (most commonly described by a grading curve)
- The shape of the particles
- The method of processing the packing (i.e. the energy imparted to the particulate mixture)

Furthermore, chemical and mineralogical properties influence particle morphological properties and thereby influence packing density through particle surface texture. Therefore, the origin and composition of particulate materials have an indirect but significant effect on packing density (Fennis, 2010).

Experimentally, it is very difficult to separate and determine the extent to which each of these factors influence the resulting packing density. It is therefore important to acknowledge the influence of these factors but also arrive at a simplified, engineering solution which can indirectly account for these influences but might not accurately describe each of them. This is especially the case for the inclusion of such knowledge into the concrete mix design process.

2.3.2 Particulate material properties

2.3.2.1 Size and particle size distribution

The absolute size of a particle within a particulate mixture does not have a significant influence on the packing density achievable when considering the case of coarse particulate materials. Yet, with decreasing particle size, below approximately 125 μm, packing density decreases due to the large surface area relative to the solid volume of material, lower particle mass and increasing influence of surface forces (Fennis, 2011).

Packing density is usually increased when the void space between larger particles is filled by smaller particles and therefore, the packing density of a mixture of particles that is approximately uniformly distributed will be increased if the range of particle sizes is increased. The introduction of larger particles to a uniform distribution of particles will always increase the packing density of the mixture. This is due to the bulk volume that was previously occupied by small particles (with significant interstitial space between particles) becoming completely occupied by the solid volume

of the large particle, eliminating previously existing interstitial space. However, the addition of smaller particles to a uniform distribution of particles can either increase or decrease the packing density (Fennis, 2011).

A wider particle size distribution does not necessarily guarantee better packing of particles. The proportion of various particle size classes within a distribution is more important as an excessive proportion of one size class can detrimentally affect the packing density of the overall mixture (e.g. excessive small particles push large particles apart, Figure 2-7). Continuously graded mixtures (a particle distribution where there are particles representing all size classes between absolute minimum and maximum particle sizes) tend to enable void space between particles to be reduced. However, this also has the implication of increasing the number of contact points within a mix, increasing internal friction and commonly, decreasing concrete workability.

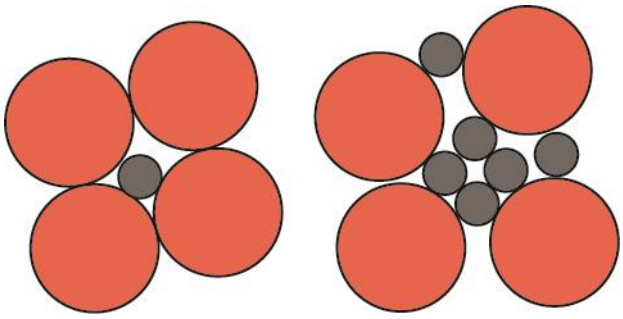

Figure 2-7: Packing of larger particles to maximum packing density (left). Packing of larger particles negatively impacted by presence of excess small particles (right) (Adapted from Fennis, 2011)

The influence of particle size distribution, or any particulate material property, on packing density and overall concrete properties cannot be considered in isolation of other properties. Continuously graded mixtures comprising particles with spherical shape and smooth surface texture should enable a more workable mix compared to the same grading comprising low sphericity, angular particles. To make use of more angular particles, such as common South African coarse aggregates produced by crushing bulk rock, gap-grading was implemented (Alexander & Mindess, 2005; Grieve, 2009). This entails omitting one or more size class within a particle size distribution to prevent excessive particle interlock and reduce internal friction.

For fine and coarse aggregate materials, particle size distribution can be assessed through sieve analysis (SANS 201, 2008). Materials passing the last standard sized sieve (75µm) are usually assessed by laser diffraction techniques, such as those used in (Van Der Putten *et al.*, 2017), which require the refractive index of the material to be known and involves post-processing of experimental data using theoretical models to interpret particle size distribution results.

2.3.2.2 Particle shape

When considering particle shape, it is not only the basic particle shape that is of interest but rather the assessment of angularity and flakiness among other characteristics. Alexander & Mindess, (2005) identify three geometric properties for the global description of particle shape: 'sphericity', 'roundness' and 'form'. 'Sphericity' distinguishes the degree to which the particle approaches a spherical shape whereas 'roundness' refers to the sharpness of the edges of the particle (see Figure

2-8). 'Form' describes the dimension of the particle in each of the 3 dimensions (Alexander & Mindess, 2005) and is usually denoted by a form or shape factor. Particle shape is dependent on the source and nature of the particulate material as well as the efficacy of the crushing or other manufacturing process. For example, crushed aggregates may vary from being cubical and sub-angular to flat and elongated, flaky particles, the latter usually being the result of the parent rock being characterised by natural bedding planes.

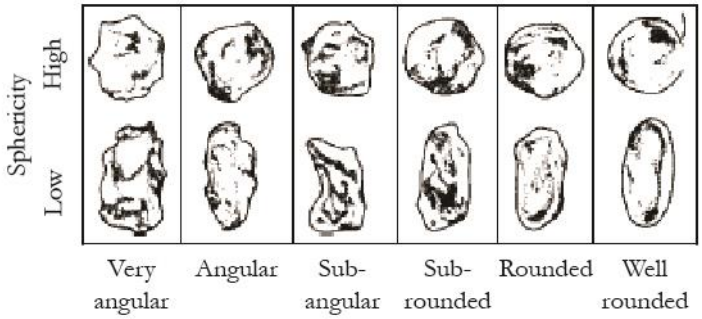

Figure 2-8: Guide for the visual assessment of particle shape from Alexander & Mindess (2005)

Concerning the modelling of particle packing, particulate materials are often idealised as spherical particles and therefore, the further from spherical particles that the real particles are, the less representative the packing models become and the more complex it becomes to account for irregular particle shapes. Ideally, to reduce internal friction, particles of high sphericity and roundness are preferred. Particles of this form lead to higher packing densities and are desirable for their beneficial influences on workability and potential to decrease the overall water requirement of concrete.

Particle shape is usually assessed using geometric ratios or other indirect measures such as the measurement of bulk density and void content (Alexander & Mindess, 2005). However, its assessment is more difficult as particle size decreases, especially towards the range of powder material particles less than 125 μm, where particle shape is more commonly assessed subjectively using microscopic imaging techniques. However, particle shape analysis and modelling is also possible using 3D imaging techniques (Erdogan *et al.*, 2006; Latham *et al.*, 2008; Majidi *et al.*, 2015).

2.3.2.3 Surface texture

Surface texture is of importance when investigating how particles pack because, as with particle shape, surface texture influences internal friction and the ease and degree to which particles can pack together. Surface texture is dependent on the inherent properties of the parent materials such as hardness, grain size, pore structure and texture but also, to a large degree, on the extent of abrasion or attrition that may have caused the surface to become smoothed or roughened (Alexander & Mindess, 2005).

The surface texture of particulate concrete materials is usually assessed by subjective means, describing the surface as either 'rough' or 'smooth' and offering various degrees of 'roughness' between these two extremes. Two geometric properties of interest when describing surface texture are the degree of surface relief and the amount of actual surface area per unit of plane projected

area (Alexander & Mindess, 2005). However, practically, it is more common to compare the surface texture of a new material with reference to materials of a known source (Alexander & Mindess, 2005). For concrete materials derived from crushing bulk, parent material (such as coarse and fine aggregates and limestone filler), another important factor influencing surface texture, again similarly to particle shape, is the crushing process to reduce the parent material to the final product. Invariably, crushed materials fracture with surface textures particular to their composition and mineralogy (Alexander & Mindess, 2005).

2.3.3 Particle interactions

Interactions influencing the way in which concrete particulate materials pack together can be divided into two broad categories: those of geometric interaction and those due to interparticle forces (which only significantly impact the interaction of powder materials below 125μm (Kwan & Fung, 2009; Fennis, 2011; Knop & Peled, 2016). However, these two forms of interaction cannot be considered independent from one another because concrete materials comprise an entire range of particle sizes from a few microns (the packing of which is most significantly influenced by surface forces but is also dependent on the geometric characteristics of the particle) to tens of millimetres (the packing of which is usually governed by a combination of gravitational and shear forces, dependent on geometric characteristics). In addition, particle interactions are further influenced by the degree of compaction effort applied, water content and the use of dispersant admixtures.

Two different geometric particle interactions that have become widely acknowledged are defined as 'wall' and 'loosening' effects (Stovall *et al.*, 1986; de Larrard, 1999; Fennis, 2011). The wall effect is the result of larger particles preventing surrounding smaller particles from packing to the degree to which they could have packed had the larger particle not been present (Figure 2-9). This results in the porosity at the surface of the larger particles being higher compared to a bulk section of the particle mixture. This effect can extend from the surface of the large particle to a distance of 5 diameters of the smaller particles and is one of the causes of the formation of the interfacial transition zone (ITZ) in concrete (Alexander & Mindess, 2005). The loosening effect is due to the presence of relatively small particles that are too large to fit within the interstices of larger particles (Figure 2-9) and therefore prevent them from packing to the degree to which they might have, had the smaller particles not been present.

For coarse and fine aggregates, increased compaction effort usually leads to an increase in the packing density of the particulate structure. For example, applying vibration leads to the movement of particles relative to one another (as particles overcome the shear stress holding them in place within the particle structure) and can enable the opening of void space, allowing appropriately sized particles to fall under gravity into the created space, increasing the packing density. However, if an additional compressive load is applied to the particle structure, the ability for the particles to overcome shear stresses and pack to higher packing density will be increased (Fennis, 2011).

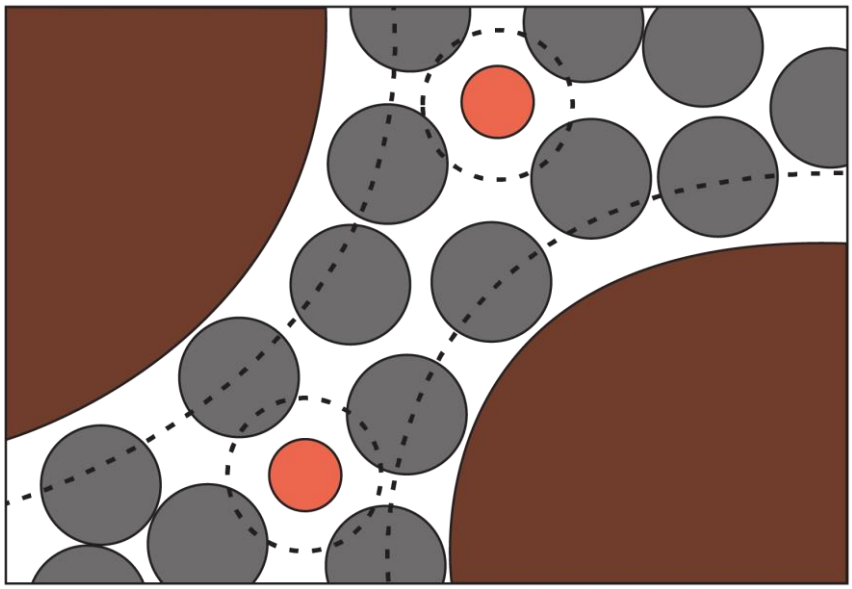

Figure 2-9: Large (brown) particles inducing a wall effect and small (orange) particles inducing a loosening effect on respective smaller and larger particles (adapted from de Larrard (1999))

However, as particle size decreases, there is a vast increase in the surface area to volume ratio and the influence of gravitational and shear forces on packing is substantially reduced. Instead, interparticle forces begin to govern their interactions (Fennis, 2011). Concerning powder material packing, interparticle forces are the attractive Van der Waals's forces and repulsive electric double layer and steric forces (Fennis, 2011). Van der Waal's forces are the result of the interaction of atomic and molecular dipoles causing attractive interparticle forces between particles of the same material composition. Electric double layer repulsion results from electrostatically charged particles being in the presence of a polar fluid (comprising ions in solution). The charged particle surface attracts ions of the opposite charge and will repel particles which have an equivalent charge (Holdich, 2002). Steric repulsion occurs due to the adsorption of a polymer to the surface of a small particle and has been used as a mechanism to disperse powder particles. Depending on the thickness of the adsorbed layer, the polymer can enable the full or partial stabilisation of small particles, preventing them from agglomerating (Fennis, 2011).

2.4 Particle packing modelling

There has been longstanding research interest concerning particulate material packing both within the field of concrete technology as well as others such as ceramics (Funk & Dinger, 1994). This interest has resulted in the investigation of PSDs to achieve dense packing, minimum porosity, pore size distributions and permeability and the material properties which these factors influence.

Initially, in the field of concrete technology, research focus was on the packing of fine and coarse aggregate materials. This was primarily to reduce the void space between aggregate materials to reduce the cement paste volume required to fill interstitial space. This allowed increased economy of a mix and would also contribute to reducing capillary sized voids and their interconnectivity to enhance technical properties (Alexander & Mindess, 2005).

Some of the earliest investigations led to the proposal of 'ideal' grading curves that could be used to construct aggregate material proportions to give maximum packing density. Although it was eventually found that there exists no ideal grading curve suitable across all possible material combinations, grading envelopes are still incorporated in some common mix design procedures (North America, United Kingdom and South Africa) to ensure the provision of nominally sized aggregates that are relatively consistent from one batch to another (Alexander & Mindess, 2005).

This section discusses packing theories and models that have been developed for the prediction of the packing ability of particulate materials. An overview of historical packing theories is given, and commentary is offered primarily on the appropriateness of various theories for application to optimising the packing of powder materials.

Particle packing theories can be divided into two primary categories, as proposed by Funk & Dinger (1994):

- Monodisperse: where all particles are of the same size
- Polydisperse: where particles cover an entire range of sizes. Polydisperse systems can be further divided into two subclasses:
    - The packing of several discretely sized particles
    - The packing of continuous PSDs where all particle sizes between a maximum and minimum particle size are represented

Historical approaches to particle packing have been on the assumption that particles can either be modelled as discrete sizes or as continuous size distributions, however, the two approaches were subsequently shown to be fundamentally the same when satisfying certain constraints (discussed further in § 2.4.2). For this review, the theory of treating the packing of a polydisperse distribution of particles as many discretely sized particles will first be discussed, followed by a discussion of treating a polydisperse distribution of particles as a continuous particle size distribution.

In both instances, foundational work in the two fields is discussed and followed by subsequent developments. Figure 2-10 presents an overview of some of these packing models as presented by Alexander & Mindess (2005). Wall and loosing effects are described in § 2.3.3 and compaction effect refers to the ability of the model to account for the influence of applied compaction on the resulting packing density (described further in § 2.4.1.6).

2.4.1 Discrete polydisperse distributions

For clarity, discrete particle size classes are defined and differentiated from the term mono-dispersions. Each discrete size class includes the particle sizes bound by two adjacent sieves (or boundary sizes when concerning laser diffraction techniques) and is defined by a mean or median value of the sieve/boundary sizes. Therefore, more accurately defined, a discrete particle size class comprises a continuous distribution which extends over a very narrow range of particle sizes (Funk & Dinger, 1994).

The theory of the packing of discretely sized particles broadly concerns the packing of two or more discrete size classes where the contacts by particles of identical size class are maximised. This leads to the filling of available void space with the maximum possible number of particles of a single, discrete size class (usually accounting for between 40 and 70 % of available interstitial

space). Thereafter, the remaining interstitial space is similarly filled with the next, adequately smaller size class, without disturbing the packing of the larger size class. The same packing procedure, i.e. maximising contacts of one size class and then filling its interstitial void space is continued either until particle size classes reach a predetermined lower particle size class limit or become infinitely small (depending on the model considered). Fundamentally, the theory considers each size class to pack to its maximum density in the available volume, leading to an overall maximum packing density when fine particles exactly fill the void space between larger particles (Funk & Dinger, 1994).

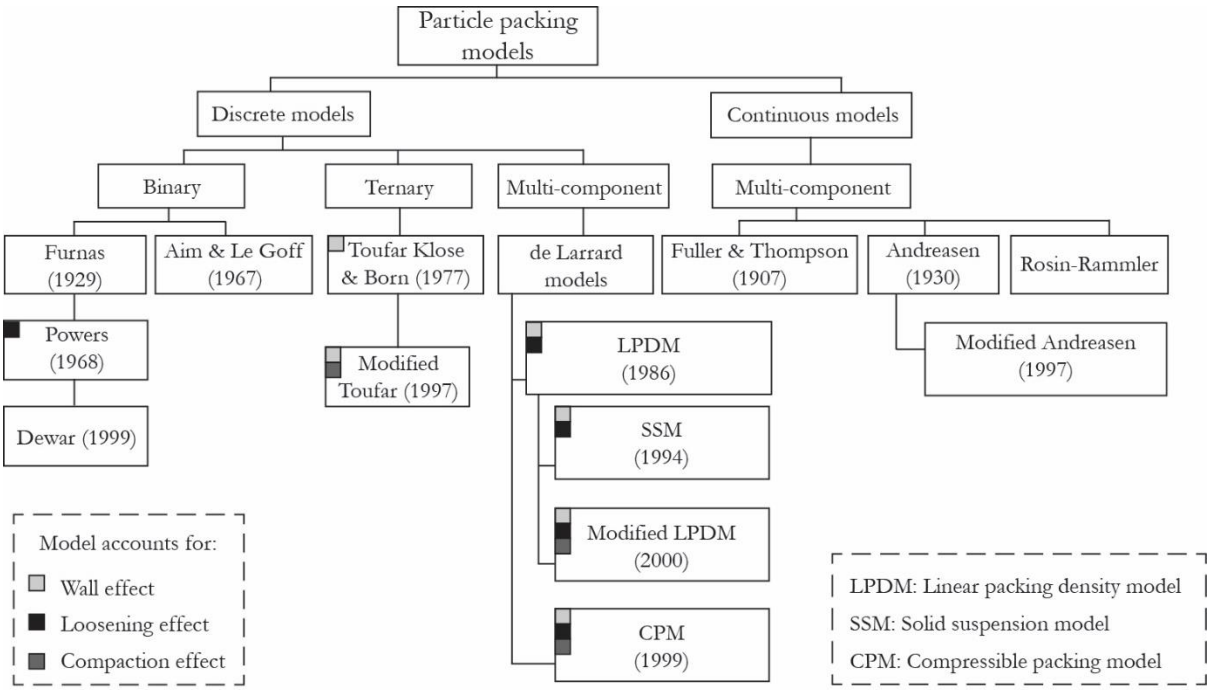

Figure 2-10: Overview of existing packing models adapted from Alexander & Mindess (2005)

2.4.1.1 Furnas Model

Discrete packing models may be categorised as either binary, ternary or multimodal models (Kumar & Santhanam, 2003). Foundational work concerning discrete packing models was completed by Furnas (1929) who initially developed the means for the calculation of the solid volumes of binary mixtures (only two size classes). Each discrete size fraction was described by its partial volume, the volume that it occupied in a unit volume. The relative volume of each size fraction was then represented as its volume fraction (*Eqn. 2-2*) and the summation of the volume fractions of all size classes equates to 1 (*Eqn. 2-3*).

$$r_i = \frac{\varphi_i}{\sum_{i=1}^{n} \varphi_i} \qquad \textit{Eqn. 2-2}$$

$$\sum_{i=1}^{n} r_i = 1 \qquad \textit{Eqn. 2-3}$$

When there is only a single size class, $r_i = 1$ and the partial volume of the size class is equivalent to the total volume which is occupied and is equivalent to the packing density α_t. Furnas' model is only valid for the case that the two particle size classes are substantially different (i.e. $d_1 >> d_2$). If the condition is not fulfilled, the packing density of the binary mixture would also be dependent on the diameter size ratio (d_1/d_2)(Funk & Dinger, 1994; Kumar & Santhanam, 2003). Fennis (2011) discusses the two scenarios that need to be considered for Furnas's case of binary packing:

Scenario 1: The volume fraction of the larger size class is substantially larger than that of the smaller size class (i.e. $r_1 >> r_2$).

Smaller particles (of diameter d_2) can be added to a container filled with the larger particles (of diameter d_1). On the addition of the smaller particles, the void space between the larger particles is filled and the overall packing density is increased. The packing density of the mixture is equivalent to the volume of the larger particles (which is limited by the maximum packing density of the larger particles) plus the volume of the smaller particles in a unit volume and is expressed in *Eqn. 2-4*.

$$\alpha_t = \varphi_1 + \varphi_2 = \alpha_1 + \varphi_2$$
$$\therefore \alpha_t = \frac{\alpha_1}{1-\alpha_2} = \frac{\alpha_1}{r_1} \qquad \textit{Eqn. 2-4}$$

Scenario 2: The volume fraction of the smaller particles is substantially larger than that of the larger particles (i.e. $r_2 >> r_1$).

Larger particles can be added to a matrix of smaller particles and contribute the value of their partial volume (φ_1) to the overall packing density of the mixture. The smaller particles then fill up the remainder of the unit volume (1- φ_1) according to their maximum packing density. The packing density of the mixture is now equivalent to the addition of the partial volume of the larger particles and the remaining volume filled with the maximum volume of smaller particles (which is limited by the maximum packing density of the smaller particles). This scenario is represented in *Eqn. 2-5*.

$$\alpha_t = \varphi_1 + \varphi_2 = \varphi_1 + \alpha_2(1-\varphi_1)$$
$$\therefore \alpha_t = \frac{1}{r_1 + (r_2 / \alpha_2)} \qquad \textit{Eqn. 2-5}$$

Furnas eventually extended this theory to multicomponent distributions with 'n' particle size classes (*Eqn. 2-6*) (Funk & Dinger, 1994) and he was able to show that the volume of each consecutively smaller, discrete particle size formed a geometric progression for a mixture achieving maximum packing density. To optimise the particle packing by this method and achieve the

densest packing possible, the ideal case is for the diameter ratio of large to small particle size to be infinitely large. However, realistically this cannot be attained. Funk & Dinger (1994) proposed a more realistic 'ideal' case to have a diameter ratio of 100:1 and, still further, more practically attainable ratios of 20:1 and 10:1.

$$\frac{CPFT}{100\%} = \frac{r^{\log D} - r^{\log D_S}}{r^{\log D_L} - r^{\log D_S}} \qquad \textit{Eqn. 2-6}$$

Where: CPFT = Cumulative percent finer than

r = Ratio of the volume of particles on one sieve to the volume on the next smaller sieve. Furnas showed that, for a standard sieve series, this ratio was constant.

D = Particle size

D_S = Smallest particle size

D_L = Largest particle size

2.4.1.2 Toufar Model

Toufar *et al.* (1976) extended work of Furnas (1929), Powers (1968) and Aim & Le Goff (1967) to incorporate the 'wall effect' in packing models for ternary and eventually multimodal particle mixtures. Packing was modelled as a series of binary mixtures and packing density was taken to be the weighted average of the total number of binary mixtures that had diameter ratios of $0.22 < d_1/d_2 < 1.0$ (Kumar & Santhanam, 2003). This was done with an understanding that smaller particles, with diameter ratios > 0.22, would be too large to fit within the interstitial space between larger particles.

2.4.1.3 Modified Toufar

Golterman *et al.* (1997) made a further, but minor, modification to the Toufar model which they found was able to better predict the packing density of binary mixtures of fine and coarse aggregate materials for the particular case of a smaller volume fraction of fine aggregate.

2.4.1.4 Linear Packing Density Model (LPDM)

Stovall *et al.* (1986) proposed the Linear Packing Density Model (LPDM) which incorporated the effects of geometrical interaction between the particles using interaction functions describing a wall and loosening effect, as described in § 2.3.3. This geometrical interaction is integrated into the model as the influence of a particular size class on the dominant size class. In this case, the dominant size class was one which was able to be fully packed (to its maximum bulk density) in the presence of other size classes. Without interaction, the LPDM is comparable to the MAAC (§ 2.4.2) with a distribution modulus of 0.44. With interaction, each particle mixture has its own optimal grading due to the influence of the particle interaction (Fennis, 2011).

2.4.1.5 Dewar Model

Dewar (1999) developed a packing model which used a mean characteristic diameter to describe

each size class to be included in a particle mixture. He constructed his model by determining the interaction of two size classes, starting with the smallest size classes, before combining them to form a new, single size class represented by a characteristic diameter. The interaction of this new size class with the next consecutive size class was then determined and the same process followed until all size classes were considered. His model accounted for the expansion of void space between larger particles due to the addition of smaller particles to the interstices of larger particles as well as the 'wall' effect of larger particles on the packing of smaller particles. However, it has been criticised for underestimating particle interaction by combining each consecutive binary mix to form a new size class and therefore not being able to accurately represent the interaction of the new size class with the next consecutive size class (Fennis, 2011).

2.4.1.6 Compressible Packing Model (CPM)

The compressible packing model (CPM) was developed as a refined version of the LPDM for particulate mixtures (de Larrard, 1999). Arguably, the most important development accompanying this model was the acknowledgement of the influence of compaction on the packing of a material mixture and the subsequent definition of a 'virtual packing density' (β). This was defined as the maximum packing density attainable for a given grain mixture with maximum compaction applied (de Larrard, 1999). From the virtual packing density, the actual packing density (α_t) of the mixture is determined with reference to a compaction index (K). This is a scalar index, entirely dependent on the compaction effort applied and therefore needed to be defined for each compaction process (de Larrard, 1999). For the ideal case of a mixture of mono-sized spheres, the virtual packing density is the packing density of a face-centred cubic lattice of spheres, equivalent to 0,74. However, a random mix of these same spheres results in the actual packing density being within the range of 0,60/0,64, depending on the compaction applied (de Larrard, 1999).

The accuracy of the LPDM and CPM depend on the interaction functions describing the wall and loosening effects but the integration of the compaction effort into the CPM by the compaction index has been found to increase the accuracy of the CPM relative to the LPDM (Fennis, 2011). However, when considering powder materials, particle interaction also occurs as a result of surface forces. Fennis (2011) found these additional interactions to influence wall and loosening effects and the distribution of the compaction energy over the various size classes. These influences are further clarified in § 4.2.1 when considering how K and loosening and wall effects are related in *Eqn. 4-5* and *Eqn. 4-6*.

2.4.1.7 Compaction Interaction Packing Model (CIPM)

Fennis (2011) discusses existing particle packing models, focusing on their potential for use in the design of 'ecological' concretes which comprise high filler material contents. As an overview, Fennis'(2011) findings suggested that existing models have been able to predict the packing density of aggregate material distributions to appreciable accuracy. Jones *et al.* (2002) made similar conclusions, showing that several packing models, although each making different assumptions, lead to similar accuracies in the prediction of the packing density of aggregate materials.

However, Fennis (2011) found that there was a lack of consideration of influences specific to powder material packing in existing models and went on to show the decreased ability of the CPM to accurately predict the packing density of powder materials relative to the ability of the model to predict the packing density of aggregate materials. Yet, Fennis (2011) still acknowledged

the CPM to be mathematically robust and provide a good foundation for implementation of the effects of surface force interactions which govern the packing of powder materials (<125 μm).

Based on these findings, numerical modelling and experimental validation, she then extended the CPM by developing new interaction formulae describing loosening and wall effects, integrating the effects of surface forces into these interactions by either increasing or decreasing the wall and/or loosening effects.

Previous models (CPM, LPDM) accounting for wall and loosening effects did so using interaction formulae based solely on the size ratio of the interacting particles. However, for the integration of surface force effects on powder packing into the interaction formulae, it was necessary to ensure the scaling of the interactions. For example, interacting particles of diameter 5 and 10 mm would have a size ratio of 0.5 but so would interacting particles of 10 and 20 μm, however the packing of the former would largely be influenced by shear and gravitational forces and the latter by van der Waal's and surface forces. Therefore, Fennis (2011) also introduced the concept of a 'cut-off' diameter, below which particle interactions would be subject to either increased or decreased wall and loosening effects but above which, the usual geometric interaction formula would be applicable.

The CIPM still only considered the effects of particle shape and texture implicitly (by incorporating an experimental packing density for each material input into the model). However, Fennis (2011) was able to increase the accuracy of the prediction of the packing density of powder materials (relative to the CPM, see Figure 2-11) and went on to apply the CIPM in the design of 'ecological' concrete mixes. More specifically, Fennis (2011) reported that, for particle mixtures with particles smaller than 125 μm, the CIPM improved the average error in the packing density predicted from 2.2 % in the CPM to 0.6 % and maximum error from 6.4 % in the CPM to 1.8 %.

2.4.1.8 Commentary on the appropriateness of discrete theory to this research

Although Furnas' approach was mathematically sound and would go on to provide the basis for the development of various other packing models (Stovall *et al.*, 1986; de Larrard, 1999; Dewar, 1999; Fennis, 2011), the applicability of his discrete theory to model the packing of real, polydisperse particulate materials, that almost invariably follow continuous distributions, has been queried (Funk & Dinger, 1994). Although Furnas extended his theory of discrete particle packing to the packing of continuous particle size distributions, he still did so on the basis of the packing of discrete particle sizes, requiring the measurement of the void volume of an ordered pack of uniformly sized particles (Funk & Dinger, 1994). The accuracy of this theory was dependent on how each discrete size class was defined. At the time of its development, this was defined coarsely, such that the ratio of a larger particle size class to smaller size class was in the region of 100:1 which clearly did not represent a real continuous distribution. However, subsequent modifications have enabled the consideration of size ratios closer to 1:1 which have enabled a considerably better representation of real, polydisperse materials.

Furthermore, Funk & Dinger (1994) also query a primary assumption of discrete particle theory, stating that although the theory requires each particle of the same size class be in contact with one another, realistically, this cannot always be assumed to be the case. A contradictory example offered was that of mixing where it could not be guaranteed that the position of a larger discrete size class would not be obstructed by a smaller size class on the completion of mixing.

Any process causing shearing would result in the dilation of the packing structure, causing a decrease in packing density. However, they do acknowledge the ability for discrete theory to improve packing efficiency of a 'static' particle structure Funk & Dinger (1994).

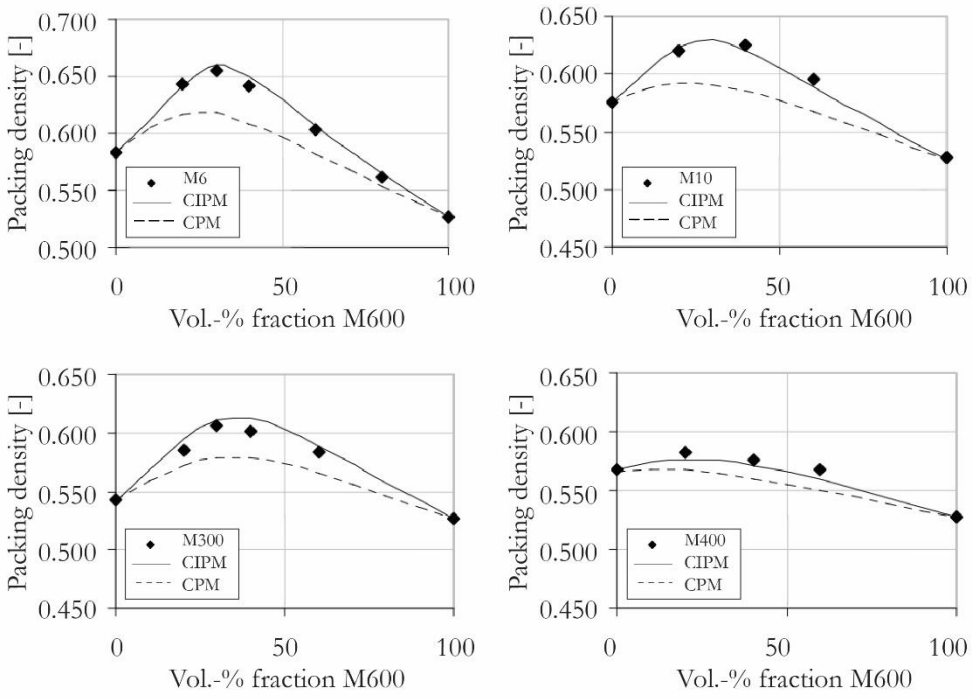

Figure 2-11: Experimental wet packing densities compared to those calculated by the CPM and CIPM for quartz powder of varying fineness (Fennis, 2011)

Commenting on the applicability of Furnas' model to the packing of powder materials, Fennis (2011) mentioned its inability to account for geometric particle interactions, let alone those due to surface forces. However, Fennis (2011) acknowledges its merit in providing foundational theory which led to the development of successive models, better accounting for particle interactions or at least providing a basis for their consideration (Fennis, 2011).

Instead of developing Furnas' theory of discrete particle size distributions, Funk & Dinger (1994) mention that, during a similar period in time, Andreasen and Andersen approached the problem of packing of polydisperse materials by basing their theory on continuous distributions of particles, primarily because they deemed it to be better representative of real, polydisperse materials. The following section presents an overview of this theory and resulting packing models, making comparisons with discrete theory where applicable.

2.4.2 Continuous polydisperse distributions

The theory for the packing of polydisperse continuous distributions of particles entails the assumption that, within a defined size range, there exist *all* size classes as opposed to the assumption made for discrete distributions of particles (where there exist only a *finite* number of size classes within a defined range). Contrary to the discrete approach (§ 2.4.1), the continuous

theory does not maximise the contacts of particles that are identical in size. Few, if any, particles that are identical in size touch one another. The foundation for this theory was largely based on geometric and similarity considerations and initially assumed that there existed an ideal PSD which would achieve maximum packing density. This section addresses some of the foundational work for the packing of particulate materials as continuous distributions.

2.4.2.1 Fuller Curve

In their reviews of particle packing models, Fennis (2011) and Funk & Dinger (1994) both mention the Fuller curve (Fuller & Thompson, 1907) as one of the earliest efforts to achieve an ideal grading curve. The proposed ideal grading is solely reliant on the maximum particle size of the aggregate mixture, as described by *Eqn. 2-7*.

$$\frac{CPFT}{100\%} = \left(\frac{D}{D_L}\right)^{0.5} \qquad \textit{Eqn. 2-7}$$

Where: CPFT = Cumulative percent finer than

D = Particle size

D_L = Largest particle size

Fuller & Thompson (1907) defined an exponent of 0.5 to give an ideal grading curve and enable maximal packing density of a particulate material proportioned according to the curve. Yet, Fuller and Thompson (1907) gave no consideration to a finite lower particle size which led to the impractical assumption that particles tend to infinite fineness (D_{min} = 0). There is also no quantitative assessment of packing density by this method. Instead, it only inferred that the 'ideal' grading would achieve maximum packing density. Therefore, it is difficult to compare the appropriateness of the selection of various mix constituents. Furthermore, no form of particle interaction is considered, preventing the application of the Fuller curve for optimising the packing of powder materials because geometric and surface force interactions are important to consider when analysing the packing of these materials (Fennis, 2011; Damineli *et al.*, 2016).

2.4.2.2 Andreasen and Andersen Curve

Andreasen and Andersen (1930) evaluated the investigations of Fuller & Thompson (1907) as well as Furnas (1928) when investigating methods to achieve dense particle packing (Funk & Dinger, 1994). Andreasen and Andersen concluded that most real distributions of particles comprise *all* particle sizes and therefore a continuous packing theory for the packing of polydisperse distributions would be more relevant than one based on discretely sized distributions (Funk & Dinger, 1994).

Andreasen and Andersen (1930) derived a more general form of Fuller and Thompson's (1907) curve based on geometry and dimensional analysis (*Eqn. 2-8*). They defined a particle size distribution modulus (q) in the range between 0.33 and 0.5 to produce an ideal grading curve which could enable the achievement of maximum packing density. The range for this exponent was

determined by building various experimental distributions which fit the distribution (according to a particular distribution modulus being tested) and determining the packing density of the resulting packs (Funk & Dinger, 1994).

$$\frac{CPFT}{100\%} = \left(\frac{D}{D_L}\right)^q \qquad \textit{Eqn. 2-8}$$

Where: CPFT = Cumulative percent finer than
D = Particle size under consideration
D_L = Largest particle size
q = Distribution modulus

However, Andreasen and Andersen's adaptation still does not resolve the issues raised when critiquing the Fuller curve. The measurement of packing density is not possible and therefore the extent to which void space can be reduced is not known. Particle interactions are also still not considered, although it could be argued that the experimental determination of a distribution modulus for a particular combination of materials could indirectly incorporate characteristics specific to the materials (such as particle shape and surface texture).

2.4.2.3 Modified Andreasen and Andersen Curve

Funk & Dinger (1994) modified the theory upon which the Andreasen and Andersen curve was developed. Their assumption was that Andreasen and Andersen were correct in stating that a packing theory for continuous distributions should be based on continuous distributions (and not discretely sized particle distributions, such as the packing models discussed in § 2.4.1). Their modification was the acknowledgement of the lower end of the particle size distribution by accounting for a finite lower particle size limit (Funk & Dinger, 1994). In this way, the entire particle size distribution of particulate materials, from powders to coarse aggregate materials, was better accounted for instead of assuming that particles sizes become infinitely small. The result of their modification was the development of *Eqn. 2-9*.

$$\frac{CPFT}{100\%} = \frac{D^q - D_s^q}{D_L^q - D_s^q} \qquad \textit{Eqn. 2-9}$$

Where: CPFT = Cumulative percent finer than
D = Particle size under consideration
D_S = Smallest particle size
D_L = Largest particle size
q = Distribution modulus

The distribution modulus was the same as the exponent proposed by Andreasen and Andersen but simulation results from Funk & Dinger (1994) suggested that optimum packing occurred at q=0.37 (which is still within the range that was previously suggested). Practically, this implies that for any value of q below 0.37 there will be sufficient interstitial space available to pack the next smallest particle size and for any value of q above 0.37, there will no longer be sufficient interstitial space (Funk & Dinger, 1994). The determination of q=0.37 is further discussed in § 4.3.3.

Figure 2-12 and Figure 2-13 portray the differences between the Andreasen and Andersen curve and the modification to the curve by Funk & Dinger (1994). The effects of varying q are also seen in Figure 2-12 (q= 0.3) and Figure 2-13 (q= 0.7). In both cases the same range of lower and maximum particle size limits are used. The lower the value of q, the higher the content of finer material in the proposed cumulative percent finer than (CPFT) plots.

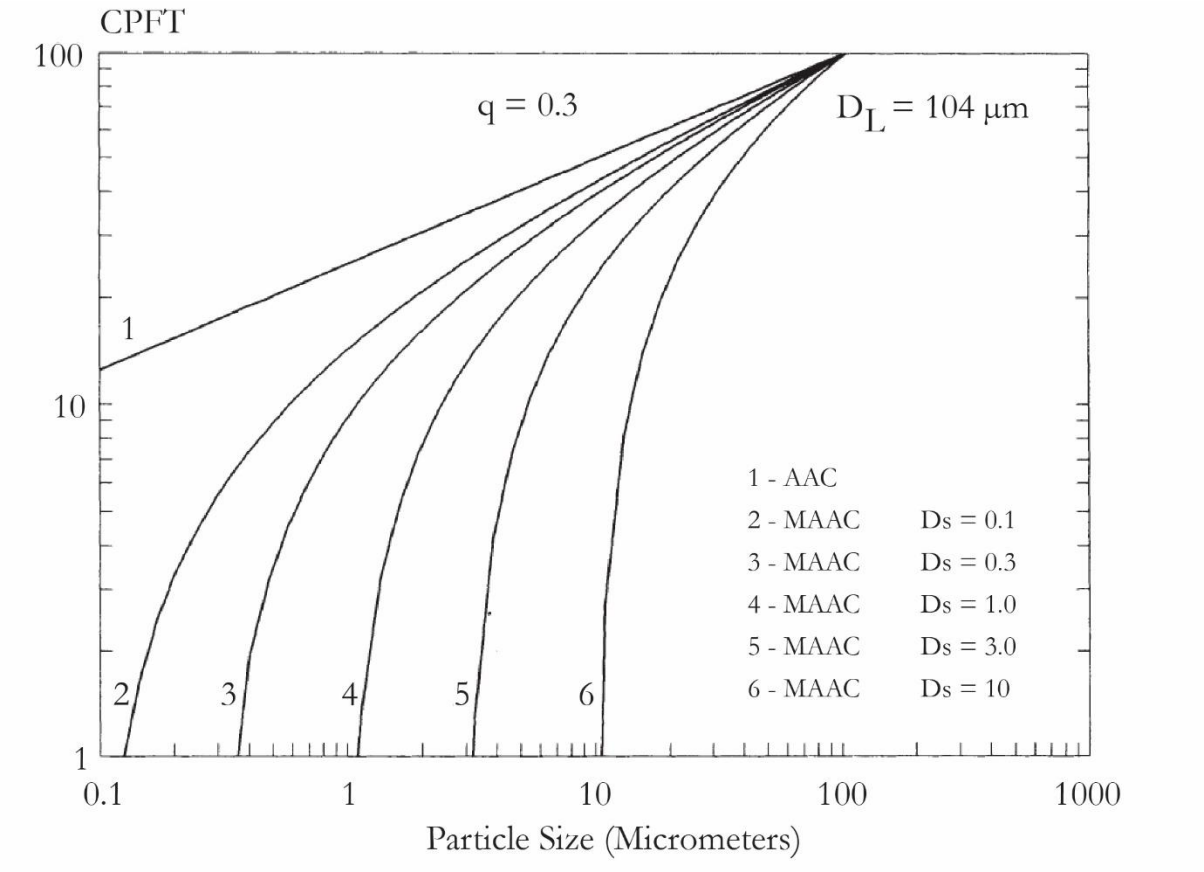

Figure 2-12: Portrayal of Andreasen and Andersen's curve and the Modified Andreasen and Andersen curve with q = 0.3 (Funk & Dinger, 1994)

Although Funk and Dinger (1994) further developed Andreasen and Andersen's work on coal/water suspensions, it has subsequently been applied in the concrete industry by several researchers (Hüsken & Brouwers, 2008; Hunger, 2010; Hüsken, 2010; Yu *et al.*, 2013). These applications varied from the design of earth moist concrete to high-strength concrete as well as self-consolidating and low-clinker concrete mix design. In all instances, q was adjusted depending on experimental packing density results and required workability/consistency. Values of q

considered were in the range of 0.22 to 0.25 for self-consolidating concrete and up to 0.37 to 0.40 for earth moist concrete.

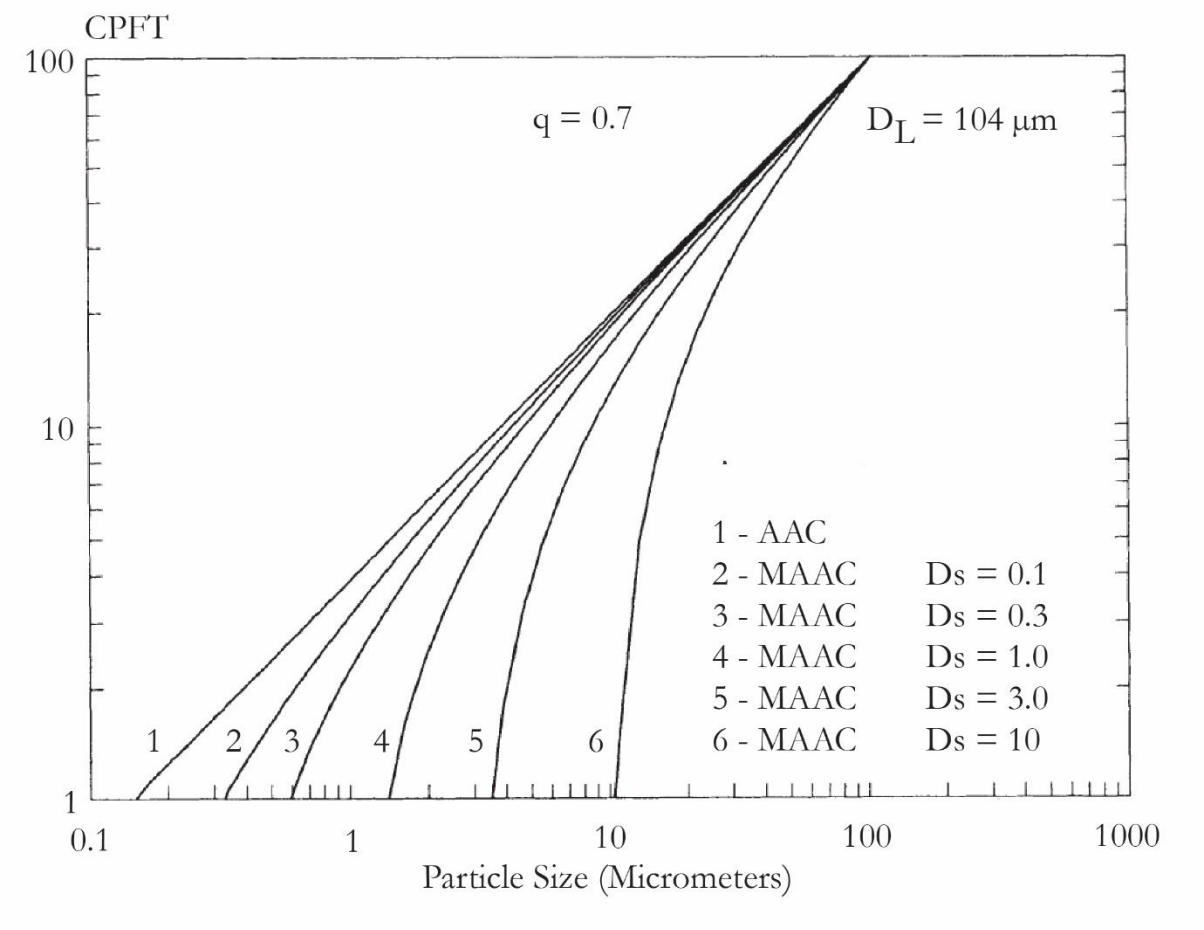

Figure 2-13: Portrayal of Andreasen and Andersen's curve and the Modified Andreasen and Andersen curve with q = 0.7 (Funk & Dinger, 1994)

While the rule of thumb has often been that the broader the distribution of particles, the better the packing, Funk and Dinger (1994) showed this was not always the case. They found this to be true for $q \leq 0.37$, but not true for distributions with $q > 0.37$. Consequently, this results in some distributions being able to pack to higher packing densities (lower porosities) than others as the range of particle sizes increases. For distributions constructed using $q > 0.37$, there exists a minimum porosity which will be reached, despite an increase in the range of the particle size distribution.

With evidence of successful application of the Modified Andreasen and Andersen Curve (MAAC) for the design of various concrete mixes and its consideration of the full spectrum of particle sizes, there is potential for its application in optimising the selection of concrete materials to reduce the clinker content of concrete. The MAAC theory of continuous distributions of particles is more representative of real distributions of particulate materials than the theory of discrete distributions of particles. Funk & Dinger (1994) also discussed the similarities of the MAAC continuous theory with that of the foundation equations for Furnas' (1929) discrete theory

which has formed the basis for various particle packing models (§ 2.4.1). Subsequently, Brouwers (2006) proved the mathematical relationship between the theories of discrete and continuous distributions of particles and showed that they are complementary for packings consisting of multiple particle size classes with the same monosized packing density.

However, the MAAC does not directly account for the important influences of compaction effort applied and how compaction effectiveness diminishes with decreasing particle size. Furthermore, aspects of particle interactions and the influence of particle characteristics such as shape and surface morphology are not able to be directly included and lead to misinterpretation of the 'optimal' combination of materials. Nevertheless, of the models based on continuous distributions of particles, the MAAC is of interest as it appears to best represent a full spectrum of particle sizes. This is important for this research which focuses on packing of the full range of concrete materials.

2.5 Viscosity prediction for increasing binder efficiency

A more recent approach to reducing clinker content is the control of the rheological behaviour of the paste phase to decrease its water demand. Damineli *et al.* (2016) emphasised rheological behaviour, arguing that it is often the practical limiting factor when defining the maximum filler content used in concrete. They focus on the importance of raw material parameters; such as surface area, density and roughness, and characteristics of the paste phase; such as water content and distance between particles, when controlling rheology.

The water demand of a paste is dependent on the volume of water required to fill void space, coat the surface area of particles, and promote spacing between particles to ensure desirable rheological properties. Therefore, the ideal case for reducing the water demand of a suspension is the reduction of porosity (to reduce the water necessary to fill voids) and reduction of surface area (to reduce the water needed to cover particle surfaces). Thereafter, only a minimum amount of excess water is needed to promote spacing between particles and improve rheological properties (Figure 2-14).

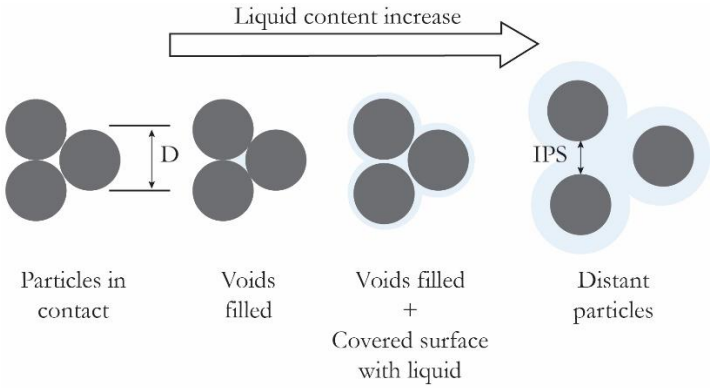

Figure 2-14: Representation of increasing water content towards the optimal water content required for the interparticle separation distance (IPS) for particle mobility (John *et al.,* 2017).

Damineli *et al.* (2016) acknowledge that the water demand of clinker-inert filler systems can be reduced (in comparison to conventional concretes/pastes) with combined techniques of particle

dispersion and packing modelling, but that this is solely due to the aim of packing modelling being the reduction of excess pore space. They argue that existing models are limited due to their ignorance of important rheological parameters, tendency of assuming particles to be perfect spheres and often lacking consideration of particle interactions, as well as important material properties of surface area and morphology.

While this is not entirely the case for the CPM and CIPM (discussed in § 2.4.1) as they indirectly include particle shape and surface characteristics through the input of an experimental packing density and account for wall and loosening effects (the latter model further accounting for the influence of surface forces on these interactions), both these models only consider the scenario of a stable (static) particle structure. Yet, the higher the packing density and lower the void space and excess water, the stiffer the fresh concrete/paste becomes due to increased friction and less lubrication for particles to move over and alongside one another.

Damineli *et al.* (2016), instead, do not consider the packing of a stable particle structure but rather approach the problem by considering the flow of pastes as highly concentrated suspensions and how particles interfere with each other's movement. Their interest is in rheological models which aim to predict the water content required for suitable rheological behaviour in terms of yield stress and viscosity parameters.

Although these approaches differ by considering the static and dynamic (flowing) state of a particle structure, the ultimate objective of both is the same: the reduction of excess porosity. However, the inability of the packing density modelling approach to directly consider the dynamic state may result in more experimental trial to achieve adequate fresh concrete properties. Modelling viscosity, instead, has the potential to simultaneously minimise porosity and achieve adequate fresh properties and ultimately, may require less experimental trial to arrive at a final mix design.

Developing the idea of modelling the viscosity of PC mixtures to reduce water demand, Damineli *et al.* (2016) applied the 'Particle Interference Model' - which was originally applied for predicting the viscosity of alumina ceramic suspensions. Interference is any energy dissipative interaction which includes, but is not limited to, particle collisions, friction, liquid-solid drag disturbances and instant localised capillary bridges. The Particle Interference Model consists of the analysis of the mean interparticle separation distance (IPS) and a particle interaction concept. An assumption is made that a particle of specific size does not interfere with the movement of other particles 10 times larger or 10 times smaller than its diameter during the flow of a highly concentrated suspension. This concept enables well-dispersed suspensions to be modelled as several sub-suspensions, each made up of a liquid phase and the particles within a diameter ratio of 10 around the particle size of concern. This has been described practically as treating each particle class as being suspended in a 'fluid' of particles of the adjacent size classes, each with their own assigned viscosity.

Damineli *et al.* (2016) related the IPS of various sub-suspensions to factors governing energy dissipation during the movement of particles, such as surface and mass forces, to incorporate aspects of friction, drag, collision, blockage, inertia, density and attractive/repulsive forces. These enabled a description of particle mobility in available space defined by the IPS and the prediction of the viscosity of the suspensions. The basis of the model is therefore the establishment of spatial conditions for particle mobility by the comparison of particle size and the mean free path between particles, which is defined by the IPS. This infers that larger particles require a larger IPS than

smaller particles to be able to have similar freedom conditions (Figure 2-15) In addition to this spatial analysis, the model assesses how the dissipation of energy affects particle movement by calculating the potential decay distance (distance travelled until stillness) travelled by a particle which is immersed in a liquid phase. This leads to the calculation of the 'natural interference' (INT_{ni}) which is the time required for a particle to travel a unit distance (Damineli *et al.,* 2016).

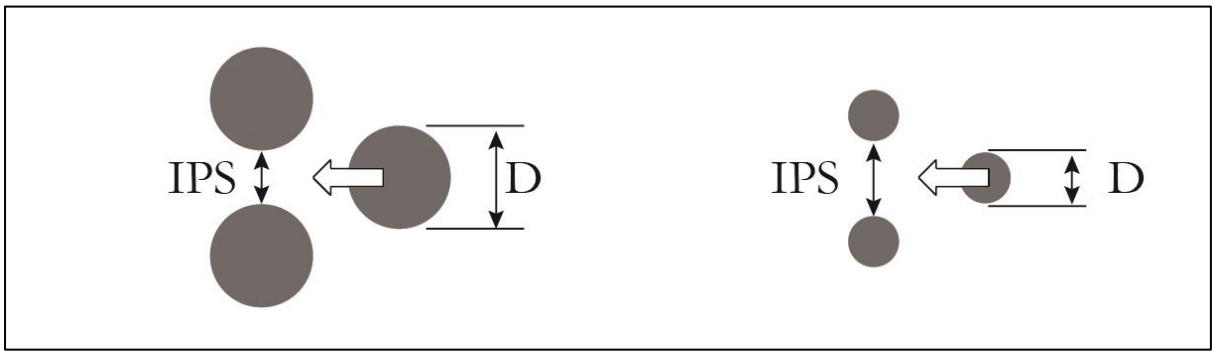

Figure 2-15: Left: Particle size is larger than the IPS, hindering the movement of the particle and therefore increasing energy dissipation and viscosity. Right: Particle size is smaller than the IPS, therefore there is increased mobility with lower probability of energy dissipative interactions. (Adapted from John *et al.,* 2017).

Ultimately, the interference of multimodal suspensions is defined as the summation of the natural interference for each diameter multiplied by its volumetric contribution to the suspension. Furthermore, the interference model requires the experimental relation of a dissipative parameter (H) to the solid volumetric content of the paste to predict its viscosity.

The calculation of interference values is based on fundamental characteristics of the suspensions and has enabled good prediction of the Casson viscosity (a steady state viscosity model) of several different suspensions of pure and blended pastes (Damineli *et al.,* 2016). For a material following the Casson model, there is a linear relationship between the square root of the shear rate and the square root of the shear stress, described by *Eqn. 2-10*. The Casson yield stress (τ_c) is calculated as the square of the intercept ($\tau_c = K_{0c}{}^2$) and the Casson plastic viscosity as the square of the slope ($\eta_c = K_c{}^2$).

This portrays the material as a solid for the scenario that internal shear stress is less than the yield stress and as a plastic fluid for shear stress greater than the yield stress, which must be overcome for the onset of flow. Casson viscosities were found to represent experimental data well (R^2 approximately 0.9), instilling confidence in the ability of the model to predict the viscosity of real paste mixtures.

$$\sqrt{\tau} = K_{0c} + K_c\sqrt{\dot{\gamma}} \qquad \textit{Eqn. 2-10}$$

Where: $\dot{\gamma}$ = Shear rate

τ = Shear stress

Based on these results, the model could enable the systematic selection of SCMs for clinker replacement by estimating water demand and corresponding particle mobility necessary for a specified viscosity. Minimisation of the water content for a desired workability can then be achieved by minimising the interference in a multimodal packing (John *et al.*, 2017). John *et al.* (2017) propose the following approach for the development of high-filler cements:

- Incorporation of clinker with an optimised PSD for effective hydration
- Inclusion of a dilution filler of approximately the same PSD as clinker,
- Inclusion of an ultrafine filler to reduce interparticle pore volume
- Use of a dispersant admixture to prevent particle agglomeration and the disruption of mobility

Damineli *et al.* (2016) mention that, although their viscosity prediction model has shown promising results, further investigation is still required for its application, particularly regarding the experimental relation of a dissipative parameter. Furthermore, the method requires additional considerations to be made such as ensuring sufficient mixing energy for the proper dispersion of particles and compatibility of binders with dispersants (high doses being more likely to retard hydration and affect dispersion with time).

2.6 Summary

Although concrete has a relatively small quantity of associated GHGs when compared to other common construction materials, the vast quantity of concrete produced annually calls for the need to reduce these emissions. Of all concrete constituents, clinker has the most substantial associated GHGs and therefore the most plausible strategies for reducing GHGs associated with concrete are to reduce the clinker content of concrete.

Existing strategies commonly entail the use of filler and SCMs to replace a portion of clinker in cement. The use of these materials has been standardised globally and allowable replacements are as high as 35 % for filler materials (such as limestone) and 80 % for composite cements comprising SCM and filler material. However, despite these high allowable replacements, actual replacement levels are substantially lower, with these materials accounting for only 20 % of total cementitious materials produced, which is likely a result of the dilution of clinker causing diminished concrete properties.

More recent investigations aiming to reduce GHGs associated with concrete have proposed the use of alternate binders (non-Portland cement clinker), but the consensus is that these are capital intensive and require further research before becoming viable solutions. Instead, one of the most economically viable solutions is the increase of clinker efficiency using highly reactive cements and packing optimisation techniques. Particularly, the maximisation of the packing density leads to reduced void space and less water is required to fill interstitial voids and more is available for lubrication of particle movement. Consequently, less water should be required to achieve a workable mixture and a comparatively lower water: cement ratio would be achieved. Inferring concrete properties to be largely dependent on water: cement ratio, less PC would be required to make concrete of a particular strength class. Yet, increasing packing density leads to increased particle contacts in a particle mixture and increased internal friction, reducing workability.

Therefore, packing optimisation should look to maximise packing density to an extent which does not adversely affect fresh concrete properties.

Common concrete mix design methodologies only account for the packing of constituents indirectly and therefore are not appropriate for powder packing optimisation. Several packing models have been developed, initially for use in aggregate packing optimisation but also for use in powder technology industries. These packing models have, in turn, been developed using varying theories. Two theories governing particle packing are the consideration of a particle mixture as a discrete or continuous polydisperse distribution of particles. Arguments have been offered favouring one theory over the other but subsequently, it has been shown that the theories are complementary of one another, given certain constraints.

Most particle packing models have enabled reasonably accurate predictions of aggregate material packing density but tend to less accurately predict powder (<125 μm) packing. This has been attributed to the influences of powder packing being different to those influencing aggregate packing. The latter is primarily governed by shear and gravitational forces whereas the former is primarily governed surface forces. However, two packing models, one from each of the discrete and continuous theories, have been reported to specifically account for powder materials. These should therefore enable increased accuracy of packing density prediction and be more applicable to powder packing optimisation.

A recent advancement in increasing clinker efficiency is the modelling of powder mixture viscosity to reduce void volume and therefore water demand using the 'Particle Interference Model'. Work in this field has shown the accurate prediction of the viscosity of powder-paste mixtures (powder material + water + dispersant) and its potential for selecting materials which reduce void volume (increase packing density) and minimise water demand. Ultimately, this method aims to decrease the mass of clinker required to achieve 1 MPa of compressive strength while ensuring the attainment of desired workability. While the method shows potential for application in reducing concrete clinker content, further investigation is required for the relation of experimental parameters used in the model.

3 Preliminary experimental investigation

The experimental investigation for this research comprised 2 phases. A preliminary phase consisted of the quantitative and qualitative description of material characteristics as well as an evaluation of appropriate test methods. Subsequently, this phase provided inputs for use in particle packing models (described in § 4). Following the modelling procedures, an additional experimental investigation was undertaken. This entailed the construction of concrete mixtures according to model outputs and testing fresh and hardened concrete properties (§ 5).

3.1 Constituent materials

Constituent materials used in this research were primarily selected based on their availability in the Western Cape. Table 3-1 provides an overview of these materials. For consistency, a single cement type, CEM II A-L 52.5 N, was used during this research. According to the manufacturer, their product comprised 9 % limestone content by mass. The chemical composition can be found in Appendix A, Table A-1.

Table 3-1: Constituent materials

Concrete constituent	Material type
Powder materials	Cement
	- *CEM II A-L 52,5 N*
	Limestone
	- *KB2*
	- *KB5*
	- *KB10*
	- *KB45*
	Fly Ash
Coarse aggregate	Nominal 9,5 mm Granite
Fine aggregate	Philippi dune sand (FM = 2.03)
	Granite Crusher 1 (FM =2.93)
	Granite Crusher 2 (FM = 3.53)
Admixture	Superplasticiser
	- *MasterGlenium 456 ACE*
Water	Potable water

Uncalcined limestone was used as a relatively inert filler material to optimise powder material packing. Four limestones of varying fineness, produced by the same manufacturer, were considered as potential filler materials. Their chemical compositions can be found in Appendix A, Table A-1. Three limestones (KB 2, 5 and 10) were finer than the cement used, with median particle sizes of 2, 5 and 10 μm and the last (KB 45) was coarser and did not follow the same nomenclature, with an approximate 125 μm median particle size. The selection of these sizes was in accordance with literature where it was suggested that the use of filler materials coarser and finer than PC be used to enable efficient packing (Scrivener *et al.*, 2016; John *et al.*, 2017).

The manufacturer reported the raw limestone was mined from a source of calcitic and

dolomitic limestone. Processes to obtain the final products, involved crushing, screening and milling of raw material. This was followed by beneficiation through floatation to ensure a high purity calcium carbonate product (typically 95 % purity) as well as further fine milling.

FA was chosen as a pozzolanic powder material to replace a portion of cement. This binder material is a by-product of the power generation industry, extracted by electrostatic precipitators or bag filters from the flue gases of coal-fired furnaces (Grieve, 2009). FA was favourably selected for its relatively high aluminate composition which is known to stimulate the calcium-aluminate reaction of calcium carbonate and for its characteristic spherical particle shape, enabling increased workability by having a ball bearing effect. Its chemical composition can be found in Appendix A, Table A-1.

Figure 3-1 portrays the PSDs of the cement, limestones and FA. A relative measure of fineness of the powder materials was determined using their PSD with the assumption that all particles were perfectly spherical. Limestone fillers KB 2, KB 5, KB 10 and KB 45 had approximate fineness's of 13100, 7100, 4800 and 600 cm^2/g respectively. CEM II A-L 52.5 N and FA had fineness's of 2700 and 5300 cm^2/g respectively.

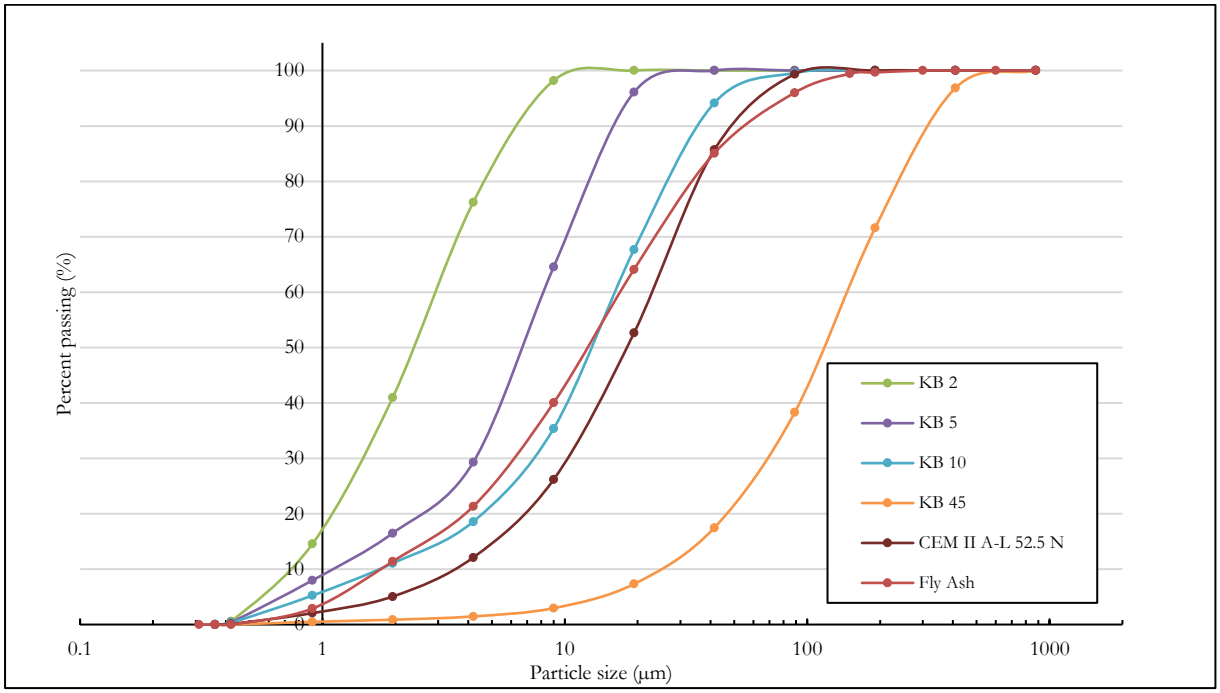

Figure 3-1: Particle size distributions of powder materials

The coarse aggregate used was limited to a nominal 9,5 mm granite stone. Fine aggregates used were Philippi dune sand and two different granite crusher sands. Phase 1 of the concrete mix design procedure (discussed in § 5.1.1) made use of a finer, granite crusher sand (fineness modulus (FM) = 2.93) which was no longer available for Phase 2 of the mix design procedure. Instead, only a coarser granite crusher sand (FM = 3.53) was available and therefore, was supplemented with Philippi dune sand, only to be completely replaced by the dune sand for the final mixtures cast in Phase 2 (see § 5.1.2). Figure 3-2 portrays the particle size distributions of the various aggregates used.

The admixture used for paste and concrete mixtures was a superplasticiser (SP). MasterGlenium 456 ACE, a new generation poly-carboxylate ether polymer was used for its effective dispersing capability. Lastly, potable water was used for all mixtures.

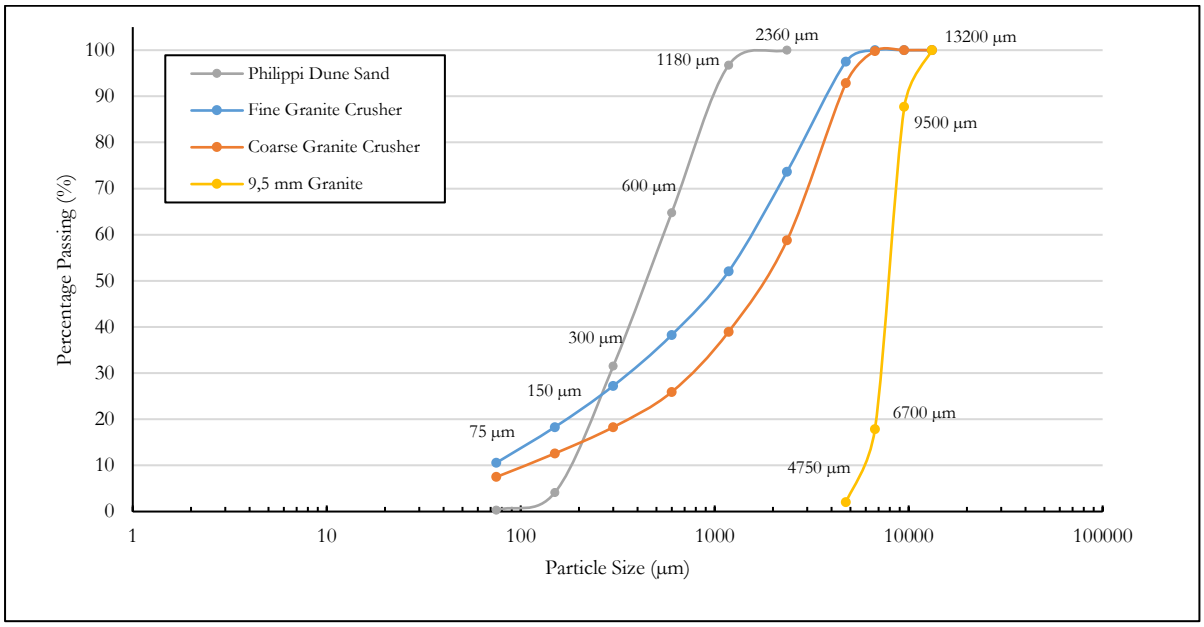

Figure 3-2: Particle size distributions of fine and coarse aggregate materials

3.2 Assessment of constituent material properties

3.2.1 Scanning Electron Microscopy

Due to the important influence of physical particle characteristics on packing density as well as water demand of powder materials, particle shape and surface texture of powder materials were qualitatively assessed using scanning electron microscopy (SEM). SEM entails scanning a specimen surface with a focused beam of electrons. The interaction of the electron beam with atoms in the specimen produces various signals which are detected and used in combination with the position of the beam to produce an image. As the assessment of particle shape and surface topography was of interest, secondary electron imaging was performed. An FEI Nova NanoSEM was used for the analysis of each powder material at varying degrees of magnification, dependent on the particle size being analysed.

3.2.1.1 Secondary electron imaging

Secondary electron imaging makes use of an Everhart Thornley detector (ETD) to describe surface topography. This method of imaging entails the detection of electrons emitted by atoms at the specimen surface which have been excited by the beam of electrons. The strength, and therefore brightness, of the signal detected depends on the number of secondary electrons reaching the detector. By scanning the specimen surface, the number of secondary electrons emitted varies depending on the angle at which the beam of electrons strikes the surface (which is in-turn dependent on the surface topography). The collation of signals of varying brightness across the specimen surface then enables the creation of an image of the surface topography.

3.2.1.2 Specimen preparation

Powder specimens each comprised a dry sample of the powder being analysed adhered to an aluminium stub. Adhesive was applied to the stub surface and powder material was lightly sprinkled onto it, ensuring an even distribution of particles. Once sufficient material was adhered to the stub, pressurised air was used to remove any remaining, loose particles. Thereafter, the material was coated with a layer of carbon to make the surface conductive and the stub placed in the sample chamber of the FEI Nova NanoSEM. See § 6.1.1 for a discussion of the results from the SEM analysis.

3.2.2 Superplasticiser demand

SP demand was determined following a combination of the methods described in ASTM C 939-02 (2002) and Agullo & Toralles-Carbonari (1999) using the standardised flow cone apparatus described in ASTM C 939-02 (2002).The method entails the relative measure of the fluidity of a paste by measuring the time taken for a certain volume of paste to flow through a cone with a small opening. The longer the flow time, the lower the fluidity. This method has proved to be useful for practical application in selecting SPs and their optimum dosage, determining loss of fluidity and accounting for the effects of mineral admixtures (SCMs) on fluidity (Agullo & Toralles-Carbonari, 1999).

The SP demand was defined by the saturation point, which is the dosage beyond which flow time does not appreciably increase. This point was determined subjectively from the shape of the curve of flow time versus SP dosage. The resulting SP demand is dependent on the cement, water: cement ratio, mineral admixture content and mixing procedure (Agullo & Toralles-Carbonari, 1999).

The SP demand was determined for the cement (CEM II A-L 52.5 N) and one of the four limestones, namely that of intermediate fineness (KB10), from which it was desired a single dosage could be applied for the later testing of all powder materials. Mixtures with total starting volumes of 2.3l were made for each of the powder materials, starting with an initial 1 % SP dose by mass of powder material and low water content. It was necessary to ensure that powder materials could be effectively dispersed at their maximum packing densities and therefore, the water content for determining SP demand was estimated using the wet packing test (described in § 3.3.1) to be near the water content that would fill the interstitial space within the particle structure at its maximum packing density. This resulted in the use of low w/p ratios (approx. 0.67 by volume and 0.22 and 0.24 by mass for CEM II A-L 52.5 N and KB10 limestone respectively, including the volume of initial SP).

For each test, the powder material was placed in a mortar mixer and briefly dry mixed. Thereafter, the initial SP dose was added to the defined water content and gradually added during approximately 90 seconds (s) of mixing at a low speed. The mixer was then stopped, and the sides of the bowl and paddle were scrapped. Thereafter, a period of approximately 2 minutes (mins) of mixing at 'medium' speed was completed. This was followed by a short resting period to allow entrained air to escape.

The flow cone orifice was blocked, and the cone filled to the designated full capacity (approx. 1.8l, but this exact same volume was used for testing each incremental addition of SP). The paste was left to rest shortly to prevent any transient flow. Thereafter, the orifice was opened and,

simultaneously, a timer was started. The paste flowed into a beaker beneath the orifice and the timer was stopped at the first break in flow from the orifice (in accordance with ASTM C 939 (2002)).

Thereafter, the paste was replaced in the mixer and the next 0.2 % increment of SP was added during a 30s period of mixing at a low speed. Thereafter, a period of approximately 2 mins of mixing at the medium speed setting was completed before repeating the flow cone test. Incremental additions of SP followed by the abovementioned mixing process was repeated until the flow time no longer decreased appreciably.

Materials with higher water demand were expected to require higher dosages for saturation. Agullo & Toralles-Carbonari (1999) mention limitations of the test method that should be considered. An assumption is made concerning the paste as a Newtonian fluid which is not always true. Furthermore, the paste within a concrete mix could have different rheology to that prepared separately and therefore the test may not be completely representative of the case for real concrete. See § 6.1.2 for a discussion of the SP demand of materials used in this research.

3.2.3 Determination of packing density

The maximum packing density of each individual powder material used was of importance for use in particle packing modelling procedures (see § 4.2). The accuracy of the prediction of packing density by the CIPM is reliant on the accuracy of the input packing density for each material. A review of some existing techniques used for powder packing density determination (Wong & Kwan, 2008a; Hunger, 2010; Fennis, 2011) showed a more accurate interpretation of the packing density using wet packing test procedures (as opposed to the usual dry packing methods used for void content determination of aggregates, such as SANS 5845 (2006)).

The preference of wet packing over dry packing techniques is specific to powder materials due to the, already acknowledged, influence of surface forces governing their interactions and therefore packing density measured. Dry packing techniques rely on the ability of gravitational and shear forces, commonly induced by rodding, vibration and application of compressive stress, to densely pack particulate materials. However, as it is extremely difficult to overcome surface forces by these means, the measurement of powder packing density by applying these techniques is usually inaccurate due to agglomerating particles.

Contrary to this, wet packing methods enable the use of a dispersant admixture within mixing water which can break agglomerates, enabling particles to act as single entities within the particulate mixture. This enables a better representation of the maximum packing density possible for a particular powder material for each test method. Furthermore, the measurement of packing density in a wet state is better representative of real concrete mixtures where SPs are used, especially when mixtures comprise a high volume of powder materials.

Following the assessment of three different wet packing techniques (discussed in § 3.3), the determination of packing density of powder materials using the mixing energy test was, similarly to Fennis (2011), found to enable the most repeatable and reproducible results. The test procedure followed is detailed in § 3.3.3.

The CIPM requires the input of a maximum packing density per powder material input into the model. Therefore, initially, mixing energy tests were completed for each of the pure powder

materials. Thereafter, various combinations of each of the limestones with cement were completed to provide experimental data for the validation of CIPM parameters (as discussed in § 4.2.4.3). Following a similar procedure to Fennis (2011), a minimum of two tests were completed for each material combination to ensure repeatability.

3.3 Assessment of packing density test methods

This section describes the procedures followed for the three wet packing tests that were of interest for this research. Reviews of other methods are available in Hunger (2010) and Fennis (2011). Discussion concerning the preference of one test over another is given in § 6.1.3 and supported by preliminary test results.

3.3.1 Wet packing test

Wong & Kwan (2008) developed a test method for measuring the packing density of powders (which they defined as particles smaller than 100 μm) entailing the measurement of the bulk density of paste formed at various water-powder ratios. For consistency with the methodology discussed in Wong & Kwan (2008), water-powder ratio is denoted as w/cm for this section.

Pastes are characteristically different at the various w/cm ratios. At a high w/cm, powder materials are suspended in water with little to no entrained air and the paste behaves as a slurry. At a low w/cm, the paste consists of agglomerates of material, poorly packed together with substantial entrained air because the water content is below that of the volume required to completely fill interstitial space between particles. Excess water at a high w/cm and an insufficiency of water with entrained air at a low w/cm cause the solid volume fraction at both extremes to be low. Wong & Kwan (2008) proposed that an optimum w/cm exists somewhere between these extremes where the solid volume fraction is maximised (and void ratio minimised) and is taken to be the maximum packing density of the powder material (Figure 3-3).

Wong & Kwan's (2008) 'wet packing test' comprises the following:

1) The w/cm ratio is set and the required quantities of water, powder material and SP (if this is to be used) are batched. The authors suggested beginning at a w/cm (by volume) equal to 1.0 and thereafter running additional tests with successively reduced water-powder ratios until the maximum solid fraction was measured.
2) For mixtures comprising several different powder materials, it is suggested that the dry materials are pre-mixed first for a period of 2 mins.
3) The entire volume of water for the test is added to the mixing bowl.
4) Half of the powder material mixture and half of the SP is added to the mixing bowl and mixing commences at a low speed for 3 mins.
5) The remaining powder material and SP is divided into four equal portions which are each added separately and followed by a 3 min period of mixing at low speed in each instance.
6) The mixture is transferred to a cylindrical mould which is filled to excess.
7) The desired form of compaction can then be applied (if any) and be followed by removing excess material with a straight edge.
8) A mass reading of the paste contained in the mould is recorded.

9) The same procedure can then be repeated at successively lower w/cm ratios until a maximum solid volume fraction is recorded.

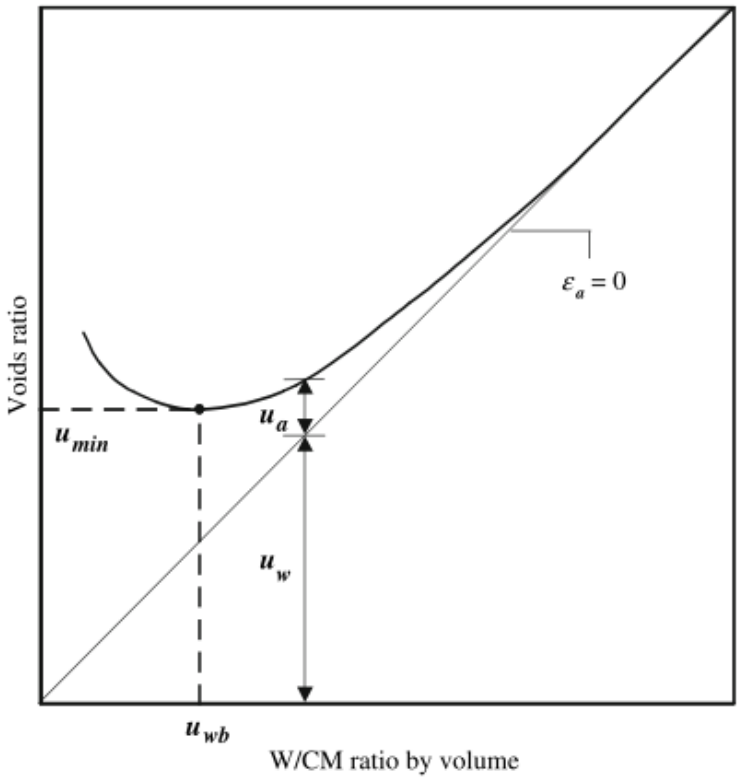

Figure 3-3: Representation of the minimisation of the voids ratio according to (Wong & Kwan, 2008).

Key for Figure 3-3

u	:	Voids ratio, defined as: $\frac{\text{volume of voids}}{\text{solid volume of powder}}$
$u_{\min}$	:	Minimum voids ratio
u_{wb}	:	Basic water ratio (w/cm which yields minimum void content)
u_w	:	Water ratio, defined as: $\frac{\text{water volume}}{\text{solid volume of powder}}$
u_a	:	Actual air ratio, defined as: $u - u_w$
ε_a	:	Air content, defined as: $\frac{\text{volume of air}}{\text{bulk volume of powder material}}$

From the mass reading at each w/cm ratio, the solid volume of powder material in the mould is determined according to *Eqn. 3-1*. The solid volume fraction is then defined by *Eqn. 3-2*. According to Wong & Kwan (2008), when starting from a w/cm = 1, the solid fraction will increase to a maximum and thereafter begin to decrease again. The maximum solid fraction is taken to be the maximum packing density.

$$V_C = \frac{M}{\rho_w u_w + \rho_\alpha R_\alpha + \rho_\beta R_\beta} \qquad \textit{Eqn. 3-1}$$

Where: M = Mass of paste in mould

V_c = Solid volume of powder materials

R_α = Volumetric ratio of powder material α

R_β = Volumetric ratio of powder material β

ρ_w = Density of water

ρ_α = Particle density of material α

ρ_β = Particle density of material β

$$\phi = \frac{V_C}{V} \qquad \textit{Eqn. 3-2}$$

Where: V = Volume capacity of mould

ϕ = Solid volume fraction

The method followed for this research was largely equivalent to that proposed by Wong & Kwan (2008) but the following adaptations were necessary:

- The mould used had the following dimensions: approx. Ø = 60 mm, height = 60 mm and volume of 200 ml (i.e. within the range of dimensions proposed by the authors)
- The total starting volume (powder material + first increment of water) was kept constant at 0.75 l for all mixtures.
- Instead of manufacturing a new paste mixture for each w/cm ratio to be tested, the same powder material was used to test several w/cm ratios. The primary reason therefore was to prevent the use of excessive volumes of material. Instead of beginning at a high w/cm ratio, the mixing regime began at a low w/cm ratio (0.4 by volume) and the water content was increased incrementally during the test after filling the mould at each w/cm and taking a mass reading.
- Two variations in the method of filling and compacting material in the mould were investigated. The first variation was the filling of the mould to excess followed by vibration

on a vibrating table for a fixed period. The second was the filling of the mould to the approximate halfway mark followed by vibration for 30 s. Thereafter it was filled to excess and vibrated for a further 30 s and any remaining material was removed with a straight edge, being careful not to further compact the specimen.

- After measuring the mass of material required to fill the cylindrical mould at each w/cm, the material was placed back into the mixer and a further increment of water was added. Then, a further 3 mins of mixing at a low speed was completed before repeating the mass measurement.
- To prevent the evaporation of moisture from the mixture for the duration of testing, an impermeable sheet was placed over the mixing bowl while the mould was being filled. Furthermore, the material was replaced timeously, and the next increment of water was added immediately thereafter. It was ensured that the entire test, covering approximately 7 different w/cm, was completed within a maximum time of 90 mins so that the onset of initial setting of cement did not influence the packing or any other behaviour of the powder material mixture.

The adaptations made to the Wet Packing Method were not expected to have an adverse effect on the measured packing density. The loss of some material was inevitable when filling the mould to excess, however it was ascertained that this was negligible, and the material volume used for the test was sufficiently large so that any losses did not have a significant effect on test results. Losses were at most between 1-5g of powder paste. To portray the insignificance of this loss on the measured packing density, the extreme case of losing 30g of paste at a low w/cm (0.40) and the resulting impact this had on packing density once the w/cm had increased to the maximum of 0.913 is presented in Table 3-2. The maximum error associated herewith is less than one standard deviation associated with the packing density result for a given material combination (see § 6.1.3.1) and therefore not significant.

Table 3-2: Error associated with loss of powder-paste during testing

	Packing density (-)		
w/cm	0.400	0.540	0.913
Scenario 1: No losses	0.306	0.359	0.521
Scenario 2: 30g paste lost when w/cm = 0.4	0.306	0.358	0.518
Difference (-)	-	-0.001	-0.003
% Difference	-	-0.16	-0.54

3.3.2 Centrifugal consolidation

Centrifugal consolidation has been used to determine the packing density of powder materials in the past (Fennis, 2011; Van Der Putten *et al.*, 2017). The method comprises the compaction of a powder-paste sample (with known solid and liquid volume) by centrifugal force. During centrifuging, excess water surrounding particles is expelled, leaving only the water which is contained between the interstices of the powder material and a layer of water on the surface. The

volume of excess liquid is removed and recorded. This value can then be subtracted from the initial water content to calculate the water content remaining within the paste which is assumed to be equivalent to the void volume after compaction. Packing density can then be determined according to *Eqn. 3-3*. m_{powder} (kg) is the mass of powder material, m_{water} (kg) is the mass of water remaining in the particle structure after centrifuging and ρ_{avg} (kg/m^3) is the density of the powder (taken as the harmonic mean of the densities of various powders in the mixture)

$$PD_{after} = \frac{1000kg/m^3}{1000kg/m^3 + \rho_{average} \cdot \frac{m_{water}}{m_{powder}}} \qquad Eqn.\ 3\text{-}3$$

The measured packing density is dependent on the water powder ratio used in the analysis and therefore, testing of a range of w/p ratios is necessary. Methods proposed by Fennis (2011) and Van Der Putten (2017) are slightly different in the way that the packing density is determined. According to Fennis (2011), centrifugal consolidation can only be used to determine maximum packing density if used in combination with another test method which determines packing density indirectly (such as via water demand). Furthermore, she advised a minimum of three w/p ratios be tested to achieve repeatable results.

Van Der Putten (2017) also tested paste mixtures of three different w/p ratios. Van Der Putten (2017) defined these ratios based on flow requirements such that the mixture with highest ratio had a mini-slump flow of no greater than 300 mm and did not segregate and the lowest ratio was sufficiently fluid for transferring the paste into a test tube for centrifuging. All mixtures contained SP of a predetermined saturation dosage to ensure effective dispersion of particles.

Paste mixtures with the highest w/p were tested first. A value for the packing density of the paste before centrifuging (PD_{before}) was calculated according to *Eqn. 3-4*. The mixture was mixed in a mechanical mixer, ensuring proper distribution of water and SP and then paste samples of known mass were contained in four test tubes. Thereafter, test tubes were centrifuged for 15 mins at 3500 rpm. During centrifuging, powder particles are compacted, and less water is required to fill the interstitial space between particles. This results in the accumulation of a layer of excess water forming on the surface of the compacted paste. On the completion of centrifuging, the volume of excess water is removed by pipette and recorded. Packing density of the centrifuged sample (PD_{after}) can then be calculated using *Eqn. 3-3*.

$$PD_{before} = \frac{V_{powder}}{V_{powder} + V_{water}} \qquad Eqn.\ 3\text{-}4$$

The volume of water remaining in the sample is then determined and the w/p describing the centrifuged sample after this water has been removed is determined. This w/p is then used for the next test specimen as well as to calculate a new value of PD_{before}. Testing is continued until the packing density calculated before (PD_{before}) and after (PD_{after}) centrifuging converges. The packing density at which these values converge is then taken to be the maximum packing density. An attempt was made to follow methodology similar to Van Der Putten (2017) but no specific

requirement was defined for the fluidity of the starting paste mixture, besides being required to be placed in test tubes.

3.3.3 Mixing energy test

The mixing energy test entails the indirect measurement of packing density by measuring the water demand of a powder material (Hunger, 2010; Fennis, 2011).The experiment entails the measurement of the power consumption of a mixer while mixing a powder-paste as the water content is gradually increased. The water demand corresponds to the water content at the maximum power consumption and can be used to calculate the solid volume fraction of the mixture which equates to the maximum packing density when maximal power consumption is registered. Figure 3-4 portrays the experimental setup and the test procedure is described in the remainder of this section.

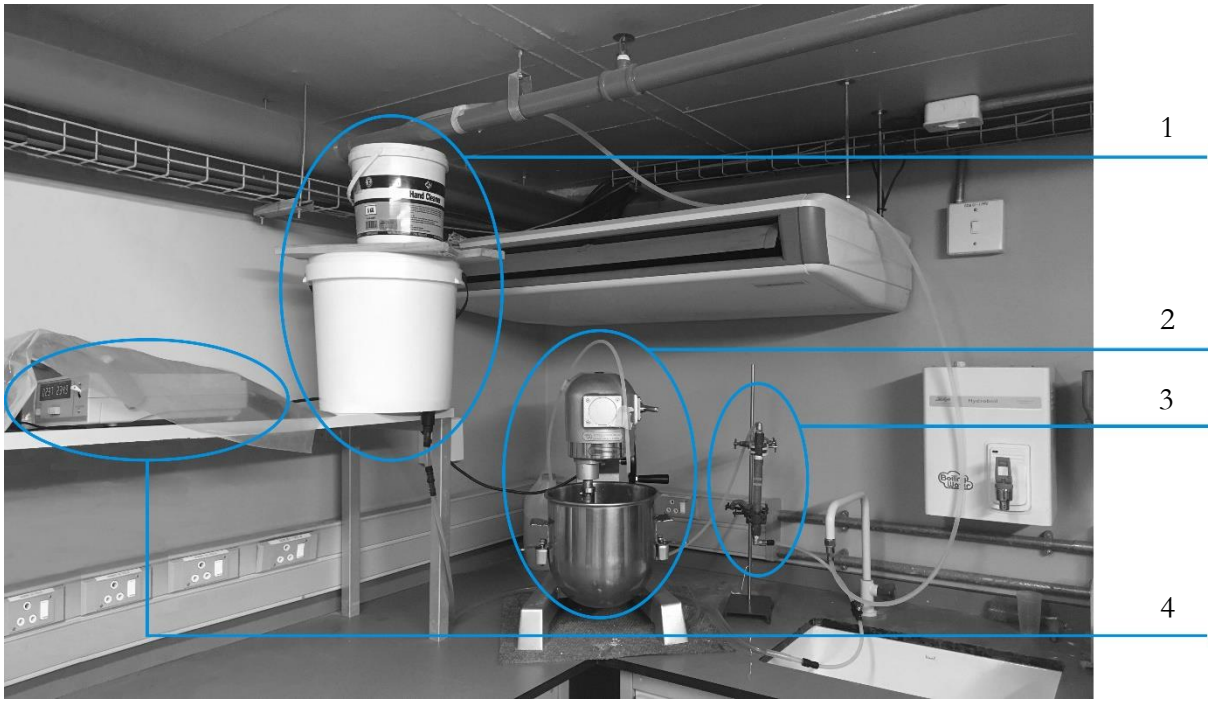

Figure 3-4: Mixing energy experimental setup. 1. Constant pressure head apparatus. 2. Mortar mixer and water inflow pipe. 3. Flowmeter 4. Power meter

As a starting point for the measurement of water demand, the solid volume of powder material was fixed at 850 ml. For consistent transferral of mixing energy to the powder mixture, the combined solid volume of powder and starting water volume was kept in the range between 1.1 and 1.2l. This was determined subjectively by trial and error and corresponds to the size of the mixing bowl used. Furthermore, the volume used could influence the K value assigned to the test method (due to ineffective mixing occurring when a subminimum amount of material is used) and therefore, it was important that the volume of the mixtures remained relatively constant from one material test to another. However, it was still necessary to ensure the starting water content was sufficiently below the material's water demand. This resulted in the starting w/p being in the range of 0.3 - 0.4 (by volume) for all tests.

Powder material was placed in the mortar mixer and dry mixed for approximately 1 min.

Approximately 80 % of initial mixing water was then gradually added to the mortar mixer at the beginning of a 2 min mixing period at medium speed. This was followed by scraping the sides of the bowl and paddle. SP (1.6 % mass of powder material, see § 6.1.2) was then added to the remaining mixing water and added to the mortar mixer at the beginning of another 2 min mixing period at a medium speed, ensuring even distribution of water and SP. Thereafter, the mixture rested for approximately 1 min.

Following this resting period, mixing speed was set to medium and the measurement of power consumption of the mortar mixer with time began. Power measurement was achieved by attaching a power meter (Topward Digital Watt Ammeter 1310) in series between the mortar mixer and AC power supply. The display of the power meter was recorded for the duration of the test and was later used to extract the power consumption at 0,5 s intervals. The power meter measured true power, accounting for phase shift occurring during power measurement.

Water was then allowed to flow into the mixing bowl at a constant rate (at a flow rate between 0.5 and 1 ml/s for all experiments) for the duration of the experiment so that the water content of the mixture at any given time could be calculated and related to the power consumption. The addition of water to a powder material leads to the formation of capillary bridges (pendular bonds) which are localised at particle contacts, causing the agglomeration of particles. The strength of these bonds increases with liquid-vapour surface energy and depends inversely on the square of the particle diameter (Fennis, 2011). While the mixture is still undersaturated, the strength of the agglomerates increases with the addition of liquid and corresponds to increasing power consumption of the mixer.

At the point of saturation, there is an absence of internal liquid-vapour surfaces causing a sudden decrease in bond strength and a decrease in the power consumption of the mixer with further addition of liquid. Figure 3-5 shows the progression of the saturation state of a powder mixture as more water is added. Maximum power consumption occurs at the capillary state where air is assumed to be completely displaced from the particle structure and thereby the water volume at this state is equated to the void volume.

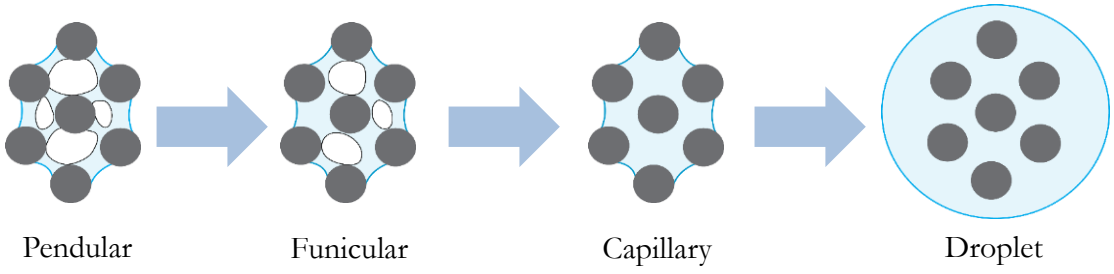

Figure 3-5: Progression of the moisture state of a powder mixture with constant addition of water (Li, 2005)

With a known solid volume of particulate material, the bulk volume at the capillary state is the summation of water volume at the time of maximum power consumption and solid volume of particulate material. Therefore, packing density (which in this instance, is the solid volume fraction at maximum power consumption) is determined according to *Eqn. 2-1*, as described in § 2.3.

$$\alpha = \frac{V_p}{V_b} \qquad \textit{Eqn. 2-1}$$

4 Particle packing modelling

4.1 Introduction

After reviewing several packing models, the CPM was identified by Fennis (2011) as having sound mathematical basis and the potential to incorporate the effect of surface forces into the equations which described geometrical interaction between particles. This led to Fennis (2011) developing an additional module to the CPM which she called the Compaction Interaction Packing Model (CIPM). Compared to the CPM, it achieved similar accuracy for the prediction of the packing density of fine and coarse aggregate materials but enabled increased accuracy of the prediction of the packing density of powder material phases of concrete. As these materials are of primary interest for this research, the application of the CIPM was favoured over the use of other models. However, when considering the entire range of particles within concrete, from a few micrometres to tens of millimetres, the way in which the CIPM was implemented in Microsoft Excel (described in § 4.2.4) limited the number of materials and size classes which could be analysed.

Therefore, this issue was resolved by optimising the packing density of powder materials using the CIPM to specifically account for surface forces and then incorporating the results into an algorithm based on the Modified Andreasen and Andersen Curve (MAAC) to enable the optimisation of the remaining fine and coarse aggregate fractions. The CIPM provides the quantitative assessment of the packing density of powder combinations, guiding the selection of powder constituents. Once defined, the powder combination serves as an input for use in the MAAC algorithm which guides the selection of materials to match an ideal grading curve. Although the MAAC provides no quantitative assessment of packing density, the degree to which the overall material combination matches the proposed ideal grading curve provides a qualitative assessment of packing density, where an exact match corresponds to the maximum packing density possible for the given input materials.

This section addresses the basis of the two models, how they were implemented in Microsoft Excel and the eventual combination of their outputs for the formation of optimised concrete mix designs.

4.2 Compaction Interaction Packing Model

4.2.1 Geometrical interaction

The CIPM improves the CPM by incorporating the effects of surface forces into the equations which previously only described geometrical particle interaction. To understand how the influences specific to powder packing have been incorporated, geometrical interaction within the CPM is first briefly described.

Effectively, particle interaction is modelled by the CPM by considering the interaction of two different particle size classes at a time, followed by the summation of these interactions over the entire range of particle sizes in a mixture of materials. Geometrical interaction is implemented by considering how the packing density of a 'dominant' size class (d_i) is affected by the presence of another size class (d_j) which can be smaller or larger in size than the 'dominant' class. Effects on the dominant class due to the presence of smaller size classes are represented by the loosening

effect (a_{ij}) and effects on the dominant class due to the presence of larger size classes are represented by the wall effect (b_{ij}). These effects are constant for a given size ratio, which is defined as the diameter of a smaller size class over the diameter of a larger size class, and are therefore always a value between 0 and 1. de Larrard (1999) defined *Eqn. 4-1* and *Eqn. 4-2* describing the loosening (a_{ij}) and wall (b_{ij}) effect coefficients.

$$a_{ij} = \sqrt{1-\left(1-\frac{d_j}{d_i}\right)^{1.02}} \qquad \textit{Eqn. 4-1}$$

$$b_{ij} = 1-\left(1-\frac{d_i}{d_j}\right)^{1.5} \qquad \textit{Eqn. 4-2}$$

Experimental packing densities per size class (α_i and α_j) are used in conjunction with a compaction index (K) to determine the virtual packing density (defined in § 2.4.1) per size class (β_i and β_j) in *Eqn. 4-3* and *Eqn. 4-4*. Virtual packing density per size class, interaction coefficients and the volume contribution of each size class to the total solid volume of the mixture (r_i and r_j) is then summated over the range of all size classes present in the mixture and used to calculate the total virtual packing density of the mixture (β_{ti}) according to *Eqn. 4-5*.

$$\beta_i = (1+\frac{1}{K_{\exp}})\alpha_i \qquad \textit{Eqn. 4-3}$$

$$\beta_j = (1+\frac{1}{K_{\exp}})\alpha_j \qquad \textit{Eqn. 4-4}$$

$$\beta_{ti} = \frac{\beta_i}{1-\sum_{j=1}^{i-1}[1-\beta_i+b_{ij}\beta_i(1-1/\beta_j)]r_j-\sum_{j=i+1}^{n}[1-a_{ij}\,\beta_i/\beta_j]r_j} \qquad \textit{Eqn. 4-5}$$

Once the virtual packing density is known, the CPM accounts for the effect of compaction effort to differentiate the theoretical virtual packing density (β_{ti}) from the actual packing density. This is done by assigning a compaction index (K) (introduced in § 2.4.1) to solely describe the compaction process used to achieve a certain packing density. As K tends to infinity, the real packing density (α_t) tends to the virtual packing density (β_t). Fennis (2011) reported data from de Larrard (1999) who defined a range of K values for various packing processes (portrayed in Table 4-1).

Table 4-1: Compaction indexes for various packing processes

Mixture state	Packing process	K value
Dry	Pouring	4.1
	Rodding	4.5
	Vibration	4.75
	Vibration and compression of 10 kPA	9
Wet	Smooth thick paste	6.7
	Mixing energy test	12.2
Virtual	-	∞

The packing density (α_t) for any mixture of materials can then be determined indirectly from *Eqn. 4-6*. This requires that *Eqn. 4-5* and *Eqn. 4-6* are simultaneously satisfied and that the summation portrayed in *Eqn. 4-6* equates to the K value assigned to the experimental packing process used. Finally, analysing all possible combinations of materials, each with their own resulting packing density (α_t), enables the determination of the material combination that gives maximum packing density.

$$K_t = \sum_{i=1}^{n} K_i = \sum_{i=1}^{n} \frac{r_i/\beta_i}{1/\alpha_t - 1/\beta_{ti}} \qquad \textit{Eqn. 4-6}$$

4.2.2 Surface force interaction

Fennis (2011) found the defining equations in the CPM for loosening and wall effects to be potentially problematic when extending the model to size ratios that approach 1 (which is required to more accurately represent a real, continuous distribution of particles). Therefore, she introduced new interaction formulae *(Eqn. 4-7* and *Eqn. 4-8)* where $w_{0,a}$ and $w_{0,b}$ could potentially be used to implement the effects of surface forces on loosening and wall effects. Fennis (2011) based these equations on work by Schwanda (1966) as they satisfied the criteria of $a_{ij} = b_{ij} = 0$ for zero interaction (representing the case for very small size ratios) and $a_{ij} = b_{ij} = 1$ for full interaction (representing the case for a size ratio equal to 1).

$$a_{ij} = \begin{cases} 1 - \dfrac{\log(d_i/d_j)}{w_{0,a}} & \log(d_i/d_j) < w_{0,a} \\ 0 & \log(d_i/d_j) \geq w_{0,a} \end{cases} \qquad \textit{Eqn. 4-7}$$

$$b_{ij} = \begin{cases} 1 - \dfrac{\log(d_j/d_i)}{w_{0,b}} & \log(d_j/d_i) < w_{0,b} \\ 0 & \log(d_j/d_i) \geq w_{0,b} \end{cases} \qquad \textit{Eqn. 4-8}$$

Fennis (2011) then used numerical modelling techniques to investigate the effect of cohesive forces

(which are the result of electrostatic and van der Waal's forces) on the packing and interaction of small spherical particles in the size range of powder materials. The model showed that particles subject to such forces tend to agglomerate with one another as well as adhere to the surfaces of larger particles. Agglomerated particles do not readily fit into the interstices of larger particles (due to their relatively increased size) and cause an increased loosening effect. This results in maximum packing density occurring at a lower volume of larger particles in comparison to particle mixtures not affected by surface forces. Furthermore, adhering of smaller particles to the surface of larger particles also causes larger particles to be pushed away from one another and can also be portrayed as having an increased loosening effect.

The attraction of smaller particles by larger particles also causes the ordered packing of smaller particles near the larger particle. Therefore, a relative decrease in the usual wall effect of large particles on smaller particles is observed. This is not to say that the presence of the larger particle does not influence the packing of the smaller particles, but instead, does so to a lesser extent. The degree to which loosening and wall effects are increased or decreased is dependent on the volume of small particles within the mix. Figure 4-1 portrays the apparent decrease in wall and increase in loosening effects for micrometre (powder) sized particles compared to millimetre-sized particles in binary mixtures with the same size ratio but with the latter not being subject to surface forces.

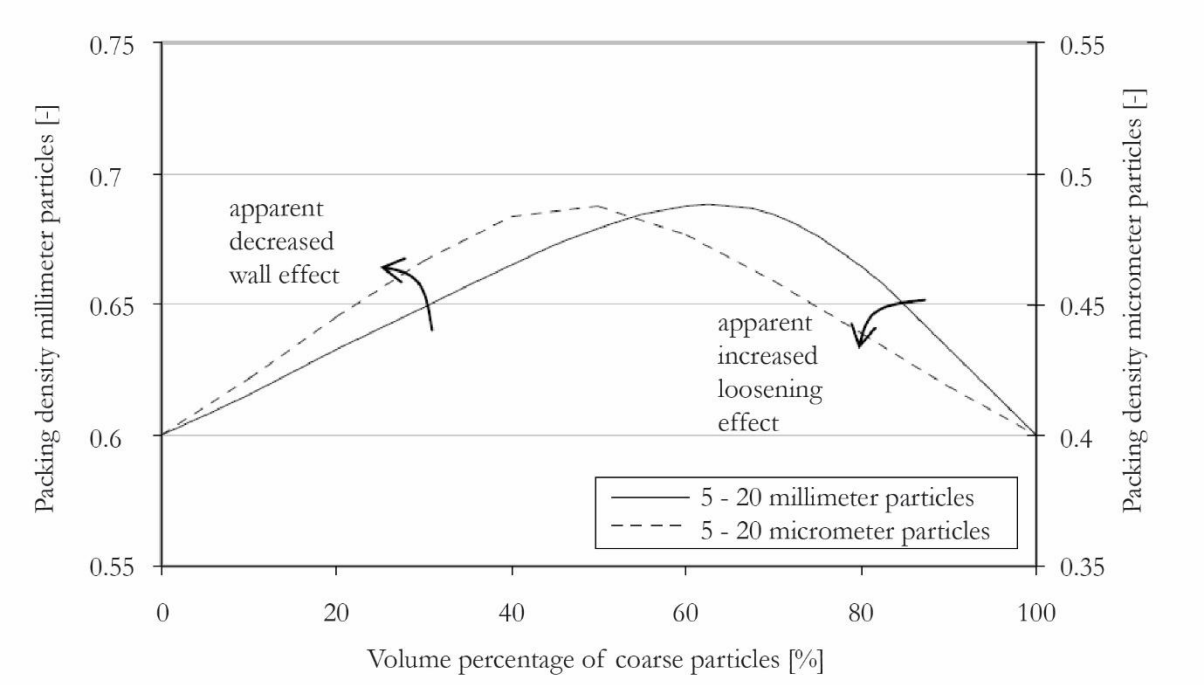

Figure 4-1: Portrayal of increased loosening and decreased wall effects for a micrometre-sized binary mixture compared to a millimetre-sized binary mixture, both with size ratio = 0.5 (Fennis, 2011).

To account for these findings in the new interaction formulae, Fennis (2011) assigned functions to describe $w_{0,a}$ and $w_{0,b}$ which are defined by *Eqn. 4-9* and *Eqn. 4-10* respectively. Fennis (2011) also defined a particle size of $25\mu m$ to be the cut-off diameter size below which the previously mentioned phenomena have a significant effect on the particle interactions. L_a and L_b were

defined as constants that could either increase or decrease the loosening and wall effects, respectively, and w_a and w_b were defined as $w_a = w_b = 1$.

$$w_{0,a} = f_{\text{int},a}(d_j) = \begin{cases} w_a L_a & d_j < 25\mu m \\ w_a & d_j \geq 25\mu m \end{cases} \qquad \textit{Eqn. 4-9}$$

$$w_{0,b} = f_{\text{int},b}(d_i) = \begin{cases} w_b L_b & d_i < 25\mu m \\ w_b & d_i \geq 25\mu m \end{cases} \qquad \textit{Eqn. 4-10}$$

4.2.3 Compaction effectiveness

In addition to increased loosening and decreased wall effects, Fennis (2011) also identified a decreasing effectiveness of compaction effort with a decrease in particle size. This was attributed to the increased interparticle friction due to the presence of surface forces and the inability of compaction to overcome these as they become prevalent. The CPM was able to model the packing density of coarse particles relatively well as there was a good relation between loose packing density, compacted packing density and virtual packing density. This was achieved using the compaction index (K) where higher values represented the application of larger compaction effort and increased shear deformation causing particles to pack closer to one another. Yet, applying equivalent compaction effort to coarse particles and powder particles does not result in equivalent shear deformation or packing density due to the decreased effectiveness of compaction effort. Therefore, Fennis (2011) revised the way to account for this so that a decreased effectiveness could be implemented for powder materials.

For a mixture of mono-sized particles, the compaction energy imparted on a mixture is described within the CPM by a compaction index according to *Eqn. 4-11*. Experimental packing density (α_{exp}) is related to the virtual packing density of the size class by a constant (K_t) which is equivalent to the compaction index (K) of the compaction process. However, for the case of a mixture comprising two mono-size groups of particles (size class 1 and size class 2), the compaction effort is distributed between them according to their size-related geometric interactions (*Eqn. 4-6*) and K_t is now defined as $K_t = K_1 + K_2$, where K_i represents the portion of compaction effort attributed to size class *i*. K_t is still a constant and equivalent to the compaction index (K) of the packing process but K_i varies according to *Eqn. 4-6*.

$$K_t = \frac{1}{\frac{\beta}{\alpha_{\text{exp}}} - 1} \qquad \textit{Eqn. 4-11}$$

Therefore, to implement surface forces, K_t was required to be relatively more effective for larger, more easily compacted particles and less effective for the more difficult to compact, smaller particles. For the same case as above (a mixture of two mono-sized particle groups) K_1 (compaction value for large particle size class) was required to increase relative to K_2 (compaction

value for small particle size class) and K_2 was required to decrease relative to K_1 (Fennis, 2011). To implement this, Fennis (2011) used *Eqn. 4-12* and *Eqn. 4-13,* after de Larrard (1999), which are the general forms of *Eqn. 4-5* and *Eqn. 4-6*

$$K_t = \sum_{i=1}^{n} K_i = \sum_{i=1}^{n} \frac{\frac{\varphi_i}{\varphi_i^*}}{1-\frac{\varphi_i}{\varphi_i^*}} \qquad \textit{Eqn. 4-12}$$

$$\varphi_i^* = \beta_i \left(1 - \sum_{j=1}^{i-1} \left(1 - b_{ij,c} \left[1 - \frac{1}{\beta_j} \right] \right) \varphi_j - \sum_{j=i+1}^{n} \frac{a_{ij,c}}{\beta_j} \varphi_j \right) \qquad \textit{Eqn. 4-13}$$

Where: φ_i = Actual solid volume of class *i*.

φ_i^* = Maximum volume that size class *i* may occupy given the presence of other size classes.

These definitions ensure φ_i is always lower than φ_i^*. For K_2 to be relatively larger than K_1, φ_2/φ_2^* should become lower. Representing $\varphi i/\varphi_i^*$ by *Eqn.* 4-14 (which combines *Eqn. 4-13* and the definition of φ_i) allows the increase in loosening ($a_{ij,c}$) and decrease in wall ($b_{ij,c}$) effects as, described in § 4.2.2, as well as the corresponding change in φ_i/φ_i^*. For a mixture comprising two size classes, decreasing $b_{ij,c}$ leads to an increased φ_2^* and a decreased φ_2/φ_2^* and lower K_2. Conversely, increasing $a_{ij,c}$ leads to a decreased φ_1^* and therefore an increased φ_2/φ_2^* and higher K_1. These effects become more pronounced for increasing applied compaction effort to the extreme that, with infinite compaction effort, the K_i value for the recessive size class is 0.

$$\frac{\varphi_i}{\varphi_i^*} = \frac{r_i \alpha_t}{\beta_i \left(1 - \sum_{j=1}^{i-1} \left(1 - b_{ij,c} \left[1 - \frac{1}{\beta_j} \right] \right) \varphi_j - \sum_{j=i+1}^{n} \frac{a_{ij,c}}{\beta_j} \varphi_j \right)} \qquad \textit{Eqn. 4-14}$$

Varying the compaction index in this way does not require $a_{ij,c}$ and $b_{ij,c}$ to be equivalent to a_{ij} and b_{ij}, (defined in § 4.2.2). However, Fennis (2011) defined $a_{ij,c}$ and $b_{ij,c}$ (*Eqn. 4-15* and *Eqn. 4-16)* to follow a similar format to *Eqn. 4-7* and *Eqn. 4-8 (*describing the influence of surface effects). New constants, C_a and C_b, describe the extent to which compaction becomes relatively more ineffective for smaller particles relative to larger ones. Once again, $w_a = w_b = 1$.

$$a_{ij,c} = \begin{cases} 1 - \dfrac{\log(d_i/d_j)}{w_{0,a}} & \log(d_i/d_j) < w_{0,a} \\ 0 & \log(d_i/d_j) \geq w_{0,a} \end{cases} \qquad w_{0,a} = \begin{cases} w_a C_a & d_j < 25\mu m \\ w_a & d_j \geq 25\mu m \end{cases} \qquad \textit{Eqn. 4-15}$$

$$b_{ij,c} = \begin{cases} 1 - \dfrac{\log(d_j/d_i)}{w_{0,b}} & \log(d_j/d_i) < w_{0,b} \\ 0 & \log(d_j/d_i) \geq w_{0,b} \end{cases} \qquad w_{0,b} = \begin{cases} w_b C_b & d_i < 25\mu m \\ w_b & d_i \geq 25\mu m \end{cases} \qquad \textit{Eqn. 4-16}$$

Upon running simulations incorporating the effects of the constants L_a and L_b and C_a and C_b, Fennis (2011) found that resulting packing densities were independent of the values chosen for L_a and L_b. Instead, the compaction-interaction effect was solely dependent on $a_{ij,c}$ and $b_{ij,c}$ and therefore C_a and C_b. C_a and C_b were thereby able to account for changes to the wall and loosening effects as well as reduced effectiveness of compaction with a decrease in particle size. This implied that any non-zero value might be assigned to L_a and L_b and the same packing density predicted. However, for consistency, mathematical robustness and physical interpretation, Fennis (2011) set L_a to C_a and L_b to C_b which can be portrayed as $a_{ij,c} = a_{ij}$ and $b_{ij,c} = b_{ij}$. This ensured the virtual packing density was always larger than the compacted one and enabled the application of *Eqn. 4-5* and *Eqn. 4-6* instead of the more awkward general forms in *Eqn. 4-12* and *Eqn. 4-13*.

4.2.4 Implementation in Microsoft Excel

The CIPM was implemented using Microsoft Excel and was based on spreadsheets initially developed by Fennis (2011) which were further adapted for this research. This section describes model inputs, the operations performed on these inputs and the calibration of the model for this research.

4.2.4.1 Input

4.2.4.1.1 Particle size classes

To accurately represent real particle size distributions, it is favourable to define size classes that have a size ratio $d_{\min}/d_{\max}$ close to 1. However, for practicality and reasonable computing times, input size classes were chosen to have a size ratio of at least 0.5. Each size class is determined as the geometric mean (d_i^{i+1} in *Eqn. 4-17*) of an upper and lower size used in the particle size analysis. This resulted in the definition of 12 size classes for the powder materials being considered. The particle size distribution, portrayed as the volume percent material retained at each size class, is then input into the model for each material under consideration.

$$d_i^{i+1} = \sqrt{d_i d_{i+1}} \qquad \textit{Eqn. 4-17}$$

4.2.4.1.2 Packing density per size class

The model requires an experimental packing density for each discrete size class as an input. It is possible to determine this for aggregate materials which can be manually separated into size classes defined by the geometric mean of the upper and lower sieves used in a sieve analysis. However, it is impossible to separate powder materials into their various size classes. Therefore, Fennis (2011) accounted for this by allowing for the use of an experimental packing density which is determined for each powder material and not each size class. An assumption is made that if each size class were able to be separated and the individual packing density determined per size class, these individual packing densities would be equivalent to one another. Implementing this assumption, the model is used to perform a reverse calculation, using the experimental powder packing density to work back to the packing density per size class. This calculation is further described in § 4.2.4.4.

4.2.4.1.3 Compaction index

Implementation of the model in Microsoft Excel allows the packing density of each input material to have been derived using different techniques. Each input material is assigned its own compaction index (K) corresponding to the technique used to determine its packing density. For example, powder packing densities determined using the mixing energy test would correspond to K=12.2 and the packing density of a fine aggregate material determined by pouring the material into a mould would correspond to K=4.1 (see Table 4-1 and § 4.2.4.2). These values are required to determine the virtual packing density per size class (α_i) which are eventually used to determine the virtual packing density of a defined mixture of input materials (β_{ti}). The virtual packing density of the mixture of materials is then converted to a real packing density (α_t) using a single K_t corresponding to the packing process to be used to make up the final mixture of materials. For example, Fennis (2011) uses K=9 to correspond to the making of a flowable concrete mixture.

4.2.4.1.4 Definition of interaction variables

Constants C_a and C_b are input to describe increased loosening and decreased wall effects as per *Eqn. 4-15* and *Eqn. 4-16*. The diameter below which increased loosening and decreased wall effects occur (d_j and d_i in *Eqn. 4-15* and *Eqn. 4-16* respectively) must also be defined. Fennis (2011) set these variables as $C_a = 1.5$, $C_b = 0.2$ and $d_j = d_i = 25\mu m$ with the disclaimer that these variables are sensitive to different materials and superplasticiser and should be determined for the specific materials and superplasticiser to be used. Therefore, calibration of the model using experimental packing density data was necessary. This is further described in § 4.2.4.2.

4.2.4.1.5 Material combinations

To determine the powder material combination giving the maximum packing density, a matrix was developed which represented all possible combinations of the 5 input powder materials (§ 3.1) in 5 % volume increments. For example, considering a case where the powder phase comprised only CEM II A-L 52.5N and KB2, only the packing density of the combinations in Table 4-2 would be analysed. This was imposed as a practical limitation due to exponentially increasing computing time with a decrease in the % increments analysed.

Table 4-2: All material combinations for a powder phase comprising only KB2 and CEM II A_L 52.5 N

Combination No.	Powder material volume %	
	KB2	CEM II A-L 52.5N
1	0	100
2	5	95
3	10	90
4	15	85
5	20	80
6	25	75
7	30	70
8	35	65
9	40	60
10	45	55
11	50	50
12	55	45
13	60	40
14	65	35
15	70	30
16	75	25
17	80	20
18	85	15
19	90	10
20	95	5
21	100	0

The model uses the combination matrix and particle size distribution to define the volume % contribution of each material size class to the total solid volume (r_i and r_j in § 4.2.1). Once all possible combinations have been analysed and the resulting packing density (α_t) determined for each material combination, the material combination which enabled the maximisation of α_t could be determined. Furthermore, for the case of a required minimum cement content, limiting criteria was specified to consider only the material combinations which comprised a cement volume % equal to or greater than the minimum specified content. For the same example of CEM II A-L 52.5N and KB2 above, with a defined minimum cement content of 50 %, this would result in the model considering only the material combinations up to combination number 11 in Table 4-2.

4.2.4.2 Sequence of calculation procedures

Once input parameters in § 4.2.4.1 had been defined, a macro (a set of programming instructions to automate various tasks) which has been programmed using Visual Basic for Applications (VBA) in Microsoft Excel is set to run. To clarify the operations of the macro, a sample calculation is demonstrated in.

Particle size classes for each material are arranged in descending order of particle size class. The input packing density per size class (α_i) and compaction index (K) for the corresponding packing process is used to calculate the virtual packing density per size class (β_i and β_j for each

interaction with the dominant size class). The % volume contribution of each material and size class (r_i and r_j) is determined according to the material combination matrix and the particle size distribution.

As the 'dominant' size class within the total mixture is not yet known, each particle size class is individually considered to be the 'dominant' size class. The interaction coefficient, describing either the loosening (a_{ij}) or wall (b_{ij}) effect, is calculated for the interaction of the 'dominant' size class with every other size class present in the mixture according to *Eqn. 4-15* and *Eqn. 4-16*. When the smallest size class in the mixture is considered 'dominant', the only interaction experienced with other particles will be due to the wall effect. When the largest size class in the mixture is considered 'dominant', the only interaction experienced with other particles will be due to the loosening effect. For the case of any other size class being considered 'dominant', interaction will always be the result of combined loosening and wall effects.

$$a_{ij,c} = \begin{cases} 1 - \dfrac{\log(d_i/d_j)}{w_{0,a}} & \log(d_i/d_j) < w_{0,a} \\ 0 & \log(d_i/d_j) \geq w_{0,a} \end{cases} \qquad w_{0,a} = \begin{cases} w_a C_a & d_j < 25\mu m \\ w_a & d_j \geq 25\mu m \end{cases} \qquad \textit{Eqn. 4-15}$$

$$b_{ij,c} = \begin{cases} 1 - \dfrac{\log(d_j/d_i)}{w_{0,b}} & \log(d_j/d_i) < w_{0,b} \\ 0 & \log(d_j/d_i) \geq w_{0,b} \end{cases} \qquad w_{0,b} = \begin{cases} w_b C_b & d_i < 25\mu m \\ w_b & d_i \geq 25\mu m \end{cases} \qquad \textit{Eqn. 4-16}$$

Particle interactions with the 'dominant' size class (taken to be d_i) are summated over the entire range of size classes in the mixture (i.e. interaction of d_i with d_1, d_i with $d_2 \ldots$ d_i with d_n for n size classes). This allows for the construction of the denominator of *Eqn. 4-5*, which is the summation of all the particle interactions within the mixture. The total virtual packing density of the mixture (β_{ti}) is then determined. This is portrayed as β_{ti} when particle d_i is assumed dominant (i = 1, 2, 3… n for n size classes). As each size class is individually considered to be 'dominant', this leads to the determination of a β_{ti} value for every size class in the mixture: β_{t1} for d_1 dominant, β_{t2} for d_2 dominant, β_{t3} for d_3 dominant and up to and including β_{tn} for d_n dominant in a mixture comprising n size classes.

$$\beta_{ti} = \frac{\beta_i}{1 - \sum_{j=1}^{i-1}[1 - \beta_i + b_{ij}\beta_i(1 - 1/\beta_j)]r_j - \sum_{j=i+1}^{n}[1 - a_{ij}\,\beta_i/\beta_j]r_j} \qquad \textit{Eqn. 4-5}$$

The minimum value of β_{ti} across all size classes is then used in *Eqn. 4-6* for the indirect calculation of the actual packing density (α_i) of the mixture for a given compaction process (which is described

by compaction index K). The minimum value of β_{ti} is used due to the physical interpretation of these expressions. Any value above the minimum represents an impossible case of packing density. de Larrard (1999) constructed the mathematical proof showing that for a mixture comprising multiple size classes, there exists an impenetrability constraint whereby the virtual packing density of the mixture is always equal to or less than the virtual packing density calculated for 'dominant' size class d_i (with $i = 1, 2, 3 \ldots n$ for n size classes). To satisfy this constraint for all size classes, β_{ti} must therefore be the minimum of all possible β_{ti} (with $i = 1, 2, 3 \ldots n$ for n size classes).

Solving for α_t indirectly requires that *Eqn. 4-5* and *Eqn. 4-6* are satisfied simultaneously and that K_t in *Eqn. 4-6* is equivalent to the compaction index (K) describing the applied compaction effort in the process to construct the packing. Therefore, a macro was programmed in Microsoft Excel to automatically iterate the value of α_t until these criteria are satisfied. As it is known that the actual packing density (α_t) can never be equivalent to the virtual packing density (β_{ti}), the first iteration of α_t is taken as $\alpha_t = \beta_{ti} - 0.005$. The resulting K_t is calculated and if it is not equivalent to the compaction index (K) then another iteration of α_t is made. α_t is continuously iterated until a value which satisfies the criteria in *Eqn. 4-5* and *Eqn. 4-6* is obtained.

$$K_t = \sum_{i=1}^{n} K_i = \sum_{i=1}^{n} \frac{r_i/\beta_i}{1/\alpha_t - 1/\beta_{ti}} \qquad \textit{Eqn. 4-6}$$

Once α_t is solved for the particular material combination defined at the outset, α_t for the next material combination is solved by following the same procedures. Once all combinations have been assessed, the combination enabling the maximisation of α_t is taken as the 'optimised' powder material combination.

4.2.4.3 Calibration of model

At the outset, the following constants needed to be defined to calibrate the model for the accurate representation of the materials and experimental methods used for determining packing density:

- Compaction index (K)
- Interaction constant representing the loosening effect (C_a)
- Interaction constant representing the wall effect (C_b)
- The 'cut-off' diameter (d_c) below which interaction effects due to surface forces significantly effect packing density

Calibration entailed the use of experimental packing density data and a series of parametric studies which were aimed at minimising the error between the packing density predicted by the model and the packing density which was recorded experimentally for several material combinations. Combinations are portrayed as 'powder volume fraction' in Appendix B, Table B-1.

4.2.4.3.1 Determination of the compaction index (K)

As already mentioned, only powder material packing densities were determined using the CIPM and therefore, the mixing energy test, described in § 3.3.3, was used to assess the packing density of all powder material combinations. This was the same test used by Fennis (2011) when developing the CIPM where she defined the compaction index for the procedure as K = 12,2. However, this was reassessed for the test setup in this research.

The determination of a compaction index describing an experimental method requires that the packing density of a material is first determined experimentally using the method. Thereafter, the packing density of the same material is determined experimentally using a reference method which has an already-known compaction index. Ideally the packing density should be determined for a mono-sized material so that any particle interactions can be ruled out and the resulting compaction index will be solely dependent on the compaction effort applied by the method. However, as has already been mentioned, the most realistic mixture that can be constructed to be close to a mono-sized material, is a material mixture comprising a single discrete size class, which is defined by the material retained between two standard sieve sizes.

The material used for calibration was Philippi dune sand fractions which passed a 300 μm sieve and were retained on a 150 μm sieve (represented by the geometric mean of the upper and lower sieve sizes, equivalent to 212.13 μm). This size class was chosen as it was the smallest, practically separable size class which was not expected to be significantly affected by surface forces.

The filling of a mould of known volume by pouring material from a fixed height above the mould was used as the reference test method. The solid volume fraction of the material in the mould was determined and taken to be the packing density. The compaction effort applied in this test method has been widely reported to be described by K= 4,1 (de Larrard, 1999; Fennis, 2011). Thereafter, the packing density determined by the reference method (α_{exp}) is used for the calculation of the virtual packing density (β) of the size class using *Eqn. 4-11*.

$$K_t = \frac{1}{\frac{\beta}{\alpha_{exp}} - 1} \qquad \textit{Eqn. 4-11}$$

Following this, another experimental packing density was determined for the same material using the mixing energy test. Using the virtual packing density (β) determined from the reference test method result and a new value of experimental packing density (α_{exp}) from the mixing energy test, *Eqn. 4-11* was then solved for K_t. For the instance of a mono-sized particle mixture, K_t is then equivalent to K, the compaction index describing the mixing energy test (see § 4.2.3).

4.2.4.3.2 Determination of interaction coefficients and cut-off diameter

Once a compaction index had been assigned to the mixing energy test, the remaining constants used in the CIPM could be determined. To fit the constants, material combinations analysed by the model were equivalent to those tested experimentally. To solve for the three constants, a

limited, multi-variable analysis was proposed as follows:

- The cut-off diameter (d_c), which is implemented as d_i and d_j in *Eqn. 4-15* and *Eqn. 4-16,* was first fixed at the value proposed by Fennis (2011) ($d_j = d_i = 25\mu m$)
- This allowed for the determination of C_a and C_b. Firstly, C_a was held constant while C_b was varied and the predicted packing density for each material combination was recorded for each combination of C_a and C_b with $d_j = d_i = 25\mu m$.
- Thereafter, C_b was held constant while C_a was varied and the predicted packing density for each material combination was recorded for each combination of C_a and C_b with $d_j = d_i = 25\mu m$.
- As the CIPM was developed based on there being increased loosening and decreased wall effects due to surface forces, only values of $C_a > 1$ and values of $0 < C_b < 1$ were assessed. Within these criteria, variation of each of these variables was performed in increments of 0.10.
- Following the variation of C_a and C_b, the values for these constants were finalised by assessing which combination enabled the minimisation of the average error (between predicted packing density and actual, experimental packing density) for cement combinations with each limestone type as well as across all cement/limestone combinations that were assessed experimentally (see Appendix B, Table B-2 for a description of this error analysis).
- Thereafter, the finalised combination of C_a and C_b was held constant while the cut-off diameter (d_c) was varied in increments of 5 μm from 5 μm to 125 μm.
- The value for the cut-off diameter (d_c) was finalised by assessing which value minimised the same average errors described in Appendix B, Table B-2.

4.2.4.4 Calculation of packing density per size class

Powder materials cover multiple size classes and therefore the packing density per size class (α_i), a required into to the CIPM (§ 4.2.4.1.2), cannot be realistically determined. Instead, the packing density is usually determined for the whole material (comprising multiple size classes) and cannot be used as a direct input into the CIPM. This is resolved by performing a reverse calculation within the CIPM to determine packing density per size class (α_i) from the experimental packing density for the powder material. This corresponds to using the experimental packing density as α_t in the CIPM to find α_i instead of the usual procedure of using known packing densities per size class (α_i) to determine α_t.

The CIPM was developed with the assumption that each material could be represented by a defined number of size classes, each with constant packing density α_i. Therefore, the reverse procedure is performed based on this assumption. Using the experimental packing density, virtual packing densities are calculated, and compaction-interaction effects are incorporated to arrive at

the α_i for each material size class. Due to the reliance of the value of α_i on the model, it is acknowledged as a comparative input parameter. For further clarity, see the sample calculation in Appendix C.

4.3 Modified Andreasen and Andersen Curve

4.3.1 Input parameters

As discussed in § 2.4.2, Funk and Dinger (1994) proposed the Modified Andreasen and Andersen Curve (MAAC) (portrayed in *Eqn. 2-9)* to formulate an optimal particle size distribution and indirectly achieve maximum packing density. To determine the optimal solution, the minimum and maximum particle size of the materials to be optimised (D_s and D_L respectively) need to be specified along with a distribution modulus (q) which practically influences the relative portions of coarse and fine material proposed in the optimal solution.

$$\frac{CPFT}{100\%} = \frac{D^q - D_S^q}{D_L^q - D_S^q} \qquad \textit{Eqn. 2-9}$$

Where: CPFT = Cumulative percent finer than

D = Particle size class under consideration

D_S = Smallest particle size class

D_L = Largest particle size class

q = Distribution modulus

With these inputs, a cumulative percent finer than value is determined at each predetermined size class in the range $(D_S, D_L]$. As for the CIPM, size classes were determined according to the geometric mean of an upper and lower particle size used in the particle size analysis (either upper and lower sieve size for aggregates or upper and lower size class used in the laser diffraction procedure for powder materials). For consistency with the application of the CIPM, adjacent size classes were defined to have size ratios no less than 0.5. The cumulative percent finer than curve then allows for the calculation of the amount of material in each size class and an experimental mixture can be constructed accordingly.

$$D_i^{i+1} = \sqrt{D_i D_{i+1}} \qquad \textit{Eqn. 4-18}$$

However, realistically, concrete constituent materials comprise several size classes and therefore it is impossible to match the MAAC exactly when constructing a real mixture comprising many different materials. It is usually the case that more than one material spans the same size classes and therefore, when determining the amount of material required to meet the CPFT for a certain

size class, the contribution from each of the materials needs to be considered. With increasing material constituents this becomes more difficult. At best, an attempt can be made to match the overall distribution of the combined concrete materials to the MAAC by manually changing the portions of constituent materials until the overall grading of all materials is similar to the CPFT proposed by the MAAC. The closer that the actual combined grading is to the CPFT proposed by the MAAC, the better the optimisation.

Manual optimisation becomes tedious and more complex when certain criteria are required to be met such as minimum cement or powder material content. Therefore, an algorithm developed by Hüsken (2010) is applied in this research to automate the selection process. The algorithm selects material quantities so that the overall particle size distribution best matches the ideal particle size distribution proposed by the MAAC while also making allowance for limiting criteria such as minimum cement content and water-powder ratio.

4.3.2 Implementation in Microsoft Excel

For consistency, the same nomenclature used by Hüsken (2010) is used for the description of the algorithm in this section. Hüsken's (2010) algorithm considers the volumetric proportions of all concrete constituents $(k = 1,2,...,m)$ including air and water. The particle size (D) in *Eqn. 2-9* is taken as the geometric mean (D_i^{i+1}) of the upper and lower sieve sizes as represented in *Eqn. 4-18*. This research comprised the use of materials with a maximum size passing a 13.2 mm sieve and retained on 9.5mm sieve and a minimum size passing 0.36 μm but retained above 0.31 μm. In total, 22 size classes were defined to describe all constituents across the range defined by these maximum and minimum particle sizes.

4.3.2.1 Definition of a target function

The optimisation algorithm entails the construction of a target function which is the goal of the optimisation problem. In this instance, the target function is the deviation between the desired, ideal grading curve (that proposed by the MAAC) and the particle size distribution of constituent materials. Solving the optimisation problem requires the minimisation of the target function and therefore results in a curve fitting problem which is dependent on the particle size distribution of constituent materials and their volumetric proportions within the mix design. To solve the curve fitting problem, the residual sum of squares (RSS), portrayed in *Eqn. 4-19,* was minimised.

$$RSS := \sum_{i=1}^{n} e_i^{\,2} = \sum_{i=1}^{n} (P_{mix}(D_i^{i+1}) - P_{tar}(D_i^{i+1}))^2 \rightarrow \min \qquad \textit{Eqn. 4-19}$$

$P_{mix}(D_i^{i+1})$ is the cumulative percent finer than (CPFT) fraction for each size class (D_i^{i+1}) in the overall particle size distribution of constituent materials and $P_{tar}(D_i^{i+1})$ represents the proportions proposed by the MAAC for each size class (D_i^{i+1}) according to the following:

$$P_{tar}(D_i^{i+1}) = \frac{(D_i^{i+1})^q - D_{\min}^q}{D_{\max}^q - D_{\min}^q} \qquad \forall D_i^{i+1} \in [D_{\min}, D_{\max}]$$

$$D_{\min} = D_i \qquad \text{for } P(D_{i-1}) = 0 \wedge P(D_i) > 0$$

$$D_{\max} = D_i \qquad \text{for } P(D_{i-1}) < 100 \wedge P(D_i) = 100$$

The curve fit is assessed by the evaluation of the R^2 statistic, portrayed in *Eqn. 4-20*. A value closer to 1 indicates that the proposed $P_{mix}(D_i^{i+1})$ approaches the size distribution according to the MAAC, given by $P_{tar}(D_i^{i+1})$.

$$R^2 = 1 - \frac{\sum_{i=1}^{n}(P_{mix}(D_i^{i+1}) - P_{tar}(D_i^{i+1}))^2}{\sum_{i=1}^{n}(P_{mix}(D_i^{i+1}) - \overline{P_{mix}})^2} \qquad \forall D_i^{i+1} \in [D_{\min}, D_{\max}] \qquad \textit{Eqn. 4-20}$$

$\overline{P_{mix}} = \frac{1}{n}\sum_{i=1}^{n} P_{mix}(D_i^{i+1})$ is the average CPFT across a particle size distribution with *n* size classes.

4.3.2.2 Definition of variables for optimisation

Variables control the composition of $P_{mix}(D_i^{i+1})$ and best match this value to $P_{tar}(D_i^{i+1})$. These are values that can be adjusted by the algorithm and enable the minimisation of the target function. Hüsken's (2010) algorithm requires the definition of a total solid volume (V_{sol}^{tot}) (see § 4.3.2.3) and then uses the volumetric proportion ($v_{sol,k}$) of each solid material (*Eqn. 4-21)* as controlling variables for the optimisation procedure.

$$v_{sol,k} = \frac{V_{sol,k}}{V_{sol}^{tot}} \qquad \text{for } k = 1,2,3...,(m-2) \qquad \textit{Eqn. 4-21}$$

The volumetric proportion of each solid material then influences the computed CPFT for a mixture comprising *k* different materials and *n* size classes through *Eqn. 4-22*.

$$Q_{mix}(D_i^{i+1}) = \frac{\sum_{k=1}^{m-2} \frac{v_{sol,k}}{\rho_{sol}} Q_{sol,k}(D_i^{i+1})}{\sum_{i=1}^{n}\sum_{k=1}^{m-2} \frac{v_{sol,k}}{\rho_{sol,k}} Q_{sol,k}(D_i^{i+1})} \qquad \textit{Eqn. 4-22}$$

Where: $Q_{sol,k}(D_i^{i+1})$ is the residue of material *k* on sieve *i*;

And $\rho_{sol,k}$ is the relative density of material *k*.

Finally, the computed CPFT for each size class (D_i^{i+1}) of the mixture is given by *Eqn. 4-23*.

$$P_{mix}(D_i^{i+1}) = P_{mix}(D_{i-1}^{i}) - Q_{mix}(D_i^{i+1}) \qquad \textit{Eqn. 4-23}$$

4.3.2.3 Definition of constraints

Constraints represent restrictions to variables and are used to enforce practical limitations or certain boundary conditions. Hüsken (2010) differentiates between two different types of constraints, namely, physical and policy constraints. Physical constraints are determined by the physical nature of the optimisation problem and in this case, include a non-negativity constraint and a volumetric constraint. The non-negativity constraint invalidates any solution that has a negative volumetric proportion ($v_{sol,k}$) or where the total solid volume is negative, using the inequality in *Eqn. 4-24*. The volumetric constraint ensures that the sum of the volumetric proportions of all solid materials ($v_{sol,k}$) equates to 1 (*Eqn. 4-25*) and that the total volume of all constituents (solid and liquid) equates to 1 m^3 (*Eqn. 4-26*). In this instance, V_{air} was approximated to 0 m^3.

$$v_{sol,k} \geq 0 \qquad k = 1,2,3...,(m-2) \qquad \textit{Eqn. 4-24}$$

$$\sum_{k=1}^{m-2} v_{sol,k} = 1 \qquad \textit{Eqn. 4-25}$$

$$V_{concrete} = V_{aggregate} + V_{cement} + V_{SCM} + V_{filler} + V_{water} + V_{admixture} + V_{air} = 1m^3 \qquad \textit{Eqn. 4-26}$$

Policy constraints represent the requirements of the mix design such as the water: cement ratio (w/c), water-powder ratio (w/p) and powder material ratio. Each of these are incorporated into the optimisation process through their relationship to the volumes of the various constituents. For this research, the term 'powder materials' consisted of the materials listed in Table 3-1 in § 3.1 and binder materials consisted of CEM II A-L 52,5N and FA. A minimum w/c is usually specified to achieve a desired strength class whereas w/p infers the paste content of a mix and a powder ratio can be specified to represent required blends of materials in the powder phase.

The impact of specifying constraints in this way on the optimisation target is, however, not considered and treats the optimisation target and constraints equally. Therefore, the specification of constraints has the potential to cause a deviation from the optimised grading proposed by the minimisation of the target function.

4.3.2.4 Optimisation solution

A spreadsheet was developed in Microsoft Excel which required the manual input of the parameters of maximum and minimum particle size, particle size distribution of each constituent material and distribution modulus (q) (the selection of which is discussed in § 4.3.3). Thereafter, the various relationships between the inputs and the target function were established according to § 4.3.2.1, incorporating the variables and constraints discussed in § 4.3.2.2 and 4.3.2.3 respectively. Constraints were defined depending on the mix design (discussed in § 5.1). Thereafter, the Solver tool embedded in Microsoft Excel was used to automatically adjust material quantities until the residual sum of squares defined in *Eqn. 4-19* was minimised. To assess the quality of the fit of the computed grading curve to that proposed by the MAAC, the R^2 statistic was then also quoted. Optimised mix designs are discussed in § 6.2.4

4.3.3 Selection of a distribution modulus (q)

Practically, a distribution of particulate materials following *Eqn. 2-9* could be made using *any* value for a distribution modulus and various ranges for q have been proposed in the past (Kumar & Santhanam, 2003; Brouwers & Radix, 2005; Hunger, 2010; Hüsken, 2010; Yu *et al.*, 2013). These proposals appear to have been made based on smaller values favouring greater fines contents and larger values resulting in mixtures with a large portion of coarse particles. Others report the selection of the distribution modulus to be dependent on the type of concrete being produced (e.g. self-compacting versus roller-compacted concrete) and the desired fresh concrete properties and is therefore something that can only be determined with experimental trial.

However, for maximising packing density, reasoning for the selection of the distribution modulus is offered in accordance with Funk & Dinger (1994) who developed the MAAC equation. Beginning with Andreasen's findings, that distribution moduli in the range between 1/3 and 1/2 supposedly enable maximum packing density, Funk & Dinger (1994) went on to show that maximum packing for a continuous distribution of particles following *Eqn. 2-9* occurs at 0,37. The authors established this through a series of computer modelling simulations entailing the packing of particle distributions made up according to the MAAC with various different distribution moduli. The simulations involved packing particles into a defined volume, equivalent to the total solid volume of the particles, beginning with the largest size class and then packing the consecutively smaller size classes into the interstitial (contiguous) space between the formerly packed size class. Their simulations were not intended to address whether there was enough volume to accommodate the next smallest particle size but whether there was sufficient *contiguous* volume (i.e. within the interstices of other size classes) to accommodate the next particle size.

For particle distributions with $q < 0.37$, Funk & Dinger (1994) consistently reported excess interstitial (contiguous) space after each size class had been packed and therefore potential to pack more particles of each size class to further increase the packing density of the overall mixture. For particle distributions with $q > 0.37$, the authors reported insufficient contiguous space to accommodate all the particles at each size class. Instead, if all particles were to be accommodated, there would be an overall increase in the bulk volume of the packed particle distribution and resulting decreased packing density. For a particle size distribution with $q = 0.37$, all the particles from each size class exactly filled the contiguous space remaining after the previous (larger) size class had been packed.

Therefore, Funk & Dinger's (1994) findings informed the selection of a single distribution modulus equivalent to 0.37 for use in the design of the concrete mixtures for this research. Fixing the distribution modulus meant that the ideal grading proposed by the MAAC for each mix was only dependent on the maximum and minimum particle sizes of the materials to be optimised. The extent that the PSD of the real mixture could match the ideal grading would then be dependent on the PSD of the individual constituents and their volumetric proportions within the total mixture.

4.4 Integrating the CIPM and MAAC

Out of the two models, the implementation of the CIPM in Microsoft Excel according to § 4.2.4 has the most significant computing time. Computing time also increased exponentially with an increase in the number of input materials, particle size classes and combinations considered and therefore, if an entire concrete mixture was to be optimised, computing times were expected to become unreasonable. Therefore, to optimise particle packing while ensuring reasonable computing times, the CIPM was only applied for the optimisation of the powder phase of concrete (due to its ability to specifically account for surface forces) and the remaining concrete materials were selected according to the MAAC optimisation algorithm (discussed in § 4.3.2).

Integration of the two models for concrete mix design was enabled by running the CIPM with the required cement content (see § 5.1) set as a constraint and assessing which combination of powder materials achieved maximum packing density. Thereafter, the combination of powder materials (defined by their % volume proportion of the total powder volume) were input into the MAAC algorithm as policy constraints (see § 4.3.2.3). The optimisation of the remaining coarse and fine aggregate materials could then be completed using the MAAC algorithm, accounting for the various other policy and physical constraints, as described in § 4.3.2. Aggregate quantities output from this stage were then further assessed for their practicality in comparison to common mix designs according to the C&CI Method of Mix Design (Addis and Goodman, 2009).

The integration of the two packing models in this way ensured the quantitative assessment of the packing density of the phases of importance for reducing clinker content (powder phases) but still did not neglect the packing of the entire range of concrete constituents (including fine and coarse aggregates). The quantitative output from the CIPM, although dependent on the accuracy of other variables/parameters within the modelling process, enabled the relative assessment of the potential of powder combinations to increase packing density. Although the MAAC was not capable of providing a quantitative assessment of packing density, it allowed a qualitative assessment of packing density through the R^2 statistic, representing the quality of the fit of the computed particle size distribution to the ideal MAAC grading curve.

5 Implementation of modelling outputs

5.1 Concrete mix design

Concrete mixes were designed with the materials described in § 3.1. Concrete mix design was carried out in two phases. This section describes the concrete mixes designed for each phase and the thought process surrounding their designs.

5.1.1 Phase 1

Phase 1 comprised the design of a reference mixture with no additional limestone to that already included in the reference cement (CEM II A-L 52.5 N with 9 % limestone by mass) and then the design of mixtures with successive increases in the replacement of cement with limestone filler. The C&CI 'Method of Mix Design' (Addis and Goodman, 2009) was followed to approximate the water content based on the available materials. This informed the use of 210 l/m^3, which was fixed along with a w/p ratio of 0.5, for the design of all Phase 1 mixtures. This resulted in a constant powder content across all mixtures (420 kg/m^3) but slight variations in the powder-paste volume (taken to be powder material + water content), due to differences in the densities of CEM II A-L 52.5 N (3095 kg/m^3) and limestone (2750 kg/m^3), which varied from approximately 347 to 352 l/m^3.

As described in § 4.2 and 4.4, powder material composition was determined according to the maximum packing density results from the CIPM. However, the optimisation process had to be completed within defined criteria. Phase 1 mixtures entailed the consideration of 10, 20, 30 and 40 % volume replacements of cement with limestone filler. Therefore, the criteria used for the optimisation of the powder content of each mix was a specific cement content (i.e. 90, 80, 70 and 60 % of the total powder content respectively). The remaining composition of the powder content was then made according to the combination of limestone materials which enabled a maximum packing density to be achieved (KB2 and KB45 were found to have the largest potential for use in increasing the packing density of the powder phase of concrete, see § 6.1.4).

In addition to these mixtures, another mixture comprising 20 % limestone replacement was constructed but, instead of purely selecting the powder composition according to that which gave maximum packing density, it was selected on the combined premise of maximising packing density and ensuring the inclusion of a portion of the finest limestone (KB 2). This was done to investigate the potential stimulation of hydration and formation of monocarboaluminates, which were expected to occur to a more noticeable extent with the inclusion of the high fineness limestone.

Following optimisation using the CIPM, the resulting powder composition of each mix was used as limiting criteria for optimisation using the MAAC (along with the already defined total powder and water contents of 420 kg/m^3 and 210 kg/m^3). This effectively led to the optimisation of fine and coarse aggregate quantities. Resulting concrete mix designs are portrayed in Table 5-1.

5.1.2 Phase 2

The outcome of Phase 1 was the realisation that fixing the water content with the inclusion of an increased limestone content, despite being optimised according to the modelling procedures described in § 4, was not sufficient to reduce the parameter of kg clinker/m^3 MPa^{-1} relative to the

reference mixture (see § 6.4). Therefore, in line with existing literature (Proske *et al.*, 2014; John *et al.*, 2017) it was confirmed that particle packing optimisation should be accompanied by a decreased water content if mechanical properties similar to a reference concrete are to be achieved.

Table 5-1: Phase 1 concrete mix designs. Powder composition by volume % is denoted beneath each mix number.

Constituent	Unit	Mix 1-1	Mix 1-2	Mix 1-3	Mix 1-4	Mix 1-5	Mix 1-6
		100 CEM	**90CEM 10KB45**	**80CEM 20KB45**	**80CEM 5KB2 15KB45**	**70CEM 30KB45**	**60CEM 5KB2 35KB45**
Water	kg/m³	210	210,0	210	210	210	210
Total binder	**kg/m³**	420	420,0	420	420	420	420
Cement	kg/m³	420	382,0	343,7	343,7	304,2	263,8
Limestone	kg/m³	-	37,7	76,3	76,3	115,8	156,2
KB2	kg/m³	-	-	-	19,1	-	19,5
KB45	kg/m³	-	37,7	76,3	57,3	115,8	136,7
Fly ash	kg/m³	-	-	-	-	-	-
Fine aggregate							
Granite Crusher 1	kg/m³	974	1046,0	1040,4	1053,4	1045,8	1039,9
Granite Crusher 2	kg/m³	-	-	-	-	-	-
Philippi Dune	kg/m³	-	-	-	-	-	-
Coarse Aggregate							
Nominal 9.5 mm Granite	kg/m³	760	684,0	685,3	672,3	675,7	677,2
Superplasticiser							
MasterGlenium ACE 456	kg/m³	0,63	0,47	0,37	0,68	0,55	0,54
	Mass % of binder	0,15	0,11	0,09	0,16	0,13	0,13
w/p	-	0,50	0,50	0,50	0,50	0,50	0,50
w/c	-	0,50	0,55	0,61	0,61	0,69	0,80
Powder-paste volume (Binder + Water)	l/m³	346	347	349	349	350	352
Slump	mm	60	70	75	75	75	75

However, with a decrease in the water content, the ability of the concrete to be sufficiently workable could also not be neglected. SP dosage could be increased to compensate the reduction in water content, yet this would likely need to be more than the maximum dosage specified by the manufacturer (usually about 1 % of the total binder content by mass) if a significant reduction in water content is to be achieved. Common SP dosage tends to be in the range of 0.5 to 1 % but existing research concerning high limestone content concretes show increased SP demand in the range of 3 % and still sometimes higher. However, Proske *et al.* (2014) found a water content of 145 l/m³ to be practically achievable for high limestone content concrete (36 and 72 mass % of

total powder mass) by including FA and using SP doses in the range of 0.5 to 1.7 % (% mass of total powder material).

Besides requiring minimum water content to achieve a desired workability, a minimum paste volume is required to provide cohesiveness, enable ease of placement and effective compaction. Therefore, when reducing the water content, it was important that sufficient paste was still provided to achieve desirable fresh concrete properties (Fennis, 2011; Li & Kwan, 2013; Proske *et al.*, 2014; John *et al.*, 2017). Addition of limestone filler can compensate the reduction of water content and provide an equivalent powder-paste volume, however, this requires careful optimisation because fine fillers also have the potential to increase water demand due to their high surface area.

Therefore, Phase 2 mixtures were designed with the intention of decreasing the water content by considering various strategies, eventually culminating in the definition of a minimum powder-paste content, to ensure adequate fresh concrete properties. Although Phase 2 mix designs were still constructed according to CIPM and MAAC modelling outputs, several trial mixes were necessary to obtain a mix that had a reduced water content but was still cohesive and adequately workable.

Initially, Mix 1-6 from Phase 1 (Table 5-1) was selected for further optimisation to produce Phase 2 mixtures. The w/p was set to be constant at 0.5 and the water content reduced to 150 l/m^3. The reduction in water content therefore led to a reduced powder material content (300kg/m^3) but the percentage volume contribution of the various limestones and CEM II A-L 52.5 N within this total powder content was kept the same as Mix 1-6 (60CEM 5KB2 35KB45). This led to a total powder-paste volume of approximately 250 l/m^3. Thereafter, as before, fine and coarse aggregate quantities were determined according to the MAAC outputs. Trial 2-1 was made with a coarser granite crusher sand (FM = 3.53), hereafter referred to as granite crusher sand 2, in comparison to the crusher sand used for the Phase 1 mixtures (FM =2.93), hereafter referred to as granite crusher sand 1. Optimising the mixture according to the MAAC while fixing the above-mentioned parameters led to the proposal of a blend of granite crusher sand 2 and Philippi dune sand. This effectively increased the fineness of the overall fine aggregate as opposed to only using granite crusher sand 2. Table 5-2 portrays Trial 2-1 mix quantities.

The resulting mixture was harsh and earth-moist in consistency, achieving zero slump. This was primarily attributed to the low powder-paste content (relative to Phase 1 mixtures) due to the water content being reduced without sufficient compensation to maintain the powder-paste volume. When dynamic compaction was applied to the concrete used for the slump test, the moulded concrete collapsed, and coarse aggregates separated from the paste.

To counter the harshness of the mixture, the coarse granite crusher sand 2 was then excluded from any further mix designs and instead, the only fine aggregate used was Philippi dune sand. Due to Philippi dune sand (FM = 2.03) being substantially finer than granite crusher sand 2 (FM = 3.53), it was also intended that a larger dune sand quantity would contribute to an increase in overall paste content (in this instance referring to powder + fine aggregate + water). Another trial was constructed using the Mix 1-6 powder composition in the MAAC algorithm which resulted in the initial mix design for Trial 2-2 portrayed in Table 5-2.

Table 5-2: Phase 2 trial mix designs. Powder composition by volume % is denoted beneath each trial mix number.

Constituent	Unit	Trial 2-1	Trial 2-2*
		60CEM 5KB2 35KB45	60CEM 5KB2 35KB45
Water	kg/m³	150	150
Total binder	kg/m³	300,0	300,0
Cement	kg/m³	188,4	188,8
Limestone	kg/m³	111,6	111,3
KB2	kg/m³	14,0	13,8
KB45	kg/m³	97,7	97,5
Fly ash	kg/m³	-	-
Fine aggregate			
Granite Crusher 1	kg/m³	-	-
Granite Crusher 2	kg/m³	1062,6	-
Philippi Dune	kg/m³	242,9	982,5
Coarse Aggregate			
Nominal 9.5 mm Granite	kg/m³	677,2	997,5
Superplasticiser			
MasterGlenium ACE 456	kg/m³	5,21	4
	Mass % of binder	1,74	1,33
w/p	-	0,50	0,50
w/c	-	0,80	0,79
Powder-paste volume (Binder + Water)	l/m³	252	251
Slump	mm	0	0

*Primary difference of Trial 2-2 from Trial 2-1 was the omission of crusher sand 2.

No noticeable change in the fresh properties was observed and therefore the paste content was increased first with additional water and then with the incremental addition of KB45 (approx. 20 kg/m³ at a time). A remarkable increase in workability was observed through the recorded slump. Table 5-3 details the effective mix design with an increasing paste content. The first revision comprised increased water and KB 45 content and the remainder of the revisions comprised only additional KB 45 and therefore, a decrease in the water content of the effective mix design (i.e. once converted to quantities per m³ concrete).

This informed a further trial mix with higher powder-paste content. Specifically, a powder-paste content of 300 ± 5 l/m³ was deemed a practical minimum to achieve sufficient workability (similar to Palm *et al.*, 2016). Water content was increased to 160 l/m³ and the maximum cement content to 190 kg/m³ and therefore a higher limestone content was necessary to achieve 300 ± 5 l/m³. To design the mix according to a powder composition proposed by the CIPM but satisfy the criteria for paste and cement content, it was necessary to set the cement volume % of the powder phase to 45 %.

Table 5-3: Effective mix designs of Trial 2-2 with additional water and incremental addition of KB 45

Constituent	Unit	Trial 2-2	Trial 2-2	Trial 2-2	Trial 2-2	Trial 2-2
		Add. water & KB 45	Add. KB 45	Add. KB 45	Add. KB 45	Add. KB 45
Water	kg/m³	167	166	164	163	162
Total binder		335,7	356,5	377,0	397,2	417,0
Cement	kg/m³	181,0	179,5	177,9	176,4	174,9
Limestone	kg/m³	154,6	177,1	199,1	220,8	242,1
KB2	kg/m³	13,2	13,1	13,0	12,9	12,7
KB45	kg/m³	141,5	164,0	186,2	208,0	229,4
Fly ash	kg/m³	-	-	-	-	-
Fine aggregate		-	-	-	-	-
Granite Crusher 1	kg/m³	-	-	-	-	-
Granite Crusher 2	kg/m³	-	-	-	-	-
Philippi Dune	kg/m³	942,3	934,1	926,1	918,3	910,5
Coarse Aggregate						
Nominal 9.5 mm Granite	kg/m³	956,7	948,4	940,3	932,3	924,4
Superplasticiser						
MasterGlenium ACE 456	kg/m³	4	4	4	4	4
	Mass % of binder	1,19	1,12	1,06	1,01	0,96
w/p	-	0,50	0,47	0,44	0,41	0,39
w/c	-	0,92	0,92	0,92	0,92	0,92
Powder-paste volume (Binder + Water)	l/m³	282	288	294	300	306
Slump	mm	20	30	50	70	50

Packing densities corresponding to various powder combinations with 45 % cement content were then assessed. The combination enabling maximum packing density comprised a substantial portion (25 %) of the finest limestone (KB2) and therefore was not implemented in the interest of preventing high water demand. Instead, a practical 10 % limitation was imposed on the KB2 volume, leading to the choice of a combination (45 % KB45 10 % KB2) achieving only negligibly lower packing density (0.673) than the maximum (0.674) (See Table D-5, Appendix D). From previous experimental trial and error, coarse aggregate content was set at 850 kg/m^3. The MAAC algorithm was then applied (with additional constraints for minimum powder-paste volume and coarse aggregate content), resulting in the Trial 2-3 mix design detailed in Table 5-4.

The mix still appeared to be too 'stony' but this was remedied by a minor addition of water to take the water content to 164 l/m^3 and corresponded to a decrease in coarse aggregate content to 846 kg/m^3 and an increased dune sand content (1005 kg/m^3). This informed the Mix 2-1 design portrayed in Table 5-4.

Table 5-4: Final Phase 2 trial mix and eventual mix designs. Powder composition by volume % is denoted beneath each mix number.

Constituent	Unit	Trial 2-3	Mix 2-1	Mix 2-2	Trial 2-4
		45 CEM 45 KB45 10 KB2	45 CEM 45 KB45 10 KB2	45CEM 30 KB45 5KB2 20FA	100 CEM
Water	kg/m³	160	164	164	164
Total binder		400.0	394.0	381.1	420.1
Cement	kg/m³	190.0	189.1	189.1	420.1
Limestone	kg/m³	210.0	204.8	129.3	-
KB2	kg/m³	38.0	33.6	16.8	-
KB45	kg/m³	172.0	171.2	112.5	-
Fly ash	kg/m³	-	-	62.7	-
Fine aggregate					
Granite Crusher 1	kg/m³	-	-	-	-
Granite Crusher 2	kg/m³	-	-	-	-
Philippi Dune	kg/m³	1007.3	1005.4	1005.4	1010.3
Coarse Aggregate					
Nominal 9.5 mm Granite	kg/m³	850.0	846.2	846.2	840.8
Superplasticiser					
MasterGlenium ACE 456	kg/m³	15.1	16.1	6.5	5.3
	Mass % of binder	3.8	4.1	1.7	1.3
w/p	-	0.40	0.42	0.43	0.40
w/c	-	0.84	0.87	0.87	0.40
Paste volume (Binder + Water)	l/m³	296	300	300	300
Slump	mm	0	40	40	55

Even with a large SP dosage, Mix 2-1 only achieved a 40 mm slump. Although this was below the range specified for Phase 1 mixes, this was sufficient to compact cube specimens on a vibrating table. The mix was cohesive and there was no visible separation of aggregates from the paste, however, there did appear to be extensive bleeding during compaction. This was attributed to the high SP dosage and was not expected to be detrimental to later age concrete properties. It is possible that further investigation into powder combinations which minimise internal friction may allow the use of lower SP dose, yet still achieve equivalent slump, and therefore minimise the amount bleeding.

Numerous reports of an increased formation of mono-carboaluminate when using limestone in an aluminate-rich mix informed the construction of a final mix containing 20 % FA within the total powder volume. Its spherical shape was also expected to benefit workability. Due to the FA used having a similar particle size distribution to one of the limestones (KB10), the packing density measured for KB10 was used as an initial approximation of the packing density of the FA for analysis in the CIPM. Thereafter, the cement content was fixed at 189 kg/m³ (as for

Mix 2-1) and the remaining powder material composition was selected on the premise of maximising packing density while ensuring the volume contribution of FA to total powder content was 20 %. Once the powder composition had been defined, the same water content and coarse and fine aggregate quantities were used as for Mix 2-1, resulting in Mix 2-2, detailed in Table 5-4.

Fresh concrete properties for the FA mix were similar to Mix 2-1 yet it achieved these at a substantially reduced SP volume (Table 5-4). As already mentioned, the FA mix was expected to have improved fresh properties due to its spherical particle shape having a ball bearing effect, reducing internal friction. Finally, to assess the effect of the limestone fillers on the measured slump, Trial 2-4 (see Table 5-4) was constructed to have equivalent powder-paste volume to Mixes 2-1 and 2-2 but only contained CEM II A-L 52.5 N in the powder phase. The trial mix achieved higher slump than Mix 2-1 and 2-2 and did so with considerably less SP, inferring the limestone fillers to have considerable water demand. This is further discussed in § 6.3.2.

5.2 Experimental tests

5.2.1 Slump test

A slump test in accordance with SANS 5862-1 (2006) was conducted to assess the workability of each mix. It was expected that fresh concrete properties may be decreased due to increased packing density causing increased internal friction and therefore a range of 60 to 90 mm slump was specified as a requirement for Phase 1 mixtures. Slump was measured to the nearest 5 mm and cohesiveness of the 'slumped' concrete was assessed by tapping the metal plate upon which the test was performed. A concrete sample which remained homogenous and had a slump which gradually increased due to tapping was considered to have good cohesiveness. If the sample instead broke apart when the mould was lifted, collapsed by lateral shearing or cement paste separated from the aggregates upon tapping, it would have been noted that the mix was non-cohesive.

With a further reduction in water content for Phase 2 mixtures, a requirement of slump was not specified, however slump and cohesiveness were still assessed.

5.2.2 Compressive strength

Compressive strength of Phase 1 and 2 mixtures was measured in accordance with SANS 5863 (2006) at 3, 7, 28 and 56 days after casting to observe strength development. A minimum of three 50×50×50 mm cubes were tested at each age. Specimens were demoulded 24 hours after casting and water cured up to the date of testing where they were tested in a saturated surface-dry condition. Loading was applied without shock at a rate of 0.3 MPa/s ± 0.1 MPa until failure.

5.2.3 Durability index tests

Durability index tests were only completed for Phase 1 mixes due to imposed time constraints. Standard water-cured, cube specimens (100×100×100 mm) were cast to assess each mixture's potential durability performance. A full suite of Durability Index tests, outlined in the *Durability Index Testing Procedure Manual* (Alexander *et al.*, 2017), were conducted for each mix at 28 days after casting. The durability index tests comprise the oxygen permeability, water sorptivity and chloride conductivity index tests. For further information regarding test procedures, see Alexander *et al.* (2017).

5.2.4 Accelerated shrinkage

Uniaxial (linear) shrinkage strain was only measured for Phase 1 mixtures due to imposed time constraints. Specimens were subjected to an accelerated drying regime, in accordance with SANS 6085 (2006). Three prismatic specimens (280×50×50 mm) were cast for each mix and water cured for 7 days. Thereafter the surface of the specimens was dried, and two strain targets were glued centrally and 100 mm apart in the longitudinal direction to two opposite faces of the prism (faces that were parallel to the cast direction).

An initial reading of the distance between the strain targets was recorded with a strain extensometer and specimens were placed in an oven maintained at approximately 50 °C for 7 days. Thereafter, specimens were removed and placed in a room with controlled temperature (22-25 °C) and humidity (not exceeding 60 %) and allowed to cool to ambient temperature (up to 3 hours was allowed for cooling). Strain readings were measured using the same extensometer as for the initial readings and then specimens were placed in the drying oven for another 2 days before being removed and allowed to cool once again and another strain measurement taken.

The average strain for each mix was calculated using the 6 readings from the three specimens after each measurement. The drying regime, followed by the measurement of strain, was repeated until the difference between the average strain of 2 consecutive measurements was less than 2 micrometres. Total strain was then recorded as the sum of the incremental strain measurements.

6 Results and discussion

6.1 Preliminary experimental investigation

6.1.1 Powder particle morphology

SEM images of limestone fillers are presented in Figure 6-1 to Figure 6-8. SEM images of FA are presented in Figure 6-9 and Figure 6-10 and cement images are presented in Figure 6-11 and Figure 6-12. Table 6-1 presents a key of the abbreviations used in the SEM images. Reference is made to Figure 2-8 for a qualitative description of particle shapes. KB45 images (Figure 6-7 and Figure 6-8) present sub-rounded to sub-angular particles with low sphericity. The planar structure of the parent material is also evident in Figure 6-8. Despite undergoing similar manufacturing processes, with increasing fineness, limestone particle shapes tend to be angular and there is a presence of flaky and elongated particles (Figure 6-4), although not nearly as prevalent as in the images of cement particles.

Table 6-1: Key for interpretation of symbols on SEM images

Terminology	Description
ETD	Everhart Thornley detector
HFW	Horizontal field width
Landing E	Landing energy of electron probe in electron volts
Mag	Magnification
Spot size	Diameter of electron probe at sample surface
WD	Working distance

Figure 6-1: SEM image of KB2. Full extent view showing angular particle shapes.

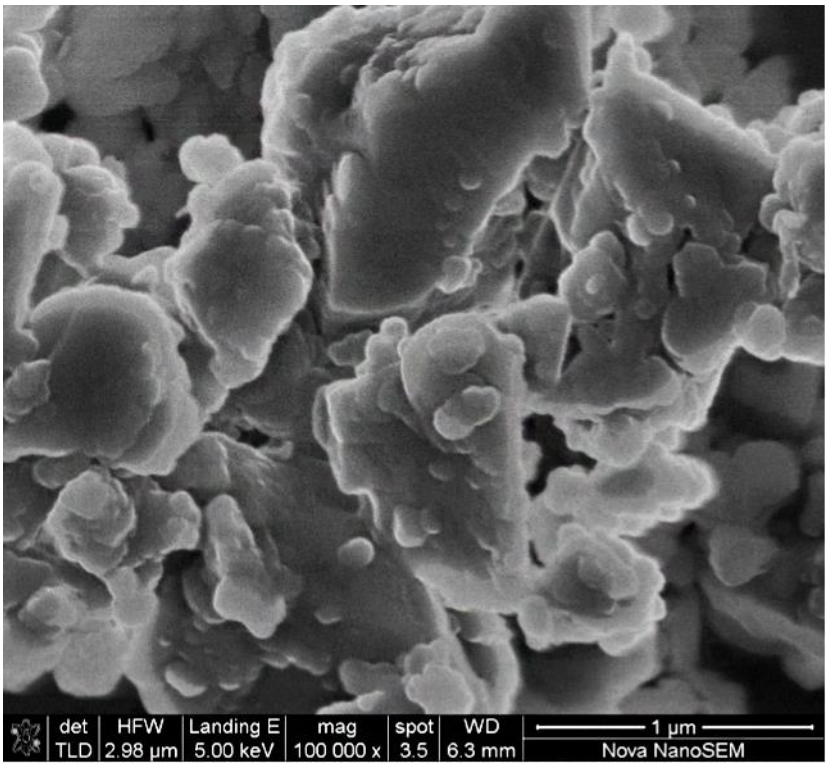

Figure 6-2: SEM image of KB2. Zoomed view with limited detail showing generally angular and flaky particle shape

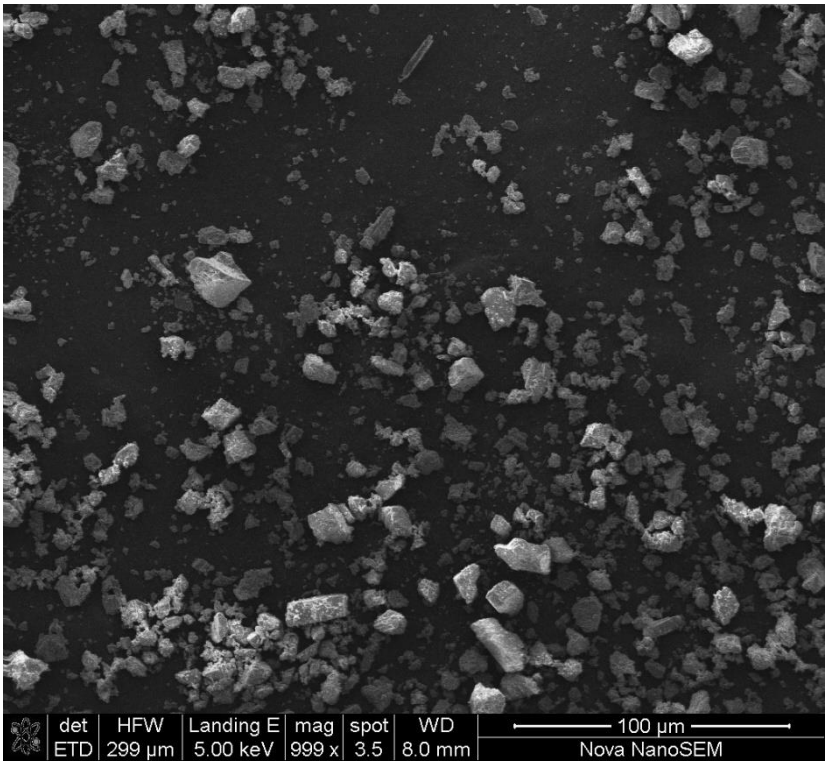

Figure 6-3: SEM image of KB5. Full extent view showing angular particle shape.

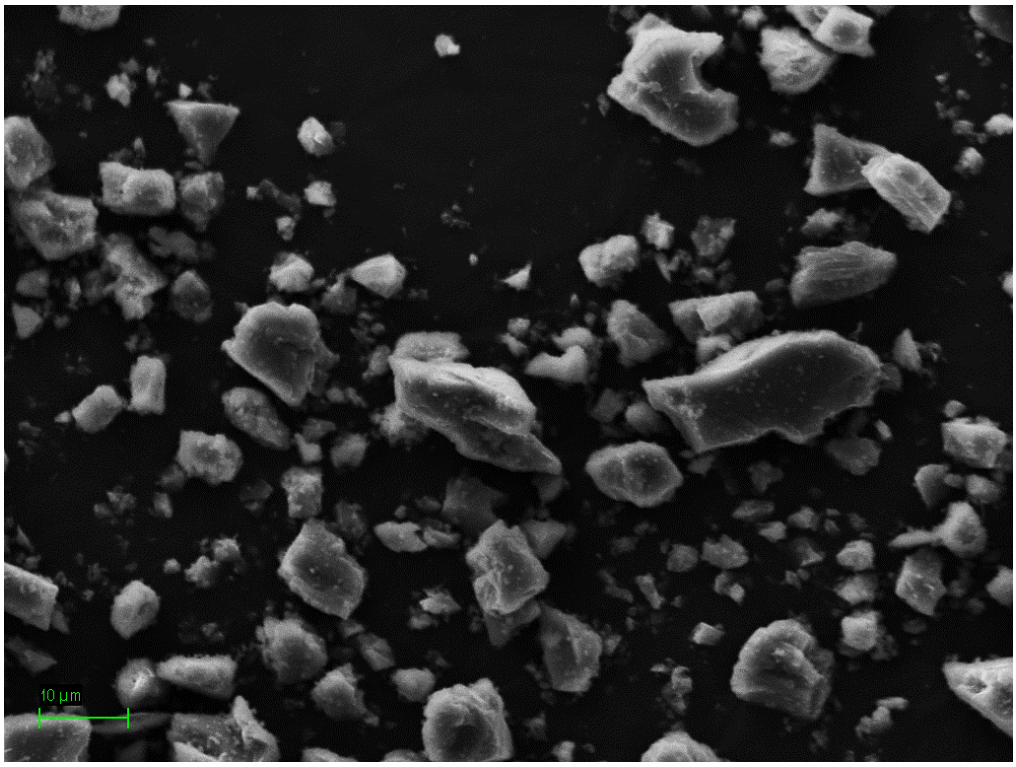

Figure 6-4: SEM image of KB5. Zoomed view showing angular as well as some flaky particles

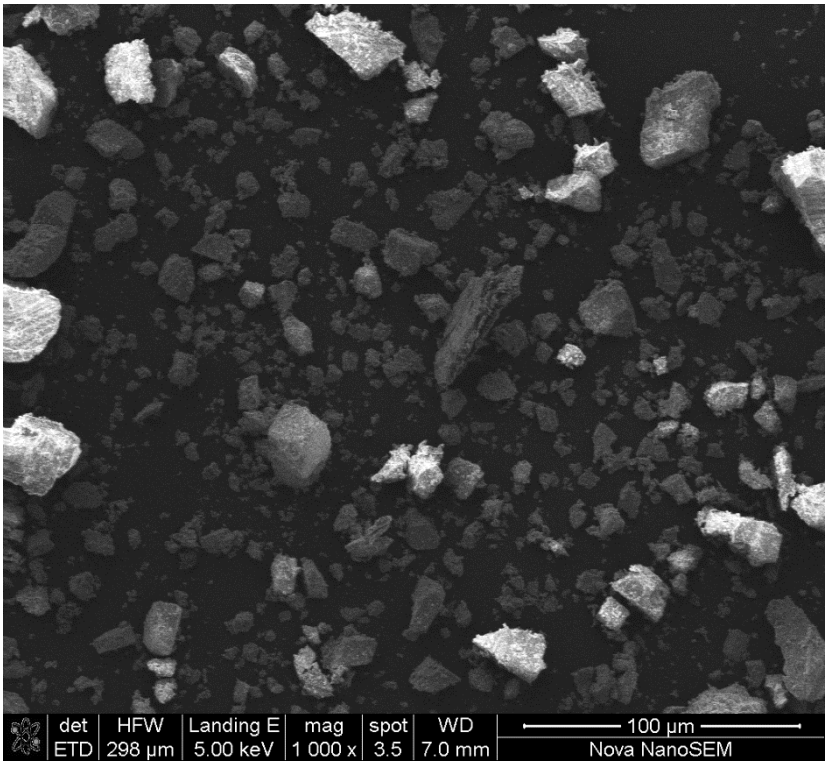

Figure 6-5: SEM image of KB10. Full extent view showing angular particle shapes

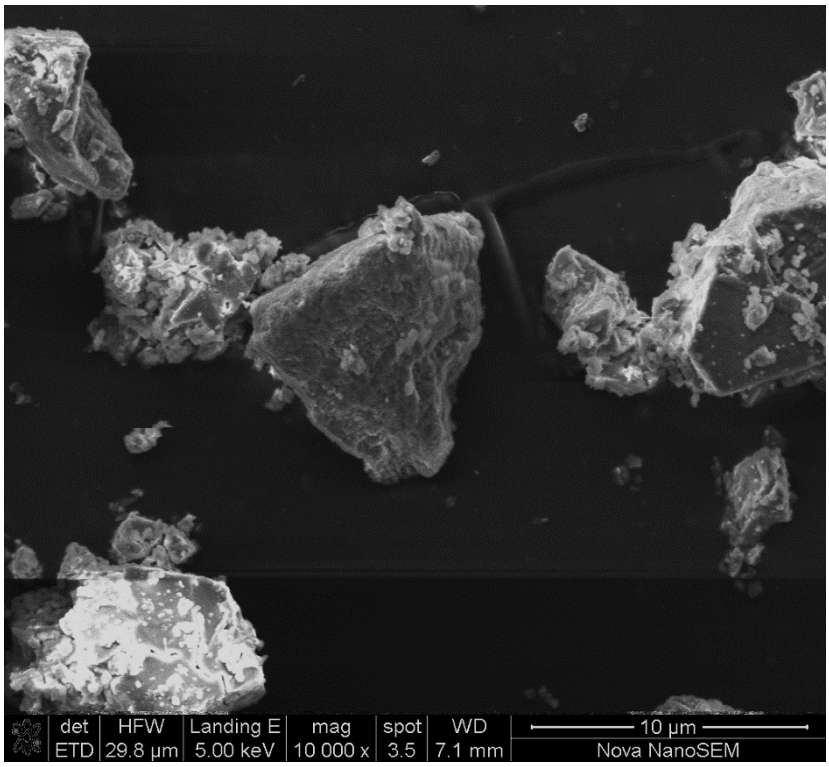

Figure 6-6: SEM image of KB10. Zoomed view showing angular particle shape and evidence of planar structure.

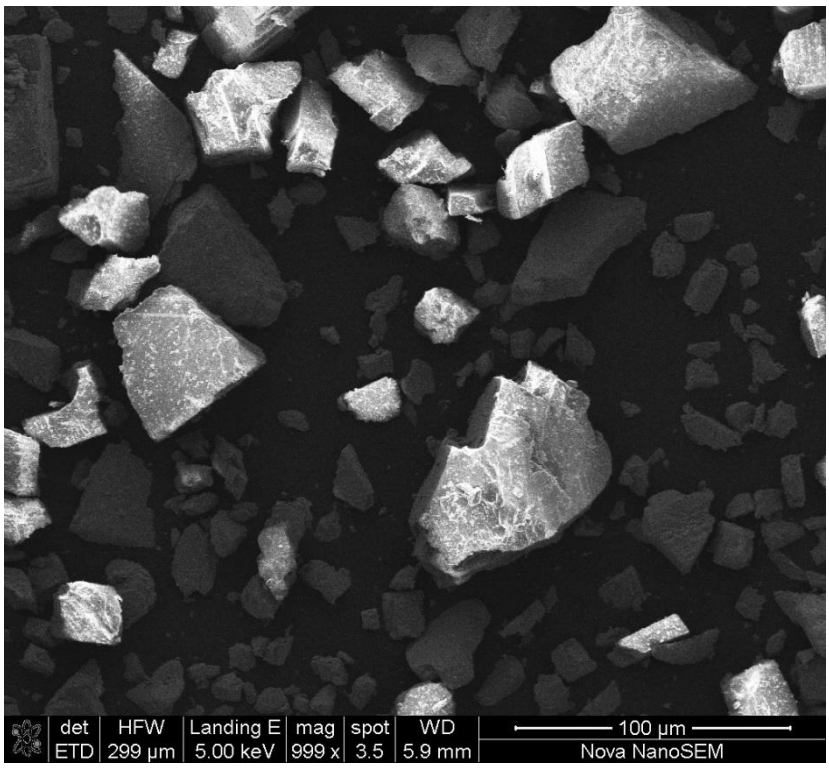

Figure 6-7: SEM image of KB45. Full extent view showing sub-angular and angular particles with varying sphericity

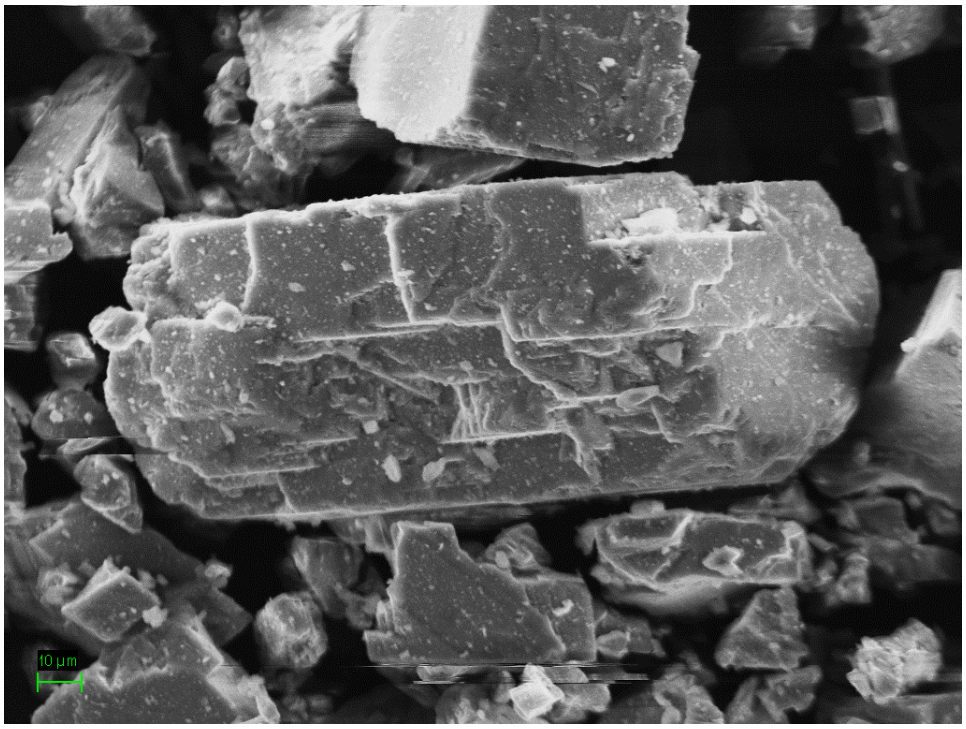

Figure 6-8: SEM image of KB45. Zoomed view showing prismatic particle shape, planar structure and relatively non-porous surface with small attached particles.

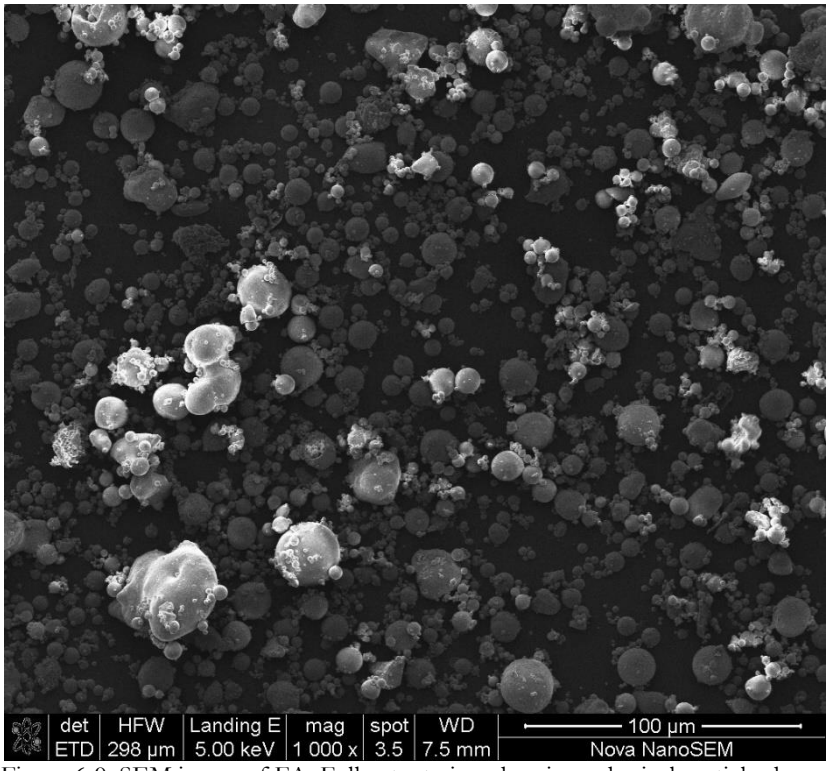

Figure 6-9: SEM image of FA. Full extent view showing spherical particle shape.

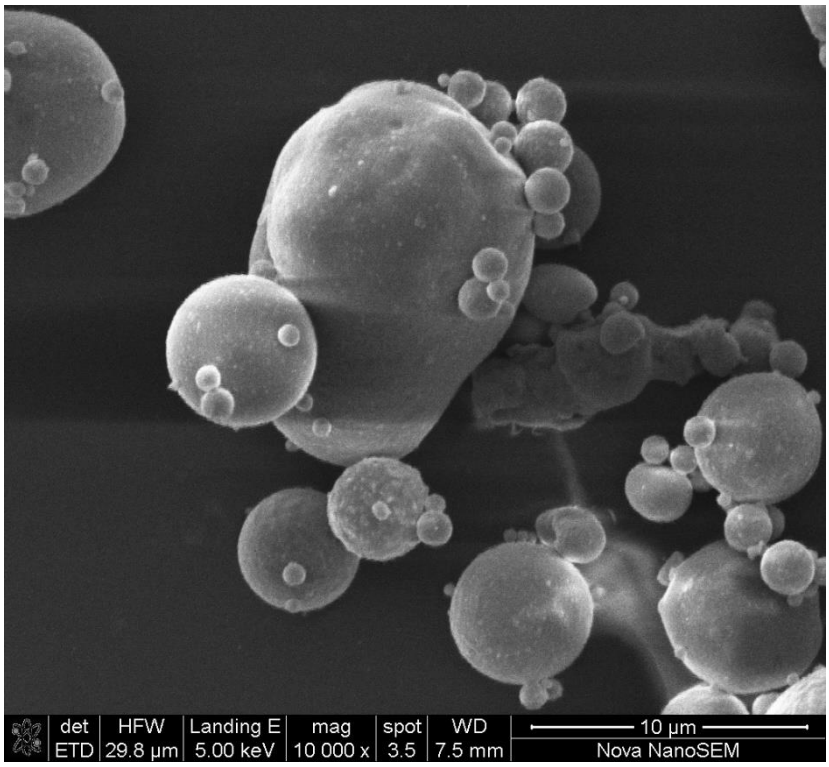

Figure 6-10: SEM image of FA. Zoomed view showing agglomerated spherical particles and non-porous surface.

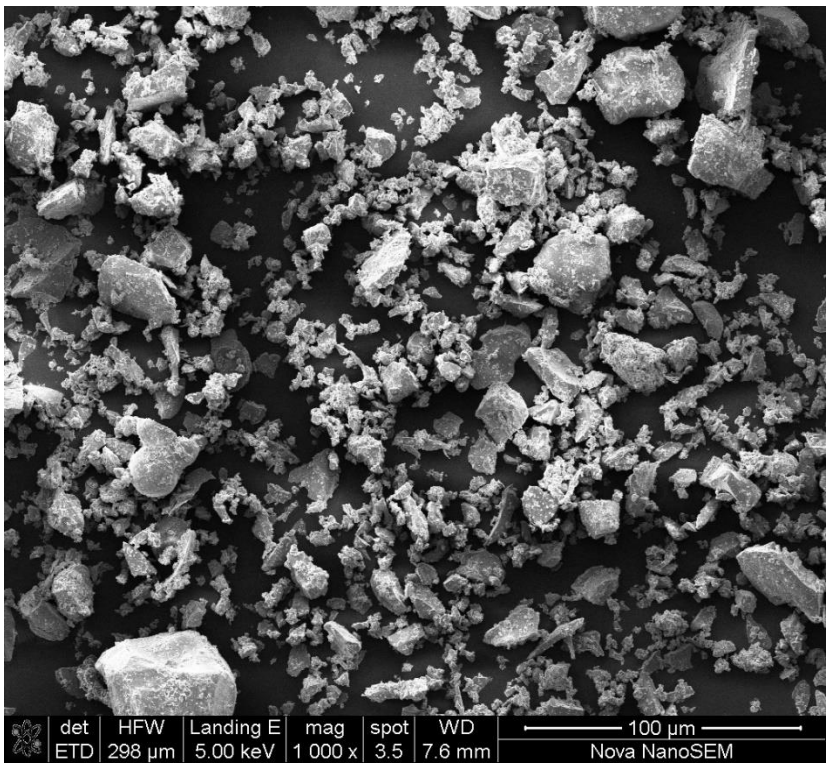

Figure 6-11: SEM image of CEM II A-L 52.5 N. Full extent view showing very angular particle shape with presence of flaky and elongated particles

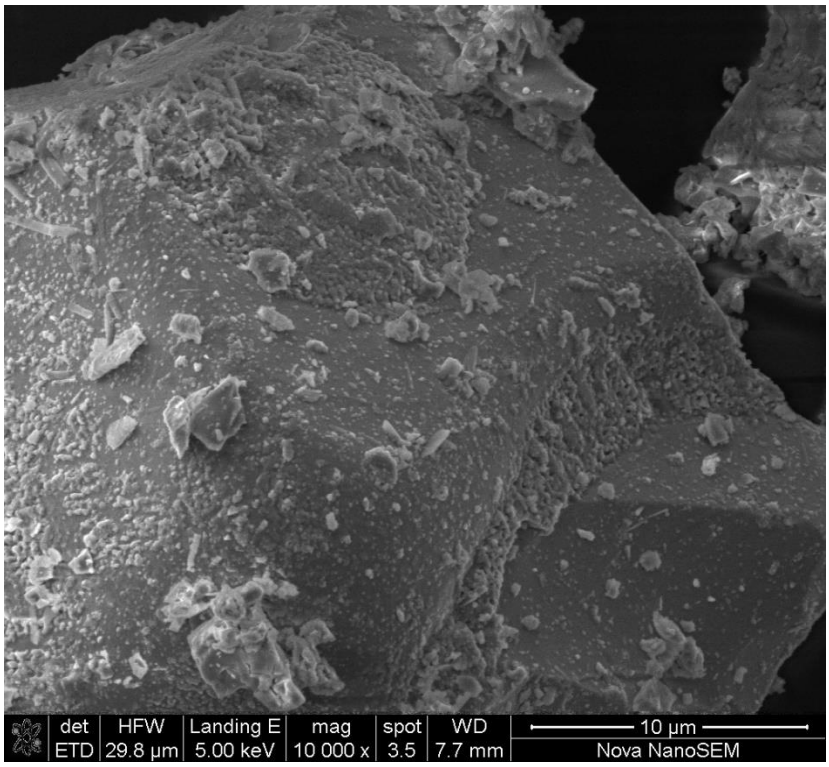

Figure 6-12: SEM image of CEM II A-L 52.5 N. Zoomed view showing non-porous surface with small attached particles

Cement particles were characterised by very angular, irregular particle shapes which included flaky elongated particle shapes. All these are characteristics of the fracture of glassy, alumino- silicate material. Contrarily, FA is characterised by uniform, rounded, spherical particle shapes (Figure 6-9).

At the practically achievable magnification, only the surface texture of larger particles could be qualitatively assessed. KB45 appeared to have relatively smooth, non-porous surfaces, probably due to the fracture of the parent material along its planar structure. The fracture of limestone parallel to these planes is also the likely cause for the formation of flaky elongated particle shapes, particularly as the material becomes increasingly fine. Although their particle shapes are considerably different, cement and FA particle surfaces also both appear to be smooth and non-porous.

As particle shapes deviate from ideal, rounded, spherical particle shapes, internal friction, experienced due to the interlock of angular particles, increases. With increasing angularity and decreasing sphericity, the ability of particles to pack closely to one another also decreases, particularly for the case of flaky and elongated particles. Increased internal friction leads to an increased water demand as a larger film of water is required to surround a particle before it can become mobile. Decreased ability to pack closely results in decreased packing density and ultimately, an increased water demand as more water is required to fill interstitial void space.

Therefore, relative to cement particles, FA particles have the most favourable particle shape but even the sub-rounded to sub-angular particle shape, characteristic of the coarser limestone, is

preferable over the cement and has potential to increase the packing ability of powder materials if blended with cement. However, despite having similar composition, the particle shape of limestone filler appears to degrade with increasing fineness and, in addition to increased surface area per volume, may result in increased water demand.

6.1.2 Superplasticiser demand

The SP saturation dosage was estimated using the plot of the time taken for a fixed volume of powder-paste mixture to exit the standard flow cone apparatus (described in § 3.2.2) as the SP dose was incrementally increased. Figure 6-13 portrays these plots for the two materials assessed, a limestone filler (KB10) and CEM II A-L 52.5 N. A more noticeable decrease in the original flow time with an increase in SP was reported for the cement yet, the flow time for both materials decreased as the SP dose was increased. Ultimately, the flow time for each material tended to converge to a set time despite further increase in SP.§

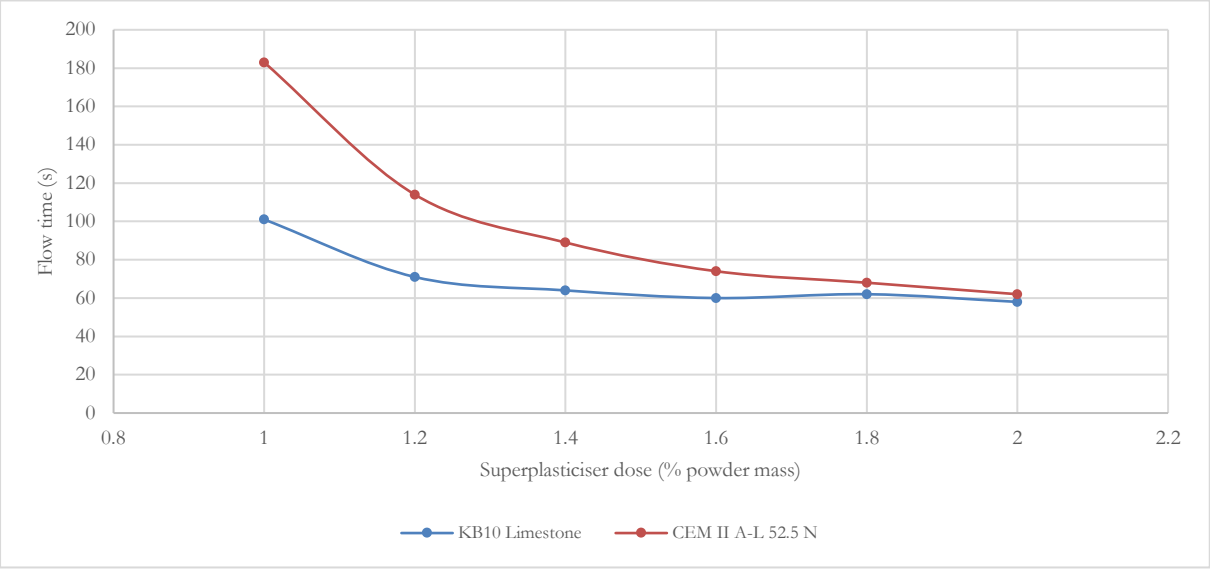

Figure 6-13: Flow time of powder-paste mixture with an increase in superplasticiser dose

The SP dose beyond which there was no significant decrease in flow time was subjectively taken as 1.6 % by powder mass for both KB10 and CEM II A-L 52.5 N. For consistency, it was deemed appropriate to use this same dose for all powder material packing density tests. Although the finer limestones (KB2 and KB5) may potentially have required higher doses to be properly dispersed, 1.6 % SP by powder mass was already more than that advised by the manufacturer and therefore it was preferred to not further increase the dose.

6.1.3 Assessment of packing density tests

6.1.3.1 Wet packing test

Preliminary wet packing tests (in accordance with § 3.3.1) were completed to determine the applicability of the test method for this research. Initially only CEM II A-L 52.5 N was tested but this was later followed by the testing of a limestone filler (KB10) as well as a blend of 2 materials

(20 % KB10 80 % CEM II A-L 52.5 N, by volume).

Results for 3 replicate cement tests, where only the volume of the increments of additional water were changed, are portrayed in Figure 6-14 and Figure 6-15. At low water contents (low water ratio (u_w)), the voids ratio (u) can be seen to decrease as the water content is increased. A local minimum in the voids ratio is reached and the solid volume fraction at this point is taken as the maximum packing density of the material. Any point above $\varepsilon_a = 0$ has its interstitial space filled with a combination of air and water but as the water content increases, data points tend to $\varepsilon_a = 0$ where interstitial space is completely filled with water. Maximum packing densities measured from the three tests were 0.571, 0.573 and 0.563, respectively, giving a standard deviation of 0.005.

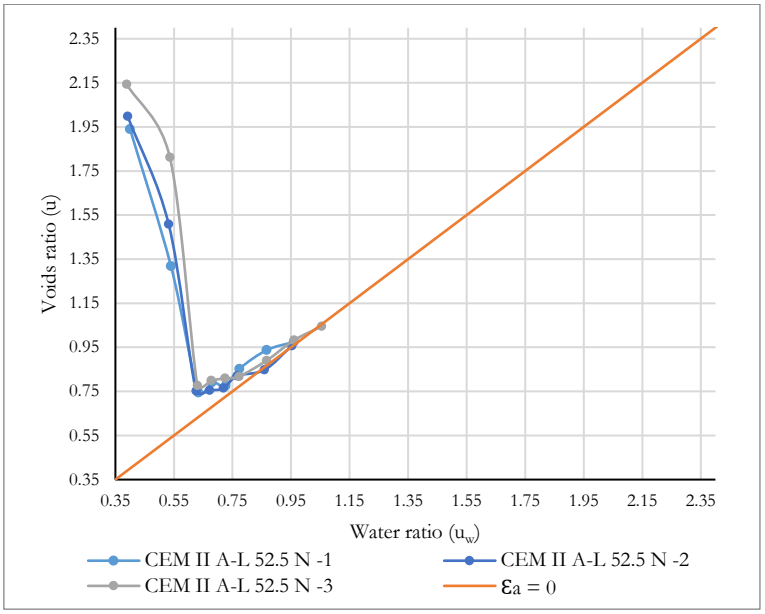

Figure 6-14: Wet packing test results for CEM II A-L 52.5 N replicate tests

The precision of the test method relied on the use of consistent increments of additional water for each replicate test and the accuracy of the result was also dependent on the increments used. With increasing fineness of the water increments, the degree of accuracy could be increased, however, wider increments were also initially necessary to determine the general location of the minimum void content (maximum packing density). Therefore, following some experimental trial, initial water increments were larger (50 - 75 ml for starting volume of 750 ml) but were decreased (to 25 ml) as the water content reached the range within which the maximum packing density was expected to occur.

Figure 6-16 portrays the combined data from the 3 replicate cement tests as well as the data from a test conducted on KB10 limestone. As observed for the cement results, the accuracy of the measured packing density relied on the increments of water used in the test. Based on the coarser increments used for the KB10 test (relative to the combined data for the cement), it was apparent that the limestone had a maximum packing density of 0.553. Although the accuracy of this finding could not be confirmed as only a single test was performed, when considering the standard deviation of the cement results, KB10 had a lower maximum packing density than the cement.

The increased fineness of KB10 relative to cement was expected to have limited its maximum packing density. An increased influence of surface forces on packing is likely to have resulted in agglomeration, reducing the packing density achievable (as the preliminary tests for assessing the method were conducted without SP).

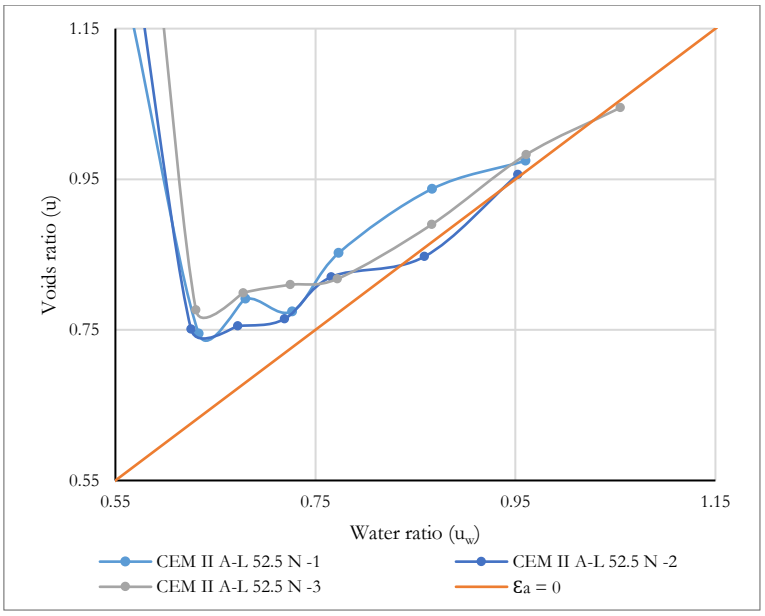

Figure 6-15: Expanded view of wet packing test results for CEM II A-L 52.5 N replicate tests

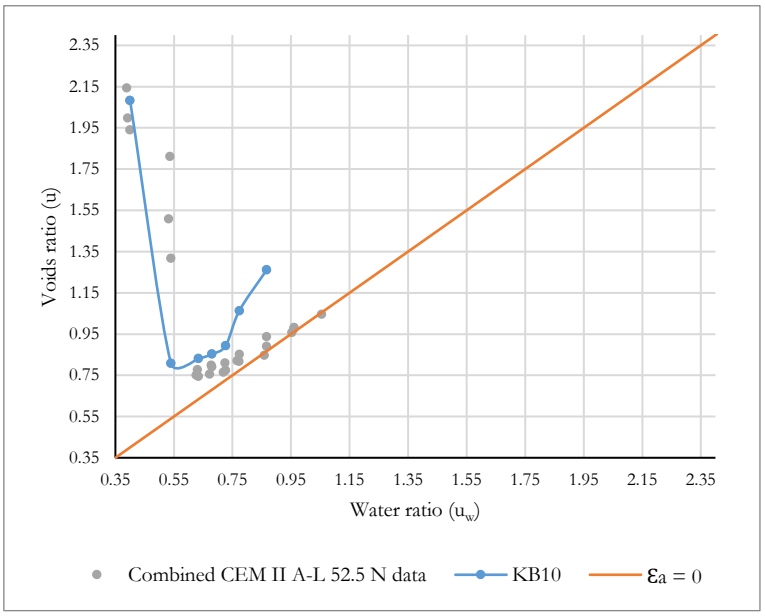

Figure 6-16: Wet packing test results for limestone (KB10) and combined CEM II A-L 52.5 N data

The 80/20 % blend of cement / limestone (by volume) is portrayed in Figure 6-17 and an expanded view of the minimisation of the voids ratio (maximisation of packing density) is given in Figure 6-18. Relative to the plain materials, the blend achieved a noticeably higher packing

density (0.575) than KB10 (0.553) but was negligibly higher than the median value for the plain cement (0.571). Therefore, the inclusion of KB10 has little influence on the overall powder packing density and appears to only result in the dilution of the cement within the powder phase as opposed to a desired increase in packing density, attributed to the similar particle size distribution of the materials.

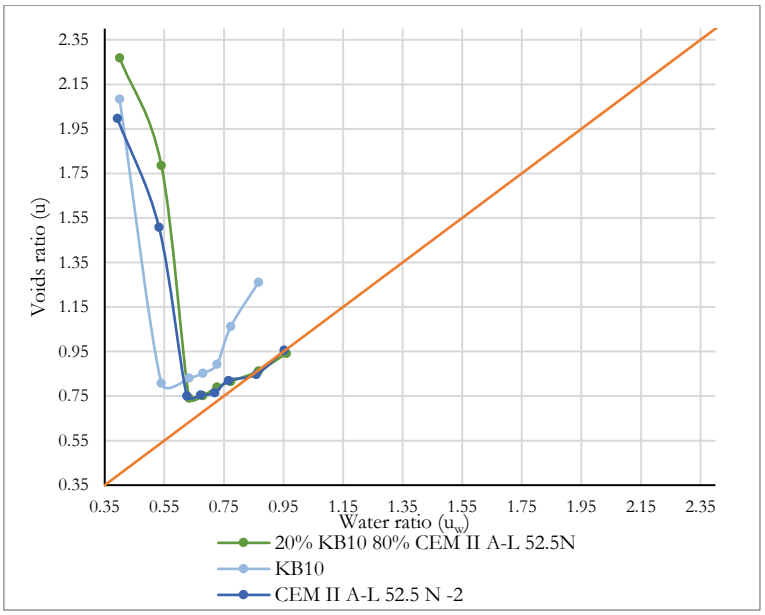

Figure 6-17: Comparison of wet packing test results for plain materials and a cement / limestone blend

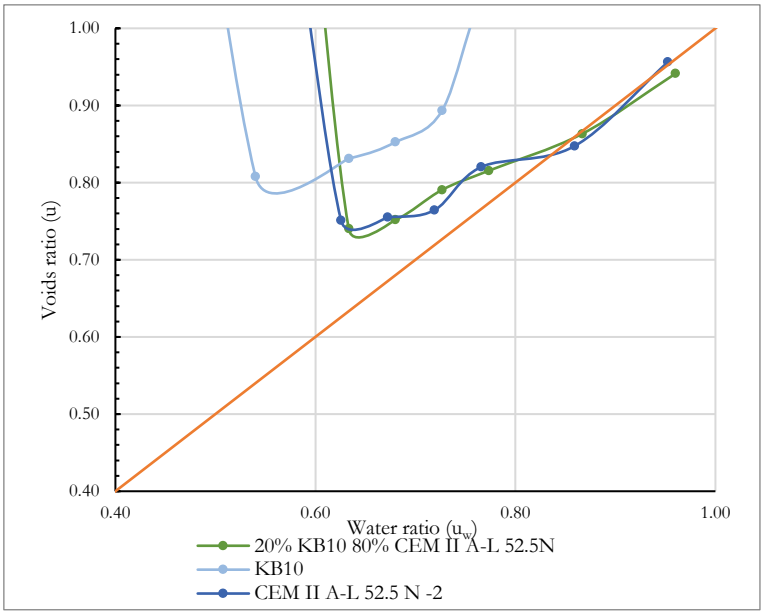

Figure 6-18: Expanded view of the comparison of wet packing test results for plain materials and a cement / limestone blend

Although the wet packing test enabled the determination of maximum packing density within an acceptable tolerance (based on the preliminary results), the method had some drawbacks with

regard to its application for this research. Difficulty was experienced when trying to maintain constant compaction effort across different specimens as the moisture content at maximum packing density was approached. It became increasingly difficult to fill the mould completely without increasing the time that vibration was applied, which affected the degree to which the sample was compacted. However, to be able to describe the compaction within the CIPM, it was necessary that this was always consistent.

Due to the number of filler materials to be tested in combination with cement, the application of the wet packing test would result in excessive quantities of material being used and would become extremely laborious. To achieve a single packing density result, the measurement of several mass readings at various w/cm ratios was required (a minimum of 7 variations was sufficient). This did not seem feasible for the assessment of several different material combinations even when completing only one replicate test per material combination. Furthermore, it was also realised that within the time frame of 90 minutes, clinker particles are likely to have already begun to hydrate, inhibiting the proper dispersion of particles and affecting the accuracy of the technique. Therefore, to aid the timeous analysis of the packing density of many powder combinations and ensure that results were repeatable and reproducible (with a focus on maintaining consistent compaction effort across all test specimens) alternative packing density methods were investigated.

6.1.3.2 Centrifugal consolidation

Preliminary centrifugal consolidation tests (in accordance with § 0) were completed to determine the applicability of the test method for this research. Initially only CEM II A-L 52.5 N was tested but this was later followed by the testing of a limestone filler (KB10). The test was investigated for its ability to provide consistent compaction for all test samples and its potential for testing several samples timeously.

A cement paste was constructed for initial testing with w/p = 0.4 by mass (approx. 1.24 by volume) and 6 test tubes were partially, but equally, filled with material. Following 10 mins of centrifuging, it was realised that 2 test tubes were defective and had lost water and therefore could no longer be considered. Relatively equal volumes of water were extracted from 3 of the remaining test tubes, with a lesser amount having surfaced on the fourth. The packing density before and after (PD_{before} and PD_{after}, see § 0) are displayed for the preliminary test in Table 6-2. The fourth specimen was subjectively excluded as an outlier (shown in red in Table 6-2) and the average and standard deviation of PD_{after} was calculated using the remaining results.

Table 6-2: Preliminary CEM IIA-L 52.5 N centrifugal consolidation results

Specimen	PD before	PD after
1	0.447	0.531
2	0.447	0.530
3	0.447	0.530
4	0.447	0.494
Average		0.530
Standard deviation		0.001

The precision of the test method was notably increased relative to the wet packing test, however,

additional mixtures were necessary to achieve a PD_{after} that was equivalent to the value of PD_{before}. Therefore, an additional mixture with w/p = 0.2 by mass (approx. 0.620 by volume) was constructed. This yielded a mixture which was considerably less flowable than the first and difficult to place in test tubes. Furthermore, on the completion of centrifuging, a negligible amount of water was able to be extracted from only 1 of 6 test tubes. This result led to the approximate convergence of PD_{before} and PD_{after} to 0.618, which explained the negligible amount of excess surface water. Therefore, it would have been preferable to have first constructed a mixture with intermediate w/p between 0.4 and 0.2 to confirm the point of convergence (i.e. the maximum packing density of CEM II A-L 52.5 N).

The same procedures were then performed for a plain KB10 limestone paste with w/p = 0.23 by mass (approx. 0.630 by volume). Of the 6 specimens, surface water removed from the surface of 3, but each contained some very fine material still in suspension. Table 6-3 portrays results for the packing density before and after (PD_{before} and PD_{after}) for the preliminary KB10 test.

Table 6-3: Preliminary KB10 limestone centrifugal consolidation results

Specimen	PD before	PD after
1	0.615	0.697
2	0.615	0.705
3	0.615	0.701
Average		0.701
Standard deviation		0.004

Similar precision was achieved for the KB10 test (of the specimens that were usable) yet no additional w/p was tested due to difficulty experienced when extracting excess water with a pipette. Solid material near the surface was easily disturbed and accidently removed with the surface water. For this reason, and the possibility of segregation due to high centrifugal force (raised as a potential concern by Fennis (personal communication 2017, February 23)) causing false measures of packing density, it was preferred to investigate yet another test technique.

6.1.3.3 Mixing energy test

As for the other powder packing density tests, the mixing energy test was first performed using plain CEM II A-L 52.5 N before testing other materials. Mixtures were constructed according to descriptions given in § 3.3.3. Figure 6-19 portrays the raw power consumption data plotted against the solid volume fraction for cement, CEM II A-L 52.5 N, as well as a plot of the same data which had been smoothed using a median filter. Solid volume fraction is taken as the ratio of the solid volume of powder to the combined volume of water and powder solid volume in the paste. At the beginning of the test, the starting water content is low, and solid volume fraction is its highest but decreases as the water content increases. As the assumption of the test method is that interstitial space is completely filled with liquid at the peak in power consumption (i.e. no entrained air), the maximum packing density is equivalent to the solid volume fraction at the peak in power consumption.

Significant 'noise' in the power consumption data is portrayed in Figure 6-19, particularly leading up to the peak. This was attributed to the moisture state of the material as the particle

mixture moves through various degrees of saturation as well as imperfections in the planetary movement of the mixer, resulting in spontaneous collisions of the paddle with the side of the mixing bowl. At the beginning of the test, the initial mixing water produced a heterogenous, earth-moist mixture resulting in more substantial 'noise' leading up to a peak. As the water content increased with time, the mixture became more homogenous and power consumption increased up to a point before it became over-saturated with water, leading to a decrease in power consumption. As a result of the increased consistency of the mixture, less 'noise' is associated with the latter period.

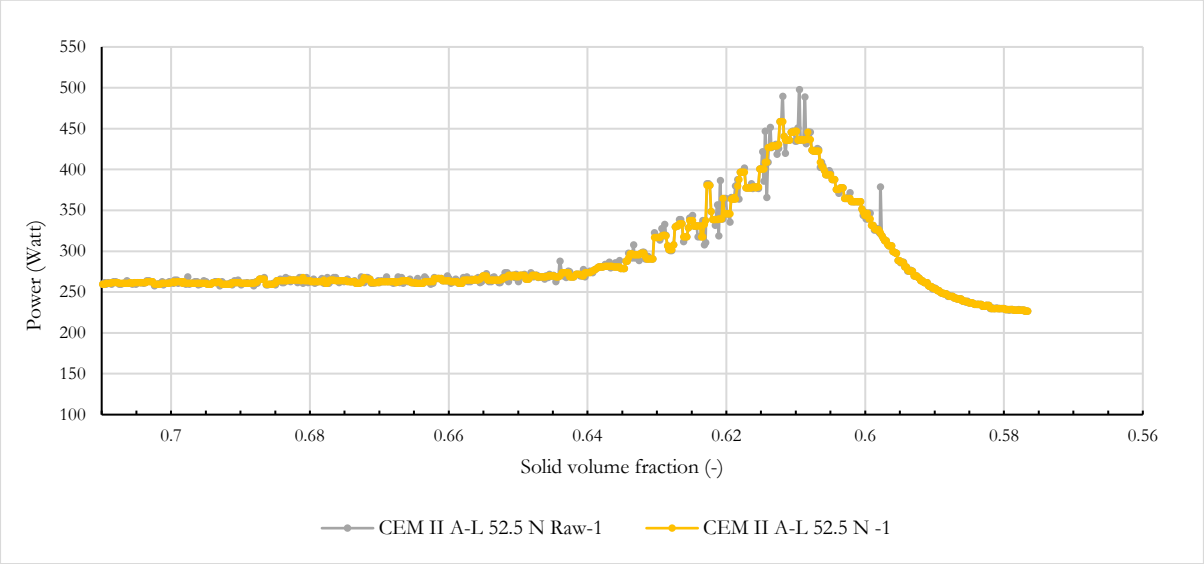

Figure 6-19: Raw and filtered mixing energy test results for plain CEM II A-L 52.5 N

To assess more accurately the solid volume fraction at which the maximum power consumption occurs, a median filter was applied to the raw power consumption data. This transformed each raw data point to be the median of 5 data points, encompassing 2 raw data points each side of the point being considered, and corresponded to describing the power consumption at any point in time as the median power consumption recorded over a 2.5 s period. Although the filtered data still contained noise, it allowed a more accurate judgement of the solid volume fraction at the peak in power consumption (0.610 ± 0.002). The repeatability of the method was investigated by conducting 2 additional replicate tests for cement (filtered test data is portrayed in Figure 6-20). The combination of these results then inferred the maximum packing density to be in the range of 0.614 ± 0.002.

Thereafter KB10 limestone was similarly tested. Filtered KB10 results for duplicate tests are portrayed in Figure 6-21. Maximum packing density (0.627 ± 0.002) was determined to an accuracy similar to the cement specimens, instilling confidence in the method. However, contradictory to the Wet Packing Test result (6.1.3.1), KB10 maximum packing density was relatively higher than the plain cement. An 80/20 % volume blend of cement / limestone was also tested, the filtered results of which are portrayed in Figure 6-22. Despite being able to differentiate the maximum packing densities of each plain powder from one another, the mixing energy test showed maximum packing density of the blend to be negligibly different to the plain cement. This finding was in line

with the Wet Packing Test result for the same blend and therefore was expected to be a characteristic of the blend and that KB10 was not capable of increasing the packing density of the powder phase.

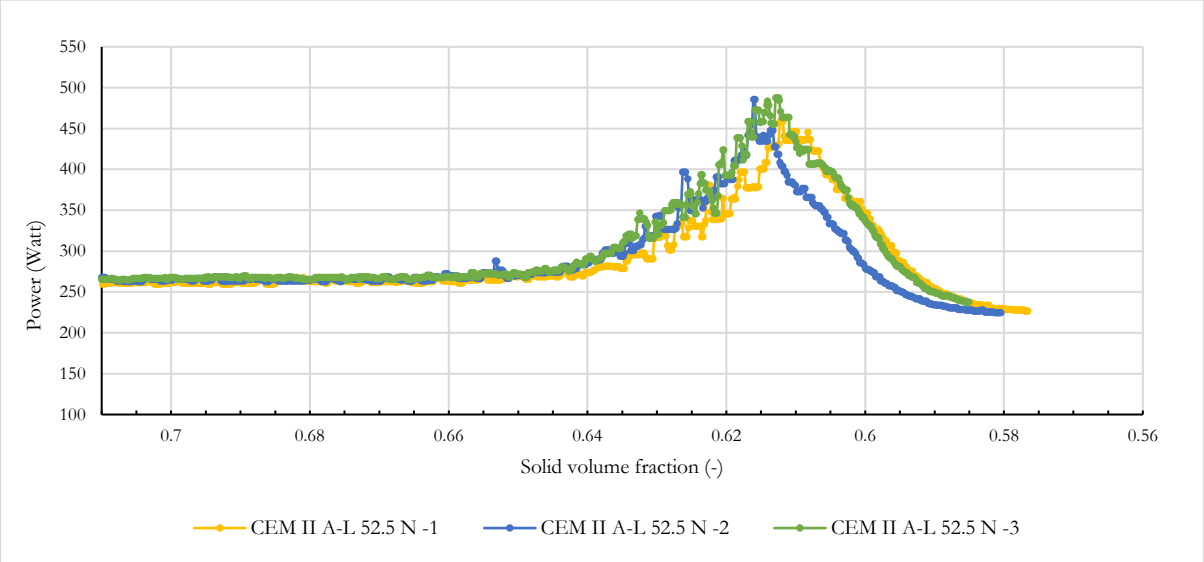

Figure 6-20: Filtered mixing energy test results for replicate tests of plain CEM II A-L 52.5N

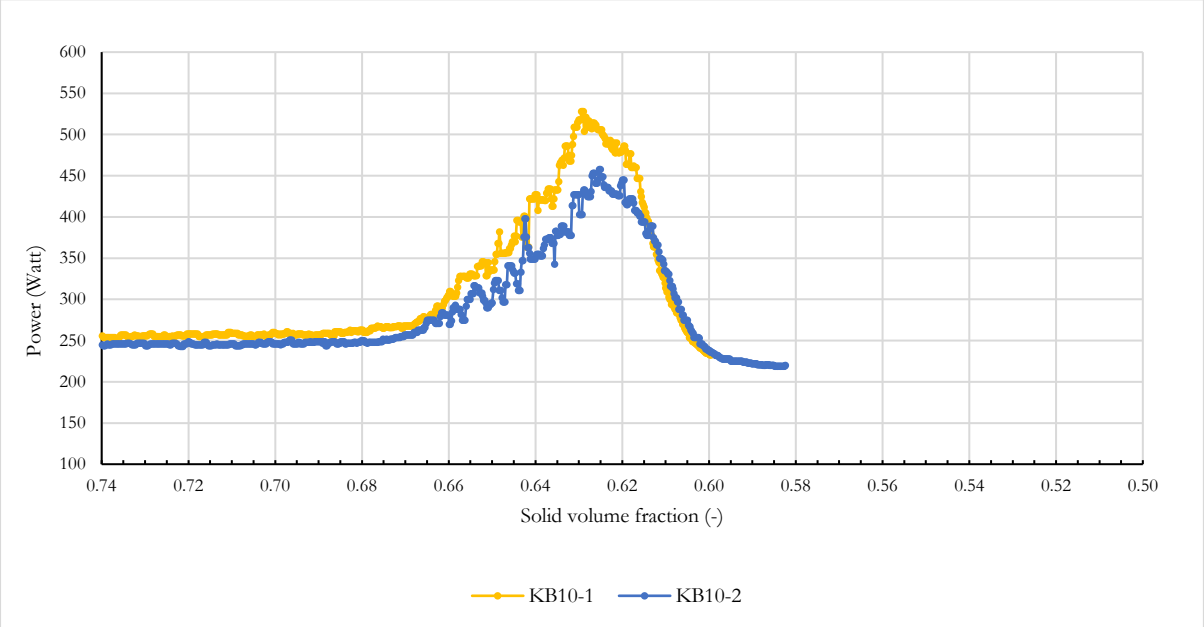

Figure 6-21: Filtered mixing energy test results for duplicate KB10 limestone tests

The consistent accuracy associated with the preliminary tests instilled confidence in the repeatability of the mixing energy test method. Furthermore, a consistent mixing regime and starting material volume ensures repeatable results. The consistent compaction effort experienced by the various material combinations allows a compaction index to be assigned to the test method. The test setup was also conducive to minimising material usage and the testing of many

combinations could be completed relatively quickly. Therefore, this method was selected for further use in assessing the maximum packing density of various powder material combinations.

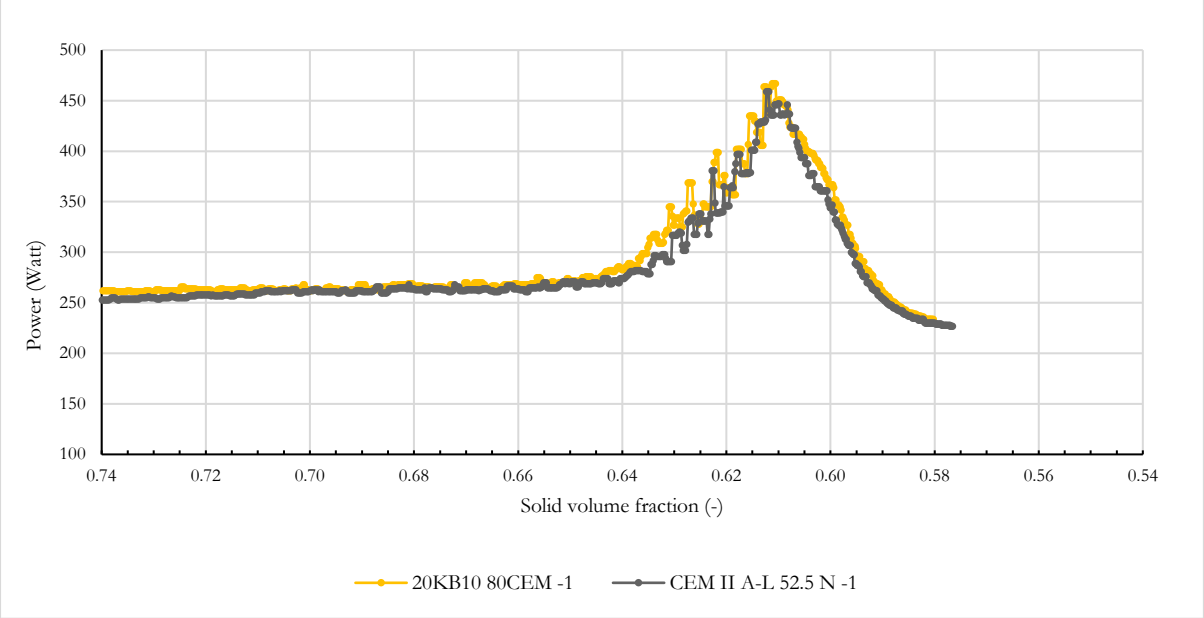

Figure 6-22: Filtered mixing energy results for plain CEM II A-L 52.5 N and an 80 / 20 % volume blend of CEM II A-L 52.5 N / KB10 limestone

6.1.3.3.1 Limitations of the mixing energy test

An attempt to determine the compaction index (K) of the method using fine aggregate (§ 6.2.1.1) was unsuccessful. Instead, a K value of 12.2 was assigned to the method for use in the CIPM, which was in accordance with Fennis (2011). It was expected that the development of smaller cohesive forces between fine aggregate particles (relative to those developed between powder particles) made the change in power consumption with an increase in moisture content more difficult to detect and led to the poor definition of a peak in power consumption (§ 6.2.1.1).

The failure of the method to account for the formation of ettringite in the pre-induction period (shortly after water and cement come into contact) and its potential influence on the measured packing density was raised as a potential concern (Schmidt, personal communication 2017, June 27). It was expected that continuous mixing for the duration of the experiment would not allow for the formation of ettringite, which could contribute to increasing the solid volume, and potentially the measured packing density if given the time to form.

To assess this, a plain cement test was conducted and once the initial water and mixing was completed, the material was left to rest for 5 mins. The intention was to allow the formation of ettringite in this period before beginning mixing again and comparing the packing density result with a result where no resting time was incorporated. The result was a negligible difference, obtaining a packing density within the tolerance already given (0.614 ± 0.002.) and therefore it was not expected to have a significant impact on other test results.

Furthermore, it has also been suggested that there is potentially a delay in the recorded power consumption for a particular moisture content and that, instead, sufficient mixing time should be

allowed in between the addition of each water increment to ensure proper distribution of the moisture in the mixture before recording the corresponding power consumption (Hunger, 2010). However, due to the small flow rate used (between 0.5 and 1 ml/s) and the use of a median filter for the analysis of power consumption data, this phenomenon was not explicitly accounted for and was considered a limitation of the method.

6.1.4 Powder mixture packing densities

The packing density of all plain powder materials was measured using the mixing energy test and was followed by measuring combinations of each limestone filler with cement. Four blends of each limestone type with cement were considered. These were, namely, limestone contents of 20, 40, 60 and 80 % of total powder volume. The measured packing density and range associated with the result for plain materials and material mixtures is summarised in Table 6-4 and all results are portrayed in Figure 6-23. Each packing density was determined using a median filter (as discussed in § 6.1.3.3) and is the average of at least two replicate tests. The range reported represents the difference between the maximum and minimum experimental result for each material combination. Mixing energy plots for each powder combination are portrayed in Appendix B, Figure B-1 to Figure B-16.

The plain materials (i.e. 100 vol.% - Table 6-4) of higher fineness were expected to have lower packing densities than coarser materials because of agglomeration being more pronounced with decreasing particle size, limiting the maximum achievable packing density. This trend was noticed when comparing packing densities of materials: KB45, KB10, KB5 and CEM II A-L 52.5 N (listed in order of decreasing packing density) but not for KB2. Instead, KB2 had a packing density almost equivalent to KB45, yet testing was inconclusive as to why this was the case. Similar observations were, however, discussed by Van Der Putten *et al.* (2017) for the packing density of high fineness, plain silica fume. They noted varying findings of either excessively high or low packing densities relative to what was expected when considering the packing densities of blends of silica fume with other materials. Therefore, the measured result for KB2 was used within the CIPM yet it was acknowledged that the method of determining the packing density of such high fineness materials may need revising.

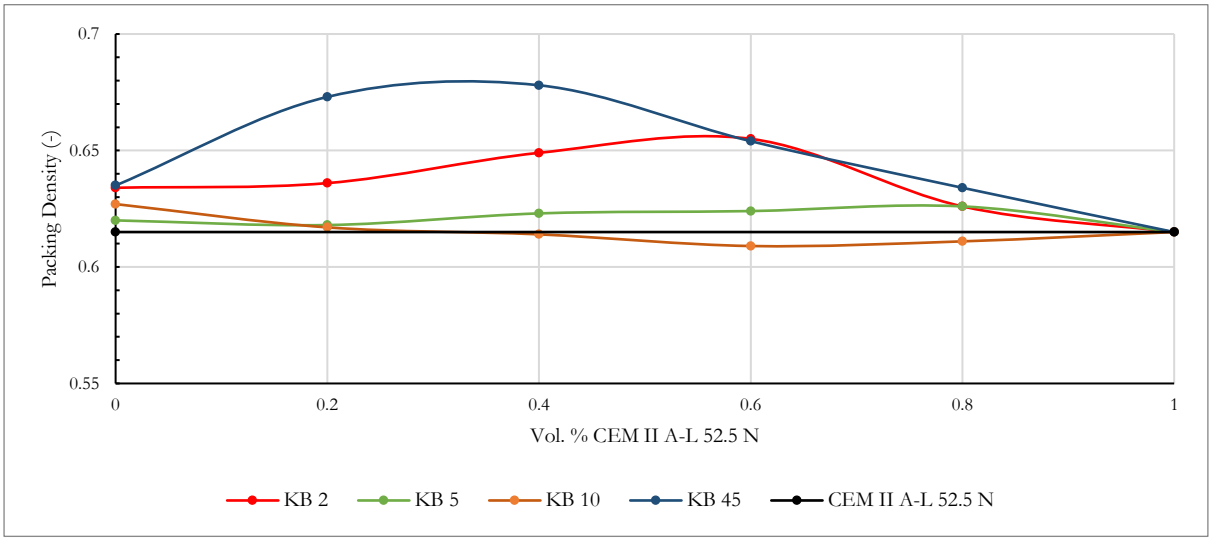

Figure 6-23: Experimental packing densities for various limestone fillers in combination with CEM II A-L 52.5 N

Table 6-4: Mixing energy experimental packing densities and corresponding range for various powder mixtures

Mixture No.	Volumetric portion of powder					Experimental packing density (α_{exp})	Range	Range as a % of (α_{exp})
	KB2	KB5	KB10	KB45	CEM II A-L 52.5			
1	0	0	0	0	1	0.615	± 0.002	0.33
2	0.2	0	0	0	0.8	0.626	± 0.004	0.64
3	0.4	0	0	0	0.6	0.655	± 0.005	0.76
4	0.6	0	0	0	0.4	0.649	± 0.003	0.46
5	0.8	0	0	0	0.2	0.636	± 0.001	0.16
6	1	0	0	0	0	0.634	± 0.002	0.32
7	0	0.2	0	0	0.8	0.626	± 0.001	0.16
8	0	0.4	0	0	0.6	0.624	± 0.002	0.32
9	0	0.6	0	0	0.4	0.623	± 0.001	0.16
10	0	0.8	0	0	0.2	0.618	± 0.002	0.32
11	0	1	0	0	0	0.620	± 0.002	0.32
12	0	0	0.2	0	0.8	0.611	± 0.001	0.16
13	0	0	0.4	0	0.6	0.609	± 0.001	0.16
14	0	0	0.6	0	0.4	0.614	± 0.002	0.33
15	0	0	0.8	0	0.2	0.617	± 0.002	0.32
16	0	0	1	0	0	0.627	± 0.002	0.32
17	0	0	0	0.2	0.8	0.634	± 0.001	0.16
18	0	0	0	0.4	0.6	0.654	± 0.002	0.31
19	0	0	0	0.6	0.4	0.678	± 0.002	0.29
20	0	0	0	0.8	0.2	0.673	± 0.001	0.15
21	0	0	0	1	0	0.635	± 0.001	0.16

Cement combinations with limestones KB5 and KB10 had negligible impact on packing density relative to plain cement. Combinations containing KB5 negligibly increased packing density to a maximum of 0.626 at 80 % KB5 whereas the inclusion of KB10 was only able to achieve a maximum of 0.617 at 80 % KB10 and caused decreased packing density (albeit negligibly) for all of the other combinations. Cement blends with KB2 and KB45 were all successful in increasing packing density relative to plain cement. For blends containing KB2, maximum packing density (0.655) was achieved at 40 % KB2. Blends containing KB45 consistently achieved the highest packing density at all replacement ratios tested, with the maximum packing density (0.678) achieved at 60 % KB45.

Therefore, KB2 and KB45 have the largest potential for use in increasing the packing density of the powder phase of concrete. As all the limestone fillers have undergone similar manufacturing processes, their particle characteristics (such as shape and morphology) were not expected to have significantly influenced their resulting packing densities, relative to one another. Instead, the varying fineness (KB2 much finer, KB45 much coarser) and particle size distribution of these materials was expected to be primarily responsible. Mechanisms influencing the mixture packing densities are further discussed in § 6.2.3.

6.2 Particle packing modelling

6.2.1 CIPM Calibration

6.2.1.1 Compaction index (K)

The methodology described in § 4.2.4.3.1 was followed for the determination of the compaction index (K) associated with the mixing energy test. The reference method used to determine the mixing energy test K was filling a container with single-sized Philippi dune sand by pouring (with no other compaction applied) and determining the packing density of the material. The consensus from the review of literature was that this reference method has a K of 4.1. Two cylindrical containers (Figure 6-24) of different volumes (197 and 2855 ml) were used to collect packing density data and ensure size-related effects did not influence packing density results. The smaller container was that used for the wet packing test (§ 3.3.1) and the larger container is the standard apparatus for determining bulk density of fine aggregate (SANS 5845 (2006)). Experimental packing density results from filling each container are shown in Table 6-5.

Table 6-5: Packing density results from filling a mould by pouring

Specimen no.	Experimental packing density results (Pouring: K=4.1)	
	Small container (V=197 ml)	Large container (V = 2855 ml)
1	0.525	0.538
2	0.527	0.536
3	0.530	0.536
4	0.530	0.535
5	-	0.534
Average	0.528	0.536
Standard deviation	0.002	0.002

Figure 6-24: Cylindrical containers of varying capacity for the determination of the compaction index (K)

Discrepancy in the average result for each container was attributed to the wall effect: material against the wall of the container has decreased packing density relative to material sufficiently far from the container wall. Due to the increased proximity of the container wall to all particles in the smaller container, the packing density measured in this container was lower relative to the larger

container. Following the reference test, a mixing energy test was then conducted using the same material. The plots of power (Watts) versus solid volume fraction (-) for two replicate tests are shown in Figure 6-25. For a further, generalised description of the interpretation of mixing energy results, see § 6.1.3.3.

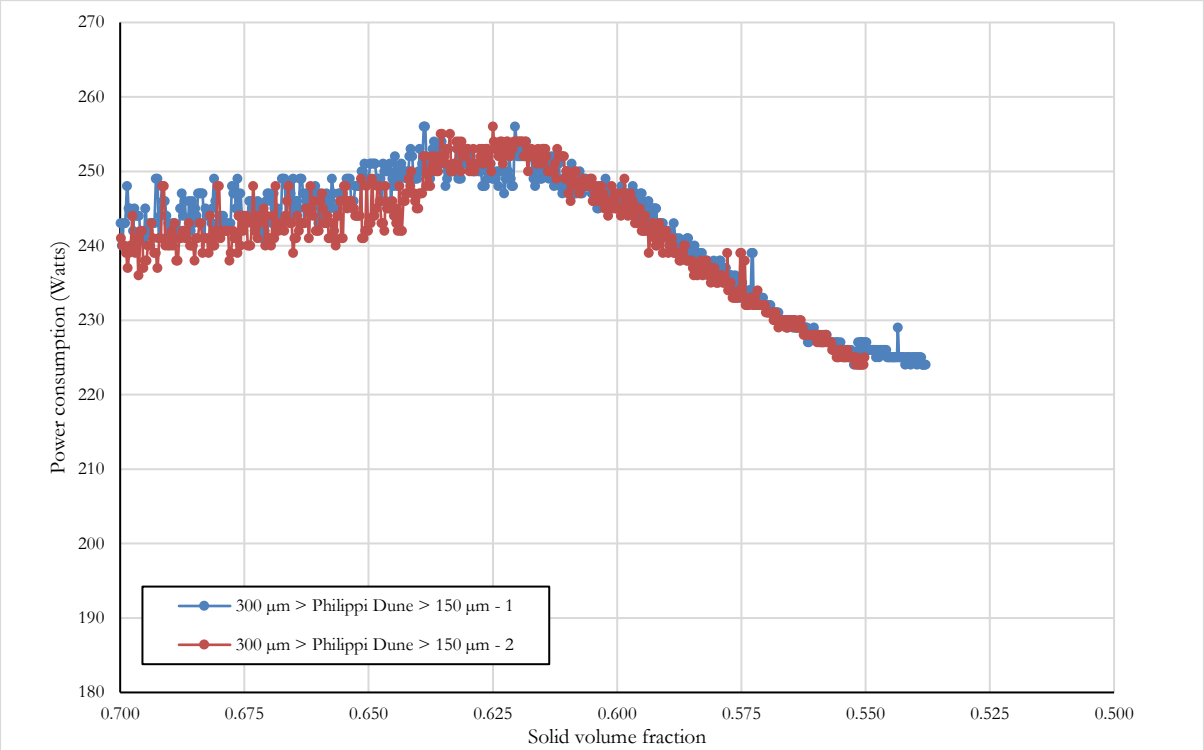

Figure 6-25: Mixing energy test results for replicate Philippi dune sand tests

A trend of increasing power consumption followed by decreasing power consumption was observed, with a peak in power consumption, although the 'noise' in the data somewhat blurred the definition of a peak. The peak was relatively flat, spanning a range of solid volume fractions, making it difficult to exactly define the maximum packing density. Furthermore, the test method was initially developed for use in assessing the water demand of powder mixtures which are characterised by the development of substantially higher cohesive forces when in contact with a liquid, due to their small particle size. Therefore, the weaker cohesive forces developed between fine aggregate particles may have contributed to a poorly defined peak in power consumption and difficulty in assigning a single solid volume fraction to the maximum power consumption.

To make use of the data, a median filter was applied to the raw power consumption data which transformed each raw data point to be the median of 5 data points, encompassing 2 raw data points each side of the point under consideration. This corresponded to describing the power consumption of the mixer at any point in time to be the median power consumption recorded over a 2,5 s period. However, a single peak could still not easily be defined and therefore an approximate analysis of the centroid of a portion of the area below the curve (within which the power consumption increased and then decreased) was assessed to approximate the maximum packing density as the point equivalent to the centroid. Performing this centroid analysis for the 2

sets of data displayed in Figure 6-25 led to a maximum packing density result of 0.620 ± 0.004.

The average packing densities from the filling of each mould (Table 6-5) were averaged again, arriving at a value of 0.532. This was used in combination with values of 0.620 ± 0.004 from the mixing energy test to determine the compaction index for the mixing energy test according to *Eqn. 4-11*. Table 6-6 portrays the variation in the calculated value of K for the range of packing densities obtained using the mixing energy test. These values differ from the K=12.2 proposed by Fennis (2011) and are outside the reasonable range which Fennis suggested for the mixing energy test (between 9 and 13).

Table 6-6: Resulting compaction index (K) for various experimental packing densities

Packing density		Resulting K
Pouring	Mixing energy	
0.532	0.616	13.5
0.532	0.620	15
0.532	0.624	16.5

Using K =12.2 in combination with the virtual packing density from the reference method in *Eqn. 4-11*, the experimental packing density that should be expected from the mixing energy test is calculated to be 0.612. Although this was outside the range of 0.620 ± 0.004, this predicted value only results in an error of 1,3 % of the mean (0.620) experimental packing density. Due to the determination of solid volume at peak power consumption only being approximate, the use of K=12.2 was preferred to describe the mixing energy test for the remaining application of the CIPM to be consistent with existing research using this method (Fennis, 2011).

6.2.1.2 Loosening (C_a) and wall effect (C_b) coefficients

Following the methodology discussed in § 4.2.4.3, experimental packing density data from testing 16 different powder combinations (reported in § 6.1.4) was used for the determination of C_a and C_b while the cut-off diameter (d_c) was held constant at 25 μm. The values of these constants were determined through the minimisation of the percentage difference (error) between packing densities predicted by the model and those observed experimentally for the same powder combination. The error was assessed at 2 levels: the average error associated with the packing densities for cement/limestone combinations per limestone type (either KB2, KB5, KB10 or KB45) and then the overall average error across all cement/limestone combinations tested.

Figure 6-26 portrays the average error in predicted packing density for all tested combinations of C_a and C_b for cement / KB2 combinations. It is evident that there is a consistent, large decrease in average error (from approximate max of 11 % to 2.0 %) as C_a increases from 1 to 6. There is a further gradual decrease in error (2 % to 1 %) as C_a increases to approximately 14 and thereafter the average error gradually begins to increase but stays within the range of 1 and 2 % average error.

The value of C_b has its greatest influence on predicted packing density while the value of C_a is relatively small (in the range of 1 to 5) but becomes less as the value of C_a is further increased. At C_a=1, the difference in prediction errors for C_b=0.1 and C_b=1 were the largest (approximately

3 %), with C_b=1 returning the lowest error. This finding is contrary to Fennis' (2011) findings, where she found C_b = 0.2 (representing a decreased wall effect) to more accurately describe powder packing density. At C_a = 5 and the same range of C_b values (0.1 and 1), the difference in error was approximately 1 % and error decreased as C_b approached 1. For any value of C_a > 6, the difference in error with a change in C_b from 0.1 to 1 was consistently less than 1 %. Therefore, for C_a values beyond 6, the C_b value had little effect on the average error recorded for combinations of cement and KB2.

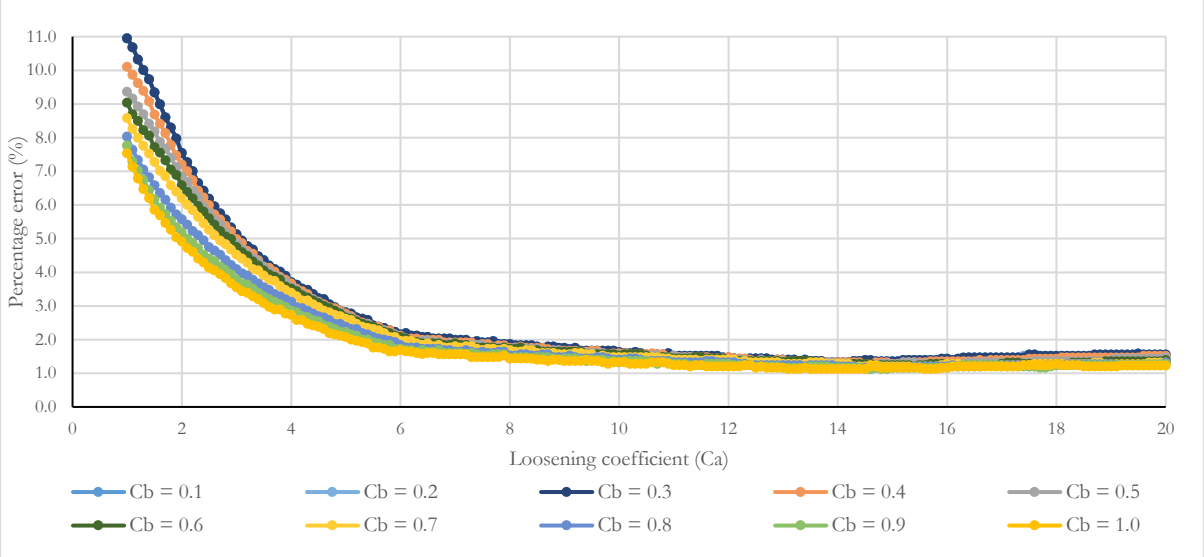

Figure 6-26: CIPM average prediction errors for CEM II A-L 52.5 N / KB2 combinations with varying C_a and C_b

Similar trends to KB2 appear in the average error plots for cement / KB5 combinations when C_a and C_b are varied (Figure 6-27). For low C_a values, average error decreases as C_a increases (with the largest error dropping from approximately 5.3 % to 1.9 % as C_a approaches a value of 6. Once again, average errors are more sensitive to a change in the value of C_b at low C_a values and from approximately C_a =10 onward, the value of C_b has negligible effect on the average error. For any C_a > 10 in combination with 0.1<C_b <1, average errors are within 1 % of one another. For the case where the influence of surface forces is not accounted for (i.e. C_a=C_b=1) average error is 2 %, remarkably lower than the average error for the same scenario when considering the mixtures using KB2 (7.5 %). Therefore, there is an apparent increase in the accuracy of the model for the mixtures comprising KB5 when compared to those using KB2 for the case of no surface forces being considered. This is due to the finer KB2 material being more affected by surface forces and the increase in the accuracy of the model as the material's average particle size increases and the influence of surface forces decreases to an extent.

The average error plots for cement / KB10 combinations with varying C_a and C_b are shown in Figure 6-28 for even C_b and in Figure 6-29 for odd C_b (for clarity). Both figures show that, as for the KB2 and KB5 combinations, average errors are more sensitive to the value of C_b at low values of C_a (approximately C_a < 5). Furthermore, for C_a > 5, the absolute value of C_a and C_b do not have a significant influence on the error. Average error tends to converge to approximately 1.5 % for C_a > 5, independent of the value of both C_a and C_b.

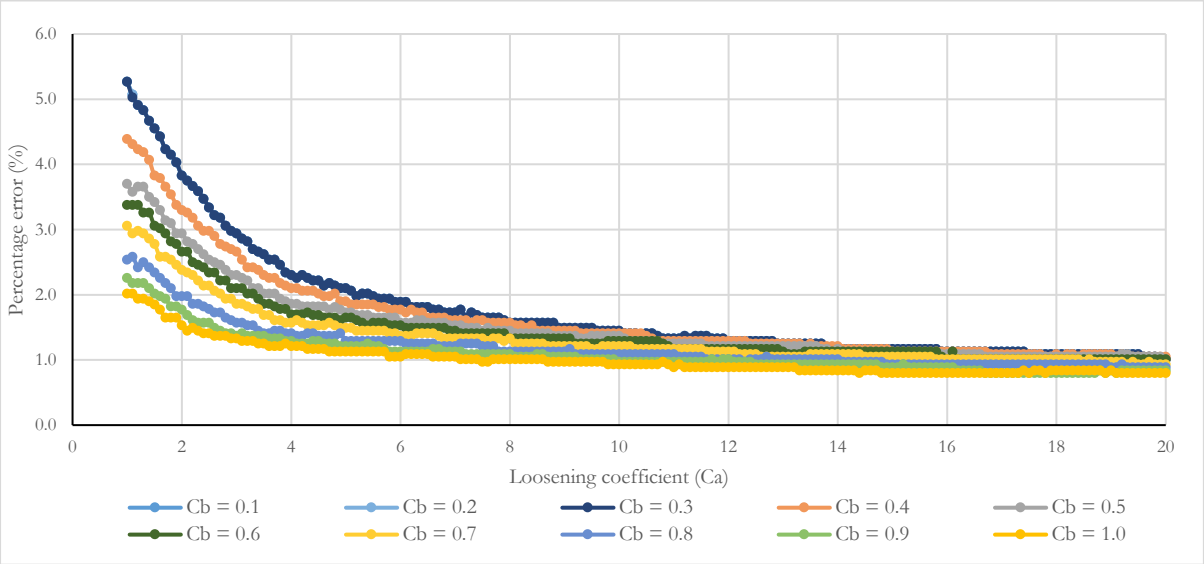

Figure 6-27: CIPM average prediction errors for CEM II A-L 52.5 N / KB5 combinations with varying C_a and C_b.

When no consideration is given to surface forces (C_a=C_b=1), average error was 1.5 %. This value is slightly reduced relative to KB5, once again, inferring an increase in accuracy of the model for coarser materials relative to finer materials when no surface force interaction is accounted for. Although there appears to be some fluctuation in the average errors across various C_b as well as for the variation of C_a for a particular C_b (the largest fluctuation being 0.15 % for $1<C_a<3$), this cannot be regarded as significant due to the range associated with each experimental result being larger than this and therefore likely responsible for the fluctuation.

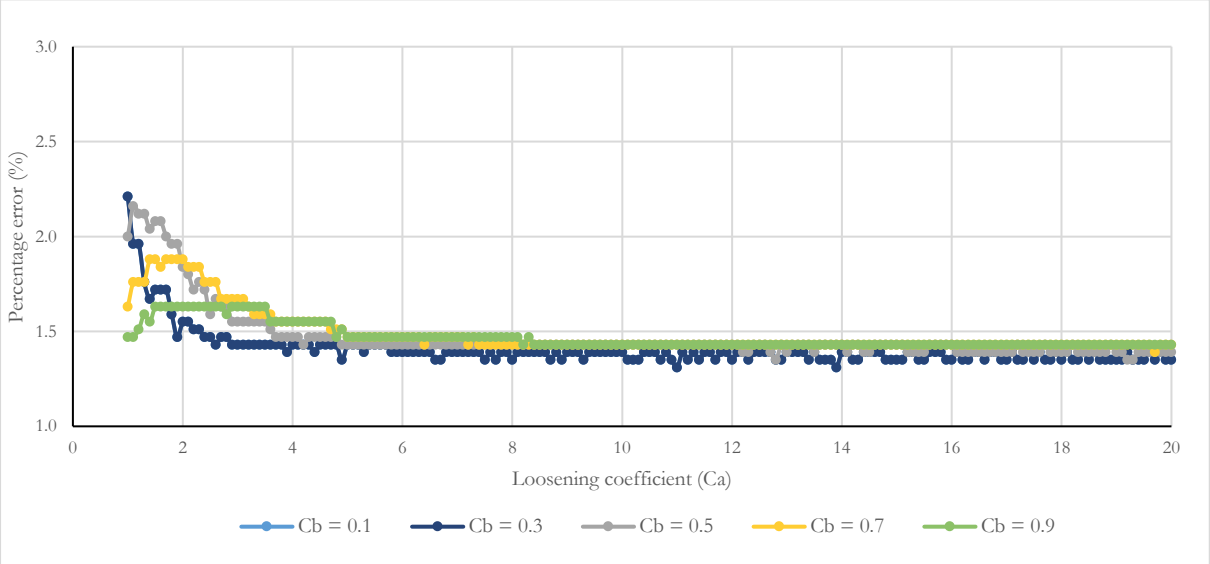

Figure 6-28: CIPM average prediction errors for CEM II A-L 52.5 N / KB10 combinations with varying C_a and C_b (for odd C_b)

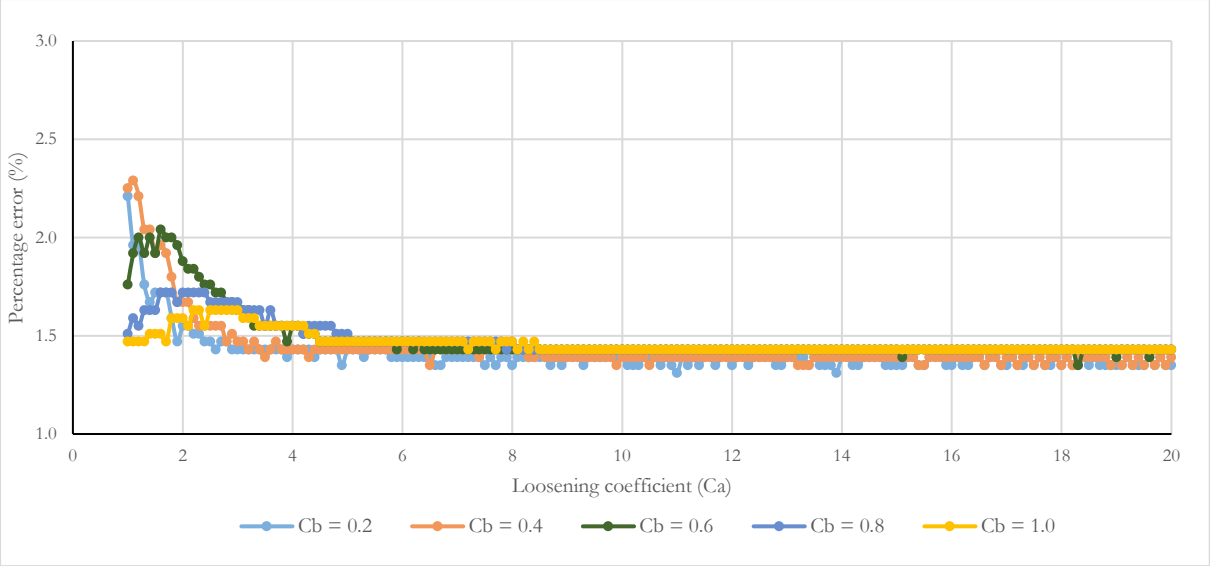

Figure 6-29: CIPM average prediction errors for CEM II A-L 52.5 N / KB10 combinations with varying C_a and C_b (for even C_b)

Figure 6-30 portrays the average error plots for cement / KB45 combinations with varying C_a and C_b. KB45 average error also initially decreased with increasing C_a but tended to a local minimum average error at lower C_a values (C_a < 2.5 for all values of C_b) than any of the other limestones. Due to the increased sensitivity of the value of C_b on packing density at low values of C_a, the value of C_b now had a greater influence on the average error when compared to the other limestone mixtures. Contrary to the other limestones, for all values of C_a, average error was minimised for lower values of C_b and increased as C_b approached 1. Plots for C_b = 0.1, 0.2 and 0.3 converge on one another in Figure 6-30 but minimum average error was achieved for C_a=1.5 with C_b=0.4.

Of all the limestones, the average error was minimised the most for KB45 mixtures, achieving average error of 0.23 % (others were all approximately 1.5 %). As the value of C_a increased from 1.5, the average errors once again increased and the influence of the value of C_b on the average error was no longer significant (discussed further in § 6.2.1.4). Similar average errors were obtained independent of the C_b value (0.1 to 1) when combined with C_a > 3. Ultimately, average error converged to 1.5 % for large C_a and was still independent of the value of C_b.

Considering the case of no surface force interaction for KB45 mixtures (C_a=C_b=1), the prediction error was its highest (2.84 %). This is contrary to the trend of decreasing error as materials become coarser, which was seen when C_a=C_b=1 for the other limestones. However, this error is still considerably lower than that recorded for KB2 mixtures (7.5 %) and is significantly reduced with relatively smaller magnitudes of C_a and C_b than for the other limestones. Therefore, the packing densities of KB45 mixtures were the only cement/limestone combinations which followed Fennis' (2011) proposal concerning the packing of powders: that powder packing density can be more accurately predicted when assuming a combined decreased wall effect (C_b<1) and increased loosening effect (C_a>1).

Comparing the average error results for the combinations of cement with each limestone type, only the KB 45 results showed a clear minimisation of average error for a specific combination of C_a and C_b. Average errors from the remaining limestones tended to converge to a

minimum error, indicating that beyond a certain C_a value and independent of the value of C_b, there was little change in average error (approximate fluctuation of 0.5 %).

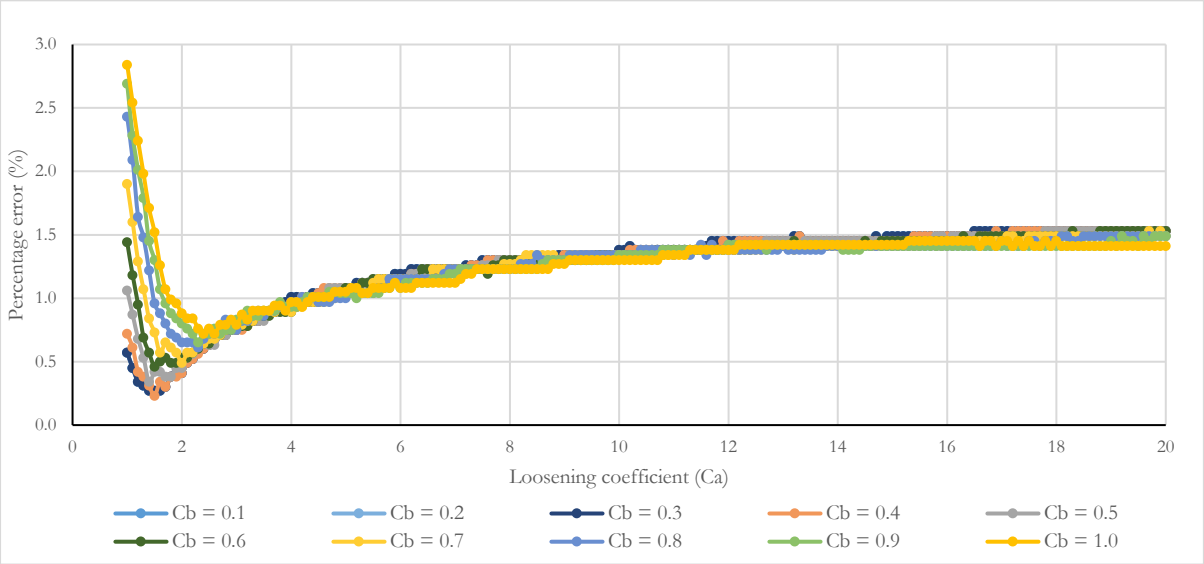

Figure 6-30: CIPM average prediction errors for CEM II A-L 52.5 N / KB45 combinations with varying C_a and C_b.

Figure 6-31 portrays the overall average error plots for all cement / limestone combinations with varying C_a and C_b (i.e. combining errors from cement combinations with KB2, KB5, KB10 and KB45. See Appendix B for description of error). The overarching trend is also the convergence of average error to a single error value which is independent of the value of C_b as C_a becomes large. This follows the same trend as KB2, KB5 and KB10 combinations but does not represent the local minimisation of the average error as seen for KB45.

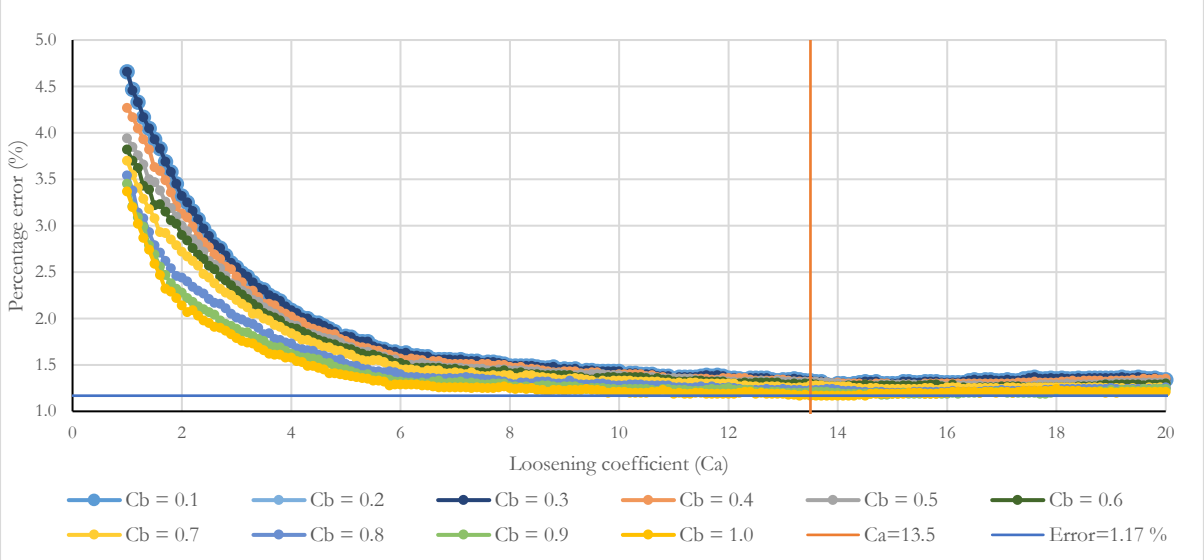

Figure 6-31: CIPM overall average prediction errors for all CEM II A-L 52.5 N / limestone combinations with varying C_a and C_b.

For all cement / limestone combinations, except those containing KB45, average error was minimised for various $C_a > 1$ that were consistently in combination with $C_b = 1$. This finding implies a minimisation in error of powder packing density when the loosening effect is increased, and the wall effect remains unchanged, which is contrary to Fennis' (2011) findings, who advised the use of $C_a = 1.5$ and $C_b = 0.2$. The overall average error results from this research imply that the effect of surface forces on powder packing density is adequately described by the CIPM through an increased loosening effect alone and that the value of C_b has negligible difference on the packing density, particularly when the value of C_a is relatively large.

However, KB45 results still counter this statement and, instead, agree with Fennis' (2011) proposal, although the wall effect is not decreased to the same degree. It is therefore clear that values of C_a and C_b cannot always be generalised across a range of different powder materials and should possibly be defined specific to each powder material. Yet, to enable the practical selection of a single combination of C_a and C_b for application across all powder materials in the CIPM, their values were chosen according to the minimisation of the overall average error in Figure 6-31.

Although this did not enable the absolute minimisation of error associated with each limestone type, it allowed a single combination of C_a and C_b to be applied across all limestone combinations with cement, despite the type (KB2, KB5, KB10 or KB45) of limestone. Furthermore, as there were only four data points available to describe packing densities of cement combinations with each limestone type, there was insufficient data to validate the choice of C_a and C_b values which minimised errors associated with one limestone over another.

The use of C_a =13.5 and C_b=1.0 led to the minimisation of overall average error to 1.2 % (displayed in Figure 6-31) when d_c was held constant at 25 μm. The selection of these values led to the average and maximum errors associated with each limestone type portrayed in Table 6-7. Despite the use of C_b=1 inferring no decrease in wall effect, in this instance it is only a value which enabled the minimisation of error and cannot necessarily be interpreted as representing no decrease in the wall effect (see § 6.2.1.4.)

Table 6-7: Average and maximum errors for each limestone type with C_a =13.5, C_b=1.0 and d_c=25 μm

Limestone type	Average error (%)	Maximum error (%)
KB2	1.1	2.3
KB5	0.8	1.1
KB10	1.4	2
KB45	1.4	3.1
Overall error	1.2	3.1

6.2.1.3 Cut-off diameter (d_c)

Although surface forces are widely acknowledged to begin to influence the packing of particles below approximately 125 μm, Fennis (2011) defined a cut-off diameter (d_c) as 25 μm, below which surface forces have a significant effect on powder packing. As this value was dependent on characteristics of the materials being used, the effect of the variation of d_c on resulting prediction error was investigated.

Once C_a and C_b were defined, the value of d_c was varied, and a similar assessment of the resulting error was conducted as for the determination of C_a and C_b. Figure 6-32 portrays the average error in the predicted packing density for each individual limestone type in combination with cement as well as the overall average error calculated across all cement / limestone mixtures. This investigation entailed the variation of d_c in increments of 5 µm and showed the overall average error to be minimised when d_c = 10 µm. Assessing the errors associated with each limestone type, KB45 results were the most sensitive to a change in the value of d_c and the error associated with the remaining limestones was considerably less sensitive, showing minimal fluctuation with changing d_c (Figure 6-32).

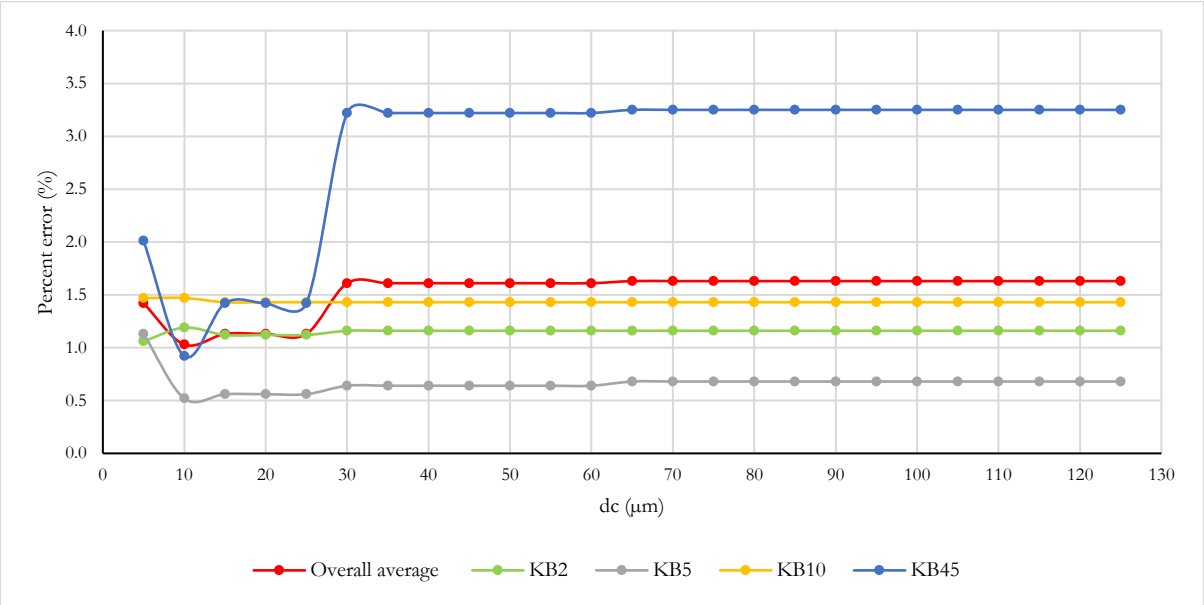

Figure 6-32: CIPM average prediction errors for C_a = 9.3 and C_b = 0.2 with varying cut-off diameter (d_c)

As for C_a and C_b, d_c was selected according to the minimisation of the overall average error to be able to apply a single value across all limestone types. This led to the use of d_c= 10 µm, which also minimised the error associated with KB45 and KB5 mixtures. The minimisation of the error associated with the other limestones all occurred when d_c= 15 µm but each had error that was negligibly different to the error corresponding to d_c= 10 µm and therefore, d_c= 10 µm was deemed the most appropriate to represent all powder materials. Further refinement of the value of d_c could not be justified due to limited experimental data and the tolerance associated with each experimental result being larger than the difference in error for differing values of d_c. Table 6-8 portrays the error results after the calibration of constants C_a =13.5, C_b=1.0 and d_c=10 µm. The overall average error achieved was equivalent to Fennis (2011) but the maximum error was increased in comparison to Fennis' (2011) reported 1.8 %.

6.2.1.4 Commentary on CIPM calibration

6.2.1.4.1 Assigning a value to the compaction index (K)

The ill-defined peak in power consumption when assessing the mixing energy of the Philippi dune sand prevented the concise definition of a compaction index (K) which was specific to the

experimental setup. However, extensive investigations by Fennis (2011) into the definition of K for the mixing energy test provided substantive basis for the use of K =12.2.

Table 6-8: Average and maximum errors for each limestone type with C_a =13.5, C_b=1.0 and d_c=10 µm

Limestone type	Average error (%)	Maximum error (%)
KB2	1.2	2.8
KB5	0.5	1.1
KB10	1.5	2
KB45	0.9	1.4
Overall error	1.0	2.8

It is possible that, by combining various other packing density test techniques, the K describing the mixing energy test could be more precisely defined. Despite difficulty in applying the centrifugal consolidation method for this research (§ 6.1.3.2), Fennis (2011) was able to use the method as an intermediate test between filling a container by pouring and the mixing energy test to increase the accuracy of the assignment of a K value. Fennis (2011) determined the packing density of discretely sized fine aggregate by filling a container by pouring and then again using centrifugal consolidation. She was then able to assign a K value to the centrifugal consolidation method and went on to use this method to determine the packing density of a powder material. Thereafter, the packing density of the same powder material was determined using the mixing energy test and the use of these two values of packing density in combination with the K value for the centrifugal consolidation method enabled Fennis (2011) to assign a K value of 12.2 to the mixing energy test.

6.2.1.4.2 Determination of C_a, C_b

Varying the values of C_a and C_b in the model resulted in different errors associated with each limestone type. These values were adjusted to minimise the errors, on the basis that this would reflect suitable model values for C_a and C_b. Errors associated with KB2, KB5 and KB10 tended to converge at different values of C_a (specific to each material), and then remain constant with further increases in C_a, and were relatively independent of the value of C_b after converging. However, KB45 error tended to a local minimum and then increased thereafter, enabling the determination of specific C_a and C_b values which minimised error.

Other than for cement combinations with KB45, the CIPM failed to adequately describe the general trend of experimental packing density with increasing limestone replacement despite the use of C_a and C_b to adjust the way in which powder materials experience compaction. This is more clearly portrayed in Appendix B, Figure B-17 through Figure B-24, which show combinations of cement with each limestone type and the resulting predicted packing densities for various C_a with the extremes of C_b (0.1 and 1) as well as experimental data points.

It is therefore apparent that C_a and C_b were able to more accurately describe the packing of cement with coarser material relative to finer material (as KB45 was substantially coarser than cement and all other limestones). Although the average error associated with the predicted packing density of cement with the finer limestones was decreased with the use of certain values of C_a and

C_b, these were not necessarily able to fit the predicted packing density values to the trend observed in the experimental data (i.e. the combination enabling maximum packing density according to the model does not match that inferred from experimental data) (Appendix B, Figure B-17 through Figure B-24).

When considering the combinations of cement with a particular limestone, accuracy of the predicted packing density for one combination might have been increased with a particular C_a and C_b value, but the same C_a and C_b would have decreased the accuracy of predicted packing density for another combination with the *same* limestone. The decreased accuracy for one combination and increased accuracy for another combination with the same limestone caused the convergence of the average error to a single value (seen in § 6.2.1.2) for KB2, 5 and 10.

However, the predicted packing densities for cement combinations with KB45 followed the same trend as the experimental packing densities (Appendix B, Figure B-23 and Figure B-24), and various combinations of C_a and C_b had the same effect on the accuracy of predictions (either an increase or decrease) for *all* combinations of KB45 with cement. The consistent increase or decrease in error with a change in C_a and C_b value across *all* combinations of cement with KB45 caused the local minimisation of error at particular values of C_a and C_b. It was therefore apparent that the way in which surface forces were implemented through C_a and C_b was appropriate for the description of the coarse limestone but still failed to represent the finer limestones.

The inability of C_a and C_b to enable consistent accuracies across combinations of cement with limestones of varying fineness speaks to the inadequacies of the model to account for the effects of varying particle size. A potential solution may be the assignment of values of C_a and C_b specific to each material so that as the proportion of a certain material in a mixture is changed, the C_a and C_b values for the mixture are weighted accordingly. Such a phenomenon could also represent the varying ability of SP to disperse materials of varying fineness or chemical composition. Materials that are more poorly dispersed would have higher loosening effects associated with them due to increased presence of agglomerates and materials that are better dispersed would have lower associated loosening effects.

For practical application of the CIPM in this research, the selection of C_a and C_b according to the minimisation of average error was deemed the most appropriate. As already shown, this led to the choice of $C_a = 13.5$ and the relatively high value of C_a renders the difference in error between extremes of C_b=0.1 and C_b=1 negligible for overall average error as well as error associated with individual limestones. The use of C_b=1 provides a practical solution to minimise error associated with predicted packing densities but does not necessarily describe the influence of surface forces on the wall effect. This is due to the predicted packing densities not following the trends observed for the experimental data. Therefore, these findings cannot disprove the occurrence of a decreased wall effect for powder material packing, but instead, point to the difficulty of modelling powder packing behaviour. The following points summarise the main outcomes from the calibration procedure:

- The way that surface force interaction is included in the CIPM results in the magnitude of C_b having negligible effect on the resulting packing density as C_a becomes large.
- Surface force effects on powder packing were able to be accounted for solely by a large value of C_a (which is dependent on the filler material used).

- The use of C_b=1 only provides a practical solution for the minimisation of prediction error relative to the experimental data and does not necessarily infer the non-existence of a decreased wall effect.
- The constants C_a and C_b are sensitive to the materials used and therefore, it may be more appropriate to implement these interaction constants in a way that each material can be assigned their own C_a and C_b. However, from the perspective of modelling, where one would want a more general and universally applicable model, this would not be ideal.
- The appropriateness of the choice of the value of C_a and C_b should be further verified with more experimental data.

6.2.2 Packing density per size class

Table 6-9 presents the packing density per size class (α_i) for each powder material. This is a required input for the CIPM (§ 4.2.4.4) to ultimately calculate the packing density of a mixture of materials spanning several size classes. However, it is difficult to measure the packing density per size class experimentally as powder materials cannot be easily separated into their constituent size classes. Therefore, the values presented in Table 6-9 are the result of applying the CIPM in reverse. An experimental packing density (α_{exp}) was determined for each powder material (which is a mixture of different size classes) using the mixing energy test (K=12.2) and used as an input into the model to work back to a constant packing density per size class (α_i) for each material. As already mentioned, performing the calculation in this way makes the packing density per size class a function of the efficacy of the model (i.e. reliant on selection of K, C_a, C_b and d_c) and it therefore serves as a comparative input parameter. Packing densities per size class displayed in Table 6-9 were determined using K=12.2, C_a=13.5, C_b =1 and d_c=10 µm. Size classes are the geometric mean of the upper and lower size used in the particle size analysis (§ 4.2.4.1).

Table 6-9: Packing density per size class (α_i) and experimental packing density (α_{exp}) for each powder material

Size class (µm)	Packing density per size class (α_i)				
	KB 2	KB 5	KB 10	KB 45	CEM II A-L 52.5 N
599.81	-	-	-	0.504	-
279.51	-	-	0.579	0.504	-
130.25	-	-	0.579	0.504	0.554
60.69	-	-	0.579	0.504	0.554
28.28	-	0.598	0.579	0.504	0.554
13.18	0.615	0.598	0.579	0.504	0.554
6.14	0.615	0.598	0.579	0.504	0.554
2.86	0.615	0.598	0.579	0.504	0.554
1.33	0.615	0.598	0.579	0.504	0.554
0.62	0.615	0.598	0.579	0.504	0.554
0.39	0.615	0.598	0.579	-	0.554
0.33	0.615	-	-	-	-
Experimental packing density (α_{exp})	**0.634**	**0.620**	**0.627**	**0.635**	**0.615**

Inherently, particulate materials pack to a higher packing density in a mixture of various size classes (relative to the packing density of a mixture of particles that are equal in size). This is portrayed in the discrepancies between the experimental packing density (of the combined size classes) and packing density per size class. The assumption of an equivalent packing density per size class is a limitation of the model as this may not always be the case. Smaller particles subject to surface forces may instead have smaller packing densities per size class relative to larger particles that are not subject to surface force interaction. However, making this assumption still increases the accuracy of the consideration of powder materials in the CIPM relative to assuming all size classes pack to the same packing density as that of the experimental packing density.

6.2.3 CIPM output powder material combinations

A summary of the CIPM input parameters used for the analysis of possible powder combinations in 5 % increments is presented in Appendix C, Table C-1. Increments of 5 % were chosen as a practical limitation due to an exponential increase in computing time as increments are reduced. Analyses were conducted with defined minimum cement contents of 90, 80, 70, 60 and 45 % of total powder volume for each of the required cases discussed in § 5.1. Table D-1 through Table D-5 (Appendix D) portray output material combinations and corresponding packing densities for combinations enabling packing densities within 1.0 % of the maximum packing density achieved for each desired cement content. This range was reported to encompass all results within the range of the tolerance for experimental results, given in Table 6-4, § 6.1.4. Proportions are given as a volume fraction of the total powder volume. The % increase in packing density relative to plain CEM II A-L 52.5 N is also quoted for comparative purposes.

Packing density outputs from the CIPM show an increase in the packing density of the powder phase as the allowable limestone content is increased up to 40 % but is negligibly increased thereafter when the limestone content is 55 %. Concerning the absolute maximum packing densities for each cement content, it is apparent that the binary blends of KB45 and CEM II A-L 52.5 N consistently achieve maximum packing density. Furthermore, considering the combinations with packing densities within 1.0 % of the maximum, combinations with a substantial proportion of KB45 are still favourable.

Relative to all the other limestones, KB45 has the widest particle size distribution and it is likely that, due to it comprising particles larger and smaller than cement, it enables the best optimisation of packing. Effectively, the overall particle size distribution of the powder phase is widened, making it possible to fill interstitial space with finer material that was not previously filled, leading to increased packing density.

A broader range of possible limestone combinations becomes a possibility when those achieving packing densities within 1.0 % of the maximum packing density (for the given cement content) are considered. After KB45, larger proportions of KB2 are preferred, followed by KB5 and lastly KB10. However, all appear in ternary or quaternary blends which include KB45. These findings are in line with existing recommendations for powder packing optimisation which advise the combined use of filler materials substantially finer and coarser (or similar in size to) the cement being used.

Ternary blends of cement, KB2 and KB45 lead to the inclusion of particle sizes of upper and lower extremes and therefore potentially allow for more effective filling of interstitial space by

the same mechanism already described for cement and KB45. However, this would now happen to a further degree due to the high fineness of KB2 (§ 3.1). Although KB5 and KB10 are both finer than the cement used, their increased similarity to cement (relative to KB2 and KB45) may inhibit their ability to increase packing density of powder phases to the same extent as KB2 and KB45.

Although combinations achieving packing densities within 1.0 % error were considered, the powder combinations used for constructing concrete mixtures were made according to those which enabled maximum packing density while adhering to any imposed practical limitations (see § 5.1) at each cement content (i.e. combination numbers 90-1, 80-1, 70-1, 60-2 and 45-6 in Appendix D). However, for the case of the powder phase comprising 80 % cement content, an additional mix was made with the combined requirement of maximising packing density with at least a minimum proportion of KB2, leading to the use of combination 80-2. Reasoning guiding this selection is further described in § 5.1.1.

6.2.4 Use of modelling outputs for concrete mix design

The outputs of powder combinations from the CIPM stage of modelling were used as policy constraints within the MAAC algorithm (§ 4.3.2). For reference, mix designs are summarised in Table 6-10. The R-squared statistic is reported for each mix design and is indicative of the quality of fit of the computed grading curve (the output of the MAAC algorithm) to the ideal MAAC grading curve (portrayed in *Eqn. 2-9*). Figure 6-33 and Figure 6-34 represent the overall grading curves for Phase 1 final mix designs. The MAAC ideal grading curve in the latter figure only differs from the former by the D_{min} used (due to the use of finer KB2 in Mix 1-4 and 1-6). Figure 6-35 represents the overall grading curves for Phase 2 final mix designs.

The reference mixture (portrayed as Mix 1-1 in all figures) was designed according to the commonly applied C&CI 'Method of Mix Design' (Addis and Goodman, 2009) and although the method does not intend to achieve maximal packing density or match an ideal grading curve, the overall constituent grading curve reasonably matches the MAAC grading curve, represented by a R-squared statistic of 0.98. However, the incorporation of parameters of bulk density and fineness modulus when determining aggregate quantities imply the filling of void space between coarse aggregates with fine aggregates, likely contributing to this finding.

The selection of aggregate quantities according to the MAAC algorithm for Mixes 1-2, 1-3 and 1-5 (Figure 6-33) enabled an increase in the R-squared statistic (all achieving $R^2 = 0.99$) relative to the reference mixture. A visibly better fit is seen for all three mixtures and for the portion of constituents larger than the powder phases, despite small discrepancies in fine and coarse aggregate quantities, the three grading curves tend to the same function. As for the CIPM, increasing limestone replacement in the powder phase also results in the computed grading curve approaching the ideal grading curve (i.e. an increase in packing density), which although is negligible, can be seen in Figure 6-33.

Table 6-10: Water content and particulate material constituents for Phase 1 and Phase 2 final mix designs

Constituent	Unit	Mix 1-1	Mix 1-2	Mix 1-3	Mix 1-4	Mix 1-5	Mix 1-6	Mix 2-1	Mix 2-2
		100 CEM	90CEM 10KB45	80CEM 20KB45	80CEM 5KB2 15KB45	70CEM 30KB45	60CEM 5KB2 35KB45	45 CEM 45 KB45 10 KB2	45CEM 30 KB45 5KB2 20FA
Water	kg/m³	210	210.0	210	210	210	210	164	164
Total binder	**kg/m³**	420	420.0	420	420	420	420	394.0	381.1
Cement	kg/m³	420	382.0	343.7	343.7	304.2	263.8	189.1	189.1
Limestone	kg/m³	-	37.7	76.3	76.3	115.8	156.2	204.8	129.3
KB2	kg/m³	-	-	-	19.1	-	19.5	33.6	16.8
KB45	kg/m³	-	37.7	76.3	57.3	115.8	136.7	171.2	112.5
Fly ash	kg/m³	-	-	-	-	-	-	-	62.7
Fine aggregate									
Granite Crusher 1	kg/m³	974	1046.0	1040.4	1053.4	1045.8	1039.9	-	-
Granite Crusher 2	kg/m³	-	-	-	-	-	-	-	-
Philippi Dune	kg/m³	-	-	-	-	-	-	1005.4	1005.4
Coarse Aggregate									
Nominal 9.5 mm Granite	kg/m³	760	684.0	685.3	672.3	675.7	677.2	846.2	846.2
Quality of curve-fit									
R^2 Statistic	-	0.98	0.99	0.99	0.99	0.99	0.98	0.95	0.95

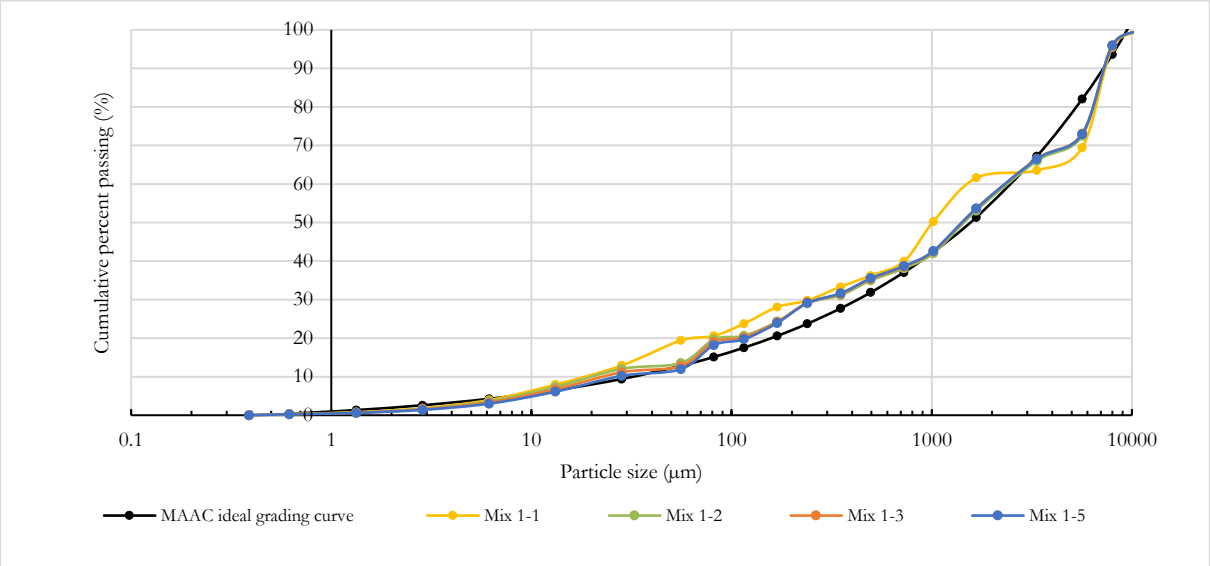

Figure 6-33: Overall constituent grading curves for Phase 1 mix designs constructed according to the MAAC algorithm with q= 0.37, D_{min}= 0.42 µm, D_{max} = 9.5 mm

Phase 1 mixtures making use of the finest limestone (KB2) are portrayed in Figure 6-34. Mix 1-4 was also able to improve on the reference mix design when comparing R^2 statistics but the increase in limestone replacement to 40 % for Mix 1-6 appeared to decrease the accuracy of the curve fit (and therefore the achievable packing density). This was despite the reported increase in packing density of the powder phases according to the CIPM results for the Mix 1-6 powder combination (§ 6.2.3). As seen for the mixtures in Figure 6-33, the largest discrepancy between Mix 1-4 and Mix 1-6 (Figure 6-34) was seen in the powder phases whereas the portion of the grading curve representing fine and coarse aggregate quantities is almost identical for both mixtures.

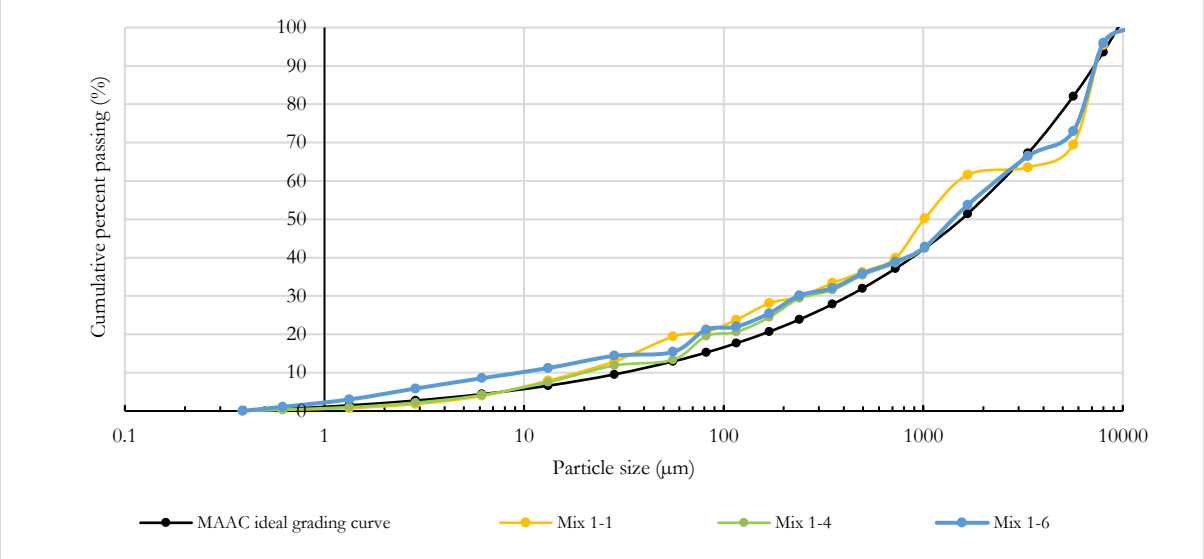

Figure 6-34: Overall constituent grading curves for Phase 1 mix designs constructed according to the MAAC algorithm with q= 0.37, D_{min}= 0.36 µm, D_{max} = 9.5 mm

Due to the necessary practical adjustments to the material quantities for Phase 2 mixtures and the omission of one of the fine aggregates used for the optimisation of the previous mixtures (see § 5.1.2), the computed grading curves for the two final Phase 2 mixtures (Figure 6-35) followed the ideal MAAC relatively poorly. Both mixtures had an R^2 statistic of 0.95, being the lowest of all the mixtures constructed, including the reference mixture. However, the poor curve fit is primarily the result of a lack of available material in the approximate range of 1.5 to 5 mm and practical limitations such as required workability (described in § 5.1.2) rather than a failure of the modelling technique.

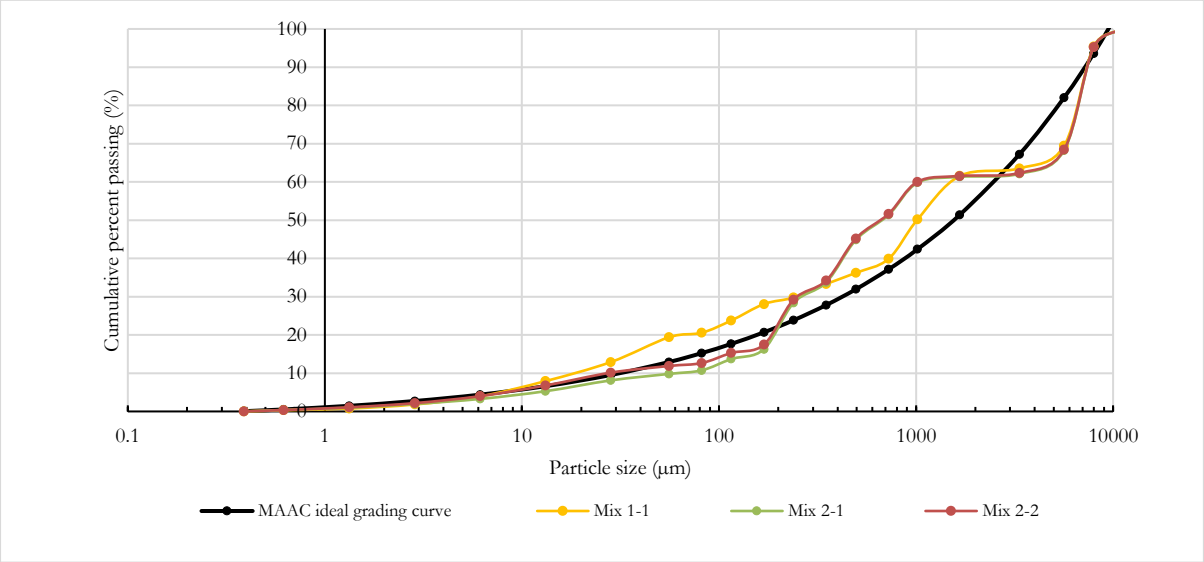

Figure 6-35: Overall constituent grading curves for Phase 2 mix designs constructed according to the MAAC algorithm with q= 0.37, D_{min}= 0.36 µm, D_{max} = 9.5 mm

It is also acknowledged that for each mix design, although constructed with the intention of achieving a grading equivalent to the ideal MAAC grading, there exists more than a single optimal solution with an equivalent R^2 statistic. This is due to the possibility of there being mix designs with varying proportions above and below that proposed by the MAAC ideal grading for each size class but ultimately, an equivalent R^2 statistic could be achieved. Therefore, the overall mix design as proposed by the MAAC algorithm for each mix is taken to be only one of many potential solutions. The number of potential solutions will however become less as the computed grading tends to the ideal grading curve.

Furthermore, as the end goal for the research project was the achievement of a concrete mix with optimised packing density but still practically usable, the matching of concrete constituents to an ideal grading curve at the expense of desired fresh concrete properties was not feasible. Therefore, these practical limitations also resulted in a deviation of the computed grading from the ideal MAAC grading. Necessary adjustments to the computed grading to remain within the realms of practicality are discussed in § 5.1.2.

6.3 Fresh concrete properties

6.3.1 Phase 1 mixtures

Minimal variation in the workability of concrete mixtures was noticed with an increase in limestone replacement. All concretes with limestone filler achieved slightly higher slump than the reference mixture with less or similar SP doses (Table 6-11). This is primarily attributed to the maintenance of water content and w/p ratio across all mixtures in conjunction with an increasing paste volume as the limestone content was increased (due to its density being less than cement).

Due to the limestone content of all Phase 1 mixtures comprising primarily KB45, i.e. the coarsest limestone with widest particle size distribution, the extension of the overall powder phase particle size distribution may have contributed to an increased flowability of the paste phase. Of all the limestone blends, Mix 1-4 had the highest SP demand (0.16 %). The use of KB2 in this mixture led to increased wettable surface area, probably resulting in more water being adsorbed to particles and less being available for lubrication of particle movement and therefore requiring a slightly higher SP dose to maintain workability. However, the use of KB2 in Mix 1-6 did not require the same SP dose to maintain workability. Instead, the overall increase in paste volume (approx. 3 l/m^3 from Mix 1-4 to Mix 1-6) was expected to enable the maintenance of slump even with the use of the very fine KB2 limestone filler.

Additionally, all mixtures with limestone blends had significantly increased fine aggregate contents (66 – 72 kg/m^3 higher) relative to the reference mixture, Mix 1-1 (full concrete mix designs are presented in § 5.1.1, Table 5-1). These quantities were the result of best-fitting the overall constituent grading curve to the MAAC and despite a relatively increased surface area to material volume with increased fine aggregate, workability was not detrimentally affected. Increased fine aggregate led to increased paste volume and it was expected that the well-graded granite crusher sand 1 and characteristic relatively spherical, rounded particle shapes contributed to acceptable workability. Furthermore, granite crusher sand 1 had considerable material passing the 75 μm sieve (approx. 10 %) which would have further contributed to the powder-paste phase, promoting a cohesive paste.

6.3.2 Phase 2 mixtures

Despite following maximum packing density outputs from the modelling procedure, the design of Phase 2 mixtures required substantial trial and error to arrive at mixtures that were workable (§ 5.1.2). The main goal for Phase 2 was a reduction in water content to compensate the reduction in cement (clinker) content and allow the w/c ratio to be kept low. This was primarily to enable the maintenance of compressive strength relative to the reference concrete following the decreased compressive strength of limestone blended Phase 1 concrete mixtures (see § 6.4.1.1).

For reference, Table 6-12 summarises the final Phase 2 mix designs and a trial mix with a powder phase of 100 % cement. Slump and SP quantity is provided with each mix design. Initial trial mixtures (discussed in § 5.1.2) presented harsh concrete with negligible slump, some of which sheared with the removal of the slump cone or when dynamic compaction was applied. Failure of these trials was most likely due to the fixing of w/p at 0.5 with a reduction in water from 210 to 150 l/m^3. This also led to a substantial decrease in powder-paste volume relative to Mix 6-1 (from 350 l/m^3 to 250 l/m^3).

Table 6-11: Overview of Phase 1 mix designs (from § 5.1.1)

Constituent	Unit	Mix 1-1	Mix 1-2	Mix 1-3	Mix 1-4	Mix 1-5	Mix 1-6
		100 CEM	**90CEM 10KB45**	**80CEM 20KB45**	**80CEM 5KB2 15KB45**	**70CEM 30KB45**	**60CEM 5KB2 35KB45**
Water	kg/m³	210	210,0	210	210	210	210
Total binder	**kg/m³**	420	420,0	420	420	420	420
Cement	kg/m³	420	382,0	343,7	343,7	304,2	263,8
Limestone	kg/m³	-	37,7	76,3	76,3	115,8	156,2
KB2	kg/m³	-	-	-	19,1	-	19,5
KB45	kg/m³	-	37,7	76,3	57,3	115,8	136,7
Fly ash	kg/m³	-	-	-	-	-	-
Fine aggregate							
Granite Crusher 1	kg/m³	974	1046,0	1040,4	1053,4	1045,8	1039,9
Granite Crusher 2	kg/m³	-	-	-	-	-	-
Philippi Dune	kg/m³	-	-	-	-	-	-
Coarse Aggregate							
Nominal 9.5 mm Granite	kg/m³	760	684,0	685,3	672,3	675,7	677,2
Superplasticiser							
MasterGlenium ACE 456	kg/m³	0,63	0,47	0,37	0,68	0,55	0,54
	Mass % of binder	0,15	0,11	0,09	0,16	0,13	0,13
w/p	-	0,50	0,50	0,50	0,50	0,50	0,50
w/c	-	0,50	0,55	0,61	0,61	0,69	0,80
Powder-paste volume (Binder + Water)	l/m³	346	347	349	349	350	352
Slump	mm	60	70	75	75	75	75

The first Phase 2 trial used coarser fine aggregate (granite crusher sand 2) which also had less material passing the 75 µm sieve (relative to granite crusher sand 1 for Phase 1 mixtures). This caused decreased paste and powder-paste volume relative to Phase 1 mixtures, leading to increased internal friction. The subsequent use of Philippi dune sand was still not an appropriate replacement due to its narrow grading relative to granite crusher sand 1. Its use resulted in a lack of material above 1180 µm and below 150 µm and was expected to cause decreased cohesiveness.

Thereafter, attempts were made to increase the powder-paste volume by increasing limestone content. Increasing paste volume with the incremental addition of KB45 showed a remarkable improvement in workability, despite there being no increase in water content (§ 5.1.2, Table 5-3). The addition of the coarsest limestone over any of the finer limestones was expected

to have promoted workability due to its ability to increase powder-paste without substantially increasing surface area requiring wetting (as would have happened with the addition of the finer limestones). Furthermore, particle shape appeared to deteriorate with increasing fineness and therefore, the higher sphericity of KB45 particles would have benefitted workability.

Table 6-12: Phase 2 final and 100 CEM trial mix designs

Constituent	Unit	Mix 2-1	Mix 2-2	Trial 2-4
		45 CEM 45 KB45 10 KB2	45CEM 30 KB45 5KB2 20FA	100 CEM
Water	kg/m³	164	164	164
Total binder		394.0	381.1	420.1
Cement	kg/m³	189.1	189.1	420.1
Limestone	kg/m³	204.8	129.3	-
KB2	kg/m³	33.6	16.8	-
KB45	kg/m³	171.2	112.5	-
Fly ash	kg/m³	-	62.7	-
Fine aggregate				
Granite Crusher 1	kg/m³	-	-	-
Granite Crusher 2	kg/m³	-	-	-
Philippi Dune	kg/m³	1005.4	1005.4	1010.3
Coarse Aggregate				
Nominal 9.5 mm Granite	kg/m³	846.2	846.2	840.8
Superplasticiser				
MasterGlenium ACE 456	kg/m³	16.1	6.5	5.3
	Mass % of binder	4.1	1.7	1.3
w/p	-	0.42	0.43	0.40
w/c	-	0.87	0.87	0.40
Paste volume (Binder + Water)	l/m³	300	300	300
Slump	mm	40	40	55

The subsequent reduction of cement content to 45 vol. % then allowed the powder proportions to be constructed according to maximum packing density outputs. The packing density of the powder phases increased as the allowable limestone content was increased (Appendix D, Table D-1 to Table D-5). Although this had the potential to expel water which previously filled void space, making it available for the lubrication of particle movement, this was not apparent from the slump measurements at the water contents tested.

The achievement of equivalent and increased slump for Mix 2-2 and Trial 2-4, respectively, with considerably reduced SP doses, infers that the water demand of Mix 2-1 was considerably higher. Due to Mix 2-2 still having large KB45 content, the addition of beneficial spherical FA particles to Mix 2-2 and the larger portion of KB2 in Mix 2-1 was expected to have been

responsible for the differing water demands. However, as Trial 2-4 was made with only plain cement and still required substantially less SP to achieve an increased slump, it was expected that KB2 was largely responsible for the high water demand of Mix 2-1. It is likely that a poor particle shape (§ 6.1.1), high fineness and corresponding large wettable surface area increased the water demand of mixtures using this material and is something that became more noticeable with a decrease in the water content.

Further investigation into the compatibility of the SP with KB2 and its ability to adequately disperse the high fineness material should be investigated. Furthermore, concerning cement/limestone blends, the potential for preferential adsorption onto cement particles could also be investigated. Resulting fresh concrete properties inferred the importance of the water demand of powder materials, individually and when blended with other materials. Explicit consideration needs to be given to powder material water demand in addition to their potential effects on the packing density of the powder phase if a workable mixture with reduced water content is to be achieved.

6.4 Hardened concrete properties

6.4.1 Compressive strength

Early and later age compressive strength for Phase 1 and 2 mixes is discussed in this section. Detailed results can be found in Appendix E.

6.4.1.1 Phase 1 mixtures

Compressive strength results for Phase 1 mixtures are portrayed in Figure 6-36. Despite having optimised the packing density of powder materials using the CIPM and optimising fine and coarse aggregates using the MAAC, compressive strength consistently decreased with increasing replacement of CEM II A-L 52.5 N at all ages. This was primarily attributed to the relatively large water content used. Fixing the water content at 210 l/m^3 meant that there was an increase in excess water (i.e. not chemically bound by hydration reactions) as cement content was reduced, resulting in increasing capillary porosity and causing decreased strength. Figure 6-37 portrays the linear relationship of increasing water penetrable porosity with an increase in w/c (representing the decreasing cement content) for Phase 1 mixes as well as the porosity of Phase 2 mixes.

The linear relationship of Phase 1 mixes was used to extrapolate the porosity expected for Phase 2 mixes at a hypothetical 210 l/m^3 water content. Thereafter the ratio of porosity to water content was used to predict the porosity which could have been expected at 164 l/m^3. As can be seen, Phase 2 mixes had decreased porosity to what was predicted, attributed to increased packing density. However, neither Phase 2 nor Phase 1 mixes achieved strength significantly different from predicted strengths at equivalent w/c, provided by the cement manufacturer (Figure 6-38). Therefore, even with powder combinations constructed according to those enabling maximum packing density, a more substantial reduction in water content is required to maintain a low w/c and undiminished compressive strength. Furthermore, the reduction in Phase 2 porosity was not significant enough to enhance concrete strength relative to that predicted at an equivalent w/c.

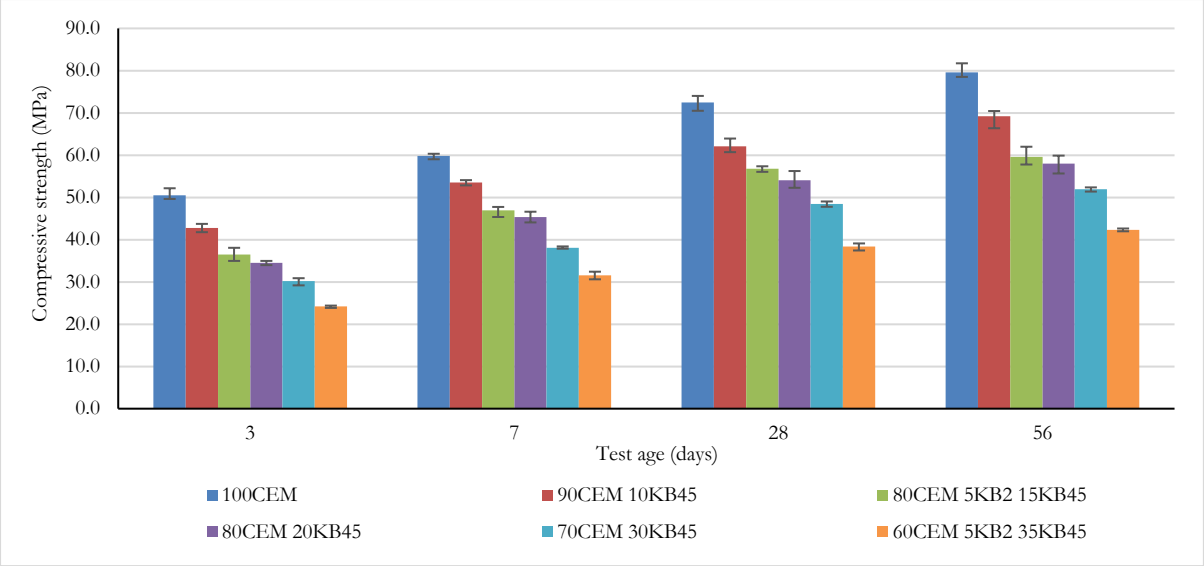

Figure 6-36: Compressive strength results for Phase 1 mixtures (water content = 210 l/m³)

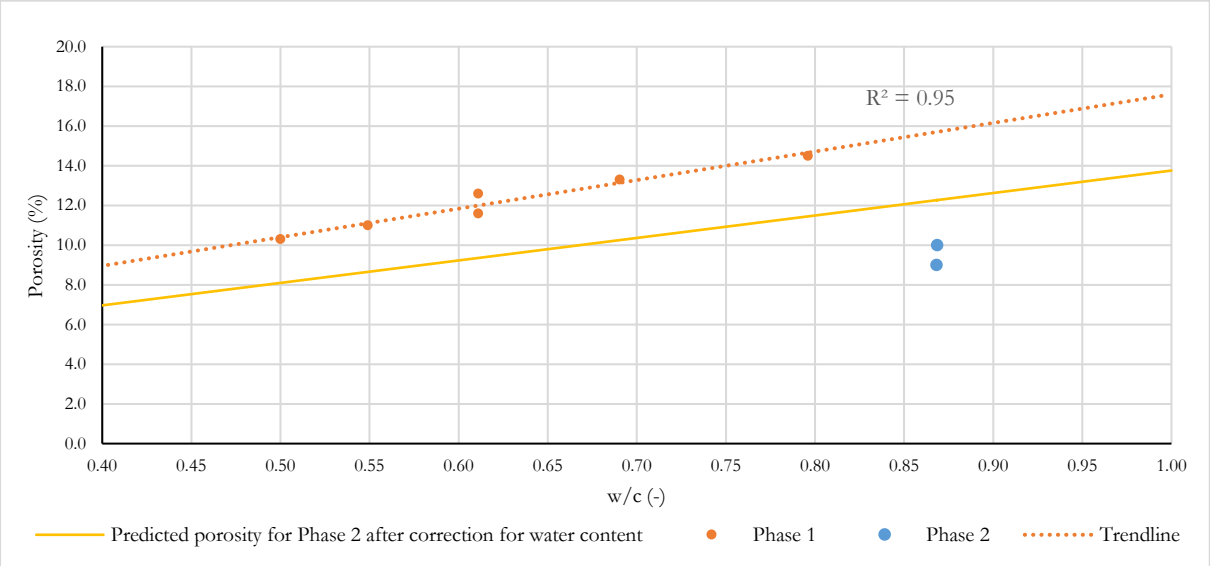

Figure 6-37: Water penetrable porosity vs water: cement ratio for Phase 1 and 2 mixes

Early age strength development was reduced as the replacement of cement with limestone was increased (Figure 6-39). The mixture comprising high fineness limestone (KB2) in combination with KB45 for the 80 vol. % cement mixture consistently achieved compressive strength approximately 2 MPa higher than the 80 vol. % cement mixture using only KB45. It was expected that the inclusion of KB2 would lead to elevated strength due to fine filler effects (discussed in § 2.1.4.2) and possibly the formation of monocarboaluminate compounds. However, the 2 MPa margin was similar to the range associated with compressive strength measurements. In addition, the composition of hydration products was not analysed and therefore conclusions concerning the influence of the high fineness filler on compressive strength could not be made with certainty. Furthermore, it is likely that these effects would have been more pronounced with an increased KB2 content.

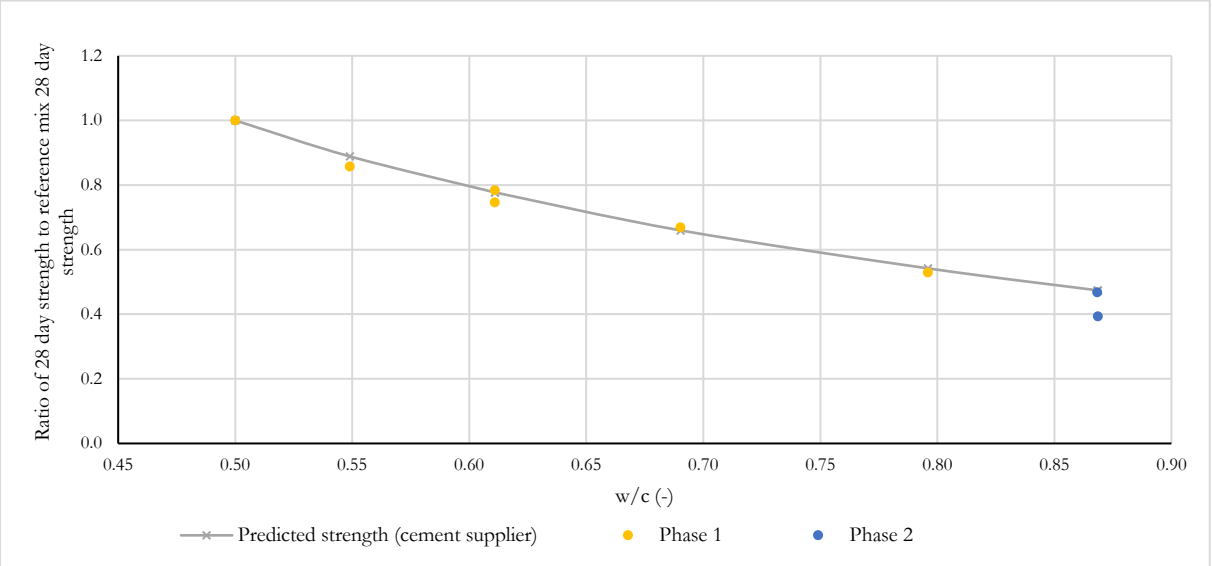

Figure 6-38: Compressive strength vs water: cement ratio for experimental results and predicted values

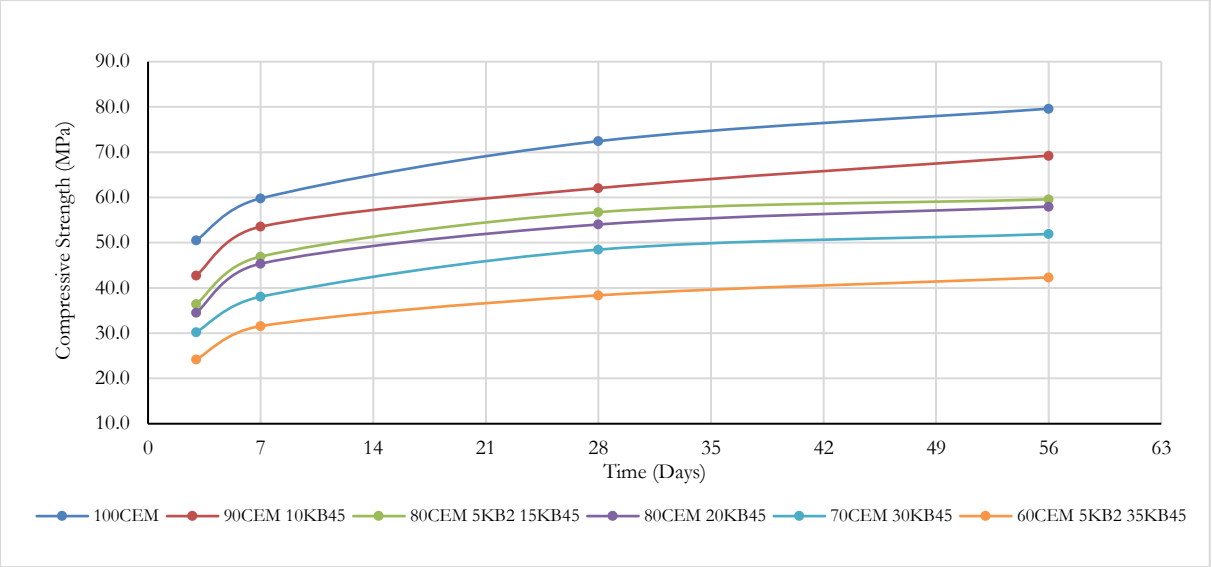

Figure 6-39: Compressive strength development for Phase 1 mixtures

6.4.1.2 Phase 2 mixtures

Phase 2 mixes were made to assess the effects of reduced water content (from 210 to 164 l/m^3). They were initially intended to be comparable to Mix 1-6 (60CEM 5KB2 35KB45) but subsequently had to have the volume % contribution of cement decreased from 60 to 45 % to increase the powder content without increasing cement content above a desired maximum of 190 kg/m^3. Resulting compressive strengths for Mix 1-6 and Phase 2 mixtures are portrayed in Figure 6-40. The best performance of Phase 2 mixtures relative to Mix 1-6 was seen in the early age strength (Day 3). Despite FA reportedly causing reduced early age strength, Mix 2-2 (45CEM 5 KB2 30KB45 20FA), obtained negligibly reduced compressive strength (approx. 1 MPa) relative

to Mix 1-6 (60CEM 5KB2 35KB45). This discrepancy at an early age was attributed primarily to the provision of nucleation sites by limestone particles, causing the earlier onset of FA hydration.

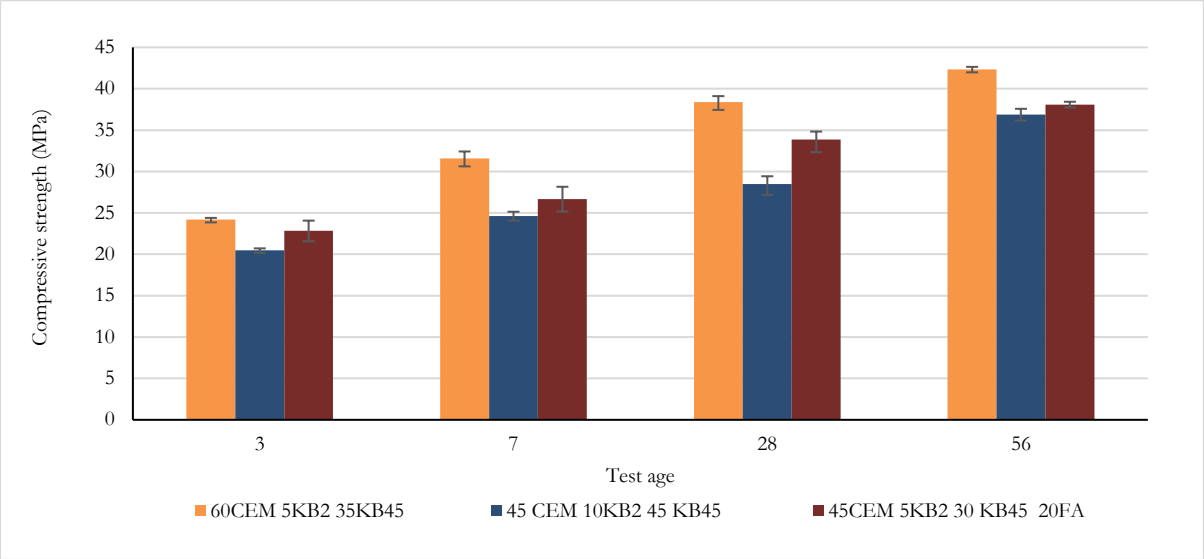

Figure 6-40: Compressive strength results for Mix 1-6 (60CEM, 210 l/m³ water content) and Phase 2 mixes (45CEM, 164 l/m³)

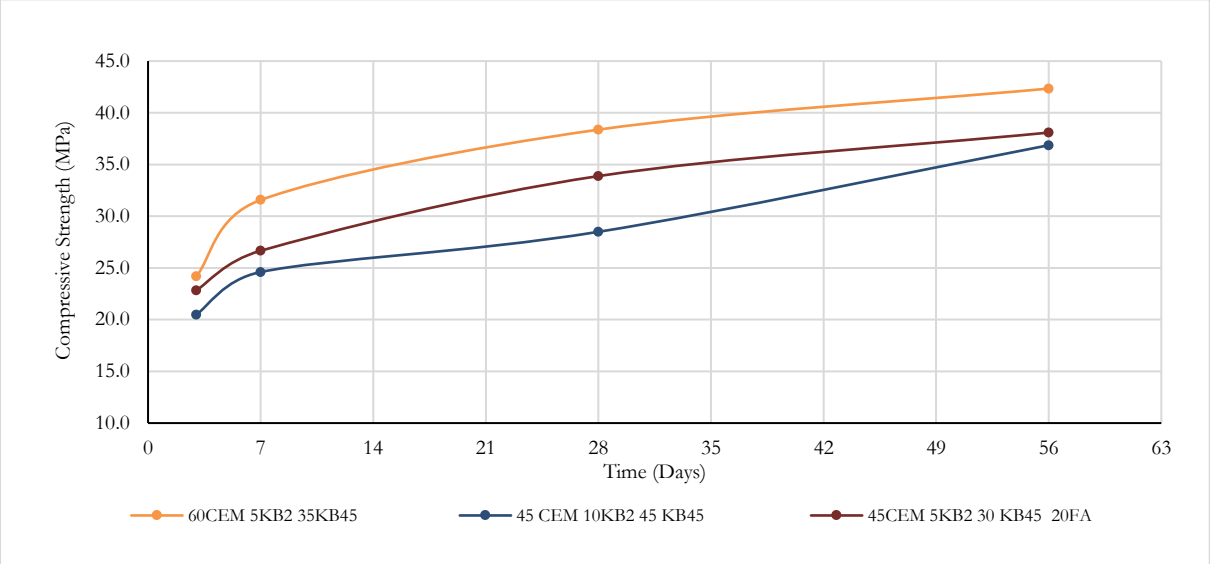

Figure 6-41: Compressive strength development for Phase 2 mixtures

However, from 7 days onward, Mix 1-6 achieved slightly higher compressive strength than Mixes 2-1 and 2-2. Therefore, the combination of decreased w/c and stimulation of FA hydration by the provision of nucleation sites was not sufficient to maintain compressive strength that was comparable to Mix 1-6. Mix 2-2 also consistently achieved higher strength than Mix 2-1 at all ages and had increased rate of strength development (approximately equivalent to Mix 1-6) between 7 and 28 days (Figure 6-41). Although Mix 2-1 had the potential to allow the formation of

monocarboaluminates, they were not expected to be prevalent due to the low concentration of aluminates in this mix. However, supplementing a portion of the limestone for FA in Mix 2-2 ensured the provision of additional aluminate material and therefore monocarboaluminate formation was thought to be responsible for the consistently higher strength of Mix 2-2 over Mix 2-1 and relatively increased strength development between 7 and 28 days. Yet, considering the later age strengths of Mixes 2-1 and 2-2 to only differ by approx. 1 MPa and there being no experimental analysis of hydration products, it was apparent that the role of monocarboaluminate formation in strength development needs to be further investigated to better understand its influence thereon.

Contradictory to the linear trend between water penetrable porosity and w/c observed for Phase 1 mixtures (Figure 6-37), Phase 2 mixtures had considerably lower porosity (comparable to the reference mix) than expected had they followed the same trend. It is therefore apparent that the increased packing density of the powder phases was successful in reducing the water penetrable porosity but was not adequate to maintain compressive strength. Once again, this is attributed to the dilution effect, whereby limestone filler dilutes clinker particles. Although the filler contributes to decreasing water penetrable porosity, a lower concentration of clinker or reactive SCM, causes a lower rate (as well as absolute) increase in the solid volume of hydration products.

6.4.1.3 General discussion

Overall, Phase 1 and Phase 2 mixtures were unable to maintain compressive strength relative to the Phase 1 reference mixture. As already discussed, the most obvious cause was the relatively high, fixed water content of 210 l/m^3 for Phase 1 mixtures, leading to the dilution effect (elaborated in § 2.1.3). Fixing the water content resulted in a substantial increase in w/c as cement was replaced with limestone. Benefits of increased packing density in Phase 1 mixtures could potentially have been more noticeable had the reduction in cement content been accompanied by a reduction in water content. This was more noticeable for Phase 2 mixtures where, despite higher w/c ratios, relatively lower water penetrable porosity was observed (Figure 6-37).

The determination of water content according to the C&CI 'Method of Mix Design' (Addis and Goodman, 2009) (§ 5.1.1) is therefore not appropriate for approximating water content for low-clinker (low-cement) mixtures. The determination of water content within the method is according to the approximation of fine and coarse aggregate water demand, however, as discussed in § 6.3, workability of low-clinker concretes is reliant on the provision of a minimum powder-paste volume. Therefore, if better consideration is given to the minimisation of water demand of the powder phases by careful material selection, water content can be reduced to achieve lower w/c, while sufficient powder-paste is still provided for fine and coarse aggregate mobility.

Figure 6-42 displays the binder efficiency indices ('bi') for Phase 1 and 2 mixtures as well as their corresponding 28-day compressive strength. The term 'binder' is taken to include only the clinker and FA components of the constructed mixes (as the reactivity of limestone was assumed low to negligible). Comparing Phase 1 and 2 mixtures against the reference mixture, binder efficiency of all mixes is decreased due to a higher binder content being required to achieve 1 MPa of compressive strength. However, Damineli *et al.* (2010) found that, generally, high strength concretes tend to be more efficient regarding the amount of binder required to achieve each unit of compressive strength. For compressive strength above 50 MPa (assuming 100×200 mm cylinder specimens), minimum 'bi' converged to 5 kg/m^3/MPa. Below 50 MPa, 'bi' values ranged from 10

to 20 kg/m^3/MPa, often due to the specification of minimum cement contents (2.1.3).

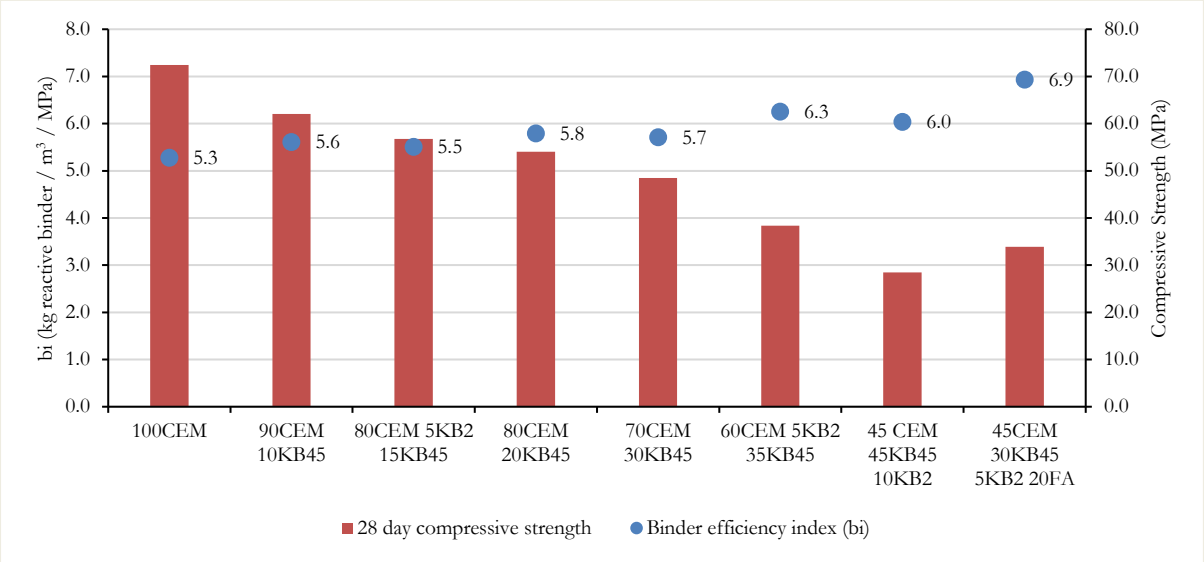

Figure 6-42: Binder efficiency index (bi) and 28-day compressive strength for Phase 1 and Phase 2 mixes

When converting 28-day cube compressive strength results to equivalent cylinder strengths using a formula proposed in Neville (2011), also used in Damineli *et al.* (2010), all limestone blended concretes have strengths < 50 MPa (Table 6-13). Therefore, the achievement of 'bi' values well below the range of 10 to 20 kg/m^3/MPa for these mixtures show increased binder efficiency relative to data collected for concretes in a similar strength class. However, there still exists further potential to achieve 'bi' < 5 kg/m^3/MPa for concretes < 50 MPa, as has been shown in subsequent research (John *et. al.,* 2017). Combining the methodology of reducing the powder phase water demand with increased SCM content (such as FA) has the greatest potential to enable clinker reduction due to a lowering of the w/c ratio and the provision of hydration products from a source other the cement, both contributing to increased compressive strength.

Table 6-13: Equivalent compressive strengths in accordance with Neville (2011)

Mix	Compressive strength (MPa)	
	28-day 50 mm cube strength	Equivalent 100×200 mm cylinder strength
100CEM	72.4	55.9
90CEM 10KB45	62.1	47.9
80CEM 5KB2 15KB45	56.8	43.8
80CEM 20KB45	54.0	41.7
70CEM 30KB45	48.5	37.4
60CEM 5KB2 35KB45	38.4	29.6
45 CEM 45 KB45 10 KB2	28.5	22.0
45CEM 30 KB45 5KB2 20FA	33.9	26.1

6.4.2 Durability index tests

The following sections discuss durability test results and their relation to the potential durability of Phase 1 concretes. Detailed results can be found in Appendix F.

6.4.2.1 Oxygen permeability index (OPI)

OPI results are portrayed in Figure 6-43 for all Phase 1 mixes. Limestone replacements up to 20 vol.% of the powder phase consistently decreased the permeability of concrete microstructure, leading to higher OPI values for Mix 1-2 (90CEM 10KB45), 1-3 (80CEM 5KB2 15KB45) and 1-4 (80CEM 20KB45) relative to the reference Mix 1-1 (100CEM). Decreased permeability was attributed to the limestone fillers isolating capillary pores, preventing their interconnectivity and thereby the permeation of oxygen through the pore structure.

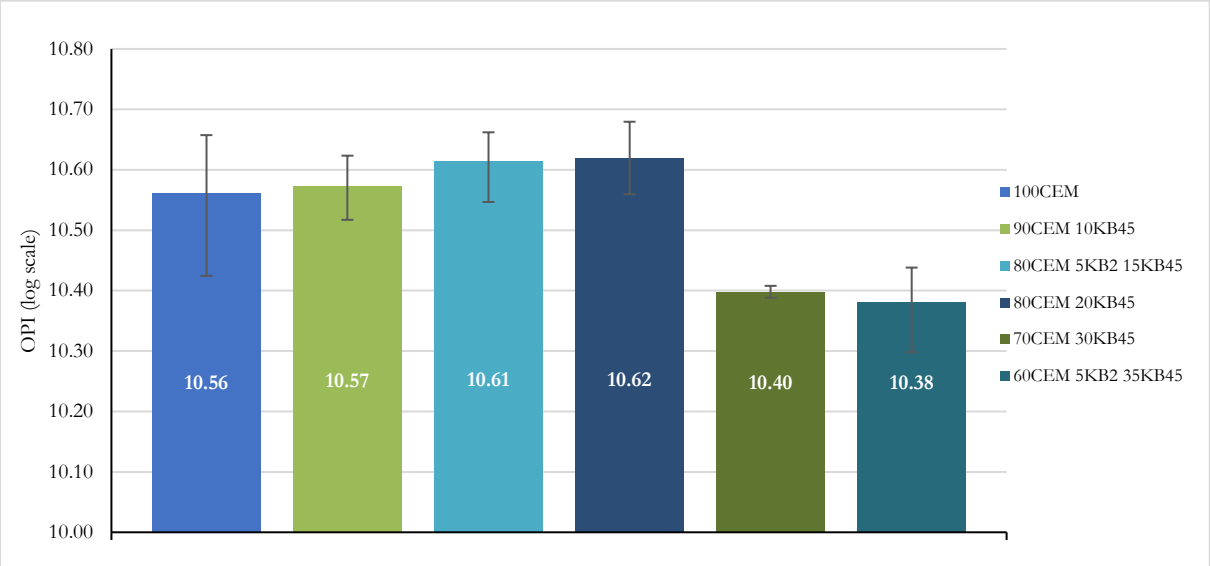

Figure 6-43: Oxygen permeability indices for Phase1 mixes

For limestone replacements of 30 and 40 vol. %, a sharp decline in the OPI value relative to the other mixes was seen. The decrease in cement (and therefore clinker) below 80 vol.% without a reduction in water content saw an increase in capillary porosity (Figure 6-46) to a degree that, by inference, the capillary pores became interconnected and had a noticeable effect on permeability. This was attributed to a percolation effect (usually ascribed to the percolation of interfacial transition zones (ITZs)) whereby the large volume of capillary porosity leads to the inter-connection of individual capillary pores, allowing the permeation of oxygen through the entire concrete microstructure. Figure 6-44 portrays this concept and its effect on the permeability of concrete. Scenario A shows a microstructure that is characterised by low porosity and individual pores are far apart, disallowing interconnectivity resulting in an impermeable concrete microstructure. Scenario B shows increased porosity and the interconnection of some pores, leading to a slightly increased permeability. Scenario C portrays high porosity and a resulting prevalence of interconnected pores causing high permeability.

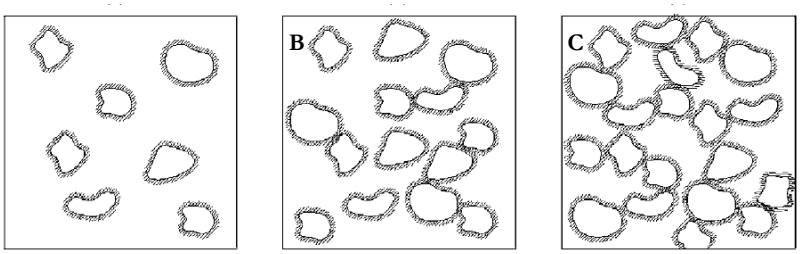

Figure 6-44: The development of a percolation effect as porosity increases (after Alexander & Mindess, 2005)

Although Mixes 1-5 and 1-6 were characterised by increased permeability relative to the other mixes, they still achieved OPI values in the same class as the other mixes, characteristic of excellent durability (Table 6-14). Therefore, limestone contents of up to 40 vol.% of the powder phase of concrete did not adversely affect oxygen permeability results and it is apparent that such blends have the potential to provide sufficient protection against carbonation.

Table 6-14: Durability classes corresponding to oxygen permeability proposed by (Alexander *et al.*, 1999)

OPI log scale	Durability class
>10	Excellent
9.5 - 10	Good
9.0 - 9.5	Poor
< 9.0	Very poor

6.4.2.2 Water sorptivity index (WSI)

Water soprtivity results for Phase 1 mixes are presented in Figure 6-45. According to guidelines for interpreting water sorptivity (Table 6-14) all results correspond to the class of 'Good' durability. Negligible difference in water sorptivity was seen across all mixtures yet a slight decrease was observed for all limestone-blended mixes relative to the reference mix, inferring increased durability performance. However, recent findings regarding the interpretation of water sorptivity and its relation to the potential durability of concrete have shown the need to consider sorptivity in conjunction with porosity (Moore & Alexander, 2017).

The reason for this is that the WSI of concrete is rate of sorption (i.e. rate of mass gain ($g/\sqrt{h}$)) 'normalised' by the porosity of concrete (% void volume). This normalisation may lead to an equivalent WSI for concretes with varying porosity. However, an increase in porosity corresponds to an increase in the rate of mass change (due to higher porosity representing greater connectivity of pores). Therefore, concrete with a given sorptivity and 'lower' porosity will potentially have greater durability than concrete with a 'higher' porosity, thus inferring the need to consider both parameters to more accurately assess durability (Moore & Alexander, 2017).

Figure 6-46 portrays water penetrable porosity and water content for Phase 1 mixtures that were determined as part of the standard WSI test procedure. Porosity results for the Phase 2 mixes

were obtained following the same drying and saturation procedure as for the standard test method but were determined using 50 mm cubes that had been sliced in half. The porosity of Phase 1 mixes increased consistently with a decrease in cement content (and increase in w/c) and corresponds to an increase in excess water (i.e. not chemically bound) due to lower clinker content in each subsequent mix. A decrease in water content for Phase 2 mixes enabled a substantial decrease in water penetrable porosity. Figure 6-37 showed the linear trend of increasing porosity with increasing w/c for Phase 1 mixtures but the deviation of Phase 2 mixtures from the linear trend. It was therefore apparent that in conjunction with the decreased water content, the increased packing density of Phase 2 powder phases caused a significant decrease in porosity.

Table 6-15: Durability classes corresponding to sorptivity proposed by (Alexander *et al.*, 1999)

Sorptivity mm/√h	Durability class
<6	Excellent
6 - 10	Good
10 - 15	Poor
> 15	Very poor

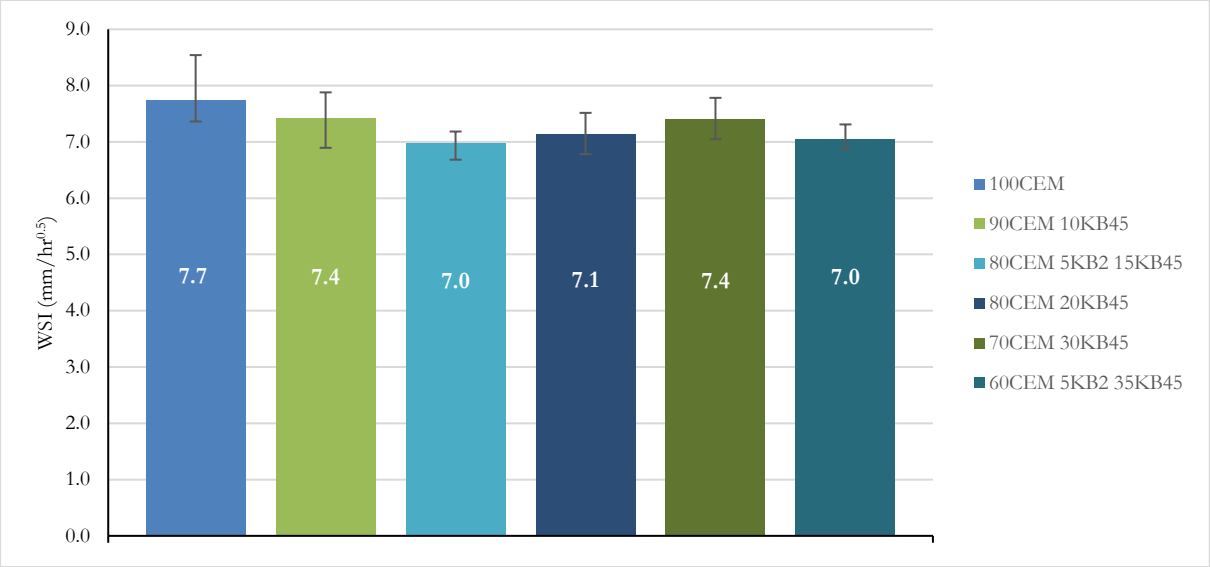

Figure 6-45: Water sorptivity indices for Phase 1 mixes

Moore & Alexander (2017) proposed new guidelines, combining sorptivity and porosity values, to better assess the potential durability of concrete. Table 6-16 summarises potential durability classes and infers varying durability performance relative to considering sorptivity alone (Table 6-15). Phase 1 mixes, including the reference mix, fall within the durability class, 'Good to Poor'. This was attributed to the relatively high porosity of Phase 1 mixes (specifically, those with high limestone content) corresponding to increased connectivity of pores, which is detrimental to durability.

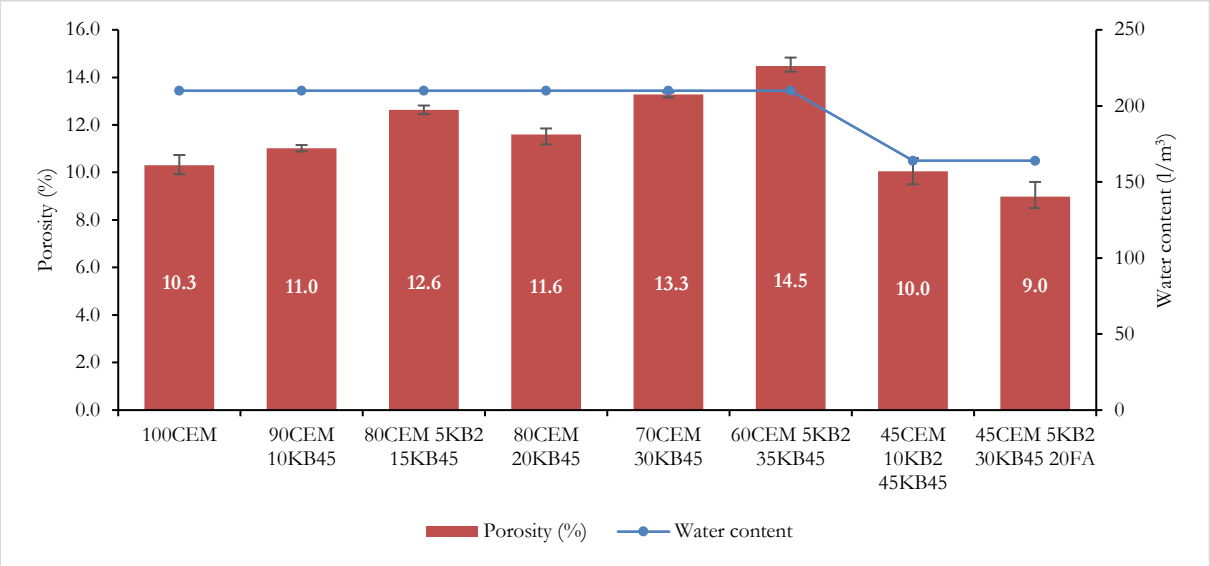

Figure 6-46: Water penetrable porosity and water content of Phase 1 and Phase 2 mixes

Table 6-16: Durability classification for various combinations of sorptivity and porosity (Moore & Alexander, 2017)

Sorptivity mm/√h	Porosity %	Durability class
< 6	< 10	Excellent
6 – 10	< 10	Excellent to Good
	> 10, < 12	Good to Poor
10 – 15	< 12	Good to Poor
	> 12, < 15	Poor to Very Poor
> 15	-	Very Poor

Although durability indices were not measured for Phase 2 mixes, the decreased porosity of these mixes show their potential for achieving improved durability relative to Phase 1 mixes. This infers the ability of the combination of low water content with high packing density to enable resistance to moisture ingress despite low cement (and clinker) content. This further displays the independence of concrete durability from w/c ratio, as Phase 2 mixes had considerably higher w/c ratios than Phase 1 mixes (see Table 6-11 and Table 6-12). Additionally, the use of SCMs, such as FA, are expected to further enhance durability through the refinement of concrete microstructure, physically, due to their fineness, as well as chemically, due to the provision of additional hydration products.

6.4.2.3 Chloride conductivity index (CCI)

Chloride conductivity indices of Phase 1 concretes are portrayed in Figure 6-47. As anticipated, CCI results infer a decrease in potential durability as the cement content is reduced. The reference mix (Mix1-1) and concretes with limestone replacement up to 20 vol.% (Mixes 1-2, 1-3 and 1-4) had CCI values corresponding with 'Good' durability, according to guidelines in Table 6-17.

Limestone replacement of more than 20 vol.% considerably worsened potential durability, resulting in CCI values within the 'Poor' durability class in Table 6-17.

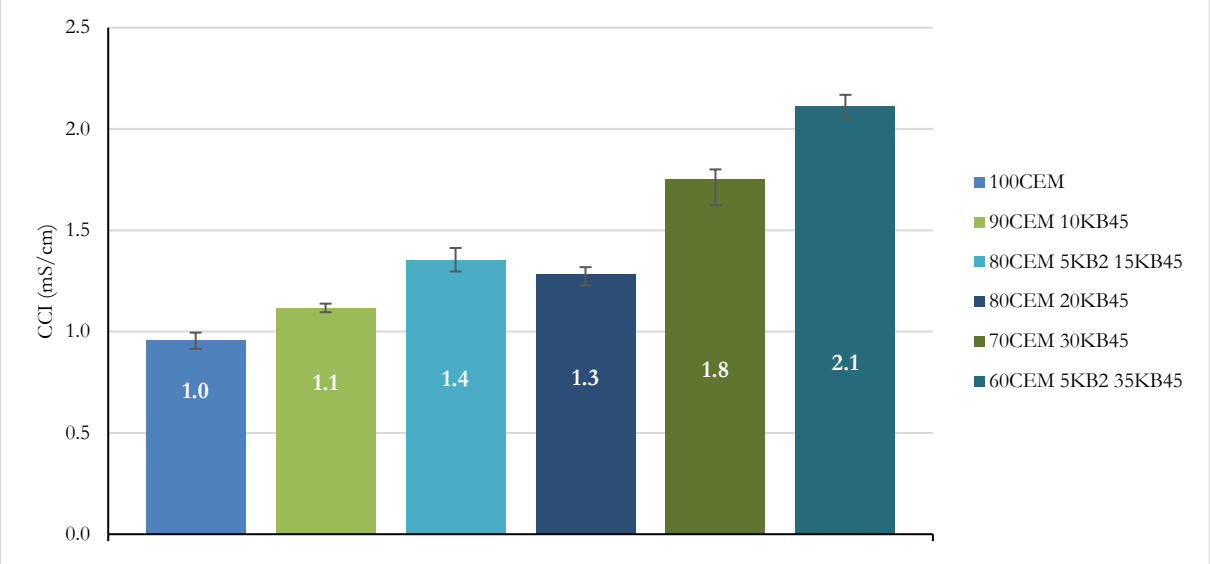

Figure 6-47: Chloride conductivity indices for Phase 1 mixes

Table 6-17: Durability classes corresponding to chloride conductivity proposed by (Alexander *et al.*, 1999)

Conductivity mS/cm	Durability class
< 0.75	Excellent
0.75 - 1.50	Good
1.50 - 2.50	Poor
> 2.50	Very poor

Resistance to chloride ingress depends primarily on binder content and binder type and their ability to 'bind' chlorides. The 'binding' process includes a physical and chemical component. The former refers to the surface area of hydration products for the physical adsorption of chlorides, while the latter refers to the reaction of chlorides with hydration products to form a chloro-aluminate compound called 'Friedels's salt', which can, to an extent, retain chloride ions within its crystallographic structure.

Due to the decreasing volume of hydration products as cement content decreases, the total surface area available for the adsorption of chlorides decreases, resulting in decreased resistance to chloride ingress. Furthermore, the lack of aluminate material (usually provided in the form of SCMs FA, GGBS and GGCS) does not allow the formation of Friedels's salt, further limiting any chloride-binding capability. Therefore, the resistance of low clinker concretes to chloride ingress will likely only be possible if the binder phase is supplemented with materials that can provide aluminates.

6.4.3 Accelerated shrinkage

The development of shrinkage strain with time is portrayed in Figure 6-48 for Phase 1 mixtures, and total accelerated shrinkage strain (after two consecutive strain readings differed no more than 2 µm per 100 mm gauge length) is portrayed in Figure 6-49. Upper and lower shrinkage limits are displayed on both figures. These limits were empirically developed by the University of Cape Town (UCT) to gauge drying shrinkage measurements. Microstrain below 350.10^{-6} is considered low shrinkage, between 350.10^{-6} and 550.10^{-6} is considered moderate shrinkage and an excess of 550.10^{-6} is considered high. Detailed results can be found in Appendix G.

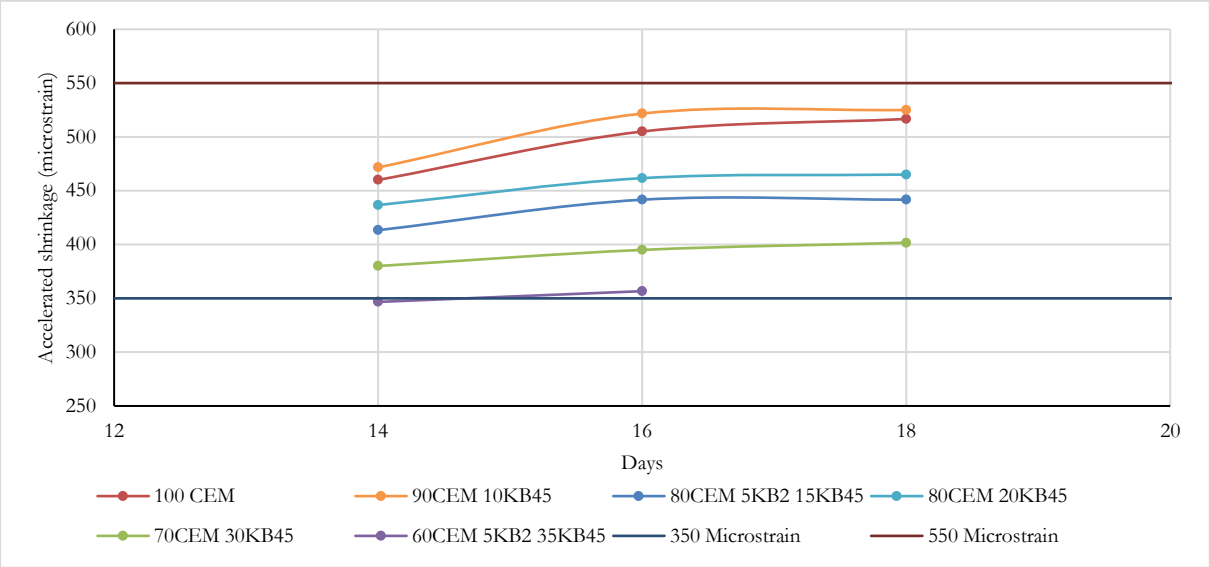

Figure 6-48: Accelerate shrinkage strain development for Phase 1 mixes

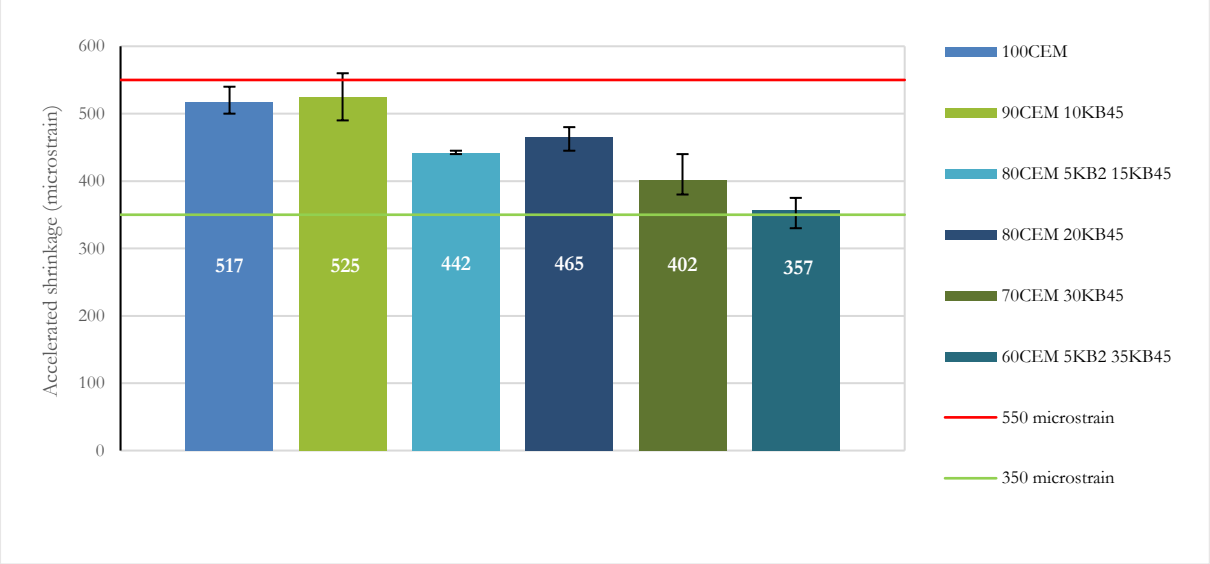

Figure 6-49: Total accelerated shrinkage strain for Phase 1 mixes

Drying shrinkage is the result of the loss of moisture from two types of pores: very small gel pores (formed by spaces between solid gel layers) and significantly larger capillary pores (formed by excess water not used in hydration) (Alexander & Beushausen, 2009). Due to larger bond energy being associated with water in gel pores relative to the 'free' water in capillary pores, significantly higher shrinkage strains are associated with loss of moisture from gel pores. Therefore, with an increase in the volume of hydration products (gel), there is an associated increase in drying shrinkage strain and vice versa.

Fixing the water content for Phase 1 mixtures resulted in a decrease in the rate of development of shrinkage strain (Figure 6-48) as well as the ultimate shrinkage strain (Figure 6-49) as the cement (clinker) content was reduced. Furthermore, a decrease in the time required to reach the ultimate shrinkage was also observed for the minimum cement content used (CEM60 5KB2 35KB45). These results corresponded to an increase in capillary pore volume and a decrease in gel, and therefore gel pores, leading to reduced shrinkage strains as cement (clinker) content was reduced. Figure 6-50 portrays the linear relation between total shrinkage strain and water penetrable porosity. Overall, according to the empirical guidelines, all concretes were characterised by moderate shrinkage, with Mix 1-6 bordering the low shrinkage category.

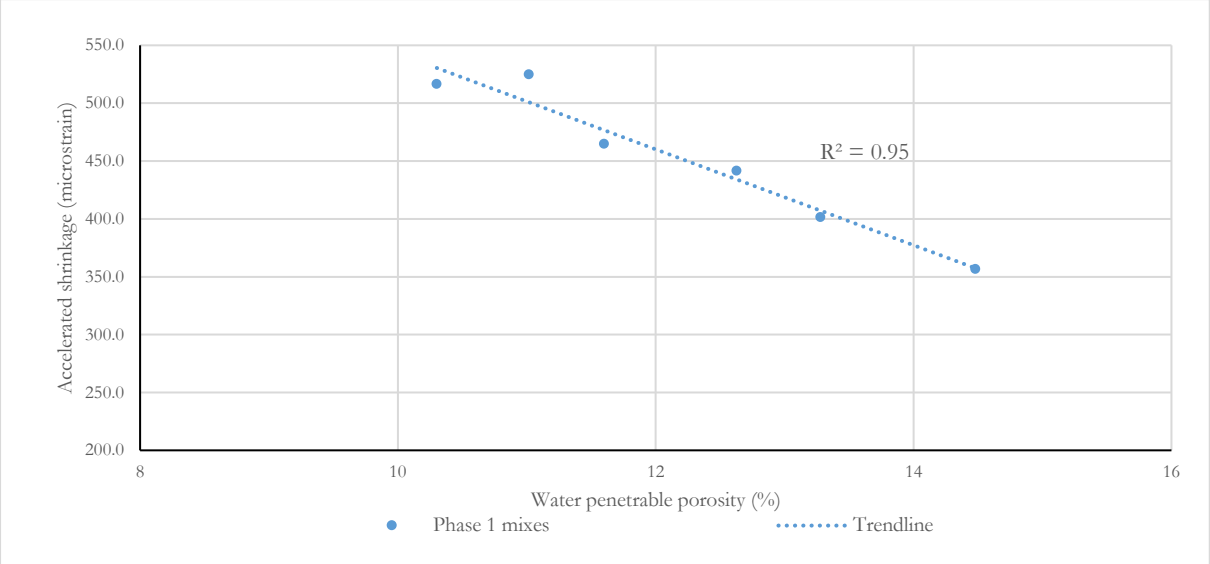

Figure 6-50: Linear correlation of accelerated shrinkage and water penetrable porosity for Phase 1 mixes

7 Conclusions and recommendations

This section first provides conclusions based on key findings in the foregoing sections. Thereafter, recommendations are made concerning future research and implementation of low clinker concrete in practise.

7.1 Conclusions

7.1.1 Packing density optimisation

7.1.1.1 Experimental determination of powder packing density

The mixing energy test was selected for powder packing density determination due to its ability to provide repeatable results while not requiring excessive material volumes or time to complete a test. Packing density of powder phases was benefitted the most for cement combinations with limestone fillers of high and low fineness and was negligibly affected when combined with limestones of fineness similar to cement.

7.1.1.2 Particle packing modelling

Of the existing packing models reviewed, the CIPM appeared to be the only model which explicitly accounted for the effect of surface forces on powder packing. The MAAC provided an accurate description of an entire range of particle size classes by defining upper and lower size limits while providing a practical optimisation solution, not requiring excessive computing. Therefore, their integration allowed surface forces to be considered for powder packing while not neglecting the packing of fine and coarse aggregate materials and ensured practical computing time.

The trends observed for experimental packing density of various powder combinations were better described (qualitatively) by the CIPM for cement combinations with limestones of high and low fineness relative to combinations with limestones of similar fineness to cement. The most accurate predictions were reported for cement combinations with the coarsest limestone, inferring that the model was able to better describe packing density combinations of cement with coarser powder materials (125 μm median particle size) relative to combinations with materials of similar and higher fineness than cement.

The calibration of the CIPM showed that prediction error converged to a minimum when a large value of C_a was used, and that prediction error was relatively independent of the value of C_b at large C_a values. This inferred the relatively larger influence of an increased loosening effect on powder material packing compared to the proposed decreased wall effect. However, results were inconclusive as to whether this inference was accurate. Ultimately, compaction indices used were those proposed by Fennis (2011), and practical values of C_a, C_b and d_c were used which enabled the minimisation of average error to 1 %. This permitted optimal material combinations to be predicted. However, the chosen values were not necessarily representative of surface force influences on wall and loosening effects as proposed by Fennis (2011).

Phase 1 mixtures proposed by the MAAC optimisation algorithm achieved good fit to the MAAC with high R^2 statistic, inferring closeness to maximal packing density. The proposed Phase 2 mixtures could not be directly applied due to their failure to meet practical, minimum workability. Therefore, practical limitations imposed on fine and coarse aggregate contents caused a deviation

of the combined constituent grading curve from that proposed by the MAAC, resulting in packing density lower than the possible maximum.

Although the CIPM and MAAC were successfully integrated to account for the entire spectrum of concrete materials, there were still some short-comings of the method when attempting to design low-clinker concrete. Extensive experimental trial was necessary to validate and calibrate the CIPM to suit particular materials as well as ensure a workable mix. These findings therefore infer the need to better understand the fundamental influences of powder packing so that advances can be made towards a fully predictive process which incorporates indicators of practical usability (such as water demand and expected workability) while maximising packing density.

7.1.2 Concrete properties resulting from optimisation

7.1.2.1 Phase 1 mixes

The fixing of a relatively high water content for Phase 1 mixes allowed the maintenance of sufficient workability for all mixtures. However, this led to decreased compressive strength relative to the reference mix as cement content was decreased. Increased packing density was insufficient to account for decreased cement (clinker) content when water content remained constant. Comparisons made with predicted strength development curves showed increased packing density to have little benefit at equivalent w/c ratios.

Besides reduced resistance to chloride ingress, durability performance was not adversely affected. This finding was attributed to the ability of fine fillers to prevent interconnectivity of the pore structure. Accelerated drying shrinkage results showed an expected trend of decreasing shrinkage strain as cement content was decreased, corresponding to a decrease in the volume of gel hydration products (C-S-H) and relative increase in capillary porosity. Therefore, despite the reduction of compressive strength, certain durability parameters were not adversely affected. This portrays the potential use of low-clinker concrete where durability is of primary concern (over structural properties).

7.1.2.2 Phase 2 mixes

Compensation of reduced water content with increased limestone filler volume reduced workability relative to Phase 1 mixes. The reduced water (164 l/m^3) and cement (45 vol.% = 190 kg/m^3) content did not sufficiently reduce the w/c to achieve compressive strength comparable to the reference mix. However, the ternary blend, 45CEM 5KB2 30KB45 20FA, was able to provide similar early age strength relative to Phase 1 mix, 60CEM 5KB2 35KB45, attributed to monocarboaluminate formation.

Reduced water content led to reduced porosity, but porosity was further decreased relative to that predicted when extrapolating from Phase 1 data and was attributed to the increased powder packing density. However, porosity was not decreased to an extent that improved compressive strength relative to predicted strength for an equivalent w/c.

7.1.2.3 General conclusions for low-clinker concrete properties

Oxygen permeability, water sorptivity and drying shrinkage of Phase 1 mixes was not adversely affected with increased limestone content. However, potential beneficial effects of increased

packing density on compressive strength were not apparent and primarily attributed to the relatively high water content causing high capillary porosity. The reduced water content of Phase 2 mixes allowed the observation of reduced porosity due to increased packing density, but this was still not sufficient to enhance compressive strength for a given w/c ratio.

The various mixes covered a wide range of w/c ratios and therefore, direct comparison with the reference mix was likely not appropriate. Comparisons made with data from the review of literature revealed that 'bi' values for Phase 1 and 2 mixes were significantly reduced (between 5.3 and 6.9 kg/m^3/MPa) relative to concrete of similar strength class (commonly between 10 and 20 kg/m^3/MPa). This inferred improved binder performance and pointed to the likelihood of further 'bi' reductions below 5 kg/m^3/MPa if water demand was carefully controlled. This confirms the inferences of existing research regarding the inappropriateness of enforcing minimum cement content. If no longer enforced, this could enable substantial clinker reduction.

Furthermore, durability indicators pointed to the potential for packing optimisation to produce durable concrete despite relatively high porosity and low cement (clinker) content. This implied the potential for clinker savings when durability is of primary concern over structural concrete properties and is something that requires further investigation.

7.1.3 Packing density optimisation for clinker reduction

The combination of the CIPM and MAAC ensured that surface force effects on powder materials were taken into consideration when optimising the packing density of concrete constituents. However, the accuracy of packing density prediction by the CIPM was reliant on the value of constants that were not able to be generalised for use across multiple different materials. Therefore, the way in which surface force effects were implemented still failed to model the packing of the tested powder material combinations with consistent accuracy. Further investigation into how surface forces can be implemented so that the effect can be generalised across all materials is necessary if packing optimisation is to be used to design low-clinker concrete.

There is clear evidence of the ability for packing optimisation to enable clinker reduction if water content is reduced and SCM content increased. However, due to practical limitations of mixing, placing and compacting, it is essential that minimum workability is achieved. Therefore, to achieve low clinker concrete that is practically usable, it is essential that packing optimisation is not solely focused on maximising packing density but also on reducing water demand, particularly of powder phases, to reduce required water content for minimum workability. Thereby, low w/c ratios can be achieved at low cement (clinker) content, but sufficient paste content can be provided by incorporating fillers and SCMs to ensure adequate workability.

Overall, powder packing optimisation did not adversely affect certain durability parameters and has potential to allow significant reductions in clinker content, specifically for concrete strength classes below 50 MPa, shown by the binder efficiency indices. However, the design of low-clinker concrete still requires substantial experimental trial. Further investigation and understanding regarding powder packing is required to approach a fully predictive process whereby optimal packing, fresh and hardened concrete properties may be predicted.

7.2 Recommendations

7.2.1 Use of the CIPM

Experimental packing density data obtained from various test methods, covering a larger range of material combinations, should be used to improve the confidence in the values of CIPM constants. The way in which surface forces are implemented in the CIPM should be reassessed, possibly assigning each material type its own C_a and C_b so that as the proportion of a certain material in a mixture is changed, the C_a and C_b values for the mixture are weighted accordingly. However, more appropriate may be the assessment of the fundamentals of powder material packing to arrive at a more general and universally applicable model.

7.2.2 Modelling techniques for packing optimisation

It is apparent that packing density should not be considered in isolation from water demand. Therefore, techniques which incorporate both parameters (such as that discussed in § 2.5) need further development so that their application can be universal. This entails the fundamental assessment of factors affecting particle packing and water demand and development of test methods to accurately assess this.

7.2.3 Low-clinker concrete mix design and materials

Dual consideration needs to be given to maximising packing density and lowering water content to obtain significant reductions in the clinker content of concrete. Focus needs to be given to minimising the water demand of the paste (and powder-paste) to enable overall water content minimisation. The potential use of low-clinker concrete for applications where durability is of primary concern should be investigated and incorporate SCMs with chloride binding capability.

Further investigation into increasing the SCM content of concrete without adversely affecting early age concrete properties is needed and could include the combined use of highly reactive cements. The contribution of mono- and hemi- carboaluminates, from the reaction of limestone with available aluminates, to compressive strength should be quantified to understand the extent to which these materials may benefit compressive strength. Investigation into the use of new SCMs, such as calcined clays, and their effects on concrete properties should be continued to allow their wide-spread use and increase the available resources of reactive, clinker replacement materials.

References

Addis, B. & Goodman, J., 2009. Concrete mix design. In: G. Owens, ed. *Fulton's Concrete Technology*. Midrand: Cement and Concrete Institute, 219 - 228.

Agullo, L. & Toralles-Carbonari, B. 1999. Fluidity of cement pastes with mineral admixtures and superplasticizer—a study based on the Marsh cone test. *Materials and Structures*. 32(7):479–485. DOI: 10.1007/BF02481631.Aim, R. & Le Goff, P., 1967. Effet de paroi dans les empilements desordonnes de spheres et application a la porosite de melanges binaires. *Powder technology*, Volume 1, 281-290.

Alexander, M. & Beushausen, H., 2009. Deformation and volume change of concrete. In: G. Owens, ed. *Fulton's Concrete Technology*. Midrand: Cement and Concrete Institute, 111-154.

Alexander, M. & Mindess, S. 2005. *Aggregates in concrete*. Taylor & Francis.

Alexander, M., Jaufeerally, H. & Mackechnie, K. 2003. Structural and durability properties of concrete made with Corex slag. Research monograph. (6):1–28.

Alexander, M.G., Ballim, Y. & Mackechnie, J.R. 2009. Durability index testing procedure manual (Ver 1.0, Feb 2009). Department of Civil Engineering, University of Cape Town: Concrete Materials and Structural Integrity Research Unit.

American Concrete Institute Committee 211. 2002. *Standard practise for selecting proportions for normal, heavyweight, and mass concrete*. (ACI 211.1-91). Farmington Hills, Michigan: American Concrete Institute

Andreasen, A.H.M. and Andersen, J. (1930) Über die beziehung zwischen kornabstufung und zwischenraum in produkten aus losen körnern (mit einigen experimenten). *Colloid & Polymer Science*, Vol. 50 (3), 217-228.

ASTM International. 2002. *Standard test method for flow of grout for preplaced-aggregate concrete (Flow cone method)*. (ASTM C 939-02). West Conshohocken: ASTM international

Bentz, D.P., Irassar, E.F., Bucher, B.E. & Weiss, W.J. 2009. Limestone fillers conserve cement part 2: Durability issues and the effects of limestone fineness on mixtures. *Concrete International*. (December):35–39.

Bentz, D.P., Sato, T., De La Varga, I. & Weiss, W.J. 2012. Fine limestone additions to regulate setting in high volume fly ash mixtures. *Cement and Concrete Composites*. 34(1):11–17. DOI: 10.1016/j.cemconcomp.2011.09.004.

Berodier, E. & Scrivener, K. 2014. Understanding the filler effect on the nucleation and growth of C-S-H. *American Ceramic Society*. 97(12):3764–3773. DOI: 10.1111/jace.13177.

Brouwers, H.J.H. 2006. Particle-size distribution and packing fraction of geometric random packings. *Physical Review E*. 74:1–14. DOI: 10.1103/PhysRevE.74.031309.

Brouwers, H.J.H. & Radix, H.J. 2005. Self-compacting concrete: Theoretical and experimental study. *Cement and Concrete Research*. 35(11):2116–2136. DOI: 10.1016/j.cemconres.2005.06.002.

Damineli, B.L., John, V.M., Lagerblad, B. & Pileggi, R.G. 2016. Viscosity prediction of cement-filler suspensions using interference model: A route for binder efficiency enhancement. *Cement and Concrete Research*. 84:8–19. DOI: 10.1016/j.cemconres.2016.02.012.

Damineli, B.L., Kemeid, F.M., Aguiar, P.S. & John, V.M. 2010. Measuring the eco-efficiency of cement use. *Cement and Concrete Composites*. 32(8):555–562. DOI: 10.1016/j.cemconcomp.2010.07.009.

de Larrard, F. 1999. Concrete mixture proportioning: A scientific approach. V. 1. DOI: 10.1017/CBO9781107415324.004.

De Weerdt, K., Kjellsen, K.O., Sellevold, E. & Justnes, H. 2011. Synergy between fly ash and limestone powder in ternary cements. *Cement and Concrete Composites*. 33(1):30–38. DOI: 10.1016/j.cemconcomp.2010.09.006.

Dewar, J.D. 1999. Computer modelling of concrete mixtures. London: E & FN Spon.

Dhir, R.K., Limbachiya, M.C., McCarthy, M.J. & Chaipanich, A. 2007. Evaluation of Portland limestone cements for use in concrete construction. *Materials and Structures*. 40(5):459–473. DOI: 10.1617/s11527-006-9143-7.

Erdogan, S.T., Quiroga, P.N., Fowler, D.W., Saleh, H.A., Livingston, R.A., Garboczi, E.J., Ketcham, P.M., Hagedorn, J.G., et al. 2006. Three-dimensional shape analysis of coarse aggregates: New techniques for and preliminary results on several different coarse aggregates and reference rocks. *Cement and Concrete Research*. 36(9):1619–1627. DOI: 10.1016/j.cemconres.2006.04.003.

European Committee for Standardisation. 2011. *Cement – Part 1: Composition, specifications and conformity criteria for common cements*. (EN 197-1: 2011). Brussels: CEN

Fennis, S.A.A.M. 2011. *Design of ecological concrete by particle packing optimisation*. Doctoral Thesis, Delft, Netherlands: Delft University of Technology

Flower, D.J.M. & Sanjayan, J.G. 2007. Greenhouse gas emissions due to concrete manufacture. *Int J LCA*. 12(5):282–288.

Fuller, W.B. and Thompson, S.E. (1907) The laws of proportioning concrete. *ASCE J*. Transport., Vol. 59, 67-143.

Funk, J.E. & Dinger, D.R. 1994. Predictive process control of crowded particulate suspensions. DOI: 10.1007/978-1-4615-3118-0.

Furnas, C.C. 1929. Flow of gases though beds of broken solids. United States Government Printing Office.

Goltermann, P., Johansen, V. and Palbøl, L. (1997) Packing of aggregates: An alternative tool to determine the optimal aggregate mix. *ACI Materials Journal*, Vol. 94 (5), 435-443.

Grieve, G., 2009. Cementitious materials. In: G. Owens, ed. *Fulton's Concrete Technology*. Midrand: Cement and Concrete Institute, 1-17.

Hewlett, P. 2004. *Lea's Chemistry of Cement and Concrete*. 4th ed. Elsevier Science & Technology Books. DOI: 10.1016/B978-0-7506-6256-7.50031-X.

Holdich, R.G. 2002. Colloids and agglomeration. In *Fundamentals of particle technology*. Midland information technology and publishing. 131–140. DOI: 10.4236/ns.2010.210132.

Hunger, M. 2010. *An integral design concept for ecological self-compacting concrete*. Doctoral thesis, Eindhoven, Netherlands: Eindhoven University of Technology.

Hüsken, G. & Brouwers, H.J.H. 2008. A new mix design concept for earth-moist concrete: A theoretical and experimental study. *Cement and Concrete Research*. 38(10):1246–1259. DOI: 10.1016/j.cemconres.2008.04.002.

Hüsken, G. 2010. *A multifunctional design approach for sustainable concrete: with application to concrete mass products*. Doctoral thesis, Eindhoven, Netherlands: Eindhoven University of Technology. DOI: 10.6100/IR693348.

Imbabi, M.S., Carrigan, C. & McKenna, S. 2012. Trends and developments in green cement and concrete technology. *International Journal of Sustainable Built Environment*. 1(2):194–216. DOI: 10.1016/j.ijsbe.2013.05.001.

InEnergy. 2010. *Cement and Concrete Institute: Concrete Industry Greenhouse Gas Emissions*. Johannesburg, South Africa.

John, V.M., Damineli, B.L., Quattrone, M., Pileggi, R.G. 2017. Fillers in cementitious materials - experience, recent advances and future potential (Pre-publication version). *Cement and concrete research*.

Jones, R., Zheng, L. & Newlands, M. 2002. Comparison of particle packing models for proportioning concrete constituents for minimum voids ratio. *Materials and Structures*. 35:301–309. DOI: 10.1007/BF02482136.

Juenger, M.C.G. & Siddique, R. 2015. Recent advances in understanding the role of supplementary cementitious materials in concrete. *Cement and Concrete Research*. 78:71–80. DOI: 10.1016/j.cemconres.2015.03.018.

Juenger, M.C.G., Winnefeld, F., Provis, J.L. & Ideker, J.H. 2011. Advances in alternative cementitious binders. *Cement and Concrete Research*. 41(12):1232–1243. DOI: 10.1016/j.cemconres.2010.11.012.

Knop, Y. & Peled, A. 2016. Packing density modelling of blended cement with limestone having different particle sizes. *Construction and Building Materials*. 102:44–50. DOI: 10.1016/j.conbuildmat.2015.09.063.

Knop, Y., Peled, A. & Cohen, R. 2014. Influences of limestone particle size distributions and contents on blended cement properties. *Construction and Building Materials*. 71:26–34. DOI: 10.1016/j.conbuildmat.2014.08.004.

Kumar, A., Oey, T., Kim, S., Thomas, D., Badran, S., Li, J., Fernandes, F., Neithalath, N., et al. 2013. Simple methods to estimate the influence of limestone fillers on reaction and property evolution in cementitious materials. *Cement and Concrete Composites*. 42:20–29. DOI: 10.1016/j.cemconcomp.2013.05.002.

Kumar, S. V. & Santhanam, M. 2003. Particle packing theories and their application in concrete mixture proportioning: A review. *Indian Concrete Journal*. 77(9):1324–1331.

Kwan, A.K.H. & Fung, W.W.S. 2009. Packing density measurement and modelling of fine aggregate and mortar. *Cement and Concrete Composites*. 31(6):349–357. DOI: 10.1016/j.cemconcomp.2009.03.006.

Latham, J.P., Munjiza, A., Garcia, X., Xiang, J. & Guises, R. 2008. Three-dimensional particle shape acquisition and use of shape library for DEM and FEM/DEM simulation. *Minerals Engineering*. 21(11):797–805. DOI: 10.1016/j.mineng.2008.05.015.

Li, L.G. & Kwan, A.K.H. 2013. Concrete mix design based on water film thickness and paste film thickness. *Cement and Concrete Composites*. 39:33–42. DOI: 10.1016/j.cemconcomp.2013.03.021.

Lollini, F., Redaelli, E. & Bertolini, L. 2014. Effects of Portland cement replacement with limestone on the properties of hardened concrete. *Cement and Concrete Composites*. 46:32–40. DOI: 10.1016/j.cemconcomp.2013.10.016.

Lothenbach, B., Scrivener, K. & Hooton, R.D. 2011. Supplementary cementitious materials. *Cement and Concrete Research*. 41(12):1244–1256. DOI: 10.1016/j.cemconres.2010.12.001.

Majidi, B., Melo, J., Fafard, M., Ziegler, D. & Alamdari, H. 2015. Packing density of irregular shape particles: DEM simulations applied to anode-grade coke aggregates. *Advanced Powder Technology*. 26(4):1256–1262. DOI: 10.1016/j.apt.2015.06.008.

Mehdipour, I. & Khayat, K.H. 2016. Effect of SCM content and binder dispersion on packing density and compressive strength of sustainable cement paste. *ACI Materials Journal*. (113). DOI: 10.14359/51688704.

Mohammadi, I. (James) & South, W. 2016. General purpose cement with increased limestone content in Australia. *ACI Materials Journal*. 113(3):335–347. DOI: 10.14359/51688703.

Moon, G.D., Oh, S., Jung, S.H. & Choi, Y.C. 2017. Effects of the fineness of limestone powder and cement on the hydration and strength development of PLC concrete. *Construction and Building Materials*. 135:129–136. DOI: 10.1016/j.conbuildmat.2016.12.189.

Moore, A.J. & Alexander, M.G. 2017. A critical review of the water sorptivity index (WSI) parameter used in potential durability assessment: Can WSI be considered in isolation of porosity? (In-review). University of Cape Town.

Muigai, R.N. 2014. *A framework towards the design of more sustainable concrete structures*. Doctoral thesis, Cape Town, South Africa: University of Cape Town.

Müller, H.S., Breiner, R., Moffatt, J.S. & Haist, M. 2014. Design and properties of sustainable concrete. *Procedia Engineering*. 95: 290–304. DOI: 10.1016/j.proeng.2014.12.189.

Neville, A.M. (2011) *Properties of concrete*. 5th ed. Pearson Education.

Palm, S., Proske, T., Rezvani, M., Hainer, S., Müller, C. & Graubner, C-A. 2016. Cements with a high limestone content – Mechanical properties, durability and ecological characteristics of the concrete. *Construction and Building Materials*. 119:308–318. DOI: 10.1016/j.conbuildmat.2016.05.009.

Powers, T., 1968. *The properties of fresh concrete*. New York: Wiley & Sons.

Proske, T., Hainer, S., Rezvani, M. & Graubner, C. 2013. Eco-friendly concretes with reduced water and cement contents — Mix design principles and laboratory tests. *Cement and Concrete Research*. 51:38–46. DOI: 10.1016/j.cemconres.2013.04.011.

Proske, T., Hainer, S., Rezvani, M. & Graubner, C.A. 2014. Eco-friendly concretes with reduced water and cement content - Mix design principles and application in practise. *Construction and Building Materials*. 67(PART C):413–421. DOI: 10.1016/j.conbuildmat.2013.12.066.

Ramezanianpour, A.A. 2014. *Cement Replacement Materials*. Springer. DOI: 10.1007/978-3-642-367212.

Schwanda, F. 1966. Das rechnerische Verfahren zur Bestimmung des Hohlraumes und Zementleimanspruches von Zuschlägen und seine Bedeutung für Spannbetonbau. *Zement und Beton*. 37: 8-17

Scrivener, K.L., John, V.M. & Gartner, E.M. 2016. *Eco-efficient cements: Potential, economically viable solutions for a low-CO2, cement-based materials industry*. UNEP: Paris, France.

Siddique, R. & Khan, M.I. 2011. *Supplementary Cementing Materials*. Springer. DOI: 10.1007/978-3-642-17866-5.

South African National Standards. 2006. *Bulk densities and voids content of aggregates*. (SANS5845:2006). Pretoria: SANS Standards.

South African National Standards. 2013. *Cement – Part 1: Composition, specifications and conformity criteria for common cements*. (SANS 50197-1: 2013). Pretoria: SANS Standards.

South African National Standards. 2006. *Concrete tests - consistence of freshly mixed concrete-slump test*. (SANS5862-1:2006). Pretoria: SANS Standards.

South African National Standards. 2006. *Concrete tests – initial drying shrinkage and wetting expansion of concrete.* (SANS6085:2006). Pretoria: SANS Standards.

South African National Standards. 2006. *Concrete tests - Compressive strength of hardened concrete.* (SANS5863:2006). Pretoria: SANS Standards.

South African National Standards. 2008. *Sieve analysis, fines content and dust content of aggregates.* (SANS 201: 2008). Pretoria: SANS Standards.

South African National Standards. 2006. *Specification for aggregates from natural sources – aggregates for concrete.* (SANS 1083:2006) Pretoria: SANS Standards.

Stovall, T., de Larrard, F. & Buil, M. 1986. Linear packing density model of grain mixtures. *Powder Technology.* 48(1):1–12. DOI: 10.1016/0032-5910(86)80058-4.

Talbot, A.N. & Richart, F.E. 1923. The strength of concrete, its relation to the cement aggregates and water. University of Illinois Engineering Experiment Station, Bulletin No. 137

Thomas, M.D.A. 2007. Optimising the use of fly ash in concrete. *Portland Cement Association*. 24.

Toufar, W., Born, M. and Klose, E. (1976) Beitrag zur optimierung der packungsdichte polydisperser körniger systeme. Freiberger Forschungsheft A 558, *VEB Deutscher Verlag für Grundstoffindustrie*. 29-44.

Tsivilis, S., Chaniotakis, E., Kakali, G. & Batis, G. 2002. An analysis of the properties of Portland limestone cements and concrete. *Cement and Concrete Composites*. 24(3–4):371–378. DOI: 10.1016/S0958-9465(01)00089-0.

Van Den Heede, P. & De Belie, N. 2012. Environmental impact and Life Cycle Assessment (LCA) of traditional and "green" concretes: Literature review and theoretical calculations. *Cement and Concrete Composites*. 34(4):431–442. DOI: 10.1016/j.cemconcomp.2012.01.004.

Van Der Putten, J., Dils, J., Minne, P., Boel, V. & De Schutter, G. 2017. Determination of packing profiles for the verification of the compressible packing model in case of UHPC pastes. *Materials and Structures.* 50(2):118. DOI: 10.1617/s11527-016-0986-2.

Voglis, N., Kakali, G., Chaniotakis, E. & Tsivilis, S. 2005. Portland-limestone cements: Their properties and hydration compared to those of other composite cements. *Cement and Concrete Composites*. 27(2):191–196. DOI: 10.1016/j.cemconcomp.2004.02.006.

Wong, H.H.C. & Kwan, A.K.H. 2008. Packing density of cementitious materials: part 1—measurement using a wet packing method. *Materials and Structures*. 41(4):689–701. DOI: 10.1617/s11527-007-9274-5.

Wong, H.H.C. & Kwan, A.K.H. 2008a. Packing density of cementitious materials: measurement and modelling. *Magazine of Concrete Research*. 60(3):165–175. DOI: 10.1680/macr.2007.00004.

World Business Council for Sustainable Development – Cement Sustainability Initiative. 2016. Getting the numbers right (GNR) Project, WBCSD-CSI, Available: http://www.wbcsdcement.org/GNR-2014/index.html [2017, October]

Yu, Q.L., Spiesz, P. & Brouwers, H.J.H. 2013. Development of cement-based lightweight composites-Part 1: Mix design methodology and hardened properties. *Cement and Concrete Composites.* 44:17–29. DOI: 10.1016/j.cemconcomp.2013.03.030.

Yu, R., Spiesz, P. & Brouwers, H.J.H. 2015. Development of an eco-friendly ultra-high performance concrete (UHPC) with efficient cement and mineral admixtures uses. *Cement and Concrete Composites*. 55:383–394. DOI: 10.1016/j.cemconcomp.2014.09.024.

Appendix A: Powder material chemical composition

Table A-1: Typical % chemical composition of cement and FA from material suppliers

Sample Reference	CEM II A-L 52.5N	FA
SiO_2	19.8	53.7
Al_2O_3	3.2	32.9
Fe_2O_3	3.1	3.2
Mn_2O_3	0.1	0.1
TiO_2	0.2	1.7
CaO	63.8	4.3
MgO	1.3	1.1
P_2O_5	0.1	0.5
SO_3	2.5	0.0
K_2O	0.6	0.5
Na_2O	0.2	0.0
SrO	0.3	0.0
LOI	4.6	1.0

Table A-2: Typical % chemical composition of limestone fillers from supplier

	KB2	KB5	KB10	KB45
$CaCO_3$	96.5	96.5	95	95
$MgCO_3$	2.8	2.8	4	4
Fe_2O_3	0.03	0.03	0.03	0.03
SiO_2	0.21	0.21	0.9	0.9

Appendix B: CIPM calibration

Table B-1: Powder combinations for CIPM calibration with corresponding predicted and experimental packing densities and associated % error

Mixture No.	Powder volume fraction (-)					α_{exp} *	α_t *	% Absolute error
	KB2	KB5	KB10	KB45	CEM II A-L 52.5			
1	0	0	0	0	1	0.615	0.615	-
2	0.2	0	0	0	0.8	0.626	0.626	0.00
3	0.4	0	0	0	0.6	0.655	0.637	2.75
4	0.6	0	0	0	0.4	0.649	0.645	0.62
5	0.8	0	0	0	0.2	0.636	0.645	1.42
6	1	0	0	0	0	0.634	0.634	-
7	0	0.2	0	0	0.8	0.626	0.619	1.12
8	0	0.4	0	0	0.6	0.624	0.622	0.32
9	0	0.6	0	0	0.4	0.623	0.623	0.00
10	0	0.8	0	0	0.2	0.618	0.622	0.65
11	0	1	0	0	0	0.62	0.620	-
12	0	0	0.2	0	0.8	0.611	0.618	1.15
13	0	0	0.4	0	0.6	0.609	0.621	1.97
14	0	0	0.6	0	0.4	0.614	0.623	1.47
15	0	0	0.8	0	0.2	0.617	0.625	1.30
16	0	0	1	0	0	0.627	0.627	-
17	0	0	0	0.2	0.8	0.634	0.641	1.10
18	0	0	0	0.4	0.6	0.654	0.663	1.38
19	0	0	0	0.6	0.4	0.678	0.677	0.15
20	0	0	0	0.8	0.2	0.673	0.668	0.74
21	0	0	0	1	0	0.635	0.635	-
							Average error	1
							Max error	2.75

* α_t : CIPM predicted packing density; α_{exp} : Experimental packing density

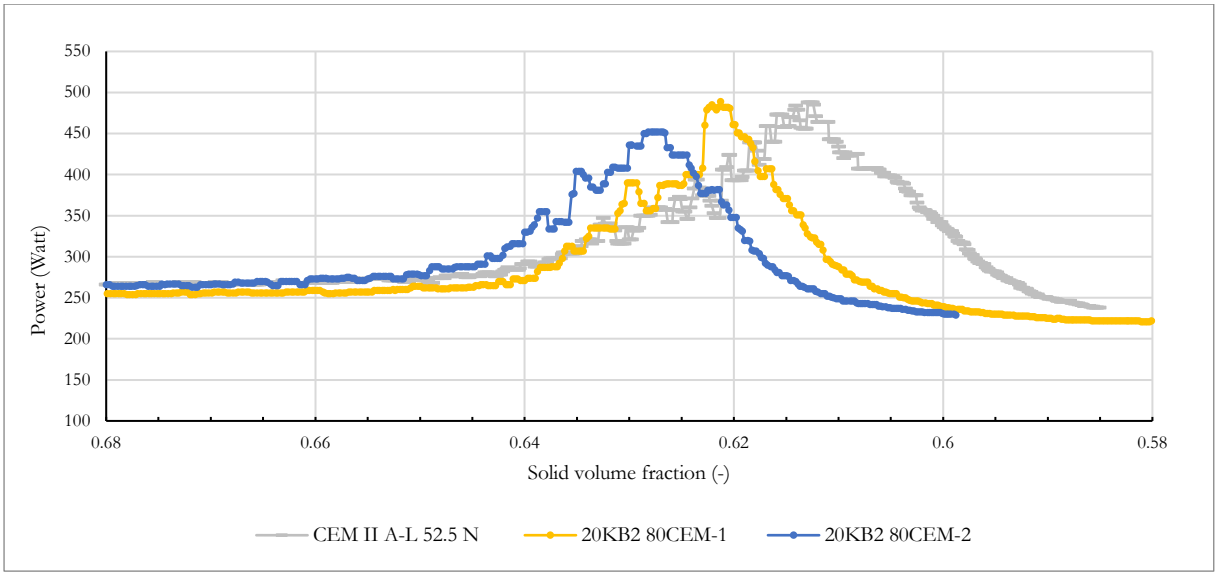

Figure B-1: 20KB2 80CEM mixing energy results

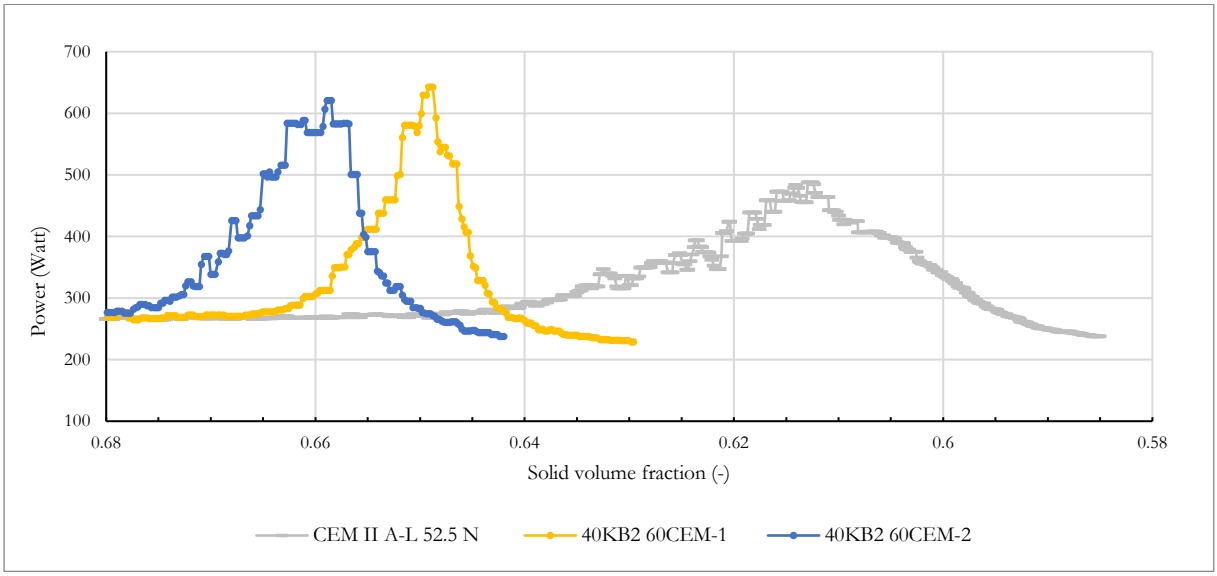

Figure B-2: 40KB2 60CEM mixing energy results

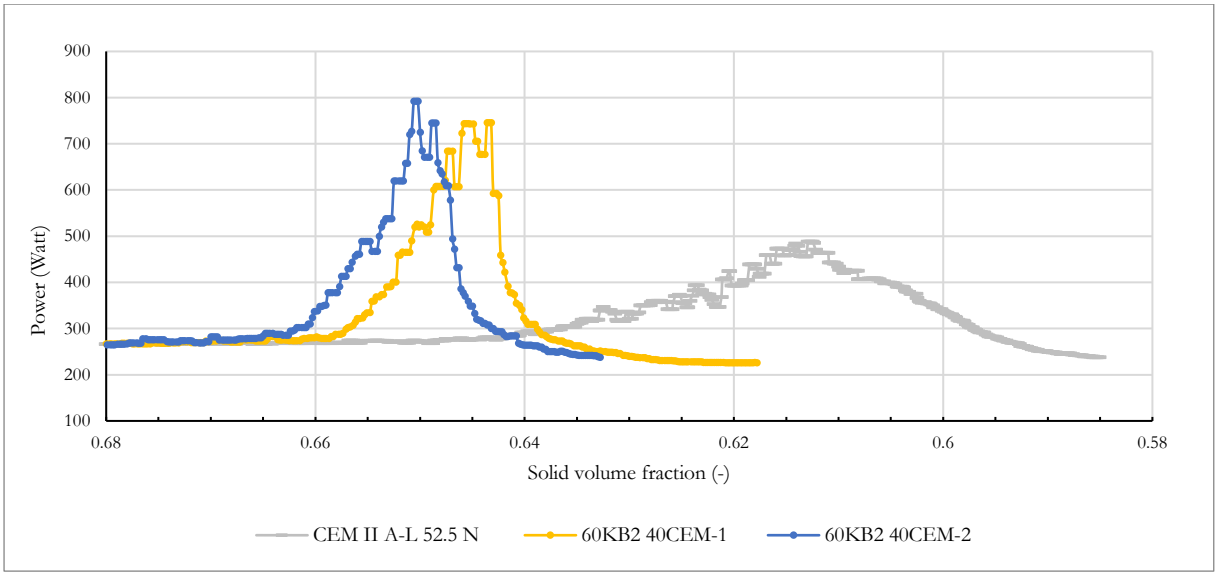

Figure B-3: 60KB2 40CEM mixing energy results

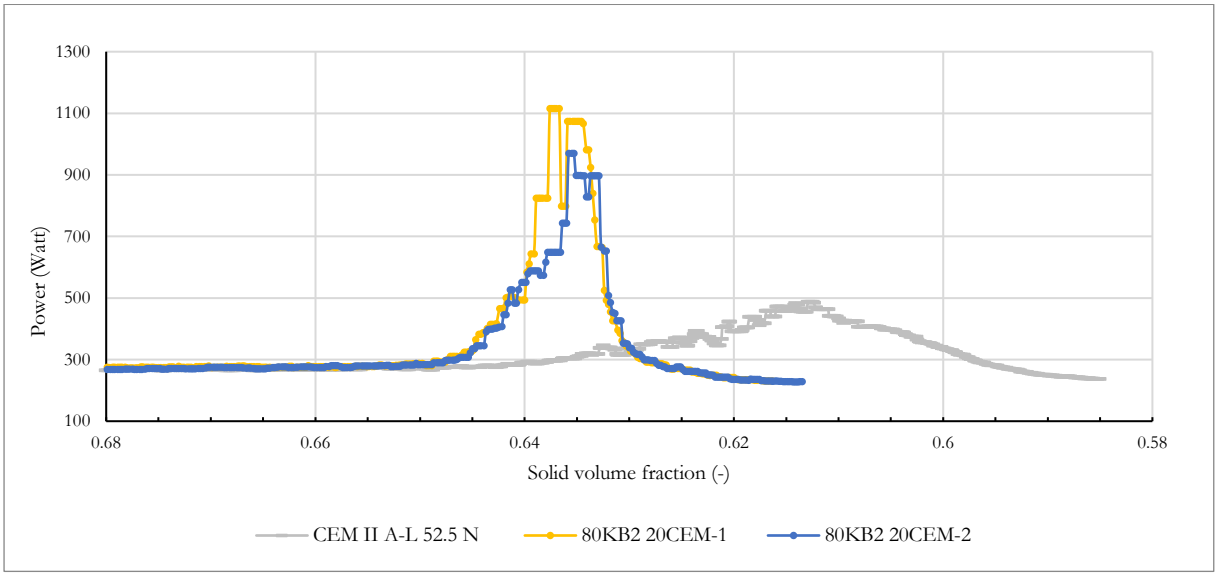

Figure B-4: 80KB2 20CEM mixing energy results

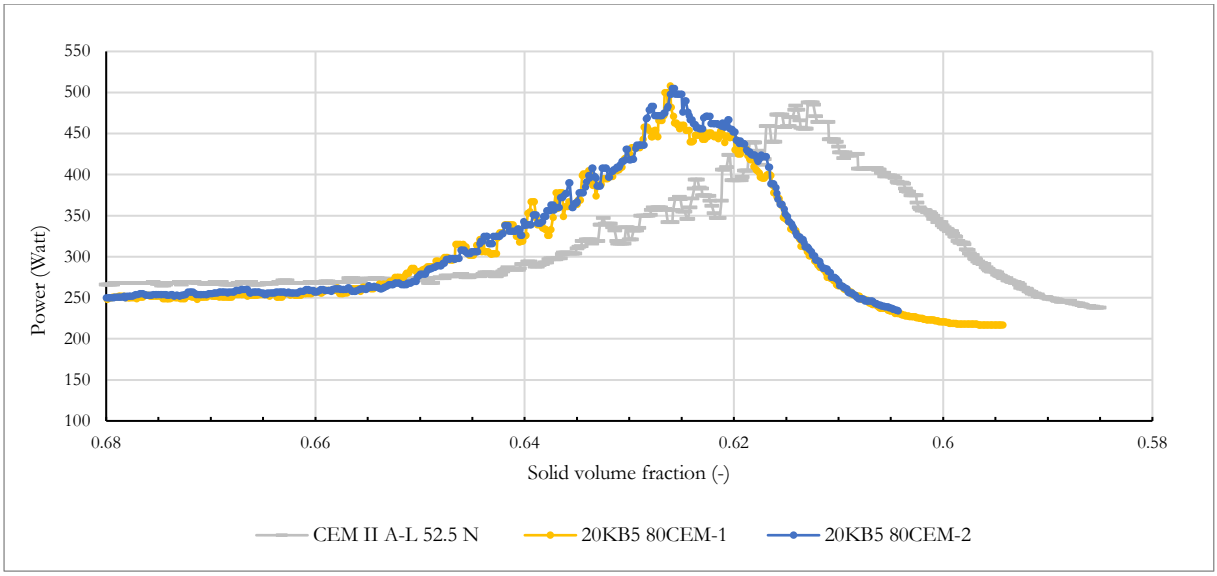

Figure B-5: 20KB5 80CEM mixing energy results

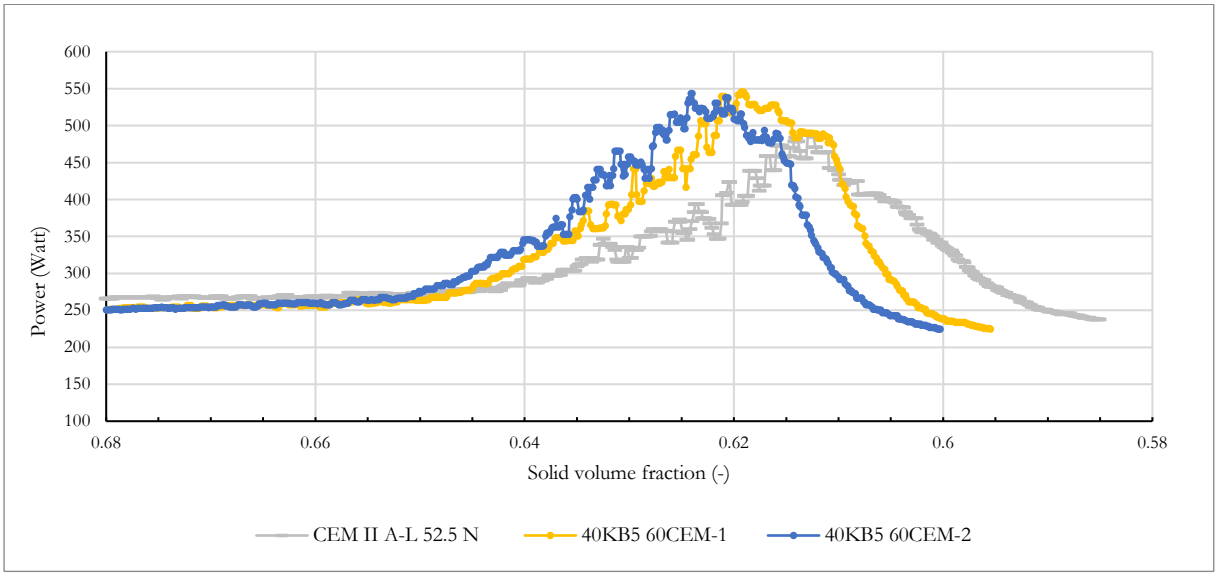

Figure B-6: 40KB5 60CEM mixing energy results

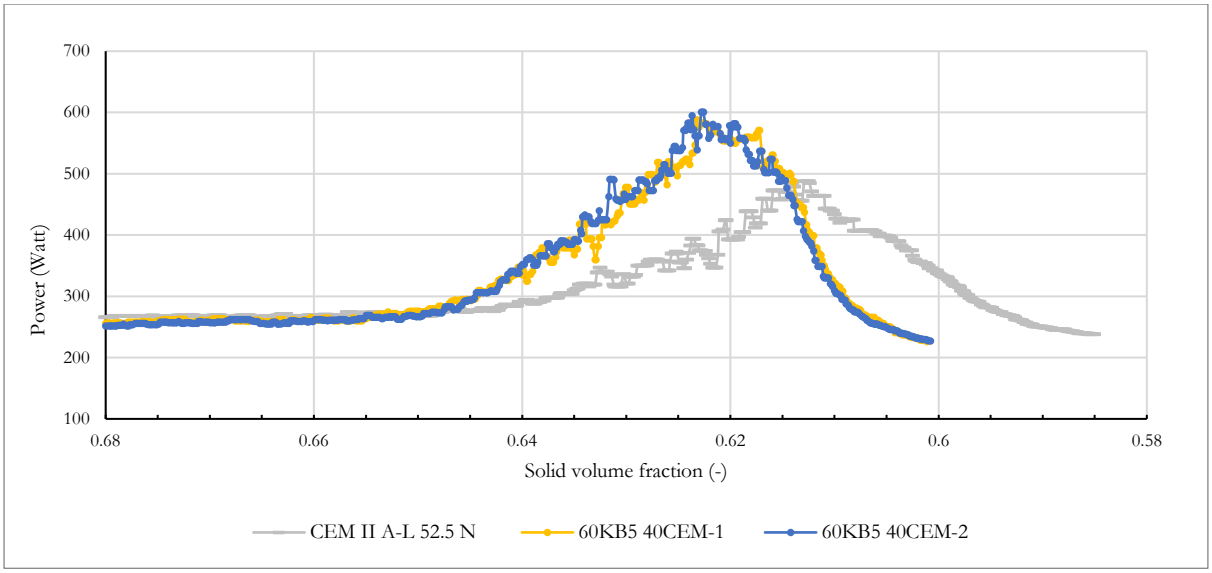

Figure B-7: 60KB5 40CEM mixing energy results

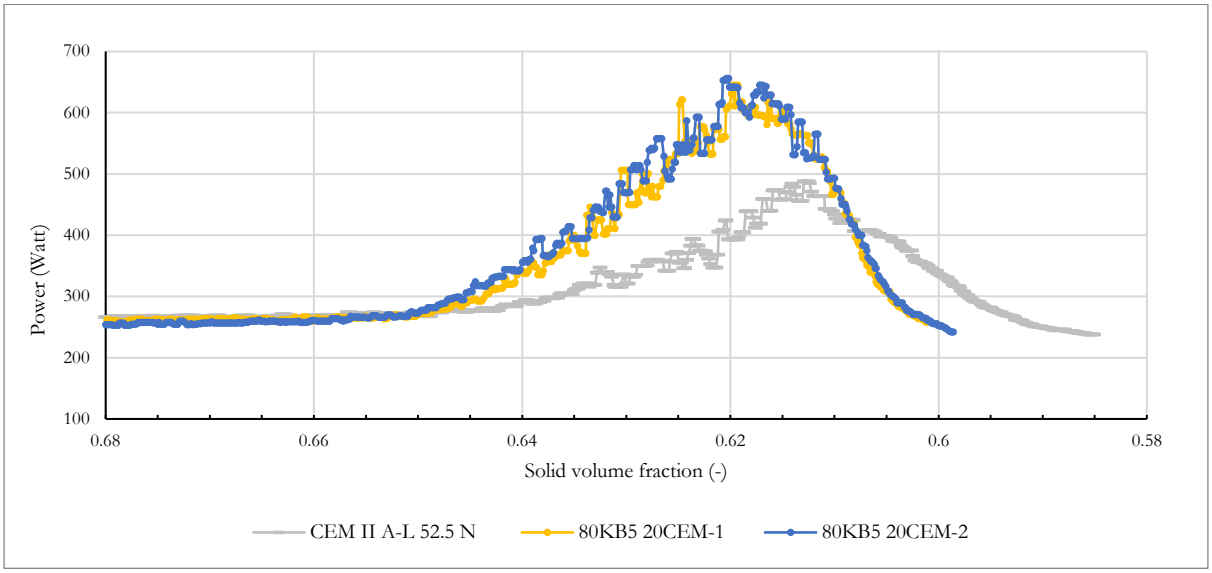

Figure B-8: 80KB5 20CEM mixing energy results

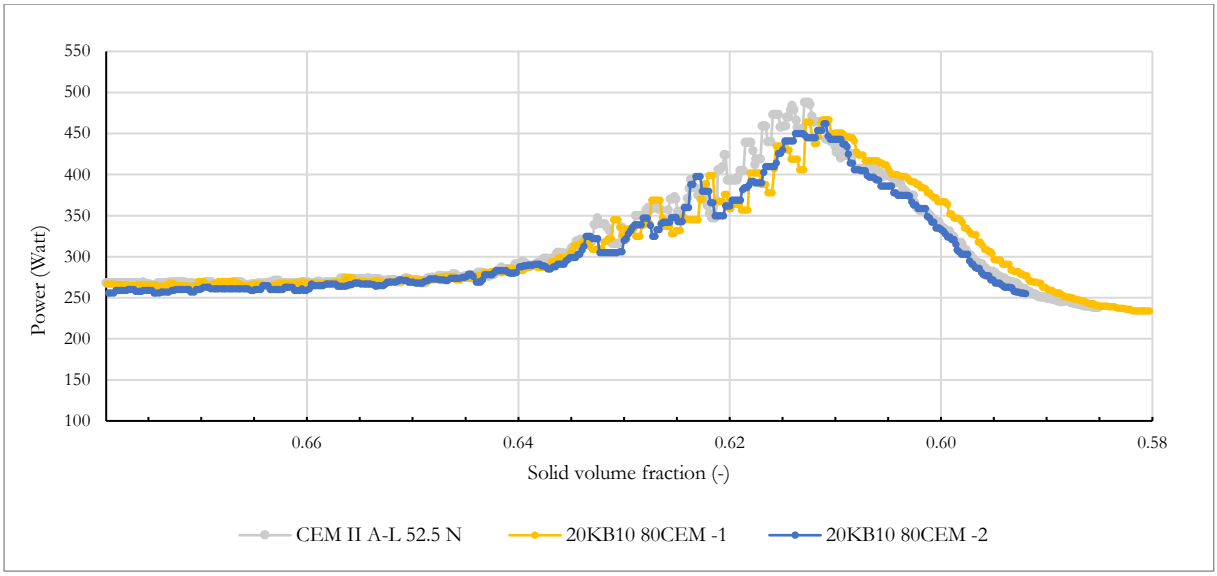

Figure B-9: 20KB10 80CEM mixing energy results

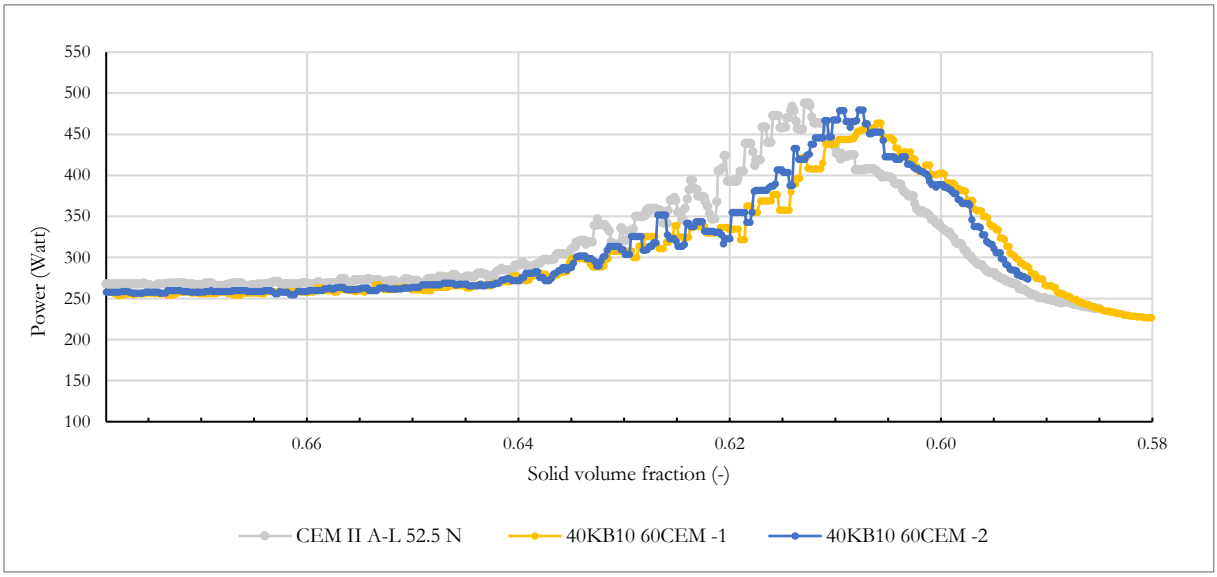

Figure B-10: 40KB10 60CEM mixing energy results

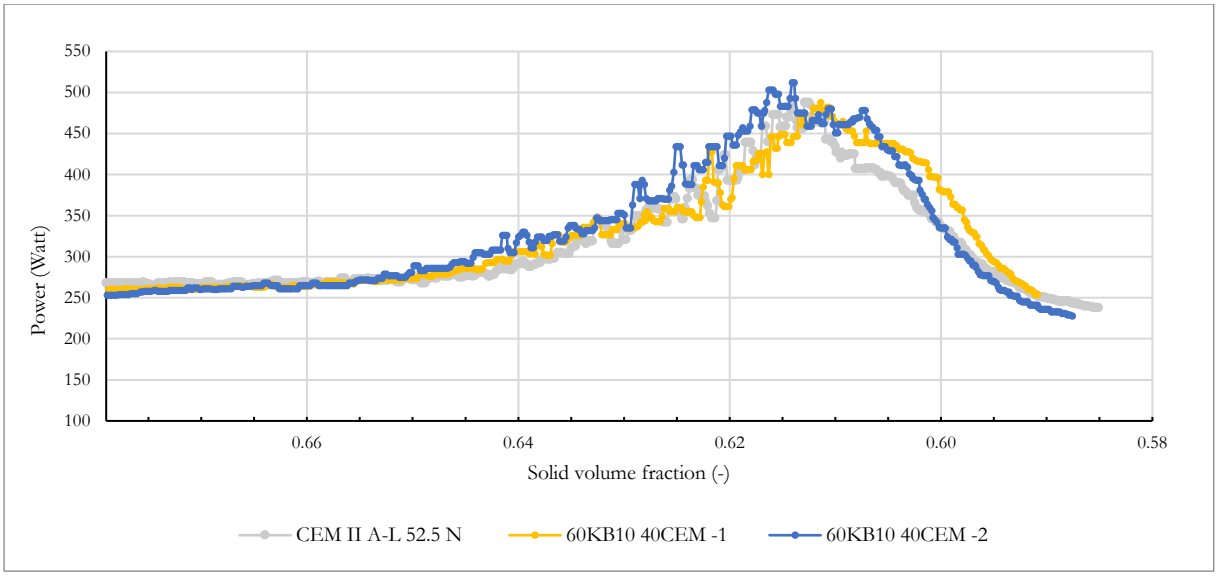

Figure B-11: 60KB10 40CEM mixing energy test results

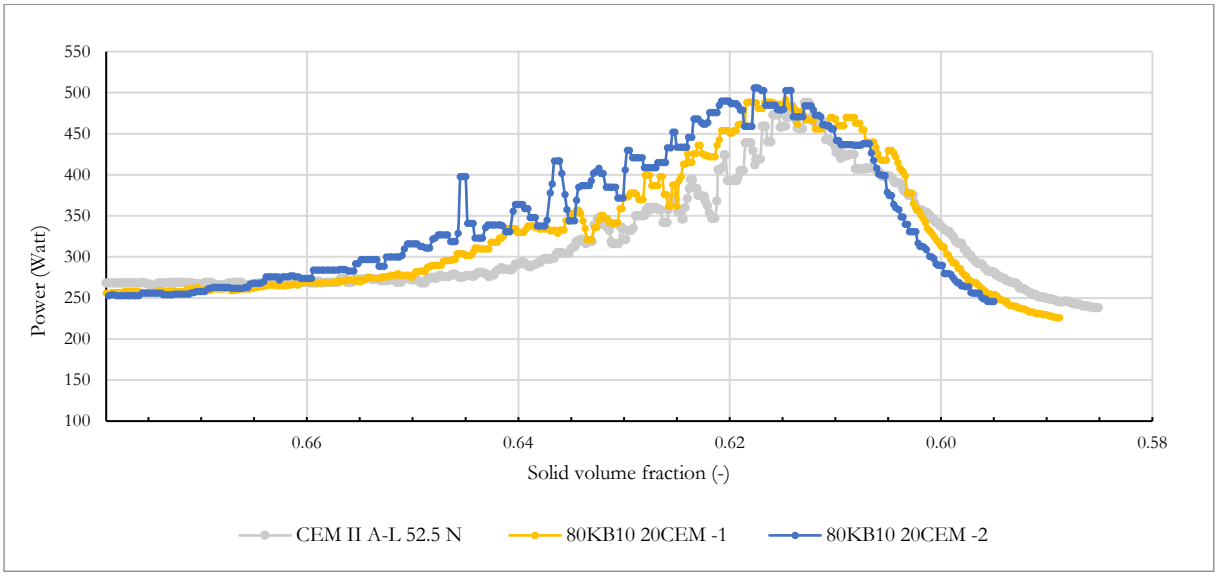

Figure B-12: 80KB10 20CEM mixing energy test results

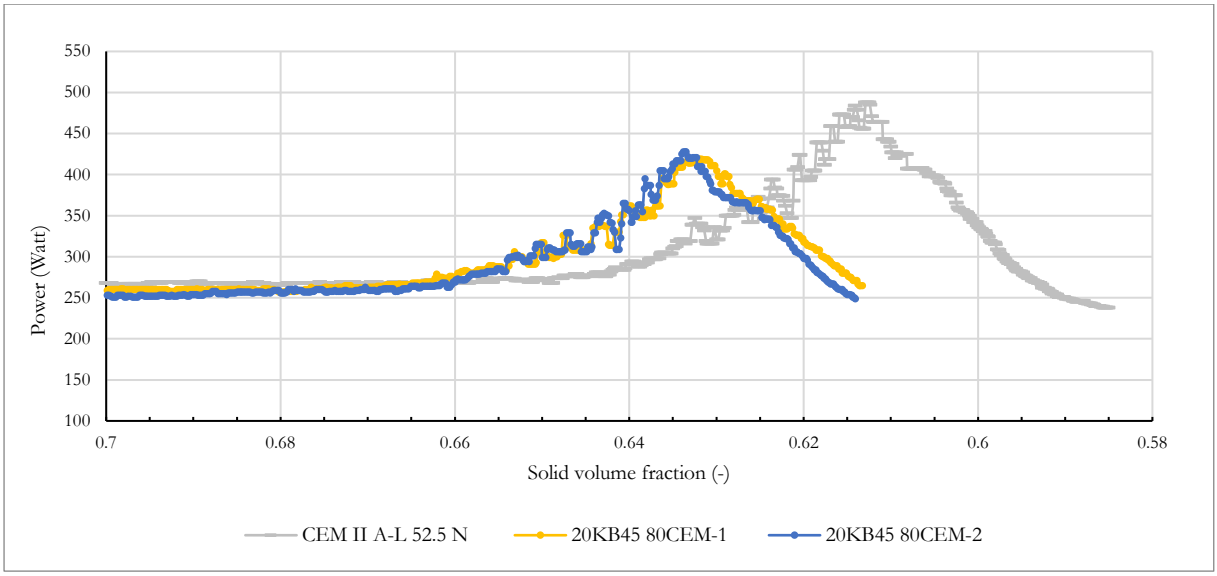

Figure B-13: 20KB45 80CEM mixing energy test results

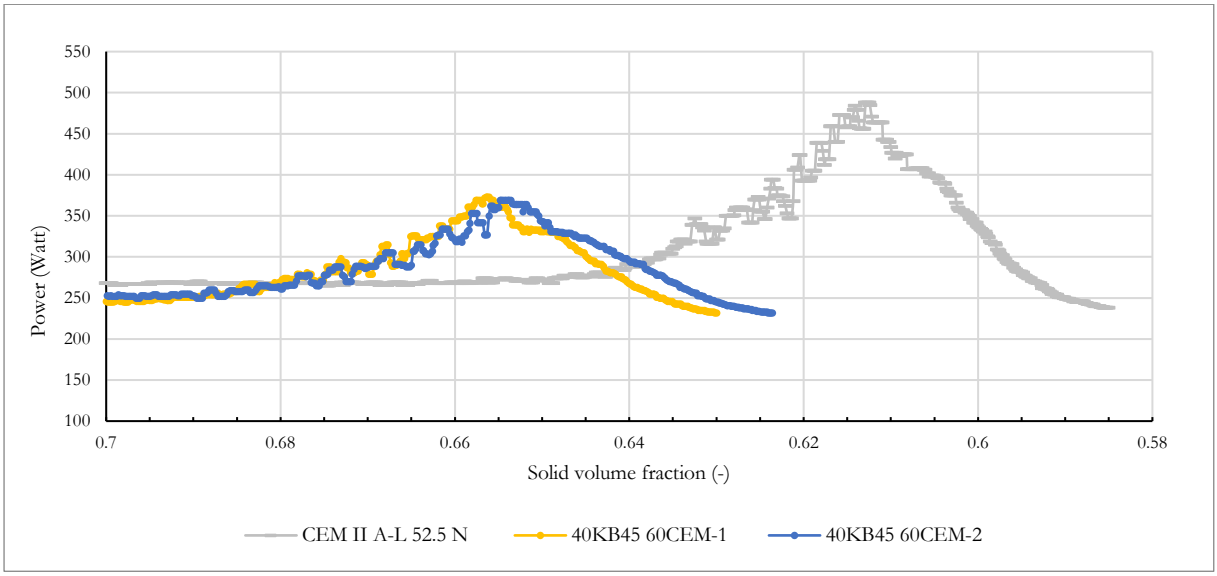

Figure B-14: 40KB45 60CEM mixing energy test results

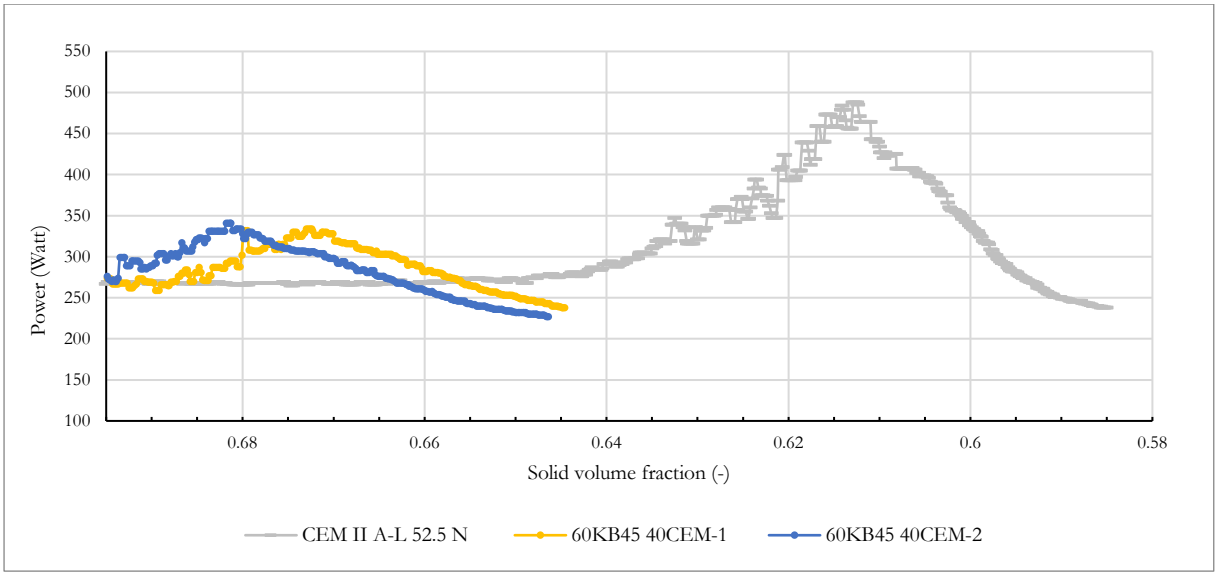

Figure B-15: 60KB45 40CEM mixing energy test results

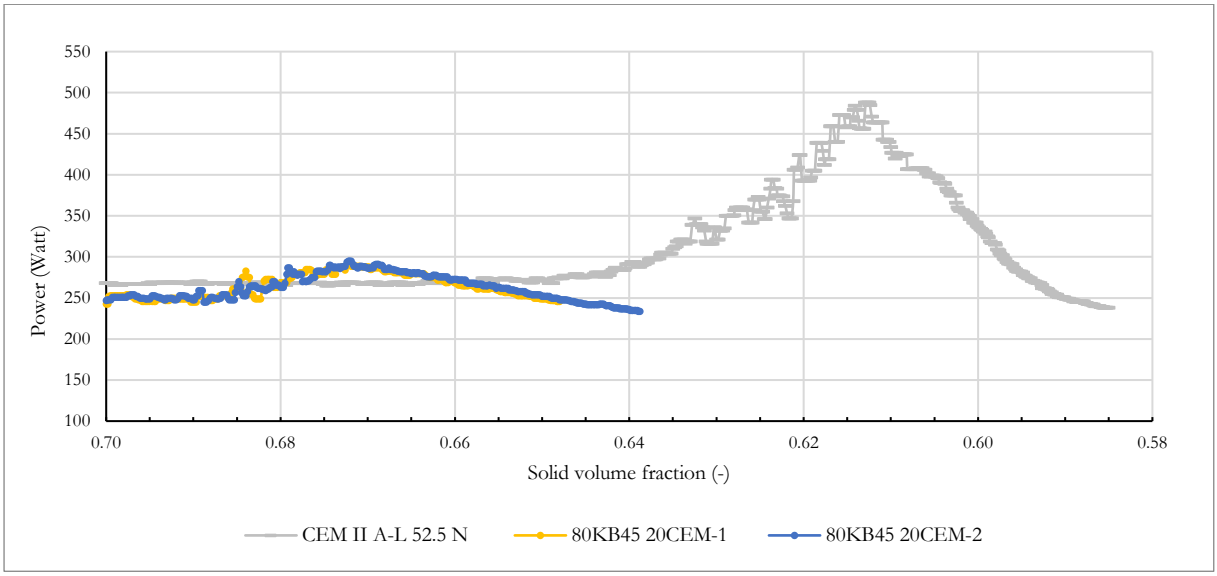

Figure B-16: 80KB45 20CEM mixing energy test results

Calculation of CIPM prediction error

Table B-2 portrays the assessment of the CIPM packing density prediction error (discrepancy between CIPM predicted value and an experimental result). The absolute difference between the predicted packing density (α_i) and experimental packing density (α_{exp}) was used to calculate a percentage error (e_{i-v}) for each cement/limestone combination that was tested, where i represents the limestone type (either KB45, KB10, KB5 or KB2) and v represents its volume % proportion of the total mixture (either 20, 40, 60 or 80 %).

This produced four data points, from the various combinations of cement and limestone, for each limestone type. An average error (e_{i-avg}) was then calculated for each limestone type. Loosening and wall coefficients (C_a and C_b respectively) were varied (see § 4.2.4.3) to determine their influence on the average error for each limestone type and the combination of C_a and C_b enabling the minimisation of the average error was reported for each limestone type.

Thereafter, an overall average error ($e_{Avg.total}$) was also assessed. This was simply an average error calculated across all cement/limestone combinations and across all limestone types. Once again, C_a and C_b were varied and the values enabling the minimisation of the overall average error were reported and compared with the values determined for each limestone type. The results from the error analysis and selection of C_a and C_b are discussed in § 6.2.1.2 .

Table B-2: Description of error calculation for calibration of CIPM constants

Powder volume fraction		% Error per powder combination	Average % error per limestone type
Limestone	Cement	$e_{i-v} = \frac{\lvert \alpha_t - \alpha_{exp} \rvert}{\alpha_{exp}} \times 100$	$e_{i-avg} = \sum \frac{e_{i-v}}{4}$
KB 45	CEM II A-L 52.5 N		
0.2	0.8	$e_{KB45\text{ - }20}$	$e_{KB45\text{ - }avg}$
0.4	0.6	$e_{KB45\text{ - }40}$	
0.6	0.4	$e_{KB45\text{ - }60}$	
0.8	0.2	$e_{KB45\text{ - }80}$	
KB 10	CEM II A-L 52.5 N		
0.2	0.8	$e_{KB10\text{ - }20}$	$e_{KB10\text{ - }avg}$
0.4	0.6	$e_{KB10\text{ - }40}$	
0.6	0.4	$e_{KB10\text{ - }60}$	
0.8	0.2	$e_{KB10\text{ - }80}$	
KB 5	CEM II A-L 52.5 N		
0.2	0.8	$e_{KB5\text{ - }20}$	$e_{KB5\text{ - }avg}$
0.4	0.6	$e_{KB5\text{ - }40}$	
0.6	0.4	$e_{KB5\text{ - }60}$	
0.8	0.2	$e_{KB5\text{ - }80}$	
KB 2	CEM II A-L 52.5 N		
0.2	0.8	$e_{KB2\text{ - }20}$	$e_{KB2\text{ - }avg}$
0.4	0.6	$e_{KB2\text{ - }40}$	
0.6	0.4	$e_{KB2\text{ - }60}$	
0.8	0.2	$e_{KB2\text{ - }80}$	
		$e_{Avg.total}$	$\sum \frac{e_{KB45-avg} + e_{KB10-avg} + e_{KB5-avg} + e_{KB2-avg}}{4}$

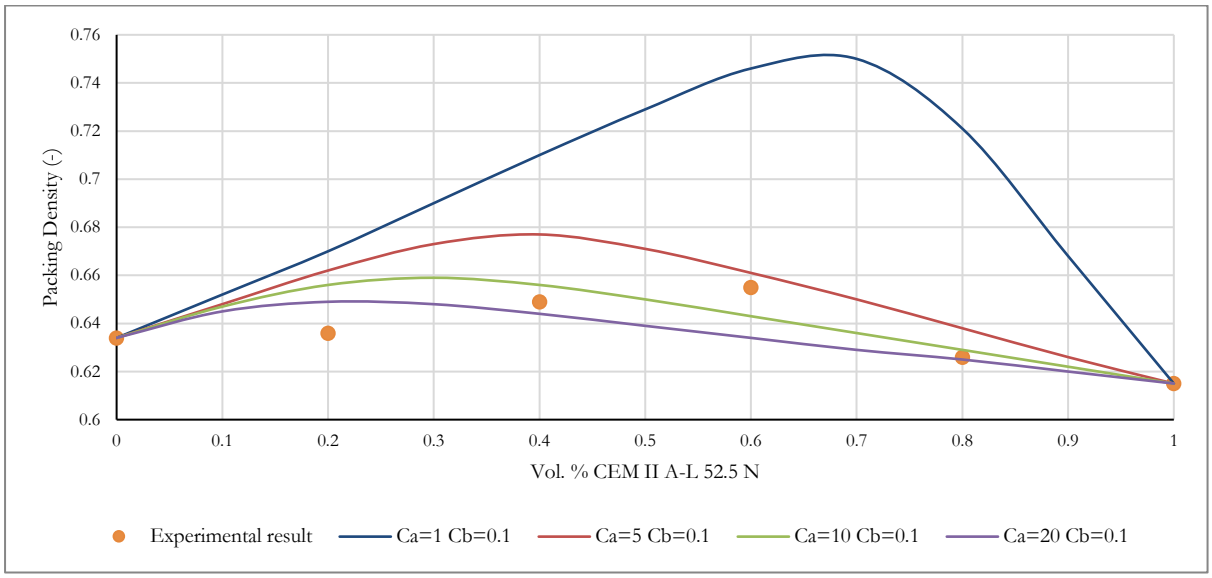

Figure B-17: CIPM predicted packing density for KB2/cement combinations for various C_a with C_b=0.1

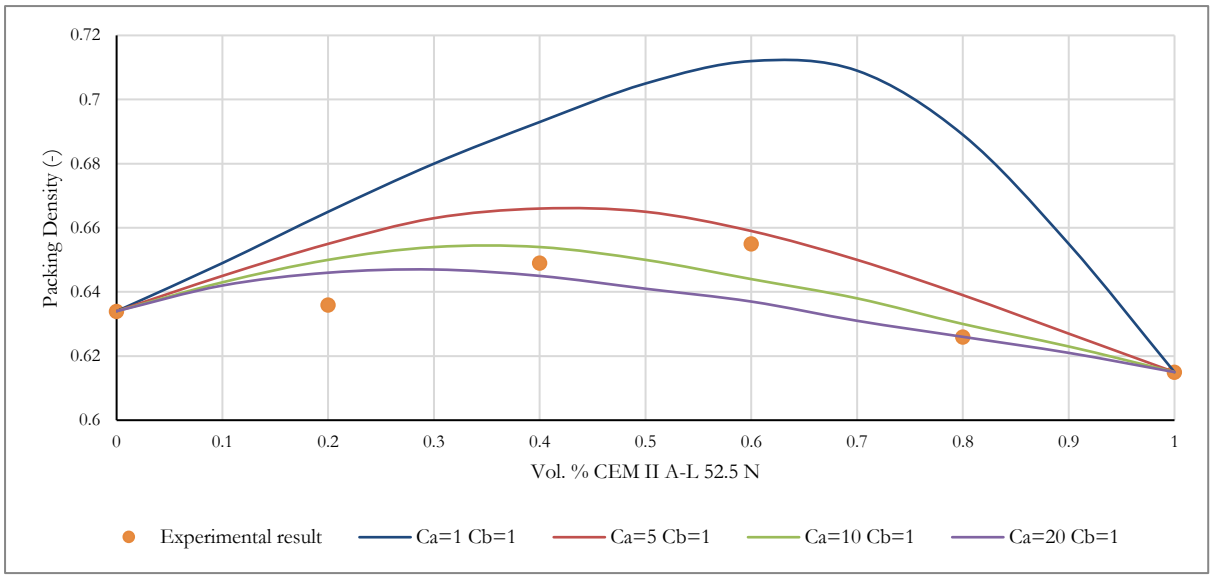

Figure B-18: CIPM predicted packing density for KB2/cement combinations for various C_a with C_b=1

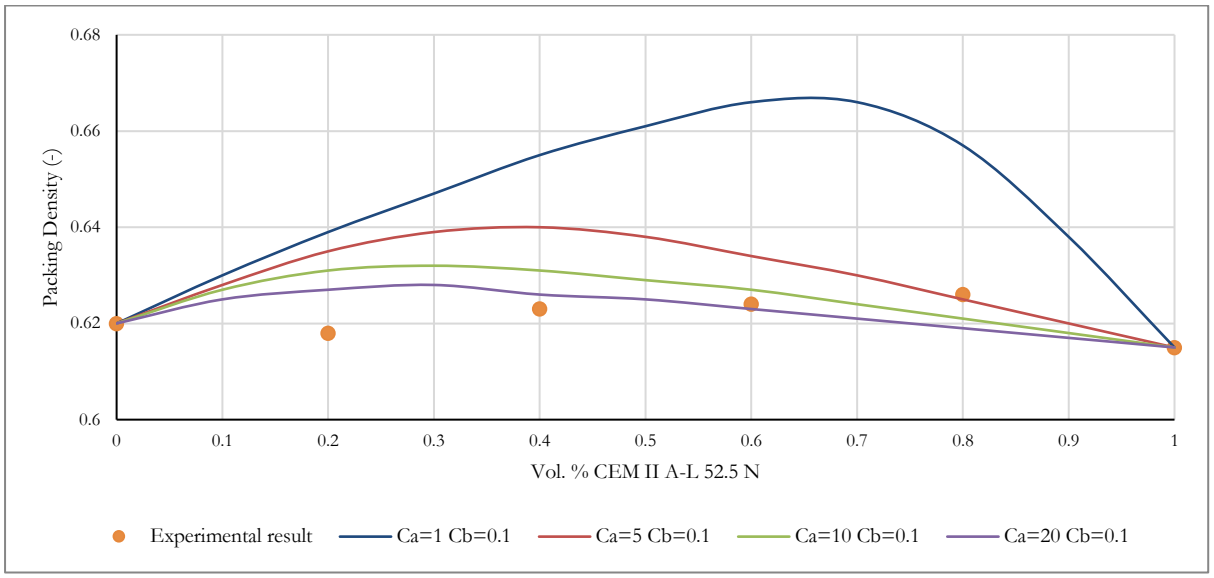

Figure B-19: CIPM predicted packing density for KB5/cement combinations for various C_a with C_b=0.1

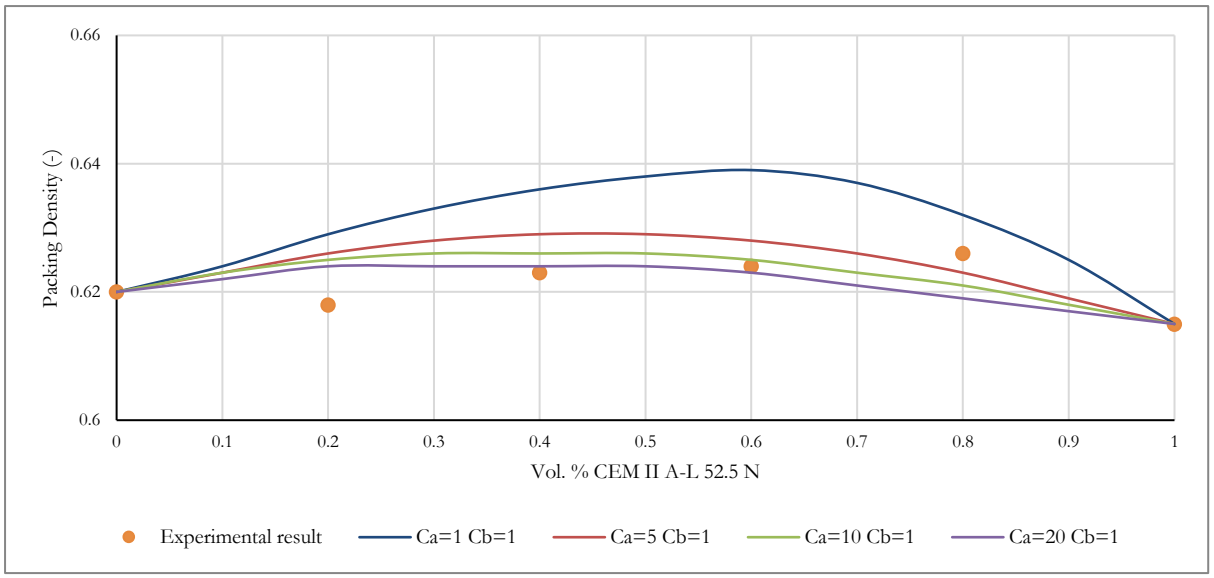

Figure B-20: CIPM predicted packing density for KB5/cement combinations for various C_a with C_b=1

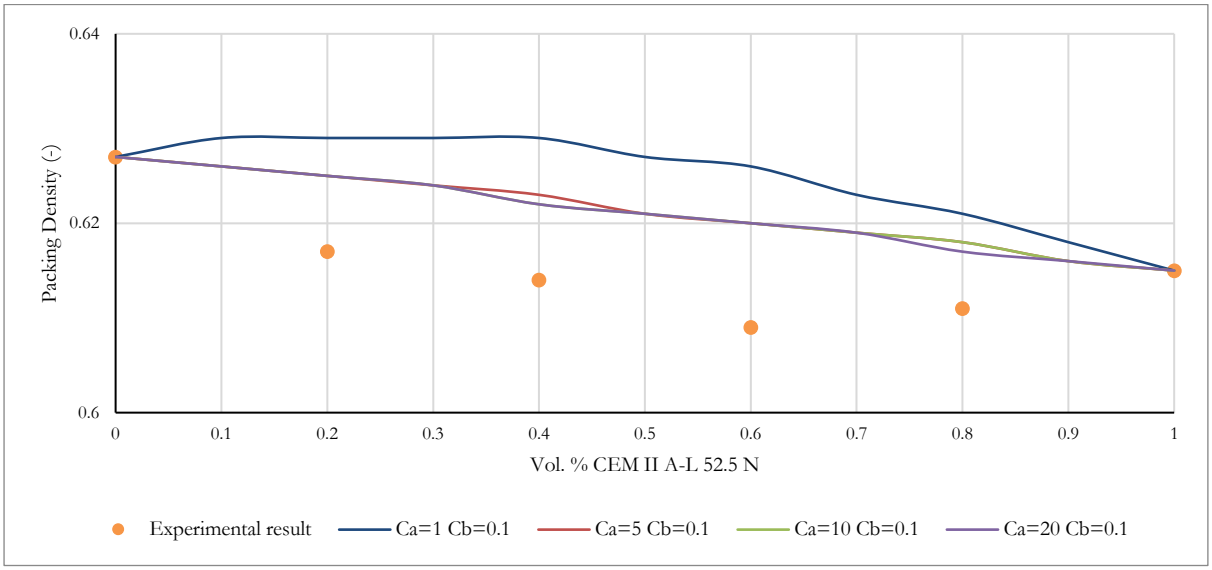

Figure B-21: CIPM predicted packing density for KB10/cement combinations for various C_a with C_b=0.1

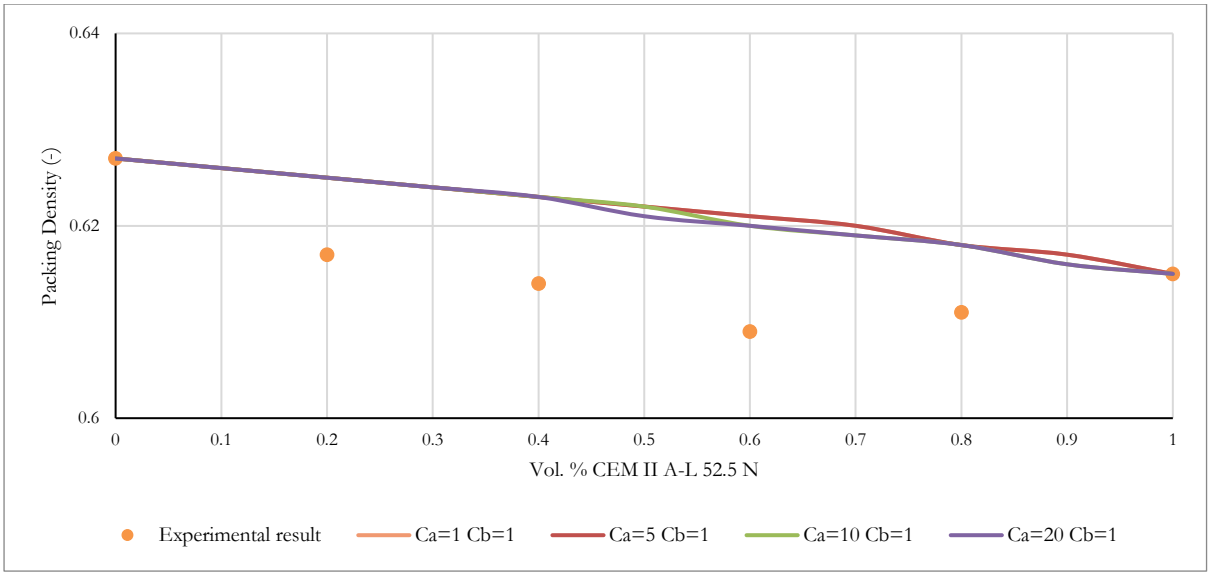

Figure B-22: CIPM predicted packing density for KB10/cement combinations for various C_a with C_b=1

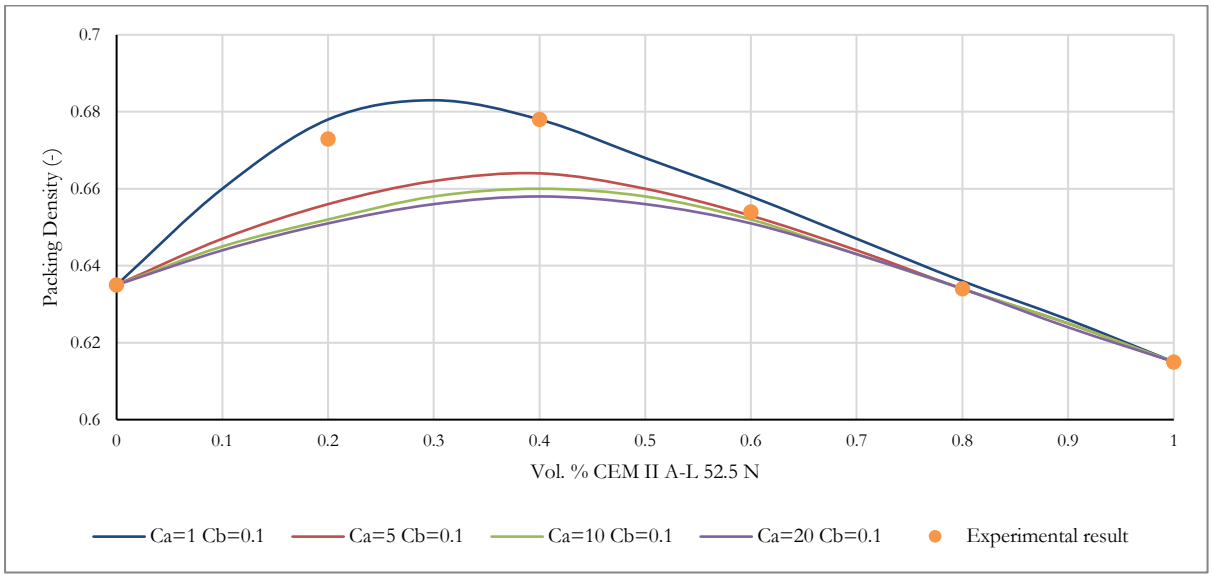

Figure B-23: CIPM predicted packing density for KB45/cement combinations for various C_a with C_b=0.1

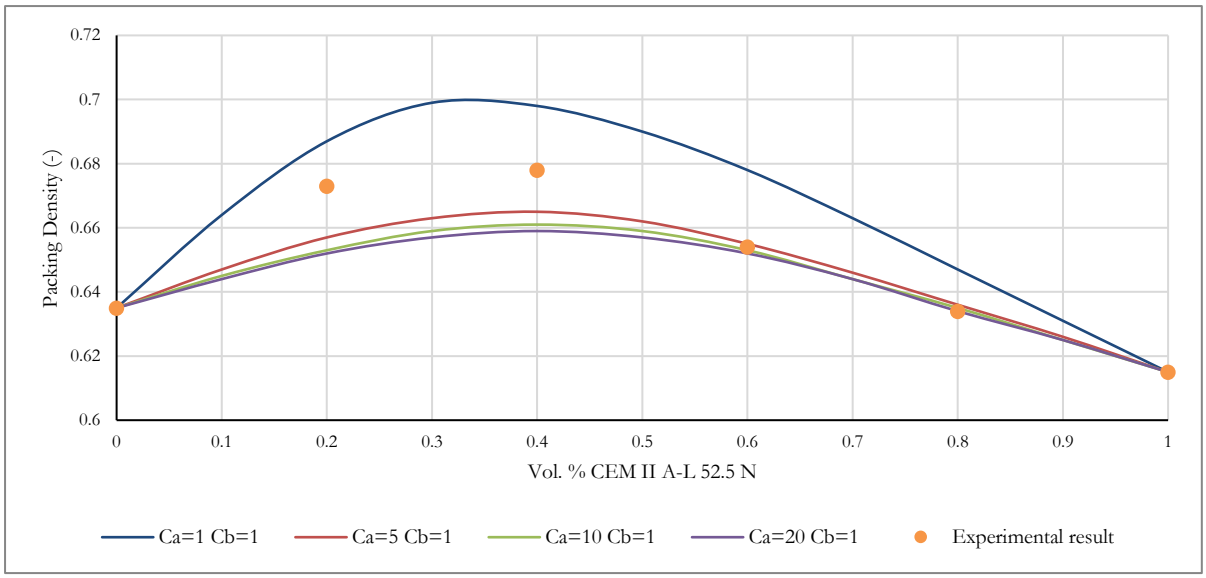

Figure B-24: CIPM predicted packing density for KB45/cement combinations for various C_a with C_b=1

Appendix C: CIPM sample calculation

Figure C-1 is a screenshot from the input for the CIPM in Microsoft Excel, portraying the particle size classes being used in the analysis and volume percentage material retained at each size class for each material. Experimental packing density ($\alpha_{\exp}$) per material and the associated compaction index and resulting packing density per size class (α_i) (from the reverse calculation) is also shown in Figure C-1.

A hypothetical scenario is considered for the demonstration of a sample calculation. A particle mixture comprising 80 % CEM II A-L 52.5 N and 20 % KB2 by volume. Only the calculation and resulting packing density of mixture of size classes n23 and n24 (Figure C-2) are given. Usually, the calculation procedures described hereafter are conducted for the interaction of each size class with every other size class present in the mixture.

	A	B	C	D	E	F	G
1		Material name	%	Pdensity α_i	K_{exp}	Experimental Pdensity per material α_{exp}	
2	1	Kulubrite 2	0.2	0.6153	12.2	0.634	
3	2	Kulubrite 5	0	0.5979	12.2	0.620	
4	3	Kulubrite 10	0	0.5794	12.2	0.627	
5	4	Kulubrite 45	0	0.504	12.2	0.635	
6	5	CEM II A-L 52.5	0.8	0.5539	12.2	0.615	
7		*Leave blank if the value is N/A*					
8		Size Class	Kulubrite 2	Kulubrite 5	Kulubrite 10	Kulubrite 45	CEM II A-L 52.5
9	1	599.809				3.15	
10	2	279.505			0.01	25.28	
11	3	130.246			0.42	33.28	0.66
12	4	60.692			5.42	20.81	13.66
13	5	28.285		3.92	26.48	10.16	33.06
14	6	13.183	1.81	31.54	32.28	4.36	26.44
15	7	6.141	21.98	35.25	16.81	1.49	14.08
16	8	2.858	35.23	12.79	7.53	0.6	7.04
17	9	1.332	26.41	8.51	5.81	0.38	2.99
18	10	0.618	14.01	7.57	4.9	0.49	1.97
19	11	0.389	0.53	0.42	0.34		0.1
20	12	0.334	0.03				
21							
22							
23							

Figure C-1: Screenshot from Microsoft Excel input for CIPM

	A	B	C	D	E	F	G	H
25		**Name**	**Name**	**Size**	**Size**	**PDensity**	**Kvalue**	**Beta**
26			**(No.)**	**(No.)**	**[µm]**	**[-]**	**[-]**	**[-]**
27	**n1**	Kulubrite 45	4	1	599.809	0.504	12.200	0.545
28	**n2**	Kulubrite 10	3	2	279.505	0.579	12.200	0.627
29	**n3**	Kulubrite 45	4	2	279.505	0.504	12.200	0.545
30	**n4**	Kulubrite 10	3	3	130.246	0.579	12.200	0.627
31	**n5**	Kulubrite 45	4	3	130.246	0.504	12.200	0.545
32	**n6**	CEM II A-L 52.5	5	3	130.246	0.554	12.200	0.599
33	**n7**	Kulubrite 10	3	4	60.692	0.579	12.200	0.627
34	**n8**	Kulubrite 45	4	4	60.692	0.504	12.200	0.545
35	**n9**	CEM II A-L 52.5	5	4	60.692	0.554	12.200	0.599
36	**n10**	Kulubrite 5	2	5	28.285	0.598	12.200	0.647
37	**n11**	Kulubrite 10	3	5	28.285	0.579	12.200	0.627
38	**n12**	Kulubrite 45	4	5	28.285	0.504	12.200	0.545
39	**n13**	CEM II A-L 52.5	5	5	28.285	0.554	12.200	0.599
40	**n14**	Kulubrite 2	1	6	13.183	0.615	12.200	0.666
41	**n15**	Kulubrite 5	2	6	13.183	0.598	12.200	0.647
42	**n16**	Kulubrite 10	3	6	13.183	0.579	12.200	0.627
43	**n17**	Kulubrite 45	4	6	13.183	0.504	12.200	0.545
44	**n18**	CEM II A-L 52.5	5	6	13.183	0.554	12.200	0.599
45	**n19**	Kulubrite 2	1	7	6.141	0.615	12.200	0.666
46	**n20**	Kulubrite 5	2	7	6.141	0.598	12.200	0.647
47	**n21**	Kulubrite 10	3	7	6.141	0.579	12.200	0.627
48	**n22**	Kulubrite 45	4	7	6.141	0.504	12.200	0.545
49	**n23**	CEM II A-L 52.5	5	7	6.141	0.554	12.200	0.599
50	**n24**	Kulubrite 2	1	8	2.858	0.615	12.200	0.666

Figure C-2: Screenshot from CIPM in Microsoft Excel. The two size classes used for demonstration of sample calculations are highlighted in yellow.

The assumption of this sample calculation is that the reverse calculation has already been performed to determine the packing density per size class per material and that the model constants defined in Table C-1 are used. Commentary on the reverse calculation is given at the end of this section. The model output compaction index (K_t) is set to 9 as the powder mixtures were to be used in the context of a full concrete mixture (not just powders alone) and this value is associated with a flowable concrete mixture according to Fennis (personal communication 2017, February 23).

Table C-1: CIPM model constants

Model constant	Symbol	Value	Unit
Loosening effect constant	C_a	13.5	-
Wall effect constant	C_b	1	-
Cut-off diameter	d_c	10	µm
Experimental compaction index	K_{exp}	12.2	-
Model output compaction index	K_t	9	-

Size class n23 is a cement size class with diameter 6.141 µm (determined from the geometric mean of upper and lower size classes). Size class n24 is a KB2 size class with diameter 2.858 µm. Input experimental packing densities per size class are quoted to 3 decimal places and although intermediate steps in this calculation show numbers rounded to 3 decimals, usually only the final packing density for a material mixture is rounded to 3 decimal places.

Initially, the 'dominant' size class is not known. Therefore, the cement size class is considered to be dominant first. The virtual packing density for each size class is then calculated.

$$\beta_i = (1 + \frac{1}{K_{\exp}})\alpha_i$$

$$\beta_{23} = (1 + \frac{1}{12.2}) \times 0.554$$
$$\beta_{23} = 0.599$$

$$\beta_j = (1 + \frac{1}{K_{\exp}})\alpha_j$$

$$\beta_{24} = (1 + \frac{1}{12.2}) \times 0.615$$
$$\beta_{24} = 0.666$$

The volumetric proportion of each size class in the total mixture (r_i) is then required:

$$r_{23} = \frac{vol_{23}}{vol_t} = 0.8$$

$$r_{24} = \frac{vol_{24}}{vol_t} = 0.2$$

Wall and loosening coefficients are then determined. As the cement size class (n23) is larger than the KB2 size class (n24), it is only subject to a loosening effect when in the presence of KB2 (and no wall effect). However, this is an ideal case. As there are usually several different size classes present in a mixture, when a particular size class is considered to be dominant, there will usually be size classes smaller and larger than it and therefore it would be subject to loosening and wall effects.

$$a_{ij} = \begin{cases} 1 - \dfrac{\log(d_i/d_j)}{w_{0,a}} & \log(d_i/d_j) < w_{0,a} \\ 0 & \log(d_i/d_j) \geq w_{0,a} \end{cases} \qquad w_{0,a} = \begin{cases} w_a C_a & d_j < d_c \\ w_a & d_j \geq d_c \end{cases} \qquad \textit{Eqn. 4-15}$$

$$d_{24} < 10\mu m$$

$$\therefore w_{0,a} = w_a C_a = 1 \times 13.5 = 13.5$$

$$\log(6.141/2.858) = 0.332 < w_{0,a}$$

$$\therefore a_{23,24} = 1 - \frac{\log(d_i/d_j)}{w_{0,a}} = 1 - \frac{\log(6.141/2.858)}{13.5} = 0.975$$

$$b_{ij} = \begin{cases} 1 - \dfrac{\log(d_j/d_i)}{w_{0,b}} & \log(d_j/d_i) < w_{0,b} \\ 0 & \log(d_j/d_i) \geq w_{0,b} \end{cases} \qquad w_{0,b} = \begin{cases} w_b C_b & d_i < d_c \\ w_b & d_i \geq d_c \end{cases} \qquad \textit{Eqn. 4-16}$$

$\therefore b_{23,24} = 0$

The virtual packing density of the mixture (when considering size class n23 dominant) is then calculated:

$$\beta_{ti} = \frac{\beta_i}{1 - \sum_{j=1}^{i-1}[1 - \beta_i + b_{ij}\beta_i(1 - 1/\beta_j)]r_j - \sum_{j=i+1}^{n}[1 - a_{ij}\,\beta_i/\beta_j]r_j}$$

$$\beta_{t23} = \frac{\beta_{23}}{1 - \sum_{j=1}^{i-1}[1 - \beta_{23} + b_{23,24}\beta_{23}(1 - 1/\beta_{24})]r_{24} - \sum_{j=i+1}^{n}[1 - a_{23,24}\,\beta_{23}/\beta_{24}]r_{24}}$$

$$\beta_{t23} = \frac{0.599}{1 - \left([1 - 0.599 + 0] \times 0.2 - [1 - 0.97 \times 0.599/0.666]0.2\right)}$$

$$\beta_{t23} = 0.634$$

Thereafter, size class n24 is considered to be the dominant size class and the same procedures are followed to determine the value of β_{t24}. As n24 is smaller than size class n23, the only interaction effect that it experiences is a wall effect (and no loosening effect).

$$b_{ij} = \begin{cases} 1 - \dfrac{\log(d_j/d_i)}{w_{0,b}} & \log(d_j/d_i) < w_{0,b} \\ 0 & \log(d_j/d_i) \geq w_{0,b} \end{cases} \qquad w_{0,b} = \begin{cases} w_b C_b & d_i < d_c \\ w_b & d_i \geq d_c \end{cases} \qquad \textit{Eqn. 4-16}$$

$d_{24} < 10\mu m$

$\therefore w_{0,b} = w_b C_b = 1 \times 1 = 1$

$\log(6.141/2.858) = 0.332 < w_{0,b}$

$$\therefore b_{24,23} = 1 - \frac{\log(d_j/d_i)}{w_{0,b}} = 1 - \frac{\log(6.141/2.858)}{1} = 0.668$$

$$a_{ij} = \begin{cases} 1 - \dfrac{\log(d_i/d_j)}{w_{0,a}} & \log(d_i/d_j) < w_{0,a} \\ 0 & \log(d_i/d_j) \geq w_{0,a} \end{cases} \qquad w_{0,a} = \begin{cases} w_a C_a & d_j < d_c \\ w_a & d_j \geq d_c \end{cases} \qquad \textit{Eqn. 4-15}$$

$\therefore a_{24,23} = 0$

The virtual packing density of the mixture (when considering size class n24 dominant) is then calculated:

$$\beta_{ti} = \frac{\beta_i}{1 - \sum_{j=1}^{i-1}[1 - \beta_i + b_{ij}\beta_i(1 - 1/\beta_j)]r_j - \sum_{j=i+1}^{n}[1 - a_{ij}\,\beta_i/\beta_j]r_j}$$

$$\beta_{t24} = \frac{\beta_{24}}{1 - \sum_{j=1}^{i-1}[1 - \beta_{24} + b_{24,23}\beta_{24}(1 - 1/\beta_{23})]r_{23} - \sum_{j=i+1}^{n}[1 - a_{24,23}\,\beta_{24}/\beta_{23}]r_{23}}$$

$$\beta_{t24} = \frac{0.666}{1 - \left([1 - 0.666 + 0.668 \times 0.666(1 - 1/0.599)] \times 0.8 - [1 - 0]0.8\right)}$$

$$\beta_{t24} = 0.376$$

The virtual packing density of the mixture is then taken as the minimum of β_{t23} & β_{t24} and a first approximation of the actual packing density of the mixture α_t is made as $\alpha_t = \beta_{ti} - 0.005$ and the summation of K_i values is checked to see that it is equivalent to the required K_t=9

$$K_t = \sum_{i=1}^{n} K_i = \sum_{i=1}^{n} \frac{r_i/\beta_i}{1/\alpha_t - 1/\beta_{ti}}$$

$$K_{23} = \frac{r_{23}/\beta_{23}}{1/\alpha_t - 1/\beta_{t23}} \qquad K_{23} = \frac{0.8/0.599}{1/0.596 - 1/0.634} = 13.28$$

$$K_{24} = \frac{r_{24}/\beta_{24}}{1/\alpha_t - 1/\beta_{t24}} \qquad K_{24} = \frac{0.2/0.666}{1/0.596 - 1/0.376} = -0.306$$

$$\therefore K_t = \sum_{i=1}^{n} K_i = 13.28 - 0.306 = 12.98$$

$$K_t > K_{\exp} = 9$$

Therefore, the value of α_t needs to be iterated again so that $K_t = K_{\exp} = 9$. The macro programmed in Microsoft Excel automatically subtracts increments of 0.005 and checks the resulting K_t after each increment. When K_t is in the range of $K_{\exp}$ + 4, the embedded Solver tool is then activated

and it iterates values of α_t to a higher precision (0.0001) until $K_t = K_{\exp}$.

The value of α_t that corresponds to $K_t = K_{\exp}$ is then the packing density for the given mixture of materials. For the more general case, once $K_t = K_{\exp}$ for a certain material combination, the next combination (defined by volume proportions of each material in the mixture) is checked, following the same procedures already described. Once all combinations have been checked, the combination enabling the maximum packing density is taken as the optimised material combination.

The reverse calculation to determine the packing density per size class from the experimental packing density per material follows a similar iterative procedure as already described. However, the model is set to consider only a pure material at a time (in this instance, either 100 % CEM II A-L 52.5N or 100 % KB2) and the packing density per size class (α_i) is iterated until $K_t = K_{\exp}$ instead of the value of α_t (which is now fixed at $\alpha_{\exp}$). The value for α_i that enables $K_t = K_{\exp}$ is then the packing per size class for the given material.

Appendix D: CIPM output powder combinations

Table D-1: Powder combinations and packing densities within 1.0 % of max packing density. 90 % cement.

Combination no.	Powder volume fraction (-)					CIPM packing density	% Increase from CEM II A-L 52.5 N
	KB2	KB5	KB10	KB45	CEM II A-L 52.5		
90-1	0	0	0	0.1	0.9	0.628	2.1
90-2	0.05	0	0	0.05	0.9	0.624	1.5
90-3	0	0.05	0	0.05	0.9	0.623	1.3
90-4	0	0	0.05	0.05	0.9	0.622	1.1

Table D-2: Powder combinations and packing densities within 1.0 % of max packing density. 80 % cement.

Combination no.	Powder volume fraction (-)					CIPM packing density	% Increase from CEM II A-L 52.5 N
	KB2	KB5	KB10	KB45	CEM II A-L 52.5		
80-1	0	0	0	0.2	0.8	0.640	4.1
80-2	0.05	0	0	0.15	0.8	0.637	3.6
80-3	0	0.05	0	0.15	0.8	0.636	3.4
80-4	0	0	0.05	0.15	0.8	0.635	3.3
80-5	0.1	0	0	0.1	0.8	0.634	3.1

Table D-3: Powder combinations and packing densities within 1.0 % of max packing density. 70 % cement.

Combination no.	Powder volume fraction (-)					CIPM packing density	% Increase from CEM II A-L 52.5 N
	KB2	KB5	KB10	KB45	CEM II A-L 52.5		
70-1	0	0	0	0.3	0.7	0.652	6.0
70-2	0.05	0	0	0.25	0.7	0.649	5.5
70-3	0	0.05	0	0.25	0.7	0.648	5.4
70-4	0	0	0.05	0.25	0.7	0.647	5.2
70-5	0.1	0	0	0.2	0.7	0.647	5.2

Table D-4: Powder combinations and packing densities within 1.0 % of max packing density. 60 % cement.

Combination no.	Powder volume fraction (-)					CIPM packing density	% Increase from CEM II A-L 52.5 N
	KB2	KB5	KB10	KB45	CEM II A-L 52.5		
60-1	0	0	0	0.4	0.6	0.662	7.6
60-2	0.05	0	0	0.35	0.6	0.660	7.3
60-3	0	0.05	0	0.35	0.6	0.660	7.3
60-4	0	0	0.05	0.35	0.6	0.659	7.2
60-5	0.1	0	0	0.3	0.6	0.658	7.0
60-6	0.05	0.05	0	0.3	0.6	0.658	7.0
60-7	0	0.1	0	0.3	0.6	0.657	6.8
60-8	0.05	0	0.05	0.3	0.6	0.656	6.7
60-9	0.15	0	0	0.25	0.6	0.656	6.7
60-10	0	0.05	0.05	0.3	0.6	0.656	6.7
60-11	0.1	0.05	0	0.25	0.6	0.655	6.5
60-12	0	0	0.1	0.3	0.6	0.655	6.5

Table D-5: Powder combinations and packing densities within 1.0 % of max packing density. 45 % cement.

Combination no.	Powder volume fraction (-)					CIPM packing density	% Increase from CEM II A-L 52.5 N
	KB2	KB5	KB10	KB45	CEM II A-L 52.5		
45-1	0	0.05	0	0.5	0.45	0.674	9.6
45-2	0	0	0	0.55	0.45	0.674	9.6
45-3	0.05	0	0	0.5	0.45	0.673	9.4
45-4	0.05	0.05	0	0.45	0.45	0.673	9.4
45-5	0	0.1	0	0.45	0.45	0.673	9.4
45-6	0.1	0	0	0.45	0.45	0.673	9.4
45-7	0	0	0.05	0.5	0.45	0.673	9.4
45-8	0	0.05	0.05	0.45	0.45	0.672	9.3
45-9	0.05	0	0.05	0.45	0.45	0.672	9.3
45-10	0.15	0	0	0.4	0.45	0.672	9.3
45-11	0.1	0.05	0	0.4	0.45	0.672	9.3
45-12	0.05	0.1	0	0.4	0.45	0.671	9.1
45-13	0	0.15	0	0.4	0.45	0.671	9.1
45-14	0	0	0.1	0.45	0.45	0.670	8.9
45-15	0.1	0	0.05	0.4	0.45	0.670	8.9
45-16	0.05	0.05	0.05	0.4	0.45	0.670	8.9
45-17	0.2	0	0	0.35	0.45	0.670	8.9
45-18	0.15	0.05	0	0.35	0.45	0.670	8.9
45-19	0	0.1	0.05	0.4	0.45	0.670	8.9
45-20	0.1	0.1	0	0.35	0.45	0.669	8.8
45-21	0.05	0	0.1	0.4	0.45	0.669	8.8
45-22	0.15	0	0.05	0.35	0.45	0.669	8.8
45-23	0	0.05	0.1	0.4	0.45	0.668	8.6
45-24	0.05	0.15	0	0.35	0.45	0.668	8.6
45-25	0.1	0.05	0.05	0.35	0.45	0.668	8.6
45-26	0.25	0	0	0.3	0.45	0.668	8.6
45-27	0.05	0.1	0.05	0.35	0.45	0.667	8.5
45-28	0	0.2	0	0.35	0.45	0.667	8.5
45-29	0.2	0.05	0	0.3	0.45	0.667	8.5
45-30	0	0	0.15	0.4	0.45	0.667	8.5
45-31	0.1	0	0.1	0.35	0.45	0.667	8.5

Appendix E: Detailed compressive strength results

A minimum of three 50 mm cube specimens per mix were tested for compressive strength at 3, 7, 28 and 56 days after casting. In accordance with SANS 5863 (2006), range/mean strength was required to be less than 15 % for a valid result.

Mix number	Mix description	Test age	Mean compressive strength	Range/Mean	Density
	-	Days	MPa	%	kg/m³
1-1	100CEM	3	50.5	5.00	2401
		7	59.8	2.17	2372
		28	72.4	4.86	2388
		56	79.6	4.04	2418
1-2	90CEM 10KB45	3	42.8	4.60	2380
		7	53.5	2.33	2372
		28	62.1	5.19	2379
		56	69.2	5.88	2376
1-3	80CEM 5KB2 15KB45	3	36.5	8.50	2355
		7	46.9	5.08	2365
		28	56.8	2.31	2371
		56	59.6	7.07	2368
1-4	80CEM 20KB45	3	34.5	2.89	2353
		7	45.4	5.59	2368
		28	54.0	7.34	2368
		56	58.0	7.30	2367
1-5	70CEM 30KB45	3	30.2	5.63	2341
		7	38.1	1.41	2328
		28	48.5	2.59	2327
		56	51.9	1.90	2340
1-6	60CEM 5KB2 35KB45	3	24.2	2.26	2340
		7	31.6	5.71	2319
		28	38.4	4.34	2336
		56	42.3	1.57	2358
2-1	45 CEM 45KB45 10KB2	3	20.5	2.66	2411
		7	24.6	4.69	2416
		28	28.5	7.97	2421
		56	36.9	5.11	2409
2-2	45CEM 30KB45 5KB2 20FA	3	22.8	10.91	2408
		7	26.7	10.34	2425
		28	33.9	7.38	2414
		56	38.1	1.40	2401

details compressive strength results for Phase 1 and 2 mixes.

Table E-1: Compressive strength results for Phase 1 and 2 mixes

Mix number	Mix description	Test age	Mean compressive strength	Range/Mean	Density
	-	Days	MPa	%	kg/m³

1-1	100CEM	3	50.5	5.00	2401
		7	59.8	2.17	2372
		28	72.4	4.86	2388
		56	79.6	4.04	2418
1-2	90CEM 10KB45	3	42.8	4.60	2380
		7	53.5	2.33	2372
		28	62.1	5.19	2379
		56	69.2	5.88	2376
1-3	80CEM 5KB2 15KB45	3	36.5	8.50	2355
		7	46.9	5.08	2365
		28	56.8	2.31	2371
		56	59.6	7.07	2368
1-4	80CEM 20KB45	3	34.5	2.89	2353
		7	45.4	5.59	2368
		28	54.0	7.34	2368
		56	58.0	7.30	2367
1-5	70CEM 30KB45	3	30.2	5.63	2341
		7	38.1	1.41	2328
		28	48.5	2.59	2327
		56	51.9	1.90	2340
1-6	60CEM 5KB2 35KB45	3	24.2	2.26	2340
		7	31.6	5.71	2319
		28	38.4	4.34	2336
		56	42.3	1.57	2358
2-1	45 CEM 45KB45 10KB2	3	20.5	2.66	2411
		7	24.6	4.69	2416
		28	28.5	7.97	2421
		56	36.9	5.11	2409
2-2	45CEM 30KB45 5KB2 20FA	3	22.8	10.91	2408
		7	26.7	10.34	2425
		28	33.9	7.38	2414
		56	38.1	1.40	2401

Appendix F: Detailed durability index results

Table F-1 to Table F-18 portray detailed durability index test results for Phase 1 mixes with mean values and coefficient of variation for each parameter.

Table F-1: Mix 1-1 (100CEM) detailed OPI results

Disk Number	k (m/s)	OPI
1	2.2E-11	10.66
2	3.8E-11	10.42
3	2.7E-11	10.58
4	2.6E-11	10.59
Mean	2.8E-11	10.56
CoV (%)	24.0	0.93

Table F-2: Mix 1-1 (100CEM) detailed WSI and porosity results

Disk Number	Sorptivity (mm/hr$^{0.5}$)	Porosity (%)
1	7.4	9.9
2	8.5	10.7
3	7.5	10.2
4	7.5	10.4
Mean	7.7	10.3
CoV (%)	7.0	3.3

Table F-3: Mix 1-1 (100CEM) detailed CCI results

Disk Number	Conductivity (mS/cm)
1	0.9
2	1.0
3	1.0
4	1.0
Mean	1.0
CoV (%)	3.6

Table F-4: Mix 1-2 (90CEM 10KB45) detailed OPI results

Disk Number	k (m/s)	OPI
1	2.4E-11	10.62
2	2.6E-11	10.58
3	2.7E-11	10.57
4	3.0E-11	10.52
Mean	2.7E-11	10.57
CoV (%)	10.1	0.41

Table F-5 Mix 1-2 (90CEM 10KB45) detailed WSI and porosity results

Disk Number	Sorptivity (mm/hr$^{0.5}$)	Porosity (%)
1	6.9	11.1
2	7.4	10.9
3	7.9	10.9
4	7.5	11.2
Mean	7.4	11.0
CoV (%)	5.5	1.1

Table F-6: Mix 1-2 (90CEM 10KB45) detailed CCI results

Disk Number	Conductivity (mS/cm)
1	1.1
2	1.1
3	1.1
4	1.1
Mean	1.1
CoV (%)	1.6

Table F-7: Mix 1-3 (80CEM 5KB2 15KB45) detailed OPI results

Disk Number	k (m/s)	OPI
1	2.8E-11	10.55
2	2.4E-11	10.62
3	2.2E-11	10.66
4	2.4E-11	10.62
Mean	2.4E-11	10.61
CoV (%)	11.5	0.46

Table F-8: Mix 1-3 (80CEM 5KB2 15KB45) detailed WSI and porosity results

Disk Number	Sorptivity (mm/hr$^{0.5}$)	Porosity (%)
1	7.1	12.6
2	6.9	12.8
3	6.7	12.5
4	7.2	12.7
Mean	7.0	12.6
CoV (%)	3.1	1.2

Table F-9: Mix 1-3 (80CEM 5KB2 15KB45) detailed CCI results

Disk Number	Conductivity (mS/cm)
1	1.4
2	1.3
3	1.4
4	1.3
Mean	1.4
CoV (%)	4.0

Table F-10: Mix 1-4 (80CEM 20KB45) detailed OPI results

Disk Number	k (m/s)	OPI
1	2.5E-11	10.61
2	2.8E-11	10.56
3	2.1E-11	10.68
4	2.3E-11	10.63
Mean	2.4E-11	10.62
CoV (%)	11.4	0.47

Table F-11: Mix 1-4 (80CEM 20KB45) detailed WSI and porosityy results

Disk Number	Sorptivity (mm/hr$^{0.5}$)	Porosity (%)
1	6.8	11.7
2	7.3	11.2
3	6.8	11.7
4	7.6	11.9
Mean	7.1	11.6
CoV (%)	5.7	2.5

Table F-12: Mix 1-4 (80CEM 20KB45) detailed CCI results

Disk Number	Conductivity (mS/cm)
1	1.3
2	1.2
3	1.3
4	1.3
Mean	1.3
CoV (%)	3.0

Table F-13: Mix 1-5 (70CEM 30KB45) detailed OPI results

Disk Number	k (m/s)	OPI
1	3.9E-11	10.40
2	4.1E-11	10.39
3	3.9E-11	10.41
4	4.1E-11	10.39
Mean	4.0E-11	10.40
CoV (%)	2.3	0.10

Table F-14: Mix 1-5 (70CEM 30KB45) detailed WSI and porosity results

Disk Number	Sorptivity (mm/hr$^{0.5}$)	Porosity (%)
1	7.0	13.3
2	7.4	13.4
3	7.8	13.3
4	7.3	13.2
Mean	7.4	13.3
CoV (%)	4.1	0.7

Table F-15: Mix 1-5 (70CEM 30KB45) detailed CCI results

Disk Number	Conductivity (mS/cm)
1	1.6
2	1.8
3	1.8
4	1.8
Mean	1.8
CoV (%)	4.9

Table F-16: Mix 1-6 (60CEM 5KB2 35KB45) detailed OPI results

Disk Number	k (m/s)	OPI
1	3.9E-11	10.41
2	3.6E-11	10.44
3	5.0E-11	10.30
4	1.0E-10*	9.99*
Mean	4.2E-11	10.38
CoV (%)	17.4	0.71

*Red text subjectively deemed an outlier

Table F-17: Mix 1-6 (60CEM 5KB2 35KB45) detailed WSI and porosity results

Disk Number	Sorptivity (mm/hr$^{0.5}$)	Porosity (%)
1	7.1	14.4
2	6.9	14.2
3	7.3	14.4
4	6.9	14.8
Mean	7.0	14.5
CoV (%)	2.8	1.7

Table F-18: Mix 1-6 (60CEM 5KB2 35KB45) detailed CCI results

Disk Number	Conductivity (mS/cm)
1	2.1
2	2.2
3	2.1
4	2.1
Mean	2.1
CoV (%)	2.4

Appendix G: Detailed accelerated shrinkage results

Cumulative accelerated shrinkage strains (microstrain) at each test day are shown for Phase 1 mixes in Table G-1to Table G-6. In accordance with SANS 6085 (2006), strain readings were taken until consecutive readings revealed strain less than 2 μm per 100 mm gauge length for each specimen. SANS 6085 (2006) requires that the range/average strain across 3 test specimens is less than 20 % for a valid test result.

Table G-1: Mix 1-1 (100CEM) accelerated shrinkage microstrain

Prism no.	Days from casting		
	14	16	18
1	485	530	540
2	455	500	510
3	440	485	500
Range	45	45	40
Average	460	505	517
Range/Average Percentage	10	9	8
Range/Average Check	okay	okay	okay
Sample/control Percentage	-	-	-
Max	485.0	530.0	540.0
Min	440.0	485.0	500.0
Standard Deviation	22.9	22.9	20.8

Table G-2: Mix 1-2 (90CEM) accelerated shrinkage microstrain

Prism no.	Days from casting		
	14	16	18
1	478	555	560
2	488	520	525
3	450	490	490
Range	38	65	70
Average	472	522	525
Range/Average Percentage	8	12	13
Range/Average Check	okay	okay	okay
Sample/control Percentage	-	-	-
Max	487.5	555.0	560.0
Min	450.0	490.0	490.0
Standard Deviation	19.4	32.5	35.0

Table G-3: Mix 1-3 (80CEM 5KB2 15KB45) accelerated shrinkage microstrain

Prism	Days from casting		
	14	16	18
1	425	455	445
2	415	440	440
3	400	430	440
Range	25	25	5
Average	413	442	442
Range/Average Percentage	6	6	1
Range/Average Check	okay	okay	okay
Sample/control Percentage	-	-	-
Max	425.0	455.0	445.0
Min	400.0	430.0	440.0
Standard Deviation	12.6	12.6	2.9

Table G-4: Mix 1-4 (80CEM 30KB45) accelerated shrinkage microstrain

Prism no.	Days from casting		
	14	16	18
1	445	470	470
2	415	445	445
3	450	470	480
Range	35	25	35
Average	437	462	465
Range/Average Percentage	8	5	8
Range/Average Check	okay	okay	okay
Sample/control Percentage	-	-	-
Max	450.0	470.0	480.0
Min	415.0	445.0	445.0
Standard Deviation	18.9	14.4	18.0

Table G-5: Mix 1-5 (70CEM 30KB45) accelerated shrinkage microstrain

Prism no.	Days from casting		
	14	16	18
1	380	390	385
2	415	430	440
3	345	365	380
Range	70	65	60
Average	380	395	402
Range/Average Percentage	18	16	15
Range/Average Check	okay	okay	okay
Sample/control Percentage	-	-	-
Max	415.0	430.0	440.0
Min	345.0	365.0	380.0
Standard Deviation	35.0	32.8	33.3

Table G-6: Mix 1-6 (60CEM 5KB2 35KB45) accelerated shrinkage microstrain

Prism no.	Days from casting	
	14	16
1	330	330
2	360	375
3	350	365
Range	30	45
Average	347	357
Range/Average Percentage	9	13
Range/Average Check	okay	okay
Sample/control Percentage	-	-
Max	360.0	375.0
Min	330.0	330.0
Standard Deviation	15.3	23.6

Appendix H: EBE faculty assessment of ethics in research projects

Application for Approval of Ethics in Research (EiR) Projects
Faculty of Engineering and the Built Environment, University of Cape Town

APPLICATION FORM

Please Note:
Any person planning to undertake research in the Faculty of Engineering and the Built Environment (EBE) at the University of Cape Town is required to complete this form **before** collecting or analysing data.The objective of submitting this application *prior* to embarking on research is to ensure that the highest ethical standards in research, conducted under the auspices of the EBE Faculty, are met. Please ensure that you have read, and understood the **EBE Ethics in Research Handbook**(available from the UCT EBE, Research Ethics website) prior to completing this application form: http://www.ebe.uct.ac.za/usr/ebe/research/ethics.pdf

APPLICANT'S DETAILS		
Name of principal researcher, student or external applicant		Matthew Stuart Holmes
Department		Civil Engineering
Preferred email address of applicant:		himmat002@myuct.ac.za
If a Student	Your Degree: e.g., MSc, PhD, etc.,	MSc Civil Infrastructure Management and Maintenance
	Name of Supervisor (if supervised):	Emeritus Professor Mark G. Alexander
If this is a researchcontract, indicate the source of funding/sponsorship		N/A
Project Title		The optimisation of the packing of powder materials for the reduction of clinker content in concrete

I hereby undertake to carry out my research in such a way that:

- there is no apparent legal objection to the nature or the method of research; and
- the research will not compromise staff or students or the other responsibilities of the University;
- the stated objective will be achieved, and the findings will have a high degree of validity;
- limitations and alternative interpretations will be considered;
- the findings could be subject to peer review and publicly available; and
- I will comply with the conventions of copyright and avoid any practice that would constitute plagiarism.

SIGNED BY	Full name	Signature	Date
Principal Researcher/ Student/External applicant	Matthew Stuart Holmes		Click here to enter a date.

APPLICATION APPROVED BY	Full name	Signature	Date
Supervisor (where applicable)	Emeritus Professor Mark Gavin Alexander	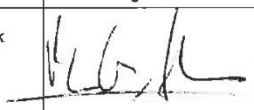	26/10/2016 Click here to enter a date.
HOD (or delegated nominee) Final authority for all applicants who have answered NO to all questions in Section1; and for all Undergraduateresearch (Including Honours).	Click here to enter text. M Vandersclmen	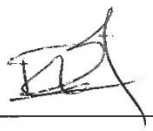	Click here to enter a date. 23/11/16
Chair : Faculty EIR Committee For applicants other than undergraduate students who have answered YES to any of the above questions.	Click here to enter text.		Click here to enter a date.

Page 1 of 1